POTENTIAL AND VISCOUS FLOW PROBLEMS USING THE BOUNDARY ELEMENT METHOD

by

Luiz Carlos Wrobel

Thesis submitted for
the degree of

Doctor of Philosophy

DEPARTMENT OF CIVIL ENGINEERING

THE UNIVERSITY OF SOUTHAMPTON

July 1981

TABLE OF CONTENTS

UNIVERSITY OF SOUTHAMPTON

ABSTRACT

FACULTY OF ENGINEERING AND APPLIED SCIENCE

CIVIL ENGINEERING

Doctor of Philosophy

POTENTIAL AND VISCOUS FLOW PROBLEMS USING THE BOUNDARY ELEMENT METHOD

by Luiz Carlos Wrobel

This work is concerned with the application of the Boundary Element Method for the solution of steady and transient potential and viscous flow problems. Two-dimensional, axisymmetric and fully three-dimensional problems are considered, the general theory developed and specific numerical procedures derived for each of the above cases.

Initially, the derivation of the boundary integral equation equivalent to Laplace's equation is reviewed within the framework of classical potential theory. Numerical procedures for the solution of this equation are discussed,being the boundary discretised by using piecewise constant, linear or quadratic variations for the potential function and its normal derivative.

Integral formulations for the solution of the diffusion equation are then studied. Three different approaches are considered: using Laplace transforms, coupling the BEM with the Finite Difference Method or employing time-dependent fundamental solutions. For the latter case, specific numerical procedures for the solution of the time-dependent boundary integral equation equivalent to the diffusion equation are developed and different time-marching schemes tested.

Finally, a BEM formulation for the solution of incompressible viscous flow problems governed by the Navier-Stokes equations together with the continuity equation is derived, following Lighthill's vorticity-velocity approach. Numerical procedures for the solution of the resulting set of non-linear integral equations are discussed in detail.

Computer programs incorporating several of these features were developed, and examples of applications of such programs are presented throughout this work.

To Ruth and the coming baby

ACKNOWLEDGEMENTS

The author wishes to thank his supervisor, Dr. C.A. Brebbia, for his guidance and helpful advice. Thanks are also due to all my colleagues at 13, University Crescent, with whom I shared frustrations and happy moments; especial thanks go to R.K. Nakaguma, J.C.F. Telles and W.J. Mansur, for many invaluable discussions; to the National Council for Scientifical and Technological Development (C.N.Pq.), Brazil, for the financial support; to my parents, for their encouragement and support in all ways; to Mrs. M. Binnie and Mrs. D. Harris for the neat typing of the manuscript; finally, I would like to thank, in particular, my wife, Ruth, who helped me with the writing and, with her love and patience, created the necessary conditions for the development of this work.

LIST OF FIGURES

CHAPTER 4 - TRANSIENT POTENTIAL PROBLEMS

CHAPTER 6 - PROGRAMMING

APPENDIX B

LIST OF TABLES

NOTATION

x_1, x_2, x_3	cartesian coordinates
R, θ, Z	cylindrical polar coordinates
ξ	intrinsic coordinate
Ω	domain of the region
Γ	boundary of the region
p,s	internal points (in Ω)
P,S	boundary points (on Γ)
$n(S)$	unit outward normal to surface Γ at point S
u	potential function
q	derivative of u with relation to n
u^*	fundamental solution
q^*	derivative of u^* with relation to n
$r(p,s)$	distance between p and s
$x_{i,n} = \partial x_i/\partial n$	
$R_{,n} = \partial R/\partial n$	
$Z_{,n} = \partial Z/\partial n$	
σ	surface density of single-layer potential
μ	surface density of double-layer potential
ρ	volume density of volume potential
$\delta(p,s)$	Dirac delta
δ_{ij}	Kronecker delta
t	time
ψ,ϕ	space interpolation functions
χ	time interpolation function
J	Jacobian
∇^2	Laplacian
$\underset{\sim}{\nabla}$	gradient vector
$\times$	vector product

$\cdot$	scalar product
$\underset{\sim}{\omega}$	vorticity vector
$\underset{\sim}{v}$	velocity vector
ν	kinematic viscosity
$\underset{\sim}{n}$	unit normal vector

1. INTRODUCTION

The Boundary Element Method is now firmly established as an important alternative technique to the prevailing numerical methods in continuum mechanics. Much attention is being given to its development over the last few years, as it can be seen by the number of recently published books and proceedings of international conferences on the subject ([1] to [10], [90]).

The technique basically consists of the transformation of the partial differential equation describing the behaviour of the unknown inside and on the boundary of the domain into an integral equation relating only boundary values, and the numerical solution of this equation. If values at internal points are required, they are calculated afterwards from the boundary data. Since all numerical approximations take place only at the boundaries, the dimensionality of the problem is reduced by one and smaller system of equations obtained in comparison with those achieved through differential methods.

The present work is concerned with the application of the Boundary Element Method for the solution of steady and transient potential and viscous flow problems. By steady and transient potential problems we mean problems governed by the Laplace and diffusion equations, respectively; viscous flow problems are problems governed by the Navier-Stokes equations. Two-dimensional, axisymmetric and fully three-dimensional analyses are considered, the general theory developed and specific numerical procedures derived for each of the above cases.

Historically, the application of integral equations to formulate the fundamental boundary-value problems of potential theory dates back to 1903, when Fredholm [11] demonstrated the existence of solutions to such equations, on the basis of a discretisation procedure. Due to the difficulty of finding analytical solutions,

the use of integral equations has, to a great extent, been limited to theoretical investigations of existence and uniqueness to solutions of problems of mathematical physics. However, the advent of high speed digital computers made it possible to implement discretisation procedures arithmetically and so enabled numerical solutions to be readily achieved.

Fredholm integral equations follow from the representation of harmonic potentials by single-layer or double-layer potentials and set up the foundations of the so-called Indirect Boundary Element Method. Vector integral equations analogous to the Fredholm integral equations of potential theory were introduced by Kupradze [12] in the context of the theory of elasticity.

Integral equations can alternatively be formulated through the application of Green's third identity [13], which represents a harmonic function as the superposition of a single-layer and a double-layer potentials. Taking the field point to the boundary, an integral equation relating only boundary values and normal derivatives of the harmonic function is obtained. Its counterpart in elasticity is Somigliana's identity [14], and their use gave rise to the Direct Boundary Element Method.

More recently, it was demonstrated that the same integral relationships can be obtained through weighted residual considerations [2]. In this way, it became easier to relate and combine the Boundary Element Method with other numerical techniques, such as the Finite Element Method, as well as to extend it for the analysis of problems governed by more complex partial differential equations, including non-linearities.

Although integral equations have been extensively employed to formulate boundary-value problems of potential theory, analytical

solutions to such equations are limited to very simple geometries, by using the Green's function for the geometry which satisfies the prescribed boundary conditions of the problem [15], [16], [17]. The Green's function method of solving boundary-value problems is most directly applicable to elliptic partial differential equations. In fact, the concept of a Green's function grew out of a detailed study of such boundary-value problems, but the method can also be extended to solve parabolic and hyperbolic partial differential equations. For general problems with complex geometry and boundary conditions, however, it may be assumed that no exact Green's function, or any other analytical treatment, is available.

In 1963, Jaswon [18] and Symm [19] presented a numerical technique to solve Fredholm boundary integral equations. The technique consists of discretising the boundary into a series of small segments (elements), assuming that the source density remains constant within each segment. By using the method of collocation, the discretised equation is applied to a number of particular points (nodes) in each element, and the influence coefficients computed approximately using Simpson's rule. Exception is made for the singular coefficients resulting from the self-influence of each element, which are computed either analytically (for Dirichlet problems) or by the summation of the off-diagonal coefficients plus the free term (for Neumann problems). This produces a system of linear algebraic equations which can be solved computationally by a direct method, e.g. Gauss elimination.

Applying such technique, they obtained accurate solutions for simple two-dimensional Neumann and Dirichlet problems. They also proposed a more general numerical formulation for solving Cauchy (mixed) boundary-value problems through the application of Green's third identity, which yields a boundary integral equation where boundary

values and normal derivatives of the physical variable play the role of the fictitious source densities. Results using this formulation are reported by Symm [19] and Jaswon and Ponter [20].

Hess and Smith [21] developed a parallel work for the solution of Neumann boundary-value problems, more specifically, the problem of potential flow about arbitrary bodies. Applying basically the same (indirect) technique, they computed the quantities of interest (potential and velocities) from the source density distribution, by using direct quadratures of the corresponding equations. They extended the method to analyse a variety of body shapes: two-dimensional, axisymmetric and fully three-dimensional results were presented. The influence coefficients were all computed analytically for the two- and three-dimensional cases although in the latter, in order to improve the computer efficiency, multipole expansions were employed to calculate the influence of elements located far from the actual node and the system of equations was solved iteratively by the Gauss-Seidel method. For axisymmetric problems, the influence coefficients were computed numerically using Simpson's rule but the number of sub-elements was scaled in such a way that the farther the element lies from the actual node, the fewer the number of sub-elements used in the calculation. The singular (self-influence) coefficients were computed analytically, by means of series expansions.

Harrington et al. [22] applied the technique to solve some two-dimensional electrical engineering problems with the more general impedance boundary condition, which is of the Robin type, i.e. it prescribes a linear relation between the potential and its normal derivative. They also proposed a piecewise linear variation for the source density. Mautz and Harrington [23] solved axisymmetric electrical engineering problems with Dirichlet boundary conditions, again employing

the indirect formulation and assuming the source density to remain constant within each element. Some of their numerical considerations were later discussed by Jaswon and Symm [1].

In 1970, Rizzo and Shippy [24] applied the direct formulation of the Boundary Element Method in conjunction with Laplace transforms to solve problems of transient heat conduction, governed by the diffusion equation. Assuming that all pertinent functions possess Laplace transforms, a boundary integral equation is derived and solved in the transform space for a sequence of real, positive values of the transform parameter. A numerical transform inversion procedure is then employed to compute the physical variables, in the real space. Using this approach, the time dependence of the problem is temporarily removed and an elliptic partial differential equation solved rather than the original parabolic one.

Butterfield and Tomlin [25], [26] extended the method for the analysis of zoned orthotropic media such as occurring in geotechnical engineering. The variables located at the interface between adjoining zones were assumed to satisfy compatibility conditions and the final system of equations obtained was banded. They solved steady and transient two-dimensional potential problems using the indirect formulation. Transient solutions were generated by distributing instantaneous sources over the problem region at zero time to reproduce the initial conditions and continuous sources over the region boundaries and interfaces, satisfying prescribed boundary and interface conditions.

Chang et al. [27] employed time-dependent fundamental solutions in the context of the direct Boundary Element Method to solve two-dimensional problems of heat conduction in isotropic and anisotropic media. The discretisation of the boundary integral equation was carried out using space and time piecewise constant values for the

variables. A similar approach was discussed by Shaw [28] for the solution of three-dimensional problems but emphasis was given on the analytical rather than numerical aspects of the method. This formulation was later extended by Wrobel and Brebbia [29] in order to allow higher order space and time interpolation functions to be included, thus making possible the analysis of more practical problems. They also derived a numerical procedure to solve transient axisymmetric problems [30] where the complexity of the fundamental solution requires the introduction of series expansions in order to enable the time integrals in the boundary integral equation to be carried out analytically.

Another alternative integral approach for the solution of transient problems is the coupled Boundary Element-Finite Difference Method proposed by Brebbia and Walker [3]. In this formulation, the time derivative is approximated in a finite difference form and a step-by-step finite difference-type procedure employed to advance the solution in time.

Problems of incompressible viscous fluid motion are governed by the Navier-Stokes equations, together with the continuity equation. The prevailing methods of solution of these equations are based on their formulation as a system of partial differential equations in terms of velocity and pressure, stream function and vorticity, or stream function alone [91]. With each of these systems, it has been necessary to compute the value of the dependent variables for the entire flowfield. Besides that, there is a difficulty associated with problems involving the flow past the exterior of a finite body, namely the fact that the flow region is infinite in extent and boundary conditions imposed at infinity need to be satisfied.

An alternative approach was proposed by Lighthill [31] employing

vorticity and velocity as the dependent variables. In this way, it is possible to separate the set of equations into a kinetic part which deals with the change of the vorticity field with time and a kinematic part which relates the velocity field ($\underset{\sim}{v}$) at any instant of time to the vorticity field ($\underset{\sim}{w}$) at that instant. The advantages of such approach have already been noticed and several formulations employing it in conjunction with the Finite Difference Method and the Finite Element Method have appeared in the literature [32],[33], [34], [35]. The usual procedure is to recast the kinematic part of the problem into an integral equation for $\underset{\sim}{v}$ in terms of $\underset{\sim}{w}$. For external flows, this equation is readily recognised as the Biot-Savart law of induced velocities [31], [36]. An extension of this equation for internal flows, taking into account the velocity boundary conditions at the solid boundaries, was derived by Wu and Thompson [33]. An immediate consequence of the above feature is that only the vorticity distribution in the viscous region of the flow contributes to the calculation of the velocity anywhere in the flow. Since this viscous region is generally embedded in a much larger, inviscid region, a great reduction in the size of the domain involved in the actual computation is achieved. Moreover, for external flow problems, the imposed boundary conditions at infinity are implicitly contained in the integral equation, thus the necessity of truncating the infinite region at a finite distance is avoided.

For a fluid in contact with a solid in motion, the no-slip condition provides a mechanism for the generation (or depletion) of vorticity at the solid surface. In the case where the fluid is initially at rest, the (irrotational) flow set up by the motion of the solid has a non-zero tangential velocity relative to the solid. A discontinuity in tangential velocity therefore results, at t=0, due to the no-slip condition, representing a sheet of vorticity at the

boundary [32], [36], [37]. For t>0, the vorticity, which is concentrated at the boundary at t=0, spreads into the interior of the fluid domain by diffusion and, once there, is carried away by both convection and diffusion. This process of transport of vorticity constitutes the kinetic part of the problem, and is governed by the vorticity transport equation.

Previous works employing the vorticity-velocity formulation kept the vorticity transport equation in the differential form, and advanced the vorticity distribution in time using finite difference [32], [33], [34] or finite element [35] schemes. However, some difficulties related to the satisfaction of boundary conditions at solid boundaries still remained, as pointed out by Wu [37].

As for the kinematic part, this differential equation can also be recast into an integral equation, and formulations using both the kinematic and kinetic parts of the problem in integral form have recently been proposed by Brebbia and Wrobel [38] and Wu and Rizk [92]. For steady state problems, the vorticity transport equation is reduced to an (elliptic) Poisson equation and a specific formulation for its solution was proposed by Wu and Wahbah [93].

The present work starts by showing how a problem governed by Laplace's equation (with prescribed boundary conditions) can be recast into an integral equation which, through a limiting process, produces a boundary integral equation relating only boundary values. Both the indirect and the direct formulations of the Boundary Element Method are discussed. The weighted residual technique is then employed to formulate (direct) integral equations equivalent to the diffusion equation with prescribed boundary and initial conditions.

Numerical formulations for the solution of the boundary integral equation equivalent to Laplace's equation are presented in chapter 3.

It is shown how several features such as special boundary conditions, internal sources, non-homogeneity, orthotropy and anisotropy can be included into the formulation. Two-dimensional, axisymmetric and fully three-dimensional problems are treated and results of some applications presented.

Chapter 4 studies numerical solutions to the time-dependent boundary integral equation equivalent to the diffusion equation, obtained through the use of time-dependent fundamental solutions. Two different time-marching schemes are considered, both adopting a time-stepping technique which allows the time integrals in the boundary integral equation to be carried out analytically, for time interpolation functions of any order. The remaining space integrals are computed numerically, apart from the singular ones. Again, two-dimensional and axisymmetric problems are treated, being extension to three dimensions straightforward. Comparison of numerical results obtained with the different time-marching schemes is effected, as well as with several finite element results.

Boundary element formulations for the solution of the Navier-Stokes equations are presented in chapter 5. Both steady and transient problems are considered, and computational procedures discussed in detail. Computer programs incorporating these procedures are currently under way.

A brief description of the computer programs developed throughout this work, for the solution of the Laplace and diffusion equations, is presented in chapter 6. All programs were written in FORTRAN, in the IBM 360/195 computer of the Rutherford Laboratory. Finally, conclusions and suggestions for further research work are discussed in chapter 7.

2. BOUNDARY INTEGRAL EQUATIONS

In this chapter, it is shown how a problem governed by a partial differential equation with prescribed boundary conditions can be recast into an integral equation which, through a limiting process, produces a boundary integral equation relating only boundary values. This transformation, together with the numerical solution of the boundary integral equation, constitutes the basis of the Boundary Element Method.

In order to clarify the ideas, we start with the simplest partial differential equation, namely Laplace's equation. The relation of the method with classical potential theory is outlined through its indirect formulation, which employs fictitious source density distributions along the boundary. All regions referred to in this formulation are assumed to be regular in the sense defined by Kellogg [13] and all surfaces to be Liapunov surfaces [39], which are smooth surfaces possessing a tangent plane and normal, but not necessarily a curvature, at each point.

Then the direct formulation of the Boundary Element Method is presented. For Laplace's equation, it follows from an application of Green's third identity. More generally, all surfaces in this formulation are assumed to be Kellogg regular surfaces [13], which may have corners or edges provided they are not too sharp. Alternatively, it is demonstrated that the same integral relationships can be derived through weighted residual considerations.

Next, the weighted residual technique is employed to formulate integral equations equivalent to the diffusion equation with prescribed boundary and initial conditions. The presence of specified initial conditions gives rise to an integral over the domain but since all values in this integral are known, the problem is still a boundary problem. These integral equations are derived in conjunction with all three previously discussed approaches, i.e. the Laplace transform, the

coupled Boundary Element - Finite Difference and the time-dependent fundamental solution methods.

2.1 Elements of Potential Theory

Some basic elements of classical potential theory will now be briefly reviewed. Concepts that are of importance to the present work are introduced and on doing so we follow Cruse [40] and Jaswon and Symm [1]. For a more formal mathematical treatment, including all necessary and relevant rigorous proofs, see for instance Kellogg [13], Courant and Hilbert [41], Sternberg and Smith [42].

If a particle of unit mass, subjected only to the force of a specific field F, is moved from a point s to a point p in space, the work done on the particle by the field during the motion is given by,

$$W = \int_s^p \underset{\sim}{F}\, d\underset{\sim}{r} \qquad (2.1.1)$$

where $\underset{\sim}{F}$ is the force field vector and $d\underset{\sim}{r}$ is the differential motion of the particle on the path from s to p.

The work is in general dependent not merely on the position of the points, but also on the path of the particle between them. If the field is such that the work is independent of the path, i.e. it has the same value when taken over any two paths connecting s and p which can be continuously deformed one into the other, the field is called conservative.

Considering the point s as fixed and p as variable, the integral (2.1.1) represents a function of p alone. This scalar function

$$u(p) = \int_s^p \underset{\sim}{F}\, d\underset{\sim}{r} \qquad (2.1.2)$$

is called the potential of the field F.

When the field is gravitational, the potential is a Newtonian one. The Newtonian potential generated by two particles of masses m_1 and m_2, located at points s (fixed) and p (variable), respectively, is of the form

$$u(p) = \int_s^p G\, m_1\, m_2\, \underset{\sim}{\nabla}\left(\frac{1}{r}\right)\, d\underset{\sim}{r} = G\, m_1\, m_2\, \frac{1}{r} + \text{constant} \qquad (2.1.3)$$

where G is the gravitational constant and r is the distance between s and p, that is,

$$r(p,s) = |p-s| = \{[x_1(p) - x_1(s)]^2 + [x_2(p) - x_2(s)]^2 + [x_3(p) - x_3(s)]^2\}^{\frac{1}{2}} \qquad (2.1.4)$$

Attractional forces of the same character as those occurring in gravitation also act between electric charges, and between the poles of magnets. For generality, we will then refer to sources rather than masses throughout this work and state that a unit simple source, located at a source point s in space, generates at a field point p the Newtonian potential

$$\frac{1}{r(p,s)} \qquad (2.1.5)$$

This potential is a continuous function of p, differentiable to all orders, everywhere except at the source point s.

Similarly, a discrete distribution of simple sources of intensities $\sigma_1, \sigma_2, \ldots, \sigma_N$ located at points $s_1, s_2, \ldots, s_N$, respectively, generates the Newtonian potential

$$u(p) = \sum_{n=1}^{N} \sigma(s_n)\, \frac{1}{r(p,s_n)} \qquad (2.1.6)$$

at point p. Again, this potential is a continuous function of p, together with its derivatives of all orders, everywhere except when p is coincident with one of the source points s_n.

Now consider a continuous distribution of simple sources of volume density ρ throughout the region Ω. The potential associated with this force field is a volume potential, obtained by the integration

$$u(p) = \int_{\Omega} \rho(s) \frac{1}{r(p,s)} \, d\Omega(s) \tag{2.1.7}$$

This volume potential is a continuous function of p, differentiable to all orders, at all points of free space, that is, points located outside the attracting region Ω. When the field point p lies inside the region Ω, the integrand in (2.1.7) contains a singularity. However, if the density ρ is bounded throughout Ω, the potential u(p) exists at all points $p \in \Omega$ and is everywhere continuous and differentiable throughout space [13]. This amounts to saying that the derivatives of the first order of u may be obtained by differentiating under the sign of integration as,

$$\frac{\partial u(p)}{\partial x_i(p)} = \int_{\Omega} \rho(s) \frac{\partial}{\partial x_i(p)} \left(\frac{1}{r(p,s)}\right) d\Omega(s) \quad i = 1,2,3 \tag{2.1.8}$$

The same is not valid for the derivatives of the second order. In fact, the mere continuity of the density does not suffice to ensure the existence of these derivatives. Therefore, it is necessary to impose that the density $\rho(s)$ satisfies a Hölder condition [13], [41] at p,

$$|\rho(s) - \rho(p)| \leq A \, r(p,s)^{\alpha} \tag{2.1.9}$$

where A and α are positive constants, $\alpha \leq 1$.

In order to investigate the partial derivatives of u of the second order, we can start by integrating (2.1.8) by parts, obtaining

$$\frac{\partial u(p)}{\partial x_i(p)} = - \int_{\Gamma} \rho(S) \frac{1}{r(p,S)} \, x_{i,n}(S) \, d\Gamma(S) + \int_{\Omega} \frac{\partial \rho(s)}{\partial x_i(s)} \frac{1}{r(p,s)} \, d\Omega(s) \tag{2.1.10}$$

through the application of the divergence theorem, and noting that

$$\frac{\partial}{\partial x_i(p)}\left(\frac{1}{r(p,s)}\right) = -\frac{\partial}{\partial x_i(s)}\left(\frac{1}{r(p,s)}\right) \tag{2.1.11}$$

Making use of the identity,

$$\frac{\partial}{\partial x_i(s)}\rho(s) = \frac{\partial}{\partial x_i(s)}\left[\rho(s) - \rho(p)\right] \tag{2.1.12}$$

taking the second derivative of (2.1.10) yields the relation

$$\frac{\partial^2 u(p)}{\partial x_i^2(p)} = -\int_\Gamma \rho(S)\,\frac{\partial}{\partial x_i(p)}\left(\frac{1}{r(p,S)}\right) x_{i,n}(S)\,d\Gamma(S) + \int_\Omega \frac{\partial}{\partial x_i(s)}\left[\rho(s) - \rho(p)\right]\frac{\partial}{\partial x_i(p)}\left(\frac{1}{r(p,s)}\right) d\Omega(s) \tag{2.1.13}$$

The second integral in (2.1.13) may be integrated by parts with respect to $x_i(s)$ and subjected to the divergence theorem once more to obtain

$$\frac{\partial^2 u(p)}{\partial x_i^2(p)} = -\int_\Gamma \rho(S)\,\frac{\partial}{\partial x_i(p)}\left(\frac{1}{r(p,S)}\right) x_{i,n}(S)\,d\Gamma(S) + \int_\Gamma \left[\rho(S) - \rho(p)\right]\frac{\partial}{\partial x_i(p)}\left(\frac{1}{r(p,S)}\right) x_{i,n}(S)\,d\Gamma(S) + \int_\Omega \left[\rho(s) - \rho(p)\right]\frac{\partial^2}{\partial x_i^2(p)}\left(\frac{1}{r(p,s)}\right) d\Omega(s) \tag{2.1.14}$$

which reduces to,

$$\frac{\partial^2 u(p)}{\partial x_i^2(p)} = \rho(p)\int_\Gamma \frac{\partial}{\partial x_i(S)}\left(\frac{1}{r(p,S)}\right) x_{i,n}(S)\,d\Gamma(S) + \int_\Omega \left[\rho(s) - \rho(p)\right]\frac{\partial^2}{\partial x_i^2(p)}\left(\frac{1}{r(p,s)}\right) d\Omega(s) \tag{2.1.15}$$

Thus, adding up the three second order derivatives (equation (2.1.15) for i = 1, 2, 3) yields the Laplacian of u,

$$\nabla^2 u(p) = \rho(p)\int_\Gamma \frac{\partial}{\partial n(S)}\left(\frac{1}{r(p,S)}\right) d\Gamma(S) + \int_\Omega \left[\rho(s) - \rho(p)\right]\nabla^2\left(\frac{1}{r(p,s)}\right) d\Omega(s) \tag{2.1.16}$$

In the second integral in the above equation, the volume may be divided into two parts: one is a small sphere of radius ε surrounding the point p, which is called Ω_ε; the other is the entirety of the remaining volume, denoted $\Omega-\Omega_\varepsilon$. As p is exterior to $\Omega-\Omega_\varepsilon$ and $1/r$ is a harmonic function (as will be demonstrated later), the Laplacian term equals zero throughout this region. The integral over Ω_ε also approaches zero with ε since $\rho(s)$ satisfies a Hölder condition at p. Thus there remains the surface integral to be evaluated.

Again, consider a small sphere of radius ε around p, with surface Γ_ε. Integrating (2.1.16) around this surface gives,

$$\int_{\Gamma_\varepsilon} \frac{\partial}{\partial n(S)} \left(\frac{1}{r(p,S)}\right) d\Gamma_\varepsilon(S) = -\frac{1}{\varepsilon^2} \int_{\Gamma_\varepsilon} d\Gamma_\varepsilon = -4\pi \qquad (2.1.17)$$

Since there are no sources in the region between Γ_ε and Γ the Newtonian field is solenoidal, i.e. there is no flux out of this region. Numerically, we can write

$$\int_{\Gamma_\varepsilon} \frac{\partial}{\partial n} \left(\frac{1}{r}\right) d\Gamma_\varepsilon + \int_{\Gamma} \frac{\partial}{\partial n} \left(\frac{1}{r}\right) d\Gamma = 0 \qquad (2.1.18)$$

where the normal is outward on Γ, but inward on Γ_ε. Combining equations (2.1.17) and (2.1.18) and noticing the reversal of the normal on Γ_ε gives

$$\int_{\Gamma} \frac{\partial}{\partial n(S)} \left(\frac{1}{r(p,S)}\right) d\Gamma(S) = -4\pi \qquad (2.1.19)$$

Inserting (2.1.19) into (2.1.16) produces the expected result,

$$\nabla^2 u(p) = -4\pi\rho(p) \qquad (2.1.20)$$

Other Newtonian potentials can be generated, including surface potentials. In particular, two of them are of importance to what follows and will be defined next. The first is the potential associated with a continuous distribution of simple sources extending over

a surface Γ and of surface density σ, which is of the form,

$$u(p) = \int_{\Gamma} \sigma(S) \frac{1}{r(p,S)} d\Gamma(S) \qquad (2.1.21)$$

and is called a single-layer potential.

Let us now consider two surfaces $\Gamma(S)$ and $\Gamma(S_1)$ separated by a small distance $h(S,S_1)$, carrying distributions of attraction of magnitude $\sigma(S)$ and $\sigma(S_1)$, respectively. These distributions are such that, for corresponding area elements,

$$\sigma(S)\, d\Gamma(S) = -\sigma(S_1)\, d\Gamma(S_1) \qquad (2.1.22)$$

The potential due to the two surfaces is then,

$$u(p) = \int_{\Gamma} \sigma(S) \frac{1}{r(p,S)} d\Gamma(S) + \int_{\Gamma_1} \sigma(S_1) \frac{1}{r(p,S_1)} d\Gamma(S_1)$$

$$= \int_{\Gamma} \sigma(S)\, h(S,S_1) \left[\frac{1}{h(S,S_1)} \left(\frac{1}{r(p,S)} - \frac{1}{r(p,S_1)}\right)\right] d\Gamma(S) \qquad (2.1.23)$$

If we let $h \to 0$ and $\sigma \to \infty$, so that $\sigma h \to \mu$ everywhere uniformly on Γ and also compute the limit of the term in brackets,

$$\lim_{h(S,S_1)\to 0} \left[\frac{1}{h(S,S_1)} \left(\frac{1}{r(p,S)} - \frac{1}{r(p,S_1)}\right)\right] = \frac{\partial}{\partial n(S)} \left(\frac{1}{r(p,S)}\right) \qquad (2.1.24)$$

the potential

$$u(p) = \int_{\Gamma} \mu(S) \frac{\partial}{\partial n(S)} \left(\frac{1}{r(p,S)}\right) d\Gamma(S) \qquad (2.1.25)$$

obtained as the limit of the potential of two single-layers of opposite signs that approach coincidence, is called a double-layer potential. The function μ is the surface density, or moment, of the double-layer.

The potentials in equations (2.1.21) and (2.1.25) are continuous functions of p, differentiable to all orders, everywhere except at $p \in \Gamma$, where the integrands in these equations contain singularities. In order to investigate the behaviour of these surface potentials near the singularity, the boundary Γ is broken into two surfaces: one is a

small disc tangent to the surface at a point P, noting that it was assumed that the surface possesses a unique tangent plane at any point; the other is the entirety of the remaining surface and contains no singularity, as $P \neq S$.

According to figure 2.1.1, the field point p is located along the normal to Γ that passes through the surface point P. The disc centred at P has a radius ε and is denoted Γ_ε; the remainder of the surface is denoted $\Gamma-\Gamma_\varepsilon$. The point p is located at a distance λ from P such that $|\lambda|<<\varepsilon$, and such that $\lambda<0$ if p is outside Ω and $\lambda>0$ if p is inside Ω. The integrals in (2.1.21) and (2.1.25) can then be separated as,

$$u(p) = \lim_{\varepsilon\to 0} \left\{ \int_{\Gamma-\Gamma_\varepsilon} \sigma(S)\, \frac{1}{r(p,S)}\, d\Gamma(S) + \int_{\Gamma_\varepsilon} \sigma(S)\, \frac{1}{r(p,S)}\, d\Gamma(S) \right\} \tag{2.1.26}$$

$$u(p) = \lim_{\varepsilon\to 0} \left\{ \int_{\Gamma-\Gamma_\varepsilon} \mu(S)\, \frac{\partial}{\partial n(S)}\left(\frac{1}{r(p,S)}\right)\, d\Gamma(S) + \int_{\Gamma_\varepsilon} \mu(S)\, \frac{\partial}{\partial n(S)}\left(\frac{1}{r(p,S)}\right)\, d\Gamma(S) \right\} \tag{2.1.27}$$

It is clear that the integrals over $\Gamma-\Gamma_\varepsilon$ are continuous as the field point p passes through the surface and will again produce the integrals in (2.1.21) and (2.1.25) when the limit is taken.

The integral over Γ_ε in (2.1.26) contains a weak singularity and is also continuous as the field point passes through the surface, provided the density σ is bounded at all points along Γ. This statement does not hold for the second integral in (2.1.27) which, because of the normal derivative term, contains a singularity of higher order. This integral can be written as,

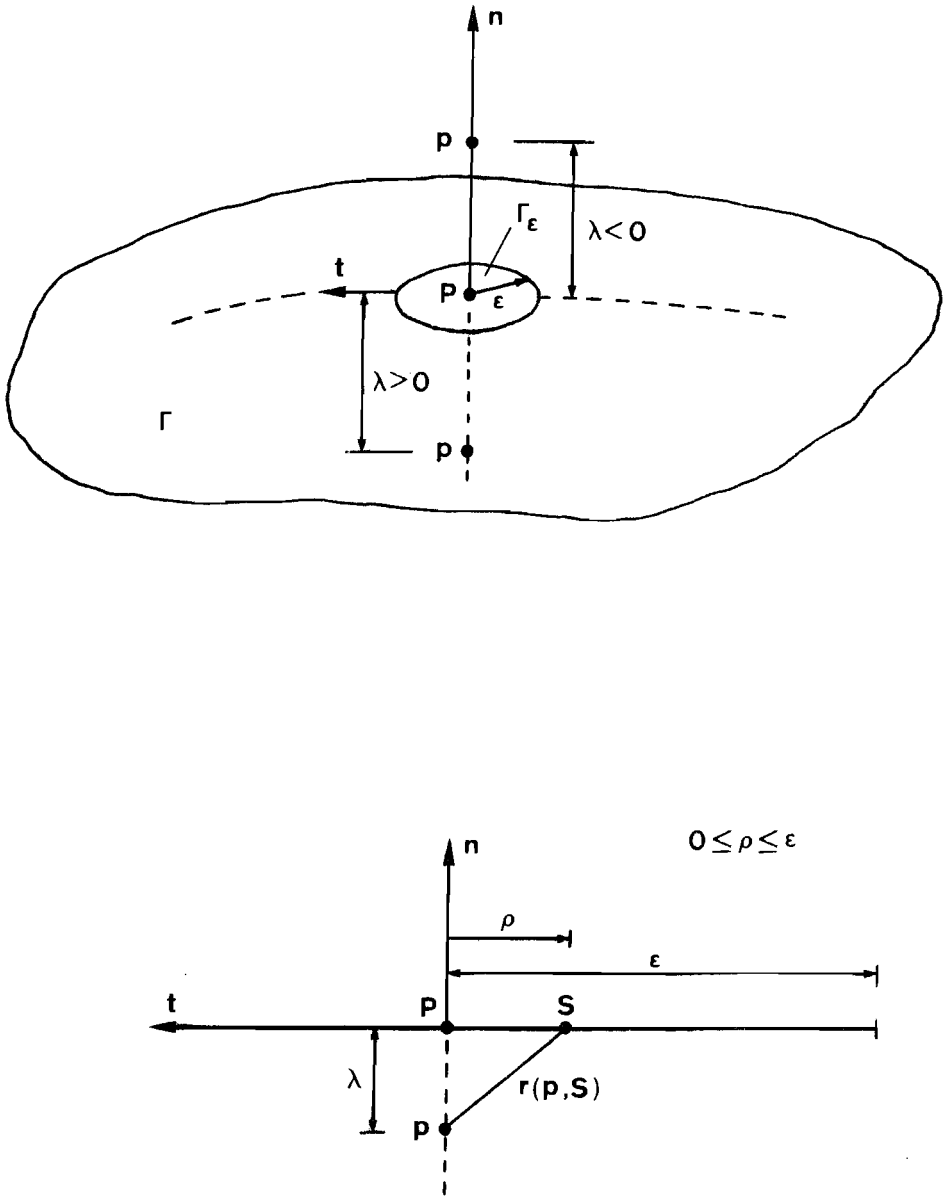

Figure 2.1.1 - Discontinuity of three-dimensional double-layer potential

$$\int_{\Gamma_\varepsilon} \mu(S) \frac{\partial}{\partial n(S)} \left(\frac{1}{r(p,S)}\right) d\Gamma(S) = \int_{\Gamma_\varepsilon} [\mu(S) - \mu(P)] \frac{\partial}{\partial n(S)} \left(\frac{1}{r(p,S)}\right) d\Gamma(S)$$

$$+ \mu(P) \int_{\Gamma_\varepsilon} \frac{\partial}{\partial n(S)} \left(\frac{1}{r(p,S)}\right) d\Gamma(S) \qquad (2.1.28)$$

This means that the potential of a surface whose density is continuous at P is the sum of the potentials of a surface whose density vanishes at P and of a surface with constant density, equal to that at P. If the density $\mu(S)$ satisfies a Hölder condition at P, then the first integral on the right-hand side of (2.1.28) is continuous as the field point passes through the surface. The second integral becomes (refer to figure 2.1.1 for notation),

$$\int_{\Gamma_\varepsilon} \frac{\partial}{\partial n} \left(\frac{1}{r}\right) d\Gamma = - \int_0^\varepsilon \frac{\lambda}{r^3} \, 2\pi\rho \, d\rho \qquad (2.1.29)$$

Since $\rho d\rho = r dr$ for a given $|\lambda| << \varepsilon$, an interchange of variables produces,

$$- \int_0^\varepsilon \frac{\lambda}{r^3} \, 2\pi\rho \, d\rho = 2\pi\lambda \int_{|\lambda|}^\varepsilon - \frac{dr}{r^2} = 2\pi \left[\frac{\lambda}{r}\right]_{|\lambda|}^\varepsilon = 2\pi \frac{\lambda}{\varepsilon} - 2\pi \, \mathrm{sgn}(\lambda) \qquad (2.1.30)$$

where the symbol 'sgn(λ)' takes the sign of λ.

Taking the limit as $\varepsilon \to 0$ (noting that $\lambda \to 0$ much quicker), (2.1.28) gives,

$$\lim_{\varepsilon \to 0} \left\{ \int_{\Gamma_\varepsilon} \mu(S) \frac{\partial}{\partial n(S)} \left(\frac{1}{r(p,S)}\right) d\Gamma(S) \right\} = - 2\pi \, \mathrm{sgn}(\lambda) \, \mu(P) \qquad (2.1.31)$$

Thus the limiting form of equation (2.1.25) as $p \to P$ from the inside can be written as

$$u^+(P) = - 2\pi\mu(P) + \int_\Gamma \mu(S) \frac{\partial}{\partial n(S)} \left(\frac{1}{r(P,S)}\right) d\Gamma(S) \qquad (2.1.32)$$

and from the outside as,

$$u^{-}(P) = 2\pi\mu(P) + \int_{\Gamma} \mu(S) \frac{\partial}{\partial n(S)} \left(\frac{1}{r(P,S)}\right) d\Gamma(S) \qquad (2.1.33)$$

The three-dimensional double-layer potential is then said to have a discontinuity or jump of $-4\pi\mu(P)$ as the point p passes from outside to inside the region, that is,

$$u^{+}(P) - u^{-}(P) = -4\pi\mu(P) \qquad (2.1.34)$$

All concepts presented thus far are also valid for two-dimensional problems, where the equivalent of the Newtonian potential is the logarithmic potential

$$\log \frac{1}{r(p,s)} \qquad (2.1.35)$$

in which r(p,s) is now,

$$r(p,s) = |p-s| = \{[x_1(p) - x_1(s)]^2 + [x_2(p) - x_2(s)]^2\}^{\frac{1}{2}} \qquad (2.1.36)$$

The logarithmic potential can be derived either by starting with two-dimensional force fields acting on a line source or by integrating the Newtonian potential for a line source at s [13], [41], [42].

The two-dimensional volume potential

$$u(p) = \int_{\Omega} \rho(s) \log \frac{1}{r(p,s)} d\Omega(s) \qquad (2.1.37)$$

satisfies Poisson's equation

$$\nabla^2 u(p) = -2\pi\rho(p) \qquad (2.1.38)$$

for every $p \in \Omega$ by an analogy to the Newtonian volume potential, noting that

$$\int_{\Gamma_\varepsilon} \frac{\partial}{\partial n(S)} \left(\log \frac{1}{r(p,S)}\right) d\Gamma_\varepsilon(S) = -\frac{1}{\varepsilon} \int_{\Gamma_\varepsilon} d\Gamma_\varepsilon = -2\pi \qquad (2.1.39)$$

where Γ_ε is now a curve in the plane region.

The single-layer potential for two-dimensional problems is given by,

$$u(p) = \int_{\Gamma} \sigma(S) \log \frac{1}{r(p,S)} \, d\Gamma(S) \qquad (2.1.40)$$

and, as in the three-dimensional case, is continuous as the field point passes through the surface, for a density σ which is bounded at all surface points.

The two-dimensional double-layer potential is of the form,

$$u(p) = \int_{\Gamma} \mu(S) \frac{\partial}{\partial n(S)} \left(\log \frac{1}{r(p,S)}\right) d\Gamma(S) \qquad (2.1.41)$$

and contains a discontinuity which can be investigated in a similar way as for the three-dimensional case.

As previously, the bounding curve Γ is divided into $\Gamma-\Gamma_\varepsilon$ and Γ_ε, the latter being a short, straight line centred at point P (figure 2.1.2), where it was assumed that the surface possesses a smooth contour. The point p is located along the normal to the surface that passes through P and the distance λ between the two points taken to be much less than 2ε, the length of Γ_ε.

Dividing the integral in (2.1.41) as was done in equation (2.1.28) and assuming that $\mu(S)$ satisfies a Hölder condition at P, the discontinuity is given by the term,

$$\lim_{\varepsilon \to 0} \left\{ \mu(P) \int_{\Gamma_\varepsilon} \frac{\partial}{\partial n(S)} \left(\log \frac{1}{r(p,S)}\right) d\Gamma(S) \right\} \qquad (2.1.42)$$

This integral contains a perfect differential since for θ defined as in figure 2.1.2 its integrand can be written as,

$$\frac{\partial}{\partial n} \left(\log \frac{1}{r}\right) d\Gamma = -\frac{\lambda}{r^2} \left(-\frac{\lambda}{\sin^2 \theta}\right) d\theta = d\theta \qquad (2.1.43)$$

Thus, evaluating the limit in (2.1.42) and noting that $|\lambda| << \varepsilon$ gives

$$\lim_{\varepsilon \to 0} \left\{ \mu(P) \int_{\Gamma_\varepsilon} \frac{\partial}{\partial n(S)} \left(\log \frac{1}{r(p,S)}\right) d\Gamma(S) \right\} = -\pi \, \mathrm{sgn}(\lambda) \, \mu(P) \qquad (2.1.44)$$

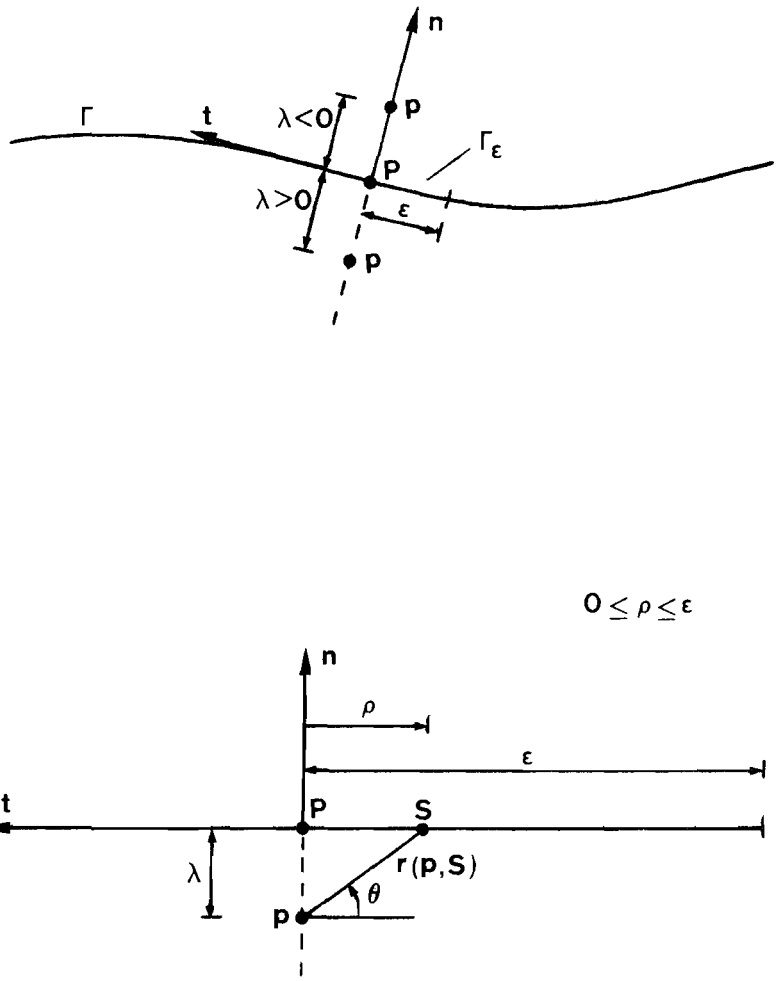

Figure 2.1.2 - Discontinuity of two-dimensional double-layer potential

The limiting form of equation (2.1.41) as the point p approaches P from the inside becomes

$$u^+(P) = -\pi\mu(P) + \int_\Gamma \mu(S) \frac{\partial}{\partial n(S)} \left(\log \frac{1}{r(P,S)}\right) d\Gamma(S) \qquad (2.1.45)$$

and from the outside is

$$u^-(P) = \pi\mu(P) + \int_\Gamma \mu(S) \frac{\partial}{\partial n(S)} \left(\log \frac{1}{r(P,S)}\right) d\Gamma(S) \qquad (2.1.46)$$

being the jump in the integral now,

$$u^+(P) - u^-(P) = -2\pi\mu(P) \qquad (2.1.47)$$

2.2 Indirect Formulation

In this section, we study solutions to Laplace's equation,

$$\nabla^2 u(s) = 0 \qquad s \in \Omega \qquad (2.2.1)$$

with boundary conditions of the Dirichlet type,

$$u(S) = \bar{u}(S) \qquad S \in \Gamma \qquad (2.2.2)$$

or of the Neumann type,

$$q(S) = \frac{\partial u(S)}{\partial n(S)} = \bar{q}(S) \qquad S \in \Gamma \qquad (2.2.3)$$

where n(S) is the unit outward normal to surface Γ at point S, $\bar{u}$ and $\bar{q}$ are prescribed values of the function and its normal derivative over the boundary Γ.

A function u is said to be harmonic within a domain Ω, bounded by a closed surface Γ, if it satisfies the following conditions:

a) u is continuous in $\Omega + \Gamma$

b) u is differentiable to at least the second order in Ω

c) u satisfies Laplace's equation in Ω

Any harmonic function can be represented by a potential distribution and conversely, every potential is a harmonic function [13], [42].

Thus, an effective method of formulating the boundary-value problems of potential theory is to represent the harmonic function by a single-

layer or a double-layer potential generated by continuous source distributions over Γ, provided these potentials satisfy the boundary conditions prescribed for u. This procedure leads to the formulation of integral equations which define the source densities concerned. These equations can be discretised and solved numerically, and values of u at internal points computed afterwards from the boundary data by using numerical quadratures as will be shown in the next chapter.

To obtain an integral equation for the solution of the Neumann problem, we assume that the unknown function u may be expressed solely as a single-layer potential with unknown density σ,

$$u(p) = \int_{\Gamma} \sigma(S)\ u^*(p,S)\ d\Gamma(S) \qquad (2.2.4)$$

The function $u^*(p,S)$ is the Newtonian potential (2.1.5) for three-dimensional problems or the logarithmic potential (2.1.35) for two-dimensional problems, and is called the fundamental solution to Laplace's equation.

Taking the derivative of (2.2.4) in the direction of the outward normal to Γ as p is taken to P yields the boundary relation,

$$q(P) = -\alpha\pi\sigma(P) + \int_{\Gamma} \sigma(S)\ \frac{\partial u^*(P,S)}{\partial n(P)}\ d\Gamma(S) \qquad (2.2.5)$$

where $\alpha = 1$ for two-dimensional problems and $\alpha = 2$ for three-dimensional problems.

This constitutes a Fredholm equation of the second kind for σ in terms of q, as the unknown appears both outside and inside the integral. After solving the system of corresponding algebraic equations, values of u at any interior or boundary point can be calculated by using (2.2.4), since $u^*(p,S)$ is continuous as $p \to P$.

It is important to note that (2.2.5) has a solution only if the Gauss condition [13]

$$\int_\Gamma q(P)\, d\Gamma(P) = 0 \qquad (2.2.6)$$

holds, and that this solution is unique only to within an arbitrary additive constant. However, a unique solution of equation (2.2.5) can be obtained by imposing some extra 'normalising' condition [1]. This will be discussed in detail in the next chapter.

The above method was extensively employed by Hess and Smith [21] to solve a series of fluid flow problems, including flow past hydrofoils, cascades and lifting aerofoils. Numerical results can also be found in [1], [19], [20].

To obtain an integral equation for the solution of the Dirichlet problem, the classical approach is to assume that the unknown function u may be expressed solely as a double-layer potential with unknown density μ,

$$u(p) = \int_\Gamma \mu(S)\, q^*(p,S)\, d\Gamma(S) \qquad (2.2.7)$$

where

$$q^*(p,S) = \frac{\partial u^*(p,S)}{\partial n(S)} \qquad (2.2.8)$$

Taking into account the jump in the double-layer potential, the limit of (2.2.7) may be taken as $p \to P$,

$$u(P) = -\alpha\pi\mu(P) + \int_\Gamma \mu(S)\, q^*(P,S)\, d\Gamma(S) \qquad (2.2.9)$$

As u(P) is known for the Dirichlet problem, the source density μ is the only unknown. Again, (2.2.9) constitutes a Fredholm equation of the second kind which, after being solved, enables us to compute u(p) everywhere in Ω using (2.2.7). Numerical results using this formulation were obtained, for instance, by Kantorowich and Krylov [43].

Since $u^*(P,S) = u^*(S,P)$, the integral equation (2.2.9) is said to contain the adjoint kernel of equation (2.2.5). The kernel is the

function of (P,S) multiplying the density under the integral sign in the integral equations. For scalar kernels, the adjoint is obtained by interchanging P and S.

An alternative approach to obtain an integral equation for the solution of the Dirichlet problem is to assume that the unknown function u may be expressed solely as a single-layer potential with unknown density σ,

$$u(p) = \int_\Gamma \sigma(S)\ u^*(p,S)\ d\Gamma(S) \qquad (2.2.10)$$

Since the kernel in this equation is continuous as p passes through the surface, the limit of (2.2.10) as $p \to P$ gives

$$u(P) = \int_\Gamma \sigma(S)\ u^*(P,S)\ d\Gamma(S) \qquad (2.2.11)$$

and, as u(P) is known, the source density σ is the only unknown in the equation.

Equation (2.2.11) is a Fredholm equation of the first kind, as the unknown appears only inside the integral. For many Dirichlet problems, formulations using such equations have proven to be more illuminating physically and more convenient mathematically then using equations of the second kind.

Regarding the numerical solution of the system of corresponding algebraic equations, obtained by discretisation, the presence of the term outside the integral, for equations of the second kind, ensures that the system matrix will always be diagonally dominant. An equation of the first kind with a non-singular kernel can be very difficult to solve, being essentially ill-conditioned [44]; however, in the present case, the singularity of the kernel ensures diagonal dominance in the system matrix and the problem is in general well conditioned.

For numerical solutions of equation (2.2.11), see for instance [1], [19], [20], [22], [23].

2.3 Direct Formulation

A conceptual disadvantage of single-layer and double-layer potentials is the introduction of formal source densities which usually bear no physical relation to the problem. This can be overcome by using Green's third identity, which leads to the direct formulation of the Boundary Element Method, where values of the function and its normal derivative over Γ play the role of the source densities in generating u throughout Ω.

First, let us introduce the Dirac delta function $\delta(p,s)$, which has the following properties,

$$\delta(p,s) = 0 \qquad \text{for } p \neq s \tag{2.3.1}$$

$$\delta(p,s) = \infty \qquad \text{for } p = s \tag{2.3.2}$$

$$\int_{\Omega} u(s)\ \delta(p,s)\ d\Omega(s) = u(p) \tag{2.3.3}$$

Now, let ϕ and Ψ be two continuous functions with continuous first and second derivatives in the region Ω. Green's theorem in its second form states that

$$\int_{\Omega} (\phi\nabla^2\Psi - \Psi\nabla^2\phi)\ d\Omega = \int_{\Gamma} (\phi\frac{\partial\Psi}{\partial n} - \Psi\frac{\partial\phi}{\partial n})\ d\Gamma \tag{2.3.4}$$

If ϕ and Ψ are harmonic functions in Ω then $\nabla^2\phi = 0$ and $\nabla^2\Psi = 0$, and (2.3.4) yields Green's reciprocal identity,

$$\int_{\Gamma} (\phi\frac{\partial\Psi}{\partial n} - \Psi\frac{\partial\phi}{\partial n})\ d\Gamma = 0 \tag{2.3.5}$$

Similarly, if ϕ is a harmonic function u in Ω and Ψ is the fundamental solution u^* to Laplace's equation, equation (2.3.4) becomes Green's third identity,

$$2\alpha\pi u(p) + \int_{\Gamma} u(S)\ q^*(p,S)\ d\Gamma(S) = \int_{\Gamma} q(S)\ u^*(p,S)\ d\Gamma(S) \tag{2.3.6}$$

This relation is derived by noting that inserting (2.1.7) into (2.1.20) (or (2.1.37) into (2.1.38)) yields the equation,

$$\nabla^2 \int_\Omega \rho(s)\, u^*(p,s)\, d\Omega(s) = -2\alpha\pi\rho(p) \tag{2.3.7}$$

Comparing equations (2.3.3) and (2.3.7), we conclude that the fundamental solution u^* satisfies the relation

$$\nabla^2 u^*(p,s) = -2\alpha\pi\delta(p,s) \tag{2.3.8}$$

and so,

$$\int_\Omega \phi\nabla^2\Psi d\Omega = -2\alpha\pi \int_\Omega u(s)\, \delta(p,s)\, d\Omega(s) = -2\alpha\pi u(p) \tag{2.3.9}$$

Equation (2.3.6) states that a harmonic function may be expressed as the superposition of a single-layer potential with density $q/2\alpha\pi$ and a double layer potential with density $-u/2\alpha\pi$. Moreover, examining each of the terms in (2.3.6) as the interior point p is taken to the boundary, we recall that the single-layer potential remains continuous as $p\to P$ but the double-layer potential jumps by an amount of $-\alpha\pi u(p)$, thus yielding the boundary formula,

$$\alpha\pi u(P) + \int_\Gamma u(S)\, q^*(P,S)\, d\Gamma(S) = \int_\Gamma q(S)\, u^*(P,S)\, d\Gamma(S) \tag{2.3.10}$$

This equation provides a functional constraint between u and q over Γ which ensures their compatibility as boundary data. If the solution of a Neumann problem is required, the right-hand side of (2.3.10) is known, and we have to solve a Fredholm equation of the second kind for the unknown boundary values of the function u. If the solution of a Dirichlet problem is required, values of u are prescribed throughout Γ and we obtain a Fredholm equation of the first kind for the unknown boundary values of the normal derivative q. Solution of Cauchy (mixed) boundary-value problems leads to a mixed integral equation for the unknown boundary data.

Note that if the point p crosses the surface Γ into the infinite domain exterior to Ω, the double-layer potential again jumps by $-\alpha\pi u(p)$, so generating the identity,

$$\int_\Gamma u(S)\ q^*(p,S)\ d\Gamma(S) - \int_\Gamma q(S)\ u^*(p,S)\ d\Gamma(S) = 0 \qquad (2.3.11)$$

This can be viewed as a particular case of (2.3.5), since both functions u and u^* are harmonic outside the region Ω.

2.4 Weighted Residual Formulation

The direct Boundary Element Method can alternatively be formulated through weighted residual considerations [2]. The advantage of using a weighted residual technique is its generality: it permits a straightforward extension of the method to solve more complex partial differential equations; since it can also be employed to formulate other numerical techniques such as the Finite Element Method, it becomes easier to relate and combine the Boundary Element Method with more classical numerical methods.

As we are seeking an approximate solution to the problem governed by equation (2.2.1) with boundary conditions of the type (2.2.2) prescribed over the part Γ_1 of the boundary and of the type (2.2.3) prescribed over Γ_2 ($\Gamma = \Gamma_1 + \Gamma_2$), the error thus introduced can be minimised by writing the following weighted residual statement,

$$\int_\Omega \nabla^2 u(s)\ u^*(p,s)\ d\Omega(s) = \int_{\Gamma_2} \left[q(S) - \bar{q}(S)\right] u^*(p,S)\ d\Gamma(S)$$

$$- \int_{\Gamma_1} \left[u(S) - \bar{u}(S)\right] q^*(p,S)\ d\Gamma(S) \qquad (2.4.1)$$

where u^* is interpreted as a weighting factor.

The integration of (2.4.1) by parts with respect to $x_i(s)$ gives

$$- \int_{\Omega} \frac{\partial u(s)}{\partial x_i(s)} \frac{\partial u^*(p,s)}{\partial x_i(s)} \, d\Omega(s) = - \int_{\Gamma_1} q(S) \, u^*(p,S) \, d\Gamma(S)$$

$$- \int_{\Gamma_2} \bar{q}(S) \, u^*(p,S) \, d\Gamma(S) - \int_{\Gamma_1} [u(S) - \bar{u}(S)] \, q^*(p,S) \, d\Gamma(S) \tag{2.4.2}$$

where $i = 1,2,3$ and Einstein's summation convention for repeated indices is implied. Integrating by parts once more,

$$\int_{\Omega} \nabla^2 u^*(p,s) \, u(s) \, d\Omega(s) = - \int_{\Gamma_1} q(S) \, u^*(p,S) \, d\Gamma(S) \tag{2.4.3}$$

$$- \int_{\Gamma_2} \bar{q}(S) \, u^*(p,S) \, d\Gamma(S) + \int_{\Gamma_2} u(S) \, q^*(p,S) \, d\Gamma(S) + \int_{\Gamma_1} \bar{u}(S) \, q^*(p,S) \, d\Gamma(S)$$

or generally,

$$\int_{\Omega} \nabla^2 u^*(p,s) \, u(s) \, d\Omega(s) = - \int_{\Gamma} q(S) \, u^*(p,S) \, d\Gamma(S)$$

$$+ \int_{\Gamma} u(S) \, q^*(p,S) \, d\Gamma(S) \tag{2.4.4}$$

Assuming u^* to be the fundamental solution to Laplace's equation and recalling (2.3.8) and (2.3.9), equation (2.4.4) becomes,

$$2\alpha\pi u(p) + \int_{\Gamma} u(S) \, q^*(p,S) \, d\Gamma(S) = \int_{\Gamma} q(S) \, u^*(p,S) \, d\Gamma(S) \tag{2.4.5}$$

which is of the same form as Green's third identity (2.3.6).

Another advantage of the direct formulation over the indirect one is that the restriction for the bounding surface to be a Liapunov (smooth) one can be relaxed. In fact, it can be applied to the more general Kellogg regular surfaces [13], thus allowing surfaces with corners or edges to be included.

So, taking the point p to the boundary and accounting for the jump of the left-hand side integral in (2.4.5) yields the more general boundary integral equation,

$$c(P)\ u(P) + \int_{\Gamma} u(S)\ q^{*}(P,S)\ d\Gamma(S) = \int_{\Gamma} q(S)\ u^{*}(P,S)\ d\Gamma(S) \qquad (2.4.6)$$

of which (2.3.10) is a particular case, when the surface Γ is smooth everywhere.

Two different procedures can be employed to calculate the value of the coefficient c: one is through the physical consideration that a constant potential applied over a closed body produces no flux, which is equivalent to the rigid-body translations of the theory of elasticity and will be discussed in detail in the next chapter; the other is herein presented for two-dimensional problems, but a similar approach is also valid for three-dimensions.

Assume that the body under consideration can be augmented by a small region Γ_{ε} which is part of a circle of radius ε centred at point P on the boundary Γ (figure 2.4.1). Proceeding as for evaluating the jump of the double-layer potential in section 2.1 and assuming that the function u(S) satisfies a Hölder condition at P, we have,

$$c(P) = 2\pi + \lim_{\varepsilon \to 0} \int_{\Gamma_{\varepsilon}} \frac{\partial}{\partial n(S)} \left(\log \frac{1}{r(p,S)}\right) d\Gamma(S) \qquad (2.4.7)$$

which, referring to figure 2.4.1 , reduces to

$$c(P) = 2\pi - \lim_{\varepsilon \to 0} \int_{\theta_1}^{\theta_2} \frac{1}{\varepsilon}\, \varepsilon d\theta = \pi + \alpha_1 - \alpha_2 \qquad (2.4.8)$$

that is, c(P) equals the internal angle of the boundary at P.

Since in a well-posed boundary-value problem only half of the boundary variables in (2.4.6) is prescribed, this equation can be employed in order to obtain the unknown boundary data. In chapter 3, a numerical scheme to solve this boundary integral equation will be presented. Then, values of the function u at any internal point p can be calculated by a numerical quadrature via equation (2.4.5). The derivatives of u at p (with cartesian coordinates $x_i(p), i = 1,2,3$), if required, can also be computed by a quadrature via the equation,

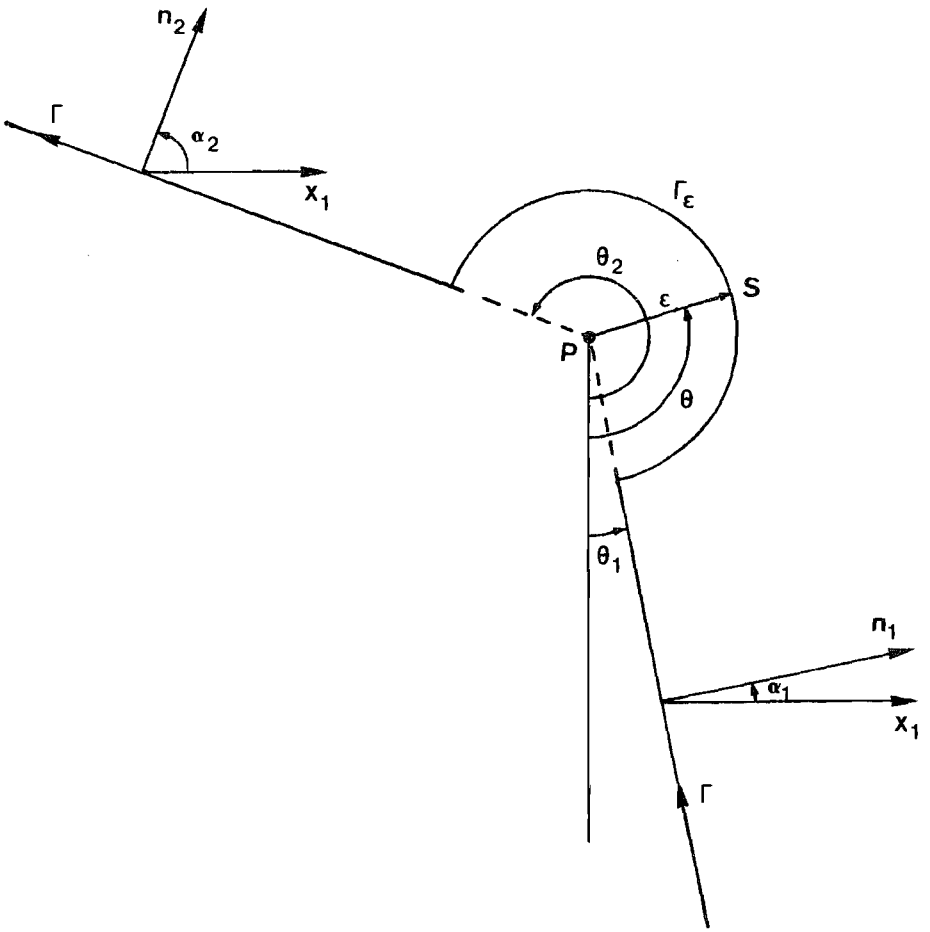

Figure 2.4.1 - Two-dimensional body augmented by region Γ_ε

$$\frac{\partial u(p)}{\partial x_i(p)} = -\frac{1}{2\alpha\pi}\left\{ \int_\Gamma q(S)\, \frac{\partial u^*(p,S)}{\partial x_i(S)}\, d\Gamma(S) - \int_\Gamma u(S)\, \frac{\partial q^*(p,S)}{\partial x_i(S)}\, d\Gamma(S) \right\} \tag{2.4.9}$$

as we may generally differentiate beneath the integral signs in (2.4.5).

2.5 Transient Potential Problems

We shall now proceed to study solutions to the diffusion equation,

$$\nabla^2 u(s,t) - \frac{1}{k}\frac{\partial u(s,t)}{\partial t} = 0 \qquad s \in \Omega \tag{2.5.1}$$

with boundary conditions of the same type as previously seen (repeated here for convenience),

$$\begin{aligned} u(S,t) &= \bar{u}(S,t) && S \in \Gamma_1 \\ q(S,t) &= \frac{\partial u(S,t)}{\partial n(S)} = \bar{q}(S,t) && S \in \Gamma_2 \end{aligned} \tag{2.5.2}$$

The coefficient k in equation (2.5.1) has different interpretations according to the physical problem concerned, and is assumed to be constant both in space and time.

Since the problem is now time-dependent, some initial conditions at time $t=t_0$ must also be prescribed,

$$u(s,t) = u_0(s,t_0) \qquad s \in \Omega \tag{2.5.3}$$

For simplicity, we shall set $t_0 = 0$ throughout this work.

The problem represented by equation (2.5.1) with boundary conditions (2.5.2) and initial conditions (2.5.3) is a mixed (boundary - initial-value) problem and as for boundary-value problems, the partial differential equation can be recast into an integral equation for the unknown function u. Three alternative formulations can be employed in order to perform this transformation: the first removes the time dependence of the problem by means of a Laplace transform [24]; the second replaces the time derivative in (2.5.1) by a finite difference

approximation and integrates the resulting equation on time in a finite difference fashion [3] while the third makes use of time-dependent fundamental solutions [29]. All three schemes will be discussed in following sections.

2.6 Laplace Transforms

Let us denote the Laplace transform of a function u(s,t), when it exists (see for instance [45]) by

$$U(s,\lambda) = \int_0^\infty u(s,t)\, e^{-\lambda t}\, dt \tag{2.6.1}$$

and assume that the transform parameter λ is real and positive.

Equation (2.5.1) in the transform space becomes,

$$\nabla^2 U(s,\lambda) - \frac{\lambda}{k} U(s,\lambda) + \frac{1}{k}\, u_0(s) = 0 \tag{2.6.2}$$

The boundary conditions must also be transformed and we assume, for simplicity, that they are constant on time. This gives,

$$\begin{aligned} U(S,\lambda) &= \overline{U}(S,\lambda) = \frac{\overline{u}(S,t)}{\lambda} && S \in \Gamma_1 \\ Q(S,\lambda) &= \overline{Q}(S,\lambda) = \frac{\overline{q}(S,t)}{\lambda} && S \in \Gamma_2 \end{aligned} \tag{2.6.3}$$

Proceeding as for Laplace's equation, we can write the following weighted residual statement,

$$\begin{aligned} &\int_\Omega \left[\nabla^2 U(s,\lambda) - \frac{\lambda}{k} U(s,\lambda) + \frac{1}{k} u_0(s)\right] U^*(p,s,\lambda)\, d\Omega(s) \\ &= \int_{\Gamma_2} \left[Q(S,\lambda) - \overline{Q}(S,\lambda)\right] U^*(p,S,\lambda)\, d\Gamma(S) \\ &- \int_{\Gamma_1} \left[U(S,\lambda) - \overline{U}(S,\lambda)\right] Q^*(p,S,\lambda)\, d\Gamma(S) \end{aligned} \tag{2.6.4}$$

where $Q^*(p,S,\lambda) = \partial U^*(p,S,\lambda)/\partial n(S)$. Integrating by parts twice the Laplacian in the above equation gives,

$$\int_{\Omega} \left[\nabla^2 U^*(p,s,\lambda) - \frac{\lambda}{k} U^*(p,s,\lambda)\right] U(s,\lambda)\, d\Omega(s) + \frac{1}{k}\int_{\Omega} u_0(s)\, U^*(p,s,\lambda)\, d\Omega(s)$$

$$= -\int_{\Gamma} Q(S,\lambda)\, U^*(p,S,\lambda)\, d\Gamma(S) + \int_{\Gamma} U(S,\lambda)\, Q^*(p,S,\lambda)\, d\Gamma(S) \tag{2.6.5}$$

Assuming U^* to be the fundamental solution to equation (2.6.2), which satisfies the following relation,

$$k\nabla^2 U^*(p,s,\lambda) - \lambda U^*(p,s,\lambda) = -\delta(p,s) \tag{2.6.6}$$

equation (2.6.5) becomes,

$$U(p,\lambda) + k\int_{\Gamma} U(S,\lambda)\, Q^*(p,S,\lambda)\, d\Gamma(S) = k\int_{\Gamma} Q(S,\lambda)\, U^*(p,S,\lambda)\, d\Gamma(S)$$

$$+ \int_{\Omega} u_0(s)\, U^*(p,s,\lambda)\, d\Omega(s) \tag{2.6.7}$$

The fundamental solution U^* for three-dimensional problems is of the form,

$$U^*(p,s,\lambda) = \frac{(k\lambda)^{\frac{1}{4}}}{\left[r^{\frac{1}{2}}(p,s)\right](2\pi k)^{3/2}} K_{\frac{1}{2}}\left[\left(\frac{\lambda}{k}\right)^{\frac{1}{2}} r(p,s)\right] \tag{2.6.8}$$

and for two-dimensional problems,

$$U^*(p,s,\lambda) = \frac{1}{2\pi k} K_0\left[\left(\frac{\lambda}{k}\right)^{\frac{1}{2}} r(p,s)\right] \tag{2.6.9}$$

where K_ν is the modified Bessel function of the second kind of order ν.

Let us now investigate the singularity of the above fundamental solutions. As $r\to 0$, so does the argument of the modified Bessel functions. The limiting form of $K_{\frac{1}{2}}(z)$ as $z\to 0$ is [46],

$$K_{\frac{1}{2}}(z) = \left(\frac{\pi}{2z}\right)^{\frac{1}{2}} \tag{2.6.10}$$

so that,

$$U^* = \frac{(k\lambda)^{\frac{1}{4}}}{r^{\frac{1}{2}}(2\pi k)^{3/2}} \left(\frac{\pi}{2r}\right)^{\frac{1}{2}} \left(\frac{k}{\lambda}\right)^{\frac{1}{4}} = \frac{1}{4\pi k r} \tag{2.6.11}$$

which means that the singularity of the fundamental solution is of the same type as that to Laplace's equation.

Analogously, the limiting form of $K_0(z)$ as $z \to 0$ is [46],

$$K_0(z) = - \log (z) \tag{2.6.12}$$

which gives,

$$U^* = \frac{1}{2\pi k} \log \frac{1}{r} - \frac{1}{4\pi k} \log \frac{\lambda}{k} \tag{2.6.13}$$

The first term is the fundamental solution to the two-dimensional Laplace's equation while the second term is a non-singular constant which adds nothing to the solution.

Taking the point p in equation (2.6.7) to the boundary and noting that the integral in Q^* is discontinuous as $p \to P$ then produces,

$$c(P)\ U(P,\lambda) + k \int_\Gamma U(S,\lambda)\ Q^*(P,S,\lambda)\ d\Gamma(S) = k \int_\Gamma Q(S,\lambda)\ U^*(P,S,\lambda)\ d\Gamma(S)$$

$$+ \int_\Omega u_0(s)\ U^*(P,s,\lambda)\ d\Omega(s) \tag{2.6.14}$$

where the coefficient c has the same value as previously.

This equation is discretised and solved numerically for a sequence of N selected values of the transform parameter λ, chosen somewhat arbitrarily. Notice that the presence of specified initial conditions gives rise to an integral over the domain Ω. One way of evaluating this integral is to divide the whole domain into cells and numerically integrate over each cell. However, if u_0 satisfies Laplace's equation, the domain integral in (2.6.14) can be transformed into equivalent boundary integrals [47]. Whatever the method of evaluating the domain integral may be, this integral introduces no further unknown since u_0 is prescribed, and equation (2.6.14) is still a boundary integral equation.

The remaining step is the transform inversion of the solution, which is carried out numerically. Following, for instance, the method of Schapery [48], we assume that the value of u at any point can be represented as a finite series by,

$$u(p,t) = u(p,\infty) + \sum_{n=1}^{N} a_n(p) \exp\left[-b_n(p)t\right] \qquad (2.6.15)$$

where $u(p,\infty)$ is the steady-state solution, a_n and b_n are functions of the position. Transforming (2.6.15) gives,

$$U(p,\lambda) = \frac{u(p,\infty)}{\lambda} + \sum_{n=1}^{N} \frac{a_n(p)}{\lambda+b_n(p)} \qquad (2.6.16)$$

The values of the coefficients b_n are now assumed to be equal to the previously selected λ. Thus there remain the N values of the coefficient a to be computed at each boundary point (plus the internal points where the solution is required). The N solutions of equation (2.6.14) provide N values of U at each point, which allow the evaluation of the coefficients a_n using equation (2.6.16) and consequently, the evaluation of the physical variable u using equation (2.6.15). A similar calculation is also required in order to obtain the real boundary (and internal) fluxes.

Numerical results using this formulation are presented in [24], [47], [49]. Notice that the transform inversion is essentially a curve fitting process and as such, it is important for the analyst to have an idea of the expected behaviour of the solution in order to select values of the transform parameter λ, since choosing too many values would quickly make equation (2.6.16) unstable while choosing too few values would not represent the curve adequately [49]. Furthermore, as pointed out in [47], the formulation is not efficient when the time history of the boundary conditions is complex and in this case, step-by-step methods of the type subsequently discussed should be preferred.

2.7 Coupled Boundary Element-Finite Difference Methods

Let us now assume that the time derivative in equation (2.5.1) can be approximated in a finite difference form, for a sufficiently small time step Δt, as

$$\frac{\partial u(s,t)}{\partial t} = \frac{u(s,t+\Delta t) - u(s,t)}{\Delta t} \tag{2.7.1}$$

Equation (2.5.1) can then be rewritten as,

$$k\nabla^2 u(s,t+\Delta t) - \frac{1}{k\Delta t}\, u(s,t+\Delta t) + \frac{1}{k\Delta t}\, u(s,t) = 0 \tag{2.7.2}$$

This equation is similar in form to equation (2.6.2) and so its fundamental solutions are of the same type as (2.6.8) and (2.6.9), replacing λ by $1/\Delta t$.

The boundary integral equation for this formulation can be obtained through weighted residual considerations, in the same way as was done in the previous section. By an analogy with equation (2.6.14), we can write

$$c(P)\, u(P,t+\Delta t) + k \int_\Gamma U(S,t+\Delta t)\, q^*(P,S,\Delta t)\, d\Gamma(S)$$

$$= k \int_\Gamma Q(S,t+\Delta t)\, u^*(P,S,\Delta t)\, d\Gamma(S) + \frac{1}{\Delta t} \int_\Omega u(s,t)\, u^*(P,s,\Delta t)\, d\Omega(s) \tag{2.7.3}$$

Starting from known initial values of u at $t = t_0$, we can advance the process on time by solving equation (2.7.3) numerically. Values of u at time $t = t_0 + \Delta t$ are then computed, at a sufficient number of internal points, in order to be used as pseudo-initial values for the next time step.

Numerical results using this formulation are presented in [50]. Notice that very small time steps have to be adopted if approximation (2.7.1) is to produce good results. As discussed in [50], the accuracy of this formulation can be significantly improved by employing second order finite difference schemes, although convergence problems become more severe.

2.8 Time-Dependent Fundamental Solutions

Considering the time dependence of the problem directly in the integration by parts process, we can write the following weighted residual statement for the governing equation (2.5.1) with boundary conditions (2.5.2),

$$\int_{t_0}^{t_F} \int_{\Omega} \left[\nabla^2 u(s,t) - \frac{1}{k} \frac{\partial u(s,t)}{\partial t}\right] u^*(p,s,t_F,t)\, d\Omega(s)\, dt$$

$$= \int_{t_0}^{t_F} \int_{\Gamma_2} \left[q(S,t) - \bar{q}(S,t)\right] u^*(p,S,t_F,t)\, d\Gamma(S)\, dt$$

$$- \int_{t_0}^{t_F} \int_{\Gamma_1} \left[u(S,t) - \bar{u}(S,t)\right] q^*(p,S,t_F,t)\, d\Gamma(S)\, dt \qquad (2.8.1)$$

where $q^*(p,S,t_F,t) = \partial u^*(p,S,t_F,t)/\partial n(S)$.

Integrating by parts twice the Laplacian and once the time derivative in the above equation gives,

$$\int_{t_0}^{t_F} \int_{\Omega} \left[\nabla^2 u^*(p,s,t_F,t) + \frac{1}{k} \frac{\partial u^*(p,s,t_F,t)}{\partial t}\right] u(s,t)\, d\Omega(s)\, dt$$

$$- \frac{1}{k} \left[\int_{\Omega} u(s,t)\, u^*(p,s,t_F,t)\, d\Omega(s)\right]_{t=t_0}^{t=t_F} = - \int_{t_0}^{t_F} \int_{\Gamma} q(S,t)\, u^*(p,S,t_F,t)\, d\Gamma(S)\, dt$$

$$+ \int_{t_0}^{t_F} \int_{\Gamma} u(S,t)\, q^*(p,S,t_F,t)\, d\Gamma(S)\, dt \qquad (2.8.2)$$

The time-dependent fundamental solution u^* is of the form [15], [16],

$$u^*(p,s,t_F,t) = \frac{1}{(4\pi k\tau)^{d/2}} \exp\left[-\frac{r^2(p,s)}{4k\tau}\right] H(\tau) \qquad (2.8.3)$$

where $\tau = t_F - t$ and d is the number of spatial dimensions of the problem, e.g. d = 3 for three-dimensional problems, etc. Note that (2.6.8) and (2.6.9) are the Laplace transforms of (2.8.3) for d = 3 and d = 2,

respectively. The Heaviside function $H(\tau)$ is included to emphasize the fact that the solution is identically zero for $t>t_F$. This condition is known as the causality condition [15].

The fundamental solution possesses the following properties,

$$k\nabla^2 u^*(p,s,t_F,t) + \frac{\partial u^*(p,s,t_F,t)}{\partial t} = -\delta(p,s)\,\delta(t_F,t) \tag{2.8.4}$$

$$\lim_{t\to t_F} u^*(p,s,t_F,t) = \delta(p,s) \tag{2.8.5}$$

Let us now investigate the singularity that occurs in the integrals in equation (2.8.2) at time $t=t_F$. In order to avoid ending the integrations exactly at the peak of the Dirac delta function, we may subtract or add to the upper limit of the integrals an arbitrarily small quantity ε. In the former case, the first integral on the left-hand side is identically zero for t in the range $0, t_F-\varepsilon$ and so, taking the limit as $\varepsilon\to 0$ and accounting for condition (2.8.3), equation (2.8.2) yields [16], [17]

$$u(p,t_F) + k\int_{t_0}^{t_F}\int_{\Gamma} u(S,t)\; q^*(p,S,t_F,t)\; d\Gamma(S)\; dt$$

$$= k\int_{t_0}^{t_F}\int_{\Gamma} q(S,t)\; u^*(p,S,t_F,t)\; d\Gamma(S)\; dt + \int_{\Omega} u_0(s,t_0)\; u^*(p,s,t_F,t_0)\; d\Omega(s) \tag{2.8.6}$$

The same relation can be obtained by adding ε to the upper limit of the integrals in equation (2.8.2). In this case, $u^*(p,s,t_F,t_F+\varepsilon)$ equals zero due to the causality condition. Thus, taking the limit of (2.8.2) as $\varepsilon\to 0$, the inclusion of condition (2.8.4) into the first integral on the left-hand side produces the expected result [15].

Another property of the time-dependent fundamental solution (2.8.3) is that, as a steady-state is reached, it reduces to the fundamental solution to Laplace's equation. That is,

$$\lim_{t_F \to \infty} \int_0^{t_F} u^*(p,s,t_F,t)\, dt = u^*(p,s) \qquad (2.8.7)$$

We shall now prove this property for three-dimensional problems, bearing in mind that a similar approach can also be applied in two-dimensions. So we have to integrate,

$$\int_0^{t_F} u^*(p,s,t_F,t)\, dt = \int_0^{t_F} \frac{1}{(4\pi k\tau)^{3/2}} \exp\left(-\frac{r^2}{4k\tau}\right) dt \qquad (2.8.8)$$

This integral can be evaluated analytically by introducing the variable $x = r^2/4k\tau$. An interchange of variables then gives,

$$\int_0^{t_F} u^*(p,s,t_F,t)\, dt = \frac{1}{4\pi^{3/2} kr} \int_a^{\infty} x^{-\frac{1}{2}} e^{-x}\, dx = \frac{1}{4\pi^{3/2} kr} \Gamma(\tfrac{1}{2},a) \qquad (2.8.9)$$

where $a = r^2/4kt_F$ and Γ is the incomplete Gamma function. Taking the limit of (2.8.9) as $t_F \to \infty$ [46],

$$\frac{1}{4\pi^{3/2} kr} \lim_{t_F \to \infty} \Gamma(\tfrac{1}{2},a) = \frac{1}{4\pi kr} \qquad (2.8.10)$$

which can be recognised as the fundamental solution to $k\nabla^2 u = 0$.

Note that the first two integrals in (2.8.6) represent the effects of boundary conditions, while the third term includes the effects of the initial value u_0 of the function u. As $t_F \to \infty$, the initial conditions distribution effect vanishes while the integrations over t for the boundary terms can be carried out assuming that u and q no longer depend on t (or at least that the contribution to the integral over t from 0 to ∞ from those values of t where u and q were still dependent on t is negligible compared to the total integral). Thus, by virtue of (2.8.7), the fundamental solution reduces to that of Laplace's equation and (2.8.6) becomes the integral equation (2.4.5) for steady potential problems.

Taking the point p in equation (2.8.6) to the boundary and accounting for the jump of the left-hand side integral yields the boundary integral equation,

$$c(P)\ u(P,t_F) + k \int_{t_0}^{t_F} \int_{\Gamma} u(S,t)\ q^*(P,S,t_F,t)\ d\Gamma(S)\ dt \tag{2.8.11}$$

$$= k \int_{t_0}^{t_F} \int_{\Gamma} q(S,t)\ u^*(P,S,t_F,t)\ d\Gamma(S)\ dt + \int_{\Omega} u_0(s,t_0)\ u^*(P,s,t_F,t_0)\ d\Omega(s)$$

where $c(P)$, as previously, is a function of the solid angle of the boundary at point P (see equation (2.4.8)).

Since the time variation of functions u and q is not known a priori, a time-stepping technique (not to be confused with the previous finite difference one) has to be introduced for the numerical solution of equation (2.8.11). However, as the fundamental solution itself is time-dependent, large time steps can generally be adopted.

Two different time-marching schemes can be employed on this numerical solution: the first treats each time step as a new problem and so, at the end of each step, computes values of the function u at a sufficient number of internal points in order to use them as pseudo-initial values for the next step; in the other, the time integration process always starts at time t_0 and so, despite the increasing number of intermediate steps as the time progresses, values of u at internal points need not be recomputed. Furthermore, if u_0 satisfies Laplace's equation, the domain integral in (2.8.11) can be transformed into equivalent boundary integrals. The necessary procedures for numerical implementation of both time-marching schemes, as well as discussions on their computer efficiency, are the object of chapter 4.

3. STEADY POTENTIAL PROBLEMS

The subject of this chapter is the solution of the boundary integral equation (2.4.6) relating boundary values and normal derivatives of the potential function u over the boundary Γ, repeated here for convenience,

$$c(P)\ u(P) + \int_\Gamma u(S)\ q^*(P,S)\ d\Gamma(S) = \int_\Gamma q(S)\ u^*(P,S)\ d\Gamma(S) \quad (3.1)$$

Rather than attempting analytical solutions to this equation for particular geometries and boundary conditions, we seek a suitable reduction of equation (3.1) to an algebraic form that can be solved by a numerical approach. This approach generally consists of the following steps (see, for instance, [1], [2], [3], [40]):

a) The boundary Γ is discretised into a series of elements over which the potential and its normal derivative are assumed to vary according to interpolation functions. The geometry of these elements can be modelled using straight lines, circular arcs, parabolas, etc.;

b) By using the method of moments [51], the discretised equation is applied to a number of particular nodes within each element where values of the potential and its normal derivative are associated;

c) The integrals over each element are carried out by using, in general, a numerical quadrature scheme;

d) By imposing the prescribed boundary conditions of the problem, a system of linear algebraic equations is obtained. The solution of this system of equations, which can be effected using direct or iterative methods, produces the remaining boundary data.

Values of the function u at any internal point, if required, can then be calculated from the boundary data by a numerical quadrature via equation (2.4.5). Similarly, the derivatives of u at any internal point can also be computed by a quadrature via equation (2.4.9).

In the following section, the above-listed steps are examined in detail in connection with two-dimensional problems defined over finite regions of homogeneous, isotropic media with Neumann, Dirichlet or Cauchy boundary conditions. In subsequent sections, it is shown how the method can be extended to include boundary conditions of the Robin-type, free surfaces and internal sources. If the region is non-homogeneous but is constituted of several homogeneous sub-regions with different physical properties, the method can be applied by first writing a system of equations for each sub-region and then introducing compatibility (in terms of potentials) and equilibrium (in terms of normal derivatives) conditions between the sub-regions.

Fundamental solutions for orthotropic and anisotropic regions are derived and it is shown that all concepts presented in the previous chapter are also valid for infinite regions fulfilling certain regularity conditions at infinity. By adopting a convenient fundamental solution which satisfies part of the boundary conditions of the problem under consideration a reduction in the amount of numerical work can be achieved, as explained in this chapter. Finally, specific numerical procedures for three-dimensional and axisymmetric problems are derived.

Computer programs incorporating several of the features presented in this chapter were developed. These programs are described in chapter 6. Whenever this is the case, numerical examples are included in order to show the validity of the numerical procedures. Although many different physical problems are governed by Laplace's equation, these examples are restricted to problems of heat conduction and flow of perfect fluids.

3.1 Two-Dimensional Problems

For the discretisation of equation (3.1), the boundary Γ is approximated by using a series of elements. The cartesian coordinates $\underset{\sim}{x}$ of points within each element are expressed (in matricial notation) in

terms of suitable interpolation functions $\underset{\sim}{\Psi}$ and nodal coordinates $\underset{\sim}{X}^m$ of each element by

$$\underset{\sim}{x} = \underset{\sim}{\Psi}^T \underset{\sim}{X}^m \tag{3.1.1}$$

where

$$x = \begin{Bmatrix} x_1 \\ x_2 \end{Bmatrix} \qquad \underset{\sim}{\Psi}^T = \begin{bmatrix} \underset{\sim}{\Psi}^T & \underset{\sim}{0} \\ \underset{\sim}{0} & \underset{\sim}{\Psi}^T \end{bmatrix} \qquad \underset{\sim}{X}^m = \begin{Bmatrix} \underset{\sim}{X}_1^m \\ \underset{\sim}{X}_2^m \end{Bmatrix} \tag{3.1.2}$$

Also, the potential u and its normal derivative q within each element are approximated through interpolation functions $\underset{\sim}{\phi}$ as,

$$\begin{aligned} u &= \underset{\sim}{\phi}^T \underset{\sim}{U}^n \\ q &= \underset{\sim}{\phi}^T \underset{\sim}{Q}^n \end{aligned} \tag{3.1.3}$$

where $\underset{\sim}{U}^n$ contains the nodal potential values and $\underset{\sim}{Q}^n$ the nodal values of normal derivatives. Note that different interpolation functions may be used for u and q [52]. The index m in equation (3.1.1) refers to the number of boundary points required to define the geometry of each boundary element while the index n in (3.1.3) refers to the number of boundary nodes within each element to which nodal values of u and q are associated.

Assuming that the boundary Γ is discretised into S elements and N nodes, the substitution of equations (3.1.3) into equation (3.1) yields

$$c_i U^i + \sum_{s=1}^{S} \left(\int_{\Gamma_s} q^* \underset{\sim}{\phi}^T d\Gamma \right) \underset{\sim}{U}^n = \sum_{s=1}^{S} \left(\int_{\Gamma_s} u^* \underset{\sim}{\phi}^T d\Gamma \right) \underset{\sim}{Q}^n \tag{3.1.4}$$

Since the interpolation functions $\underset{\sim}{\phi}$ are usually expressed in terms of some intrinsic system of coordinates, it is necessary to transform the elements of surface $d\Gamma$ from the global cartesian system of coordinates to the intrinsic system of coordinates, that is

$$d\Gamma = |J| \, d\xi \tag{3.1.5}$$

where J is the Jacobian relating both systems of coordinates.

The integrals in equation (3.1.4) can be computed analytically only for simple cases. In general, it is more convenient to compute them

numerically mainly when considering higher order interpolation functions. However, when the element s contains the node i these integrals become singular and special care has to be taken on their evaluation. For $i \notin \Gamma_s$, the integrals in (3.1.4) may be replaced by summations of the form,

$$\int_{\Gamma_s} q^*(\underset{\sim}{x})\ \underset{\sim}{\phi}^T(\xi)\ d\Gamma = \int_{-1}^{1} q^*(\xi)\ \underset{\sim}{\phi}^T(\xi)\ |J|\ d\xi = \sum_{k=1}^{K} |J|_k\ W_k (q^* \underset{\sim}{\phi}^T)_k$$

$$\int_{\Gamma_s} u^*(\underset{\sim}{x})\ \underset{\sim}{\phi}^T(\xi)\ d\Gamma = \int_{-1}^{1} u^*(\xi)\ \underset{\sim}{\phi}^T(\xi)\ |J|\ d\xi = \sum_{k=1}^{K} |J|_k\ W_k (u^* \underset{\sim}{\phi}^T)_k \qquad (3.1.6)$$

where K is the number of integration points and W is the weighting factor associated with them.

Applying equation (3.1.4) to all N boundary nodes, a final system of equations is obtained,

$$\underset{\sim}{C}\ \underset{\sim}{U} + \underset{\sim}{\hat{H}}\ \underset{\sim}{U} = \underset{\sim}{G}\ \underset{\sim}{Q} \qquad (3.1.7)$$

where the vectors $\underset{\sim}{U}$ and $\underset{\sim}{Q}$ contain all potential and normal derivative values at the boundary nodes, respectively. The diagonal matrix $\underset{\sim}{C}$ may be incorporated into $\underset{\sim}{\hat{H}}$ to form the matrix $\underset{\sim}{H}$,

$$\underset{\sim}{H}\ \underset{\sim}{U} = \underset{\sim}{G}\ \underset{\sim}{Q} \qquad (3.1.8)$$

As referred to in section 2.4, the diagonal coefficients of matrix $\underset{\sim}{H}$ (which include the free terms c_i) can be calculated by considering that a constant potential applied over a closed body produces no flux. This is equivalent to the rigid-body translations of the theory of elasticity [53] and was first employed in the context of the Boundary Element Method by Symm [19]. Its use has the further advantage of avoiding evaluating strongly singular integrals which are only integrable in the Cauchy principal value sense. Considering $\underset{\sim}{U}$ as a unit potential, equation (3.1.8) then becomes,

$$\underset{\sim}{H}\ \underset{\sim}{I} = \underset{\sim}{Q} \qquad (3.1.9)$$

and the diagonal coefficients of $\underset{\sim}{H}$ may be computed after all the off-diagonal terms are known as

$$H_{ii} = - \sum_{\substack{j=1 \\ (j \neq i)}}^{N} H_{ij} \qquad i = 1,2,\ldots,N \tag{3.1.10}$$

By applying the prescribed boundary conditions of the problem, equation (3.1.8) can be reordered in such a way that a final system of equations is obtained,

$$\underset{\sim}{K}\ \underset{\sim}{X} = \underset{\sim}{F} \tag{3.1.11}$$

where $\underset{\sim}{K}$ is a fully populated matrix of order N and $\underset{\sim}{X}$ is a vector containing all the boundary unknowns.

Notice that in computational terms H_{ij} $(i \neq j)$ and G_{ij} are assembled directly into $\underset{\sim}{K}$ (see chapter 6) so that equation (3.1.8) does not need to be formed.

Specific numerical procedures will now be developed for computer implementation purposes. Three different sets of approximations for the boundary geometry, the potential and its normal derivative are discussed (see figure 3.1.1), namely: straight line segments with piecewise constant potentials and normal derivatives, hereafter referred to as constant elements; straight line segments with piecewise linear potentials and normal derivatives (linear elements); parabolic segments with piecewise quadratic potentials and normal derivatives (quadratic elements). Although only the first and second are at present programmed, the latter is included to show that no special difficulties arise on using higher order interpolation functions.

3.1.1 Constant Elements

If the geometry of the elements is represented by straight lines, the interpolation functions $\underset{\sim}{\Psi}$ and the vector $\underset{\sim}{X}^m$ in equation (3.1.1) are given by,

$$\underset{\sim}{\Psi} = \tfrac{1}{2} \begin{Bmatrix} 1 - \xi \\ 1 + \xi \end{Bmatrix} \qquad \underset{\sim i}{X}^m = \begin{Bmatrix} X_i^1 \\ X_i^2 \end{Bmatrix} \tag{3.1.12}$$

where ξ is an intrinsic coordinate (figure 3.1.2) and $i = 1,2$, $\underset{\sim i}{X}^m$ being associated to the extreme points of each element.

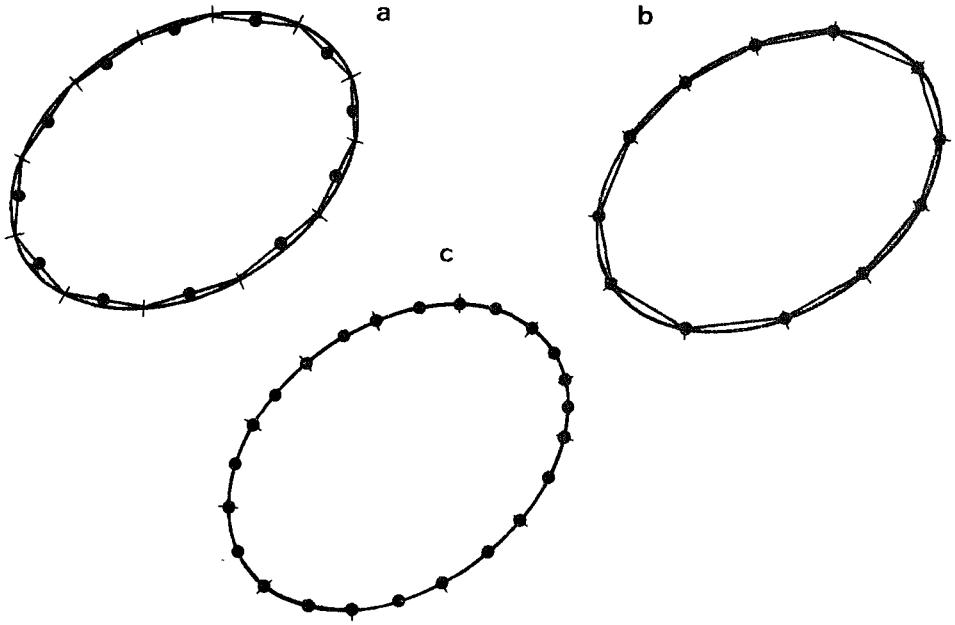

Figure 3.1.1 - Different types of boundary elements: (a) Constant element; (b) Linear element; (c) Quadratic element

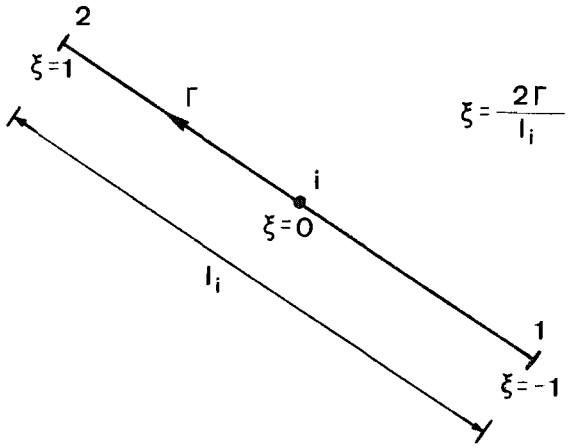

Figure 3.1.2 - Constant element

Since in this case,

$$d\Gamma = \frac{\ell}{2}\, d\xi \tag{3.1.13}$$

the Jacobian J written in equation (3.1.5) is constant at all points within each element and equal to half the length of the element.

For the constant element, equation (3.1.3) can be simply written as,

$$\begin{aligned} u &= U \\ q &= Q \end{aligned} \tag{3.1.14}$$

that is, the potential and its normal derivative values are assumed to be constant over each element and equal to their nodal values at the mid-point (figure 3.1.1a).

The integrals in equation (3.1.4) for the cases when $i \in \Gamma_s$ can be easily computed analytically [1], [40]. Analytical integration formulæ, however, are often more complicated and consequently take longer to compute than numerical quadrature formulæ. Moreover, for intervals other than straight lines it is seldom possible to obtain these integrals analytically. For generality, the terms H_{ij} and G_{ij} $(i \neq j)$ in equation (3.1.8) are then evaluated numerically using a four-points Gauss quadrature rule. With reference to equations (3.1.6), this gives,

$$\begin{aligned} H_{ij} &= \frac{d_{ij}}{2} \sum_{k=1}^{4} \frac{1}{r_{ik}^2}\, W_k \\ G_{ij} &= \frac{\ell_j}{2} \sum_{k=1}^{4} \log\left(\frac{1}{r_{ik}}\right) W_k \end{aligned} \tag{3.1.15}$$

where $d_{ij} = (X_1^i - X_1^1)(X_2^2 - X_2^1) + (X_2^i - X_2^1)(X_1^1 - X_1^2)$; ℓ_j and d_{ij} refer to the element containing node j.

For the diagonal terms H_{ii} and G_{ii}, the integrals become singular and have to be evaluated in the Cauchy principal value sense, that is, a small segment of length 2ε around the singular point is deleted from the integration and the limit as $\varepsilon \to 0$ taken. The G_{ii} coefficients may be calculated as follows (see figure 3.1.2),

$$G_{ii} = \frac{\ell_i}{2} \int_{-1}^{1} \log \frac{2}{\ell_i |\xi|} d\xi = \ell_i \left[\log(\frac{2}{\ell_i}) + 1 \right] \qquad (3.1.16)$$

and the H_{ii} terms are computed through equation (3.1.10).

3.1.2 Linear Elements

The geometry of the elements is again represented by straight lines, thus the interpolation functions $\underset{\sim}{\Psi}$ and the vector $\underset{\sim}{X}^m$ are given by (3.1.12) and the Jacobian by (3.1.13). As the functions u and q are now also assumed to vary linearly within each element, the interpolation functions $\underset{\sim}{\phi}$ and the vectors $\underset{\sim}{U}^n$ and $\underset{\sim}{Q}^n$ in equation (3.1.3) are of the form,

$$\underset{\sim}{\phi} = \tfrac{1}{2} \begin{Bmatrix} 1 - \xi \\ 1 + \xi \end{Bmatrix} \qquad \underset{\sim}{U}^n = \begin{Bmatrix} U^1 \\ U^2 \end{Bmatrix} \qquad \underset{\sim}{Q}^n = \begin{Bmatrix} Q^1 \\ Q^2 \end{Bmatrix} \qquad (3.1.17)$$

that is, the functions $\underset{\sim}{\phi}$ are the same as those employed to describe the geometry of the boundary elements and the potential and its normal derivative values are also associated to nodal values at the extreme points of each element.

The terms H_{ij} and G_{ij} $(i \neq j)$ in equation (3.1.8) for linear elements can be computed as,

$$\begin{aligned} H_{ij} &= h_{ip}^{2} + h_{iq}^{1} \\ G_{ij} &= g_{ip}^{2} + g_{iq}^{1} \end{aligned} \qquad (3.1.18)$$

where the indices p and q refer to the elements at the intersection of which node j is located. In general, we have

$$\begin{aligned} h_{ip}^{m} &= \frac{d_{ip}}{2} \sum_{k=1}^{4} \frac{1}{r_{ik}^{2}} \phi_k^m W_k \\ g_{ip}^{m} &= \frac{\ell_p}{2} \sum_{k=1}^{4} \log (\frac{1}{r_{ik}}) \phi_k^m W_k \end{aligned} \qquad (3.1.19)$$

being d_{ip} of the same form as previously and m = 1,2.

The H_{ii} coefficients are computed by using relation (3.1.10) and the G_{ii} coefficients now result from evaluating integrals of the form (see figure 3.1.3),

$$G_{ii} = \frac{\ell_p}{4} \int_{-1}^{1} \log \left[\frac{2}{\ell_p (1-\xi_p)} \right] (1+\xi_p)\, d\xi + \frac{\ell_q}{4} \int_{-1}^{1} \log \left[\frac{2}{\ell_q (1+\xi_q)} \right] (1-\xi_q)\, d\xi \tag{3.1.20}$$

which gives,

$$G_{ii} = \frac{\ell_p}{2} \left[\frac{3}{2} - \log \ell_p \right] + \frac{\ell_q}{2} \left[\frac{3}{2} - \log \ell_q \right] \tag{3.1.21}$$

3.1.3 Quadratic Elements

Here, the boundary Γ is modelled by a series of curvilinear elements using the following Lagrangian interpolation functions [2], [3],

$$\underset{\sim}{\Psi} = \begin{Bmatrix} \frac{1}{2}\,\xi(\xi-1) \\ 1-\xi^2 \\ \frac{1}{2}\,\xi(\xi+1) \end{Bmatrix} \qquad \underset{\sim i}{X^m} = \begin{Bmatrix} X_i^1 \\ X_i^2 \\ X_i^3 \end{Bmatrix} \tag{3.1.22}$$

being $\underset{\sim i}{X^m}$ in equation (3.1.1) now associated to the extreme and mid-points of each element (figure 3.1.1c).

The Jacobian related to the transformation of elements of surface $d\Gamma$ from the global cartesian system of coordinates to the intrinsic system of coordinates is given by,

$$|J| = \left[\left(\frac{dx_1}{d\xi} \right)^2 + \left(\frac{dx_2}{d\xi} \right)^2 \right]^{\frac{1}{2}} \tag{3.1.23}$$

where the derivatives in the above formula can be computed by using relation (3.1.1).

The interpolation functions ϕ in (3.1.3) are also assumed to be the Lagrangian functions (3.1.22), thus the potential and its normal derivative are also associated to nodal values at the extreme and mid-points of each element.

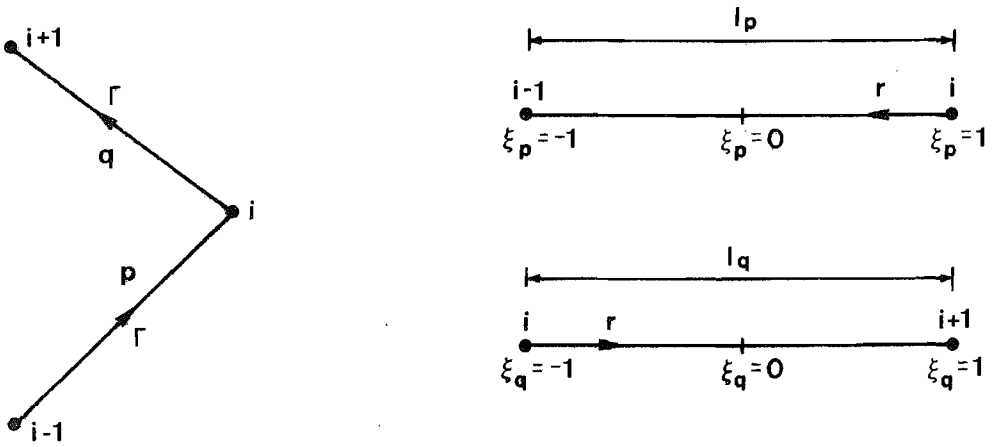

Figure 3.1.3 - Linear element

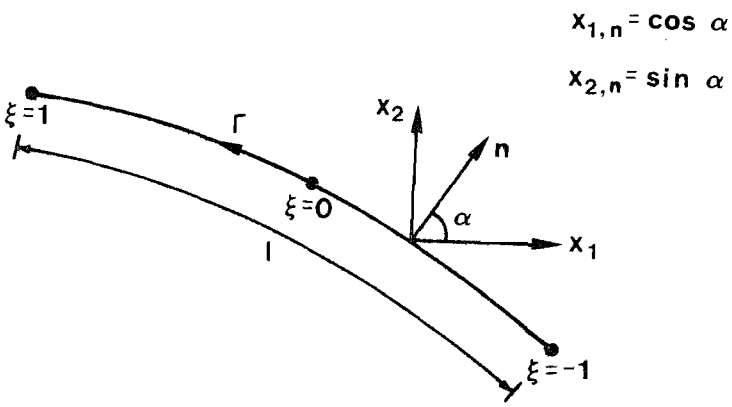

Figure 3.1.4 - Quadratic element

The terms H_{ij} and G_{ij} $(i \neq j)$ in equation (3.1.8) for quadratic elements become,

$$H_{ij} = \begin{cases} h_{ip}^{\,3} + h_{iq}^{\,1} \\ h_{ip}^{\,2} \end{cases}$$

$$G_{ij} = \begin{cases} g_{ip}^{\,3} + g_{iq}^{\,1} \\ g_{ip}^{\,2} \end{cases} \qquad (3.1.24)$$

the first occurring when node j is located at the intersection of elements p and q and the second when node j is located at the middle of element p. In general, we may write

$$h_{ip}^{\,m} = \sum_{k=1}^{4} |J|_k \, d_{ik} \frac{1}{r_{ik}^{\,2}} \, \phi_k^m \, W_k$$

$$g_{ip}^{\,m} = \sum_{k=1}^{4} |J|_k \log\left(\frac{1}{r_{ik}}\right) \phi_k^m \, W_k \qquad (3.1.25)$$

where $m = 1,2,3$ and $d_{ik} = (X_1^i - X_1^k) \; x_{1,n}^k + (X_2^i - X_2^k) \; x_{2,n}^k$, being $x_{1,n}^k$ and $x_{2,n}^k$ the direction cosines of the outward normal at point k (figure 3.1.4).

The H_{ii} coefficients may again be computed through equation (3.1.10) while the G_{ii} terms are of the form,

$$G_{ii} = \int_{-1}^{1} \log\left(\frac{1}{r(\xi)}\right) (1-\xi^2) \; |J(\xi)| \; d\xi \qquad (3.1.26)$$

if i is a mid-node, or

$$G_{ii} = \frac{1}{2} \int_{-1}^{1} \log\left(\frac{1}{r(\xi_p)}\right) \xi_p(\xi_p+1) \; |J(\xi_p)| \; d\xi$$

$$+ \frac{1}{2} \int_{-1}^{1} \log\left(\frac{1}{r(\xi_q)}\right) \xi_q(\xi_q-1) \; |J(\xi_q)| \; d\xi \qquad (3.1.27)$$

if i is an extreme node.

The presence of the Jacobian now makes it difficult to compute the above integrals analytically. Separating the integral in (3.1.26) as,

$$G_{ii} = \log\left(\frac{2}{\ell_i}\right)\int_{-1}^{1}(1-\xi^2)\,|J(\xi)|\,d\xi + \int_{-1}^{1}\log(|\xi|)\,\xi^2\,|J(\xi)|\,d\xi - \int_{-1}^{1}\log(|\xi|)\,|J(\xi)|\,d\xi \qquad (3.1.28)$$

we note that only the last integral in (3.1.28) is singular. Thus, we can evaluate the first and second integrals using a standard Gaussian quadrature and compute the last one using a Gaussian formula for integrands with a logarithmic singularity [2], [46]. The same can be applied in order to compute the integrals in equation (3.1.27).

Example 3.1.1

The first example analysed compares the accuracy of constant and linear boundary elements for the solution of a Dirichlet problem, that is, two confocal ellipses with temperatures u_i and u_e prescribed along the internal and external surfaces, respectively.

Taking the semi-axes of the ellipses to be [54],

$$a_e = c\cosh\mu_e, \qquad b_e = c\sinh\mu_e$$

$$a_i = c\cosh\mu_i, \qquad b_i = c\sinh\mu_i$$

where c is a constant and $0<\mu_i<\mu_e<\infty$, the exact solution of the problem is given by,

$$u = u_e + \frac{\mu_e-\mu}{\mu_e-\mu_i}(u_i-u_e), \qquad \mu_i \leq \mu \leq \mu_e$$

Figure 3.1.5 presents the relative error in the calculation of the temperature at the point $x_1 = 0$, $x_2 = c\sinh[(\mu_i+\mu_e)/2]$ obtained with several discretisations, for two different aspect ratios a/b of the ellipses. Assuming a unit value for the constant c, the lower curves in the figure correspond to ellipses with aspect ratios $(a/b)_i = 1.313$ and $(a/b)_e = 1.037$ while the upper curves correspond to $(a/b)_i = 10.033$ and $(a/b)_e = 5.066$. In the second case, the inner ellipse is much more distorted than the outer one such that their

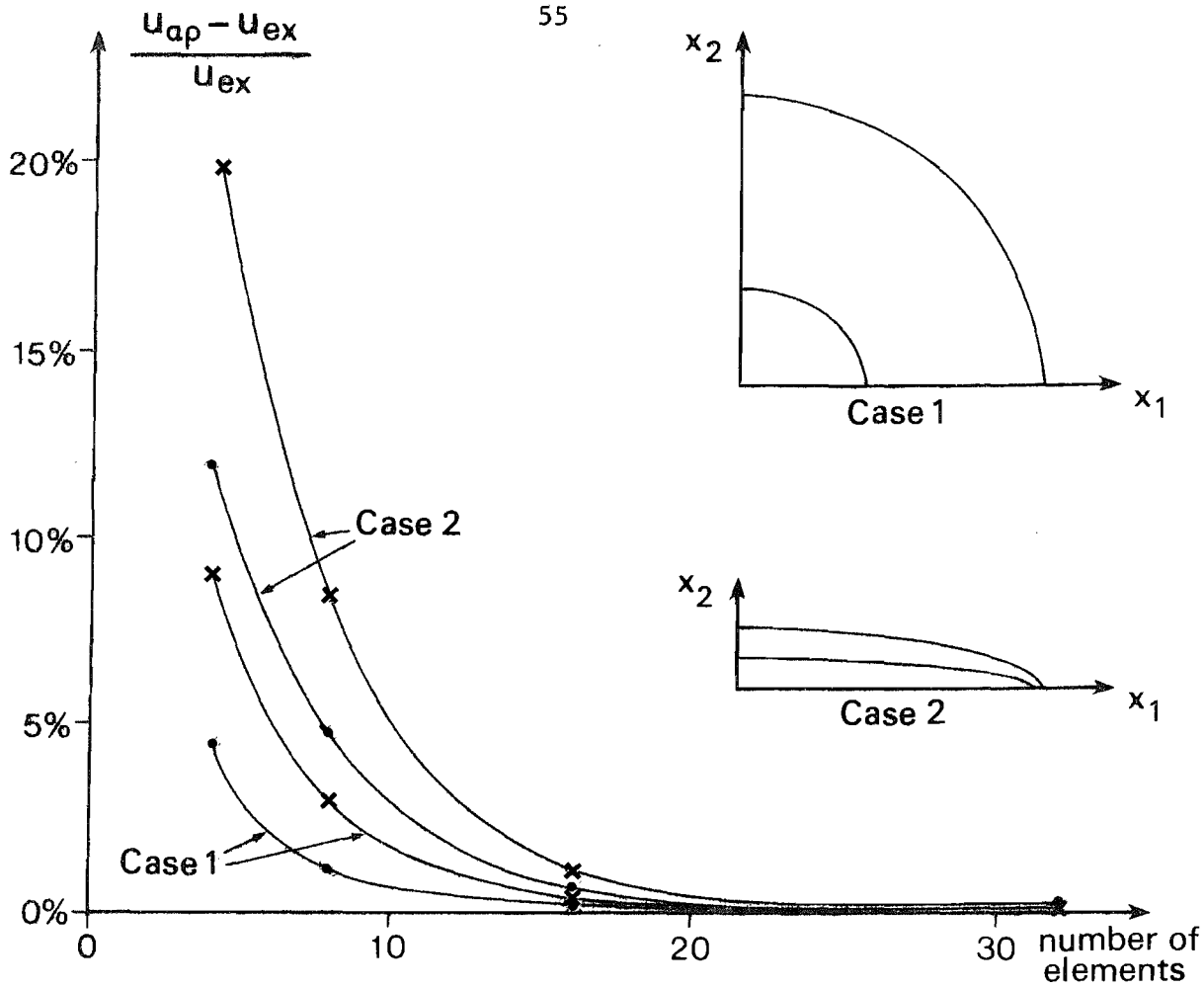

Figure 3.1.5 - Convergence of the solution

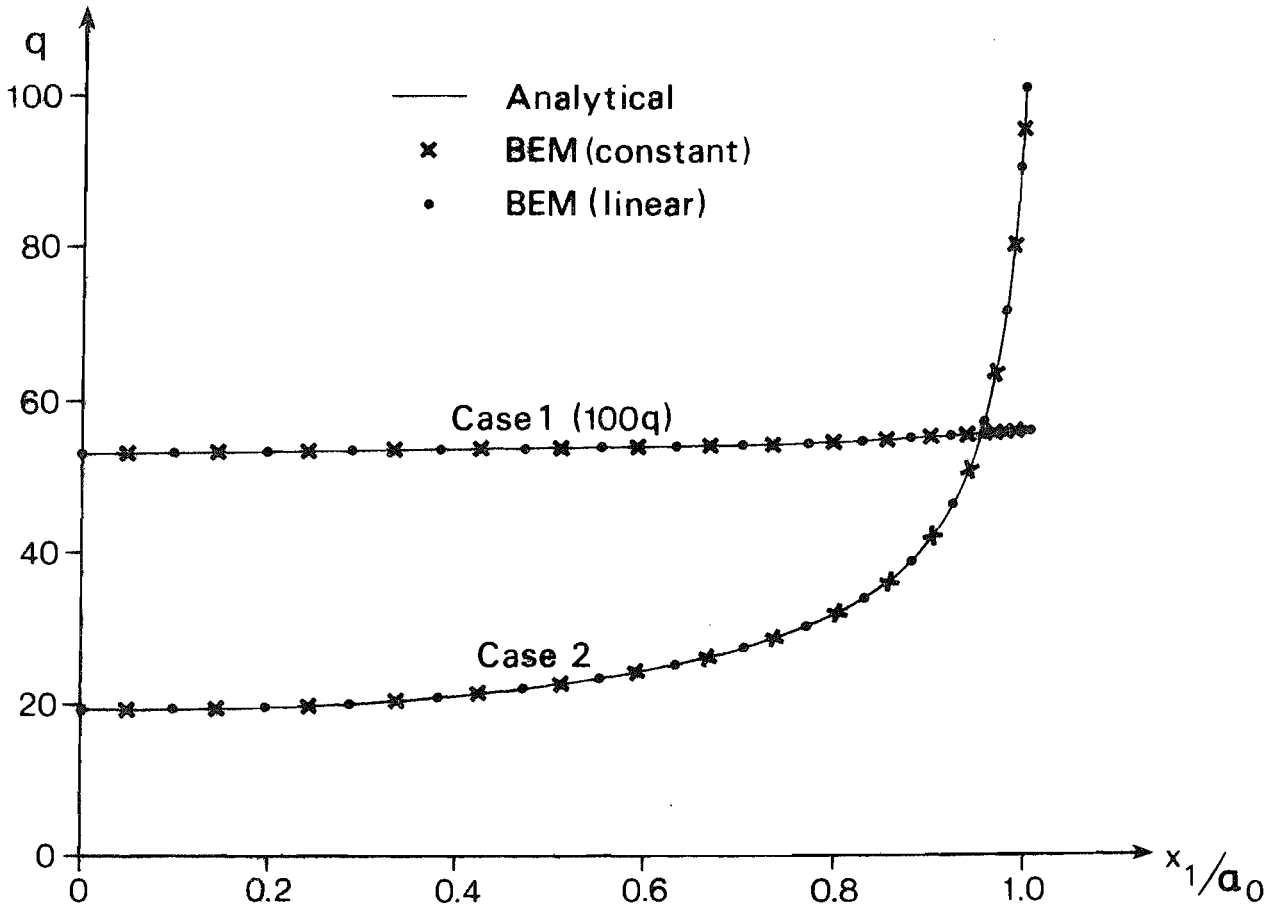

Figure 3.1.6 - Normal flux along outer surface

longer axes almost touch each other (see figure 3.1.5). The convergence of the solutions is evident in the figure. Normal fluxes along the outer surface are plotted in figure 3.1.6 for the finest discretisations employed.

Due to the double symmetry of the problem, only one quarter of the cross-section needed to be analysed. Symmetry is taken into account through a direct condensation process with integration over reflected elements such that no discretisation of the symmetry axes is necessary (see chapter 6).

Example 3.1.2

This example studies the temperature distribution over a circular region of internal radius R_i and external radius R_e with Neumann boundary conditions, i.e. radial fluxes specified on both the inner and outer boundaries (see figure 3.1.7).

Due to condition (2.2.6), the relation $q_i R_i = -q_e R_e$ has to be accomplished in order for the numerical data to be compatible. The double symmetry of the problem permits the discretisation of only one quarter of the cross-section. By adopting the same number of subdivisions over each surface, the discretised form of condition (2.2.6) holds automatically.

The exact solution of this problem is

$$u = c - q_i R_i \log r$$

that is, the solution is unique only to within an arbitrary additive constant. To enforce a unique solution to the problem, the value of the constant c must be given and this is introduced into the numerical analysis by specifying the value of u at any boundary point, for instance.

Recalling relation (3.1.8), we notice that the system matrix $\underset{\sim}{H}$ is singular since, according to equation (3.1.10),

$$\sum_{j=1}^{N} H_{ij} = 0 \qquad i = 1,2,\ldots,N$$

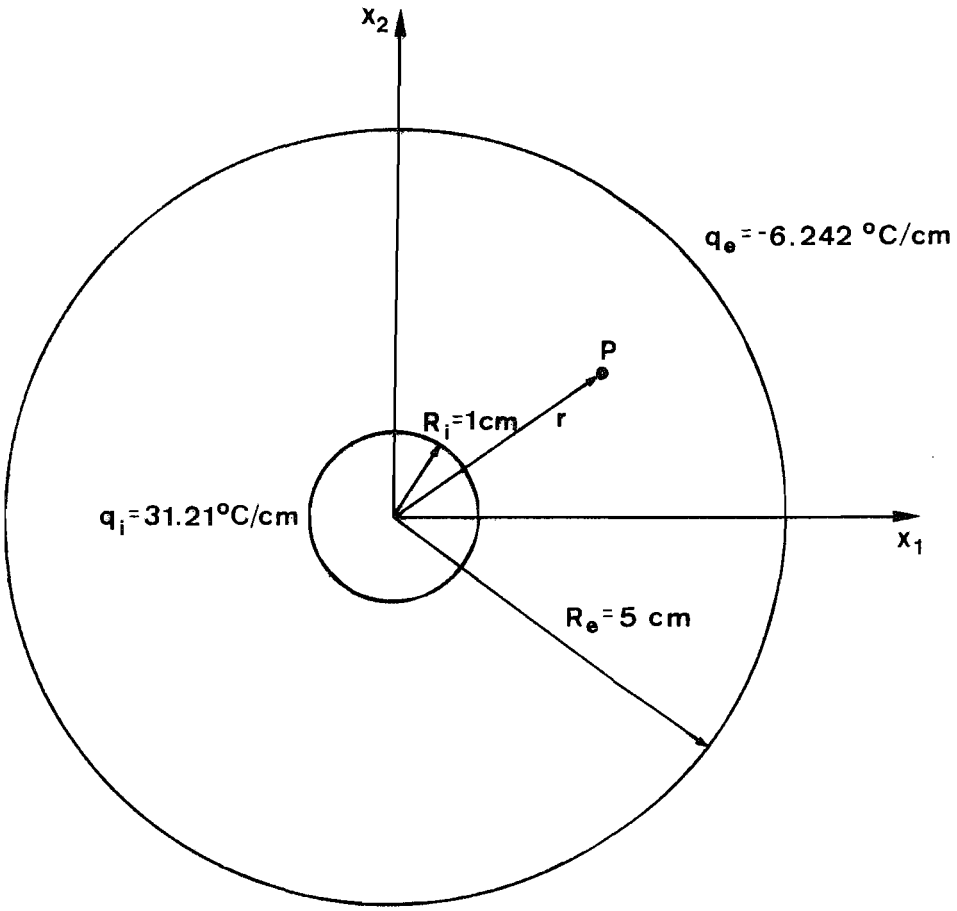

Figure 3.1.7 - Geometry and boundary conditions of circular region

r	BEM (N=4)	BEM (N=8)	EXACT
1.0	70.17	70.28	70.25
1.5	55.99	57.60	57.60
2.0	47.18	48.66	48.62
2.5	40.35	41.72	41.66
3.0	34.75	36.03	35.96
3.5	30.00	31.20	31.15
4.0	25.80	27.00	26.99
4.5	23.18	23.27	23.31

Table 3.1.1 - Temperature along the x_1-axis

r	BEM (N=4)	BEM (N=8)	EXACT
1.5	20.43	20.70	20.81
2.0	15.30	15.54	15.61
2.5	12.27	12.46	12.48
3.0	10.24	10.42	10.40
3.5	8.88	8.96	8.92
4.0	7.77	7.89	7.80
4.5	7.07	6.74	6.94

Table 3.1.2 - Radial flux along the x_1-axis

i.e. the rows of $\underset{\sim}{H}$ are linearly dependent. Indeed, each row of $\underset{\sim}{H}$ is a linear combination of the other N-1 rows of the matrix. Then any N-1 of these equations, coupled with the above 'normalising' condition, may be solved directly for the N boundary values of u.

Results for the temperature and radial flux for two different discretisations using constant elements are given in tables 3.1.1 and 3.1.2, respectively. The value of the constant c = 70.25 was introduced by prescribing u = 20°C at a node on the outer boundary.

Example 3.1.3

A case of mixed boundary conditions, i.e. u prescribed on part Γ_1 and q on part Γ_2 of a boundary Γ was considered in this example of a rectangular region with cross-section and boundary conditions as shown in figure 3.1.8.

Since the normal flux along the face $x_2 = 0.$ presents a singularity at the point $x_1 = 1.$, the discretisation adopted concentrates more elements around the singular point, as is usually done with finite elements. The problem was studied with 60 linear elements, with the following boundary sub-division: 32 elements of equal length along the faces $x_1 = 0.$, $x_1 = 2.$ and $x_2 = 1.$; 28 elements along the face $x_2 = 0.$, being 5 of equal length at $0. \leq x_1 \leq 0.5$ and 9 of decreasing logarithmic length at $0.5 \leq x_1 \leq 1.$, with the remaining 14 symmetrically located with respect to the singular point $x_1 = 1.$

Results for the function u are presented in figure 3.1.10, compared to an accurate solution obtained by conformal transformation [55]. The normal flux distribution along the face $x_2 = 0.$ is plotted in figure 3.1.9 and it can be seen that it represents well the singularity. The discontinuity on the boundary conditions at the singular point and at the three corners (2.;1.), (0.;1.) and (0.;0.) was taken into account through the use of double nodes (see chapter 6).

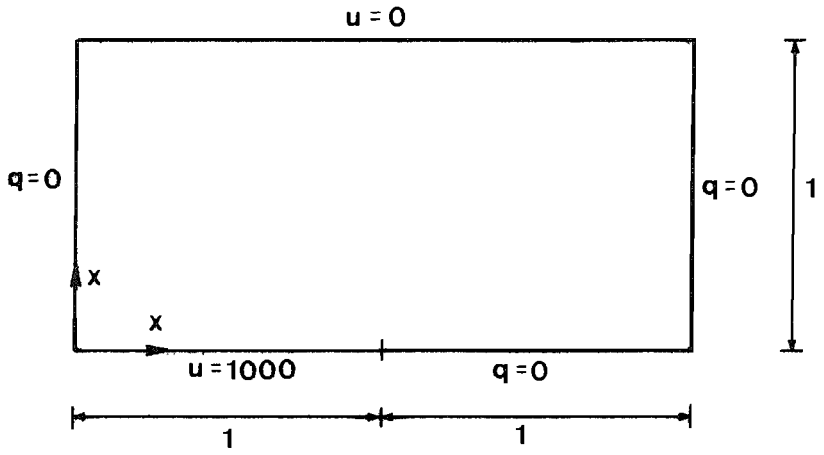

Figure 3.1.8 - Geometry and boundary conditions of rectangular region

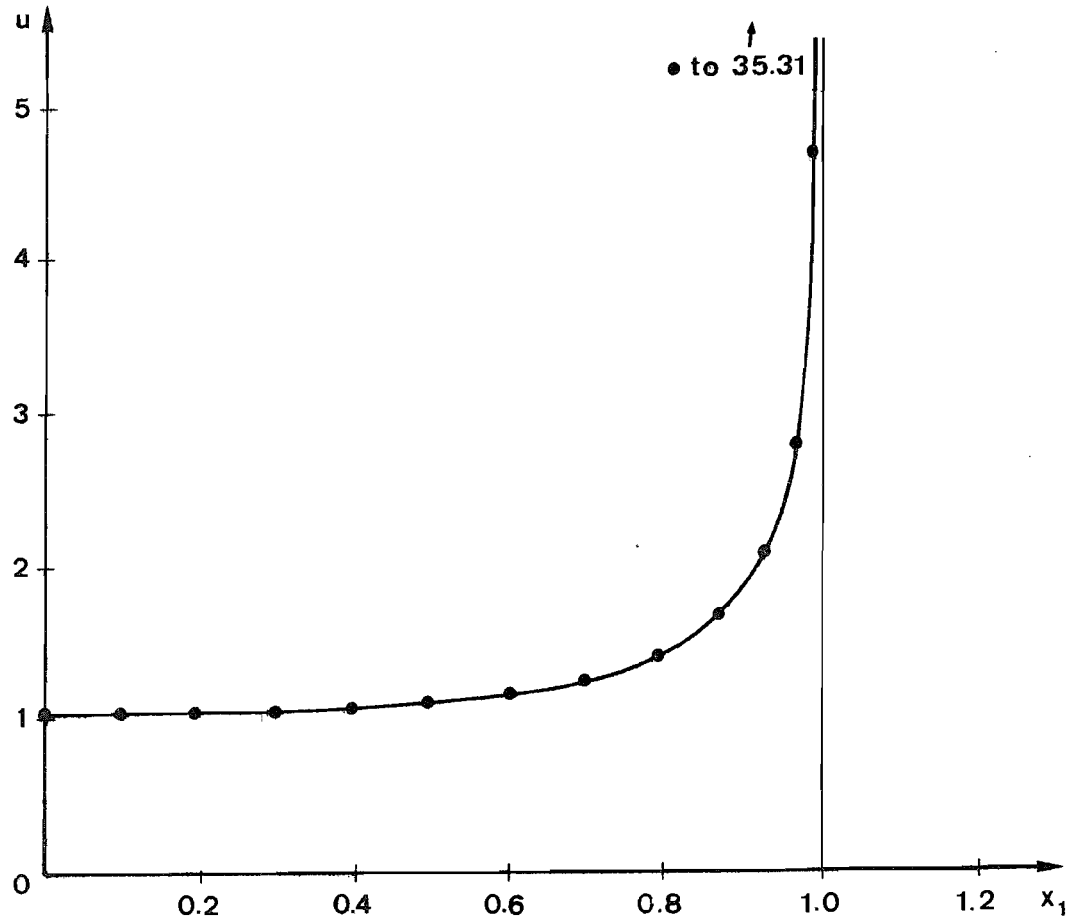

Figure 3.1.9 - Normal flux along the face $x_2=0$

0	0	0	0	0	0	0	0	0	0	0
193	192	187	179	166	148	127	107	92	82	79
193	192	187	178	166	148	127	107	92	82	79
388	386	378	363	337	299	254	211	178	157	150
388	386	378	362	336	298	253	210	177	157	150
588	585	577	558	520	457	377	303	250	219	209
588	585	577	558	520	457	376	303	250	219	209
792	791	785	770	734	638	489	374	301	261	247
792	791	785	770	733	637	488	373	300	260	247
						547	402	319	275	261
1000	1000	1000	1000	1000	1000	546	401	318	275	261

BEM
REF. [56]

Figure 3.1.10 - Values of u at boundary and internal points

The accuracy of the boundary element solution can be further improved through an analytical treatment of the singularity [1] which follows basically the same ideas as employed for the finite element method [56].

3.2 Special Boundary Conditions

Up to now, we have only dealt with the solution of problems with boundary conditions of the Neumann, Dirichlet or Cauchy types. This is not a restriction to the method presented and other boundary conditions that frequently appear on practical problems, such as Robin-type conditions and free surfaces, can easily be incorporated [29], [57], [58], [59].

The Robin condition prescribes a linear combination of the potential and its normal derivative at points along the boundary Γ as,

$$au + bq = d \tag{3.2.1}$$

where a, b and d are functions of $\underset{\sim}{x}$. Notice that (3.2.1) includes all previous boundary conditions, since for b = 0 it becomes the Dirichlet condition (2.2.2) while for a = 0 we have the Neumann condition (2.2.3). Physically, relation (3.2.1) can be recognised as the impedance boundary condition of electromagnetic problems, the convection or 'radiation' boundary condition of heat conduction problems, etc.

If equation (3.2.1) is applied at all boundary nodes, we can write,

$$\underset{\sim}{Q} = \underset{\sim}{D} - \underset{\sim}{A}\,\underset{\sim}{U} \tag{3.2.2}$$

where the vector $\underset{\sim}{D}$ and the diagonal matrix $\underset{\sim}{A}$ contain the values of d/b and a/b, respectively, at each boundary node.

Substituting (3.2.2) into (3.1.8) yields the system of equations,

$$(\underset{\sim}{H} + \underset{\sim}{G}\underset{\sim}{A})\,\underset{\sim}{U} = \underset{\sim}{G}\,\underset{\sim}{D} \tag{3.2.3}$$

or, more simply,

$$\underset{\sim}{K}\,\underset{\sim}{U} = \underset{\sim}{F} \tag{3.2.4}$$

In computational terms, the system matrix $\underset{\sim}{K}$ and the vector $\underset{\sim}{F}$ can be assembled directly so that equation (3.2.3) is not actually formed (see chapter 6). After solving the system of equations (3.2.4), the normal derivatives of potentials along the boundary can be evaluated pointwise by applying condition (3.2.1).

Free surfaces are generally related to problems of groundwater flow through saturated, unconfined porous media governed by Darcy's law [60]. If the medium under consideration is homogeneous and isotropic, the problem is reduced to that of Laplace's equation for a velocity potential u with boundary conditions of the following types (figure 3.2.1): $q = 0$ at impervious boundaries, such as the surface of soil strata and rocks (surface AF in the figure); u = constant at water boundaries (the upstream and downstream faces ABC and EF of the porous domain); $u = x_2$ at the seepage face DE where the water seeps out of the soil into the air; $u = x_2$ and $q = 0$ at the free surface CD. In addition, the exact position of the free surface is not known a priori and its determination becomes part of the analysis of the problem.

These free surface conditions are also valid for problems such as flow over spillways when the velocity head can be neglected, i.e. when the height of water over the nappe is small by comparison with the spillway height [61].

For the numerical solution of these problems, an initial position of the free surface is arbitrarily assumed and the condition $q = 0$ applied at all points on it. The calculated potential at every nodal point at the free surface is then compared with its elevation; if the difference between these two values is greater than a maximum acceptable error, this difference is algebraically added to the elevation of the nodal point and a new iteration is carried out.

Notice that the coefficients of matrices $\underset{\sim}{G}$ and $\underset{\sim}{H}$ in equation (3.1.8) corresponding to the influence of fixed boundary nodes on other

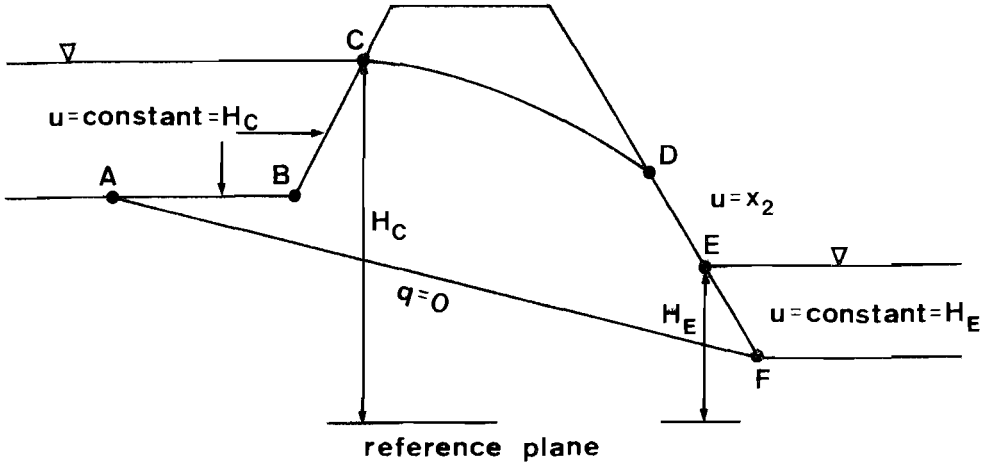

Figure 3.2.1 - Boundary conditions for free surface problem

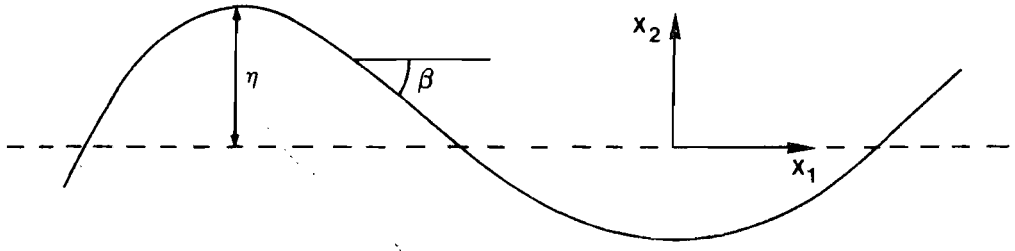

Figure 3.2.2 - Free surface elevation with relation to the x_1-axis

fixed boundary nodes remain constant during the analysis, hence they can be computed only once and stored. Potential values at internal points, if required, are calculated after the correct position of the free surface has been determined.

The Boundary Element Method may also be employed for transient free surface flow problems. For this case, the kinematic condition on the free surface is [60],

$$\frac{\partial \eta}{\partial t} = q_2 - q_1 \frac{\partial \eta}{\partial x_1} \tag{3.2.5}$$

where q_1, q_2 are the velocities in the x_1, x_2 directions and η is the elevation of the free surface with relation to an arbitrary plane (figure 3.2.2).

From geometric considerations we have that

$$\frac{\partial \eta}{\partial x_1} = - \tan \beta \tag{3.2.6}$$

in which β is the angle the free surface makes with the x_1-axis. Hence

$$\frac{\partial \eta}{\partial t} = - \frac{q}{\cos \beta} \tag{3.2.7}$$

where $q = \partial u/\partial n$ is the normal velocity.

Applying the condition $u = \eta$ at the free surface, equation (3.2.7) becomes,

$$\frac{\partial u}{\partial t} = - \frac{q}{\cos \beta} \tag{3.2.8}$$

This equation can be written in finite difference form as,

$$u^{t+\Delta t} = u^t - \frac{\Delta t}{\cos \beta^t} \left[\theta \, q^{t+\Delta t} + (1-\theta) \, q^t\right] \tag{3.2.9}$$

where θ is a weighting factor that positions the derivative between the time levels t and $t+\Delta t$. In the equation, the angle β is computed at time t even though the equation is written for the time $t+\Delta t$. Although this problem can be avoided by iteration, the use of a small time step provides sufficient accuracy [58].

As an example of how the free surface boundary condition in the form of equation (3.2.9) can be introduced into (3.1.8), consider the problem represented by figure 3.2.1 where we assume that there is a drawdown in the upstream water level. Equation (3.1.8) can be rearranged for this problem as,

$$\begin{bmatrix} -G_{ABC} & -G_{CD} & -G_{DE} & -G_{EF} & H_{AF} \end{bmatrix} \begin{Bmatrix} q_{ABC} \\ q_{CD}^{t+\Delta t} \\ q_{DE} \\ q_{EF} \\ u_{AF} \end{Bmatrix} \tag{3.2.10}$$

$$= \begin{bmatrix} -H_{ABC} & -H_{CD} & -H_{DE} & -H_{EF} & G_{AF} \end{bmatrix} \begin{Bmatrix} u_{ABC} \\ u_{CD}^{t+\Delta t} \\ u_{DE} \\ u_{EF} \\ q_{AF} \end{Bmatrix}$$

Substituting $u_{CD}^{t+\Delta t}$ by its value on equation (3.2.9) yields,

$$\begin{bmatrix} -G_{ABC} & -(G_{CD} + H_{CD} \frac{\theta \Delta t}{\cos \beta^t}) & -G_{DE} & -G_{EF} & H_{AF} \end{bmatrix} \begin{Bmatrix} q_{ABC} \\ q_{CD}^{t+\Delta t} \\ q_{DE} \\ q_{EF} \\ u_{AF} \end{Bmatrix} \tag{3.2.11}$$

$$= \begin{bmatrix} -H_{ABC} & -H_{CD} & -H_{DE} & -H_{EF} & G_{AF} \end{bmatrix} \begin{Bmatrix} u_{ABC} \\ u_{CD}^{t} - \frac{(1-\theta)\Delta t}{\cos \beta^t} q_{CD}^{t} \\ u_{DE} \\ u_{EF} \\ q_{AF} \end{Bmatrix}$$

Since all boundary-values on the right-hand side of (3.2.11) are known, the equation can be solved and the normal velocities along the free surface at time $t+\Delta t$ computed. Condition (3.2.9) is then employed to find the potential values at the free surface and the computation cycle is completed, so that the solution can be advanced on time. Numerical results using this formulation are given in [58].

Example 3.2.1

This application deals with a concrete column of rectangular cross-section where part of the boundary surface is subjected to an interior ambient condition, another part is subjected to outside weather conditions and the remainder is in contact with an abutting wall which separates both. The boundary conditions of the problem are of the 'radiation' type,

$$q + hu = hu_s \qquad (3.2.12)$$

where h is the heat transfer coefficient and u_s is the temperature of the surrounding medium.

The temperature and surface heat transfer coefficient on the interior face ($x_1 = 0$) are 100^oF and 0.5 Btu/h $ft^{2o}F$, respectively, and at the exterior face ($x_1 = \ell$) are 0^oF and 6.0 Btu/h $ft^{2o}F$. The variation of the temperature and surface heat transfer coefficient along the faces $x_2 = \pm a$ is indicated in figure 3.2.3. Note that the thermal conductivity was assumed to be 1.0 Btu/h ft^oF.

Results corresponding to three different positions for the abutting wall are presented in figure 3.2.4, compared with finite elements results [62] and an analytical solution [63] (in terms of a mean temperature over the width of the cross-section). The boundary elements analyses were performed by discretising one half of the column into 20 linear elements (see figure 3.2.3), taking into account the symmetry with respect to the x_1-axis, while the finite elements

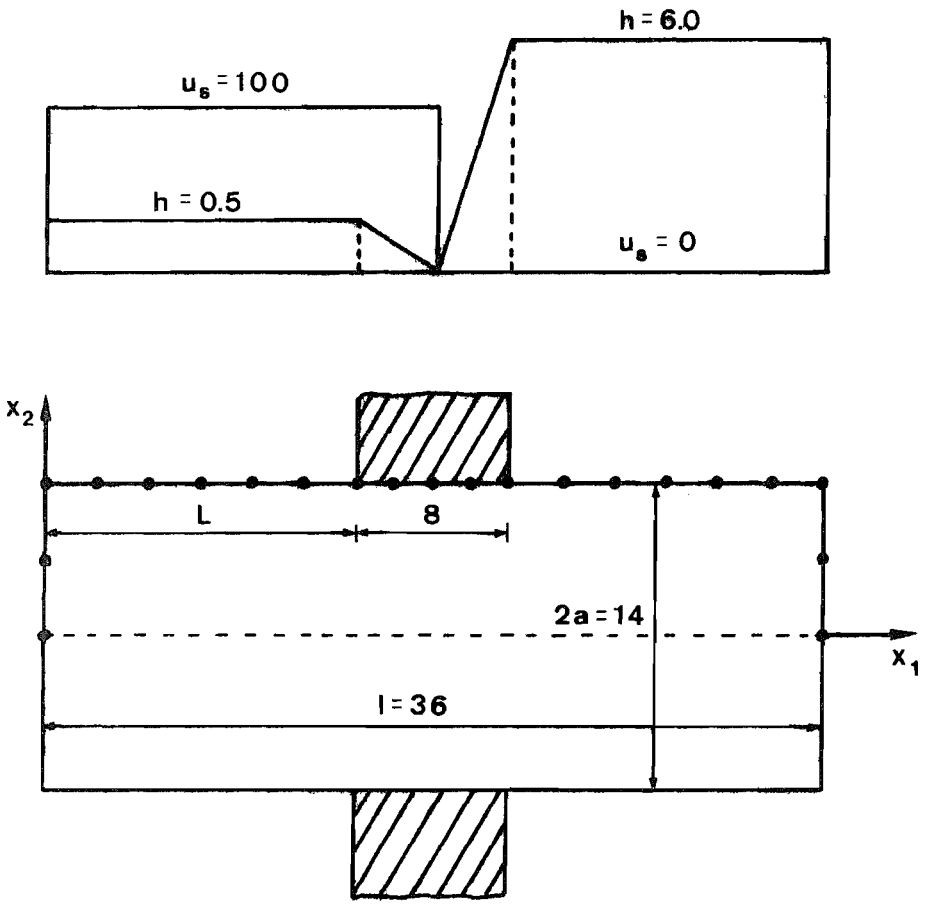

Figure 3.2.3 - Geometry, discretisation and boundary conditions for rectangular concrete column

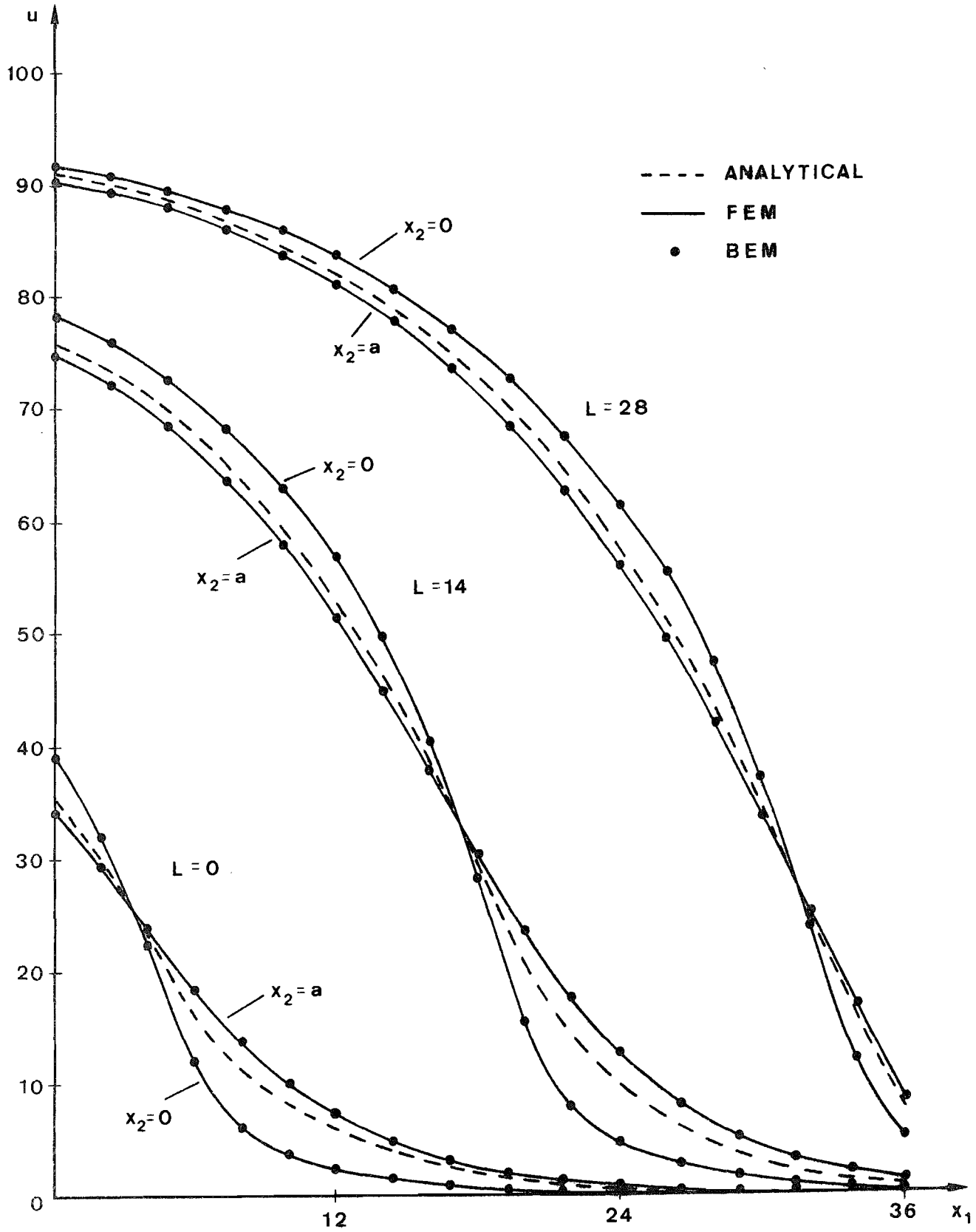

Figure 3.2.4 - Temperature distribution for three different positions of the abutting wall

ones employed 252 quadrilateral elements. The discontinuity on the value of u_s at the middle of the wall was taken into account through a double node.

Example 3.2.2

Figure 3.2.5 shows the linear boundary elements discretisation for a problem of free surface flow through a block of porous medium. The upstream and downstream water levels are maintained at 19.7 in and 1.3 in, respectively, above the horizontal impervious base. The boundary conditions of the problem are: $u = 19.7$ on the upstream face (nodes 22 to 26); $q = 0$ on the bottom (impervious) surface (nodes 1 to 8); $u = 1.3$ on the downstream face (nodes 9 and 10); $q = 0$ on the free surface (nodes 11 to 21). Note that the initial shape of the free surface was arbitrarily assumed to be a straight line and its initial position was also guessed. The final position of the free surface was obtained by iteration as previously explained.

Results are presented in figure 3.2.6 together with a finite element solution and an experimental solution obtained from an analogue model [64]. After the seventh iteration the maximum difference between the computed potential head and the elevation of each node along the free surface was less than 0.1% of the elevation and the solution was terminated.

3.3 Internal Sources

Assuming that there exist sources inside the domain Ω, as for instance internal heat generation for heat conduction problems, the governing equation of the problem becomes a Poisson-type equation,

$$\nabla^2 u = p \qquad \text{in } \Omega \qquad (3.3.1)$$

where p is a function of the position.

Boundary-value problems for Poisson's equation may be reduced to similar problems for Laplace's equation by subtracting out a particular solution independent of the boundary conditions [1], [40].

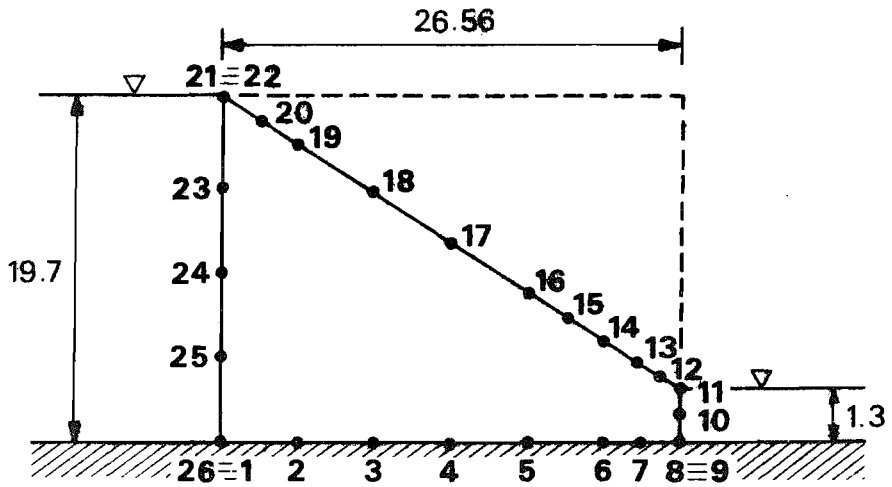

Figure 3.2.5 - Boundary elements discretisation of soil block with a free surface

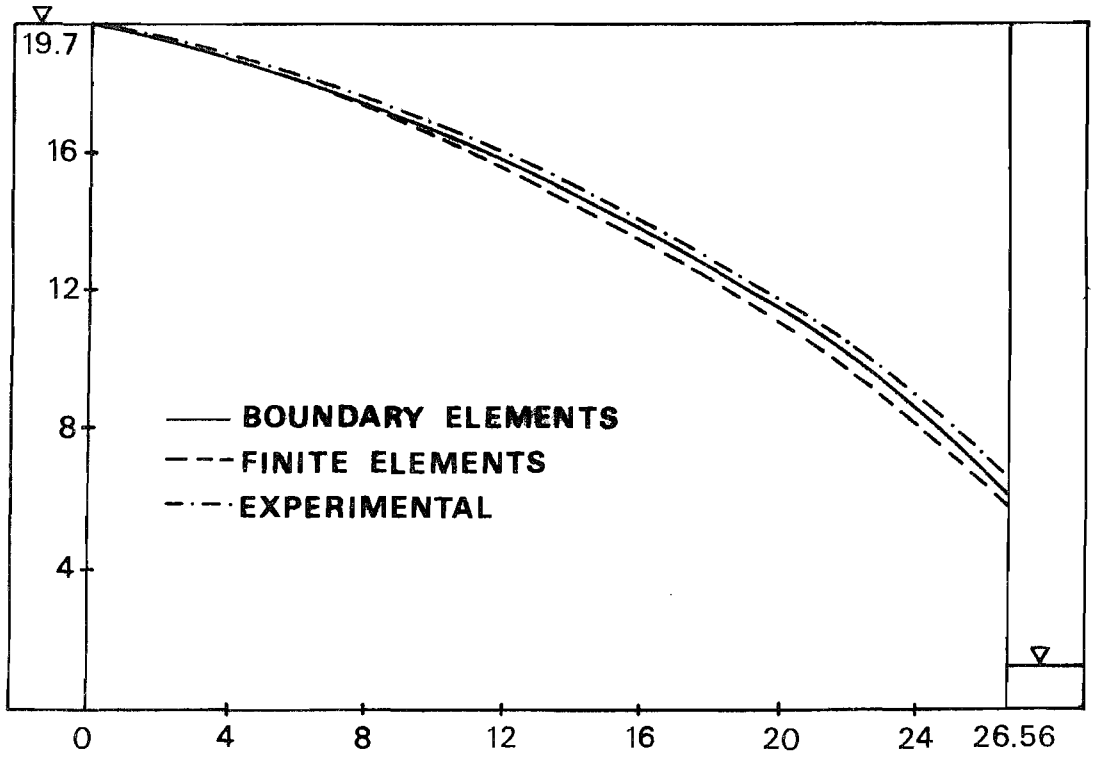

Figure 3.2.6 - Converged solution for the free surface

For some practical problems, it may occur that the function p is only defined pointwise such that a particular solution of the problem is difficult to be found. For these cases, equation (3.1) can be generalised to include a domain integral involving function p of the form [2],

$$\int_{\Omega} p(s)\ u^*(P,s)\ d\Omega(s) \tag{3.3.2}$$

to be added to the left-hand side of equation (3.1).

The above integral can be performed by sub-dividing the domain Ω into a series of cells over which a numerical integration formula can be applied.

In this work, triangular cells were employed to discretise the domain and the numerical integration carried out by applying Hammer's scheme [65] as follows,

$$\int_{\Omega_\ell} p(\underset{\sim}{x})\ u^*(\underset{\sim}{x})\ d\Omega = \int_0^1 \left[\int_0^{1-\xi_2} p(\underset{\sim}{\xi})\ u^*(\underset{\sim}{\xi})\ |J|\ d\xi_1 \right] d\xi_2 = \sum_{k=1}^{K} |J|_k\ W_k\ (pu^*)_k \tag{3.3.3}$$

where $\underset{\sim}{\xi}$ are intrinsic triangular coordinates and J is the Jacobian relating the elements of area in the two (cartesian and intrinsic) systems of coordinates.

Example 3.3.1

The equation of motion of a uniform incompressible viscous fluid in steady unidirectional flow (in the x_3-direction) is [66],

$$-\frac{\partial p}{\partial x_3} + \mu \left(\frac{\partial^2 u}{\partial x_1^2} + \frac{\partial^2 u}{\partial x_2^2}\right) = 0$$

where μ is the viscosity of the fluid, $\partial p/\partial x_3 = -G$ is a constant pressure gradient and u is the velocity component in the x_3-direction. This equation can be rewritten as,

$$\nabla^2 u = -\frac{G}{\mu}$$

For a pipe of elliptical cross-section the velocity distribution is of the form,

$$u = \frac{G}{2\mu(a^{-2}+b^{-2})}\left(1 - \frac{x_1^2}{a^2} - \frac{x_2^2}{b^2}\right)$$

where a and b are the semi-axes of the ellipse.

Taking the value of the constant $G/\mu = 2$ and the semi-axes $a = 2$ and $b = 1$, the problem to be solved is

$$\nabla^2 u = -2$$

with boundary conditions,

$$u = 0 \qquad \text{on } \Gamma$$

The solution of the above Poisson's equation can be divided into two parts,

$$u = u_1 + u_2$$

where $u_1 = -(x_1^2 + x_2^2)/2$ is a particular solution and u_2 a complementary one, which satisfies $\nabla^2 u_2 = 0$ with boundary condition $u_2 = -u_1$ on Γ.

Results for the velocity u and for the derivatives $\partial u/\partial x_1$ and $\partial u/\partial x_2$ (necessary for the evaluation of the tangential stresses $\tau_{x_1x_3}$ and $\tau_{x_2x_3}$) are presented in tables 3.3.1 to 3.3.3, compared to the analytical solution. Both previously discussed approaches were used and for the second, the domain was divided into 12 cells and a quintic (seven points) numerical integration scheme employed. Sub-dividing the domain into more cells or employing a more refined numerical integration scheme resulted in no significant improvement of the solution. Due to the double symmetry of the problem, only one quarter of the cross-section needed to be analysed.

Example 3.3.2

Flow in lakes and other water bodies can be approximated to provide an initial estimate of the circulation, which can then be checked against the full shallow-water equations. This flow is governed by the

x_1	x_2	BEM 1 (N=4)	BEM 1 (N=8)	BEM 2 (N=4)	BEM 2 (N=8)	EXACT
1.50	0.	0.334	0.345	0.353	0.351	0.350
1.20	0.35	0.401	0.410	0.422	0.416	0.414
0.90	0.	0.626	0.634	0.646	0.640	0.638
0.60	0.45	0.557	0.563	0.576	0.569	0.566
0.30	0.	0.772	0.778	0.791	0.784	0.782
0.	0.45	0.629	0.634	0.648	0.641	0.638
0.	0.	0.791	0.797	0.809	0.802	0.800

Table 3.3.1 - Results for velocity u

x_1	x_2	BEM 1 (N=4)	BEM 1 (N=8)	BEM 2 (N=4)	BEM 2 (N=8)	EXACT
2.00	0.	0.759	0.762	0.805	0.788	0.800
1.50	0.	0.602	0.597	0.621	0.604	0.600
1.20	0.35	0.490	0.482	0.485	0.481	0.480
0.90	0.	0.370	0.366	0.364	0.361	0.360
0.60	0.45	0.255	0.253	0.241	0.240	0.240
0.30	0.	0.119	0.118	0.121	0.120	0.120
0.	0.	0.000	0.000	0.000	0.000	0.000

Table 3.3.2 - Results for derivative $\partial u/\partial x_1$ (-)

x_1	x_2	BEM 1 (N=4)	BEM 1 (N=8)	BEM 2 (N=4)	BEM 2 (N=8)	EXACT
0.	1.00	1.611	1.582	1.608	1.604	1.600
0.60	0.45	0.715	0.718	0.719	0.720	0.720
0.	0.45	0.720	0.722	0.719	0.720	0.720
1.20	0.35	0.562	0.562	0.553	0.558	0.560
0.	0.	0.000	0.000	0.000	0.000	0.000

Table 3.3.3 - Results for derivative $\partial u/\partial x_2$

* BEM 1 - domain sub-divided into 12 cells

BEM 2 - solution divided into particular and complementary

following linearised equations, obtained by neglecting the inertia terms in the momentum equations [60],

$$- f\, q_2 = \rho\, g\, H \frac{\partial \eta}{\partial x_1} + (\tau_1^s - \tau_1^b) = 0$$

$$f\, q_1 = \rho\, g\, H \frac{\partial \eta}{\partial x_2} + (\tau_2^s - \tau_2^b) = 0$$

and the continuity formula,

$$\frac{\partial q_1}{\partial x_1} + \frac{\partial q_2}{\partial x_2} = 0$$

where:

f = Coriolis parameter

q_1, q_2 = vertically integrated velocity components in the x_1, x_2 directions

ρ = mass density

g = acceleration of gravity

$H = h + \eta$ = total depth of water

h = depth with relation to the mean water level

η = elevation of the free surface

τ^s = wind stresses

τ^b = bottom friction stresses

If the η values are much smaller than the h we can write $H \simeq h$, hence

$$\begin{aligned} - f\, q_2 + \rho\, gh \frac{\partial \eta}{\partial x_1} + (\tau_1^s - \tau_1^b) &= 0 \\ f\, q_1 + \rho\, gh \frac{\partial \eta}{\partial x_2} + (\tau_2^s - \tau_2^b) &= 0 \end{aligned} \qquad (3.3.4)$$

Assuming the τ^b terms to be linearly proportional to the mean momentum components,

$$\tau_1^b = \gamma q_1 \,, \quad \tau_2^b = \gamma q_2$$

we can cross-differentiate equations (3.3.4) and afterwards subtract both equations. Assuming that the derivatives of h are negligible (i.e. the bottom slope is small) this gives, taking continuity into consideration, the following equation,

$$\frac{\partial \tau_1^s}{\partial x_2} - \frac{\partial \tau_2^s}{\partial x_1} = \gamma \left(\frac{\partial q_1}{\partial x_2} - \frac{\partial q_2}{\partial x_1} \right) \tag{3.3.5}$$

We can propose a stream function ψ such that

$$q_1 = \frac{\partial \psi}{\partial x_2} \quad , \quad q_2 = - \frac{\partial \psi}{\partial x_1}$$

and formula (3.3.5) becomes,

$$\nabla^2 \psi = \frac{1}{\gamma} w(x_1, x_2) \tag{3.3.6}$$

where

$$w(x_1, x_2) = \frac{\partial \tau_1^s}{\partial x_2} - \frac{\partial \tau_2^s}{\partial x_1}$$

Note that we have included the Coriolis parameter but assumed it constant for all the lake, i.e. the lake is small enough to allow the neglect of local variations in the Coriolis forces. If we take,

$$X_1 = \frac{x_1}{L} \quad , \quad X_2 = \frac{x_2}{L}$$

$$W(X_1 , X_2) = \frac{w(x_1, x_2)}{T/L}$$

$$\psi = \frac{\psi}{(f\varepsilon/2H^2)^{\frac{1}{2}} L^2}$$

L being the lateral characteristic length of the lake, T the characteristic wind stress and ε the eddy viscosity coefficient, equation (3.3.6) takes the non-dimensional form,

$$\nabla^2 \psi = \frac{1}{\delta} W(X_1, X_2) \tag{3.3.7}$$

where

$$\delta = \frac{\gamma L (f\varepsilon/2)^{\frac{1}{2}}}{TH}$$

We analysed, using the above formulation, the wind circulation in Lagoa dos Patos, Brazil (figure 3.3.1a). As a first numerical example, we calculate the stream lines for the flow in and out of the lake without wind effects, taking $\psi = 0$ for the west shore and $\psi = 1$ for the east shore. Results are shown in figure 3.3.1b. For this case, the governing equation becomes a Laplace equation.

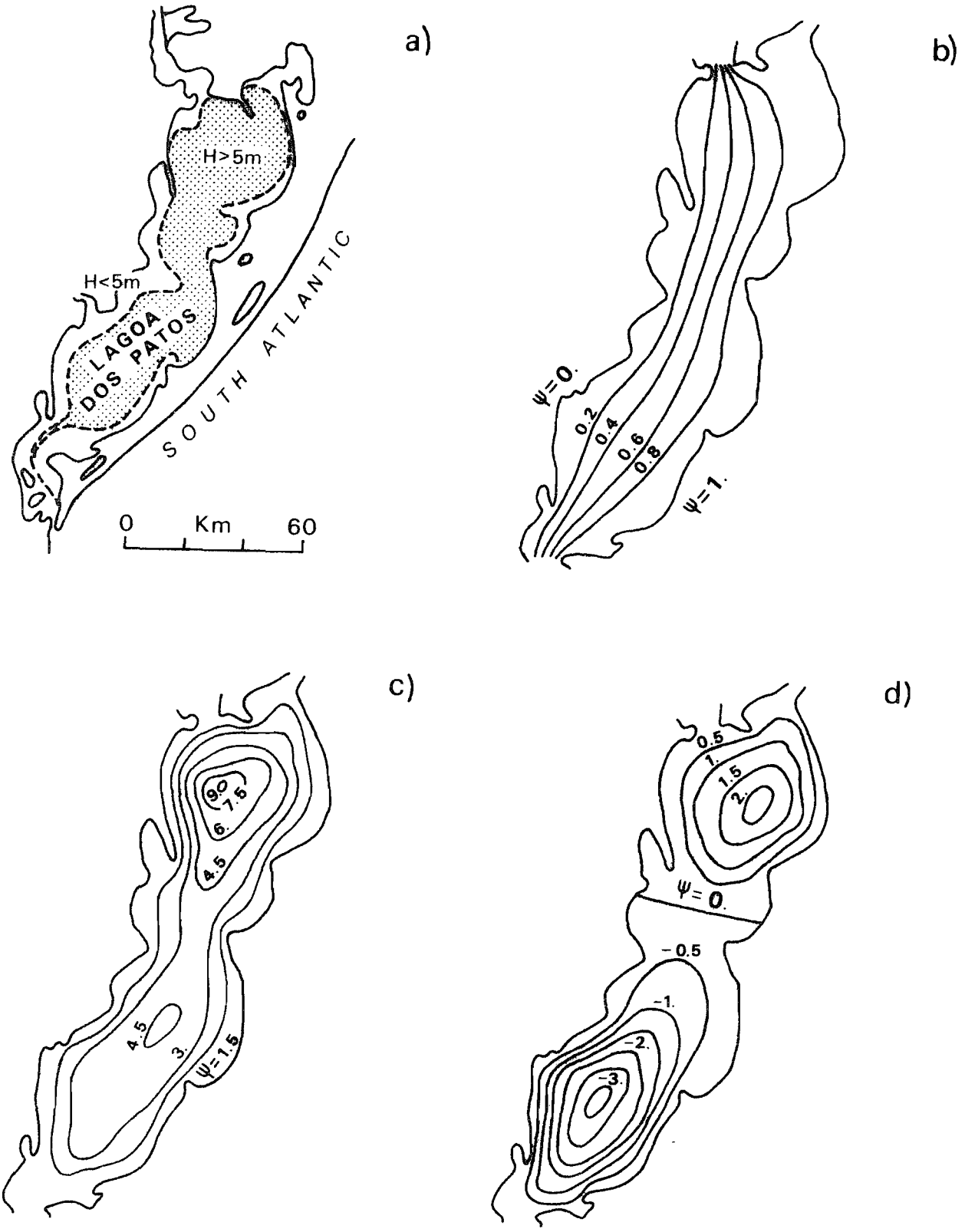

Figure 3.3.1 - Lagoa dos Patos: a) Geometry; b) Flow pattern for potential flow; c) Wind driven mean circulation pattern due to a linear stress distribution; d) Wind driven mean circulation pattern due to a quadratic stress distribution

If we consider the right-hand side of equation (3.3.7) equal to 1, X_1 and X_2, this allows for a superposition of three different sets of results in order to obtain any solution of the type,

$$\nabla^2\psi = A + BX_1 + CX_2$$

where the right-hand side represents a quadratic wind stress distribution. Results are shown in figure 3.3.1c for a linear wind stress distribution, A = 1, B = C = 0, and in figure 3.3.1d for a quadratic wind stress distribution, A = 1, B = -3, C = 0. All the previous results were obtained by discretising the boundary of the lake using 93 linear elements and subtracting out a particular solution of equation (3.3.7).

3.4 Sub-Regions

If the problem under consideration is defined over a region which is only piecewise homogeneous, the numerical procedures described can be applied to each homogeneous sub-region as they were separated from the others. The final system of equations for the whole region is obtained by adding the set of equations (3.1.8) for each sub-region together with compatibility and equilibrium conditions between their interfaces [2], [26].

To illustrate these ideas in more detail, consider for simplicity a region Ω consisting of two sub-regions Ω^1 and Ω^2 (figure 3.4.1). Over sub-region Ω^1, we define:

$\underset{\sim}{U}^1$, $\underset{\sim}{Q}^1$ - nodal potentials and fluxes ($q_1 = -k_1\ \partial u_1/\partial n$) at the external boundary Γ^1;

$\underset{\sim}{U}^1_I$, $\underset{\sim}{Q}^1_I$ - nodal potentials and fluxes at the interface Γ_I, considering it belongs to Ω^1;

Similarly, we define over sub-region Ω^2:

$\underset{\sim}{U}^2$, $\underset{\sim}{Q}^2$ - nodal potentials and fluxes ($q_2 = -k_2\ \partial u_2/\partial n$) at the external boundary Γ^2;

$\underset{\sim}{U}_I^2$, $\underset{\sim}{Q}_I^2$ - nodal potentials and fluxes at the interface Γ_I, considering it belongs to Ω^2;

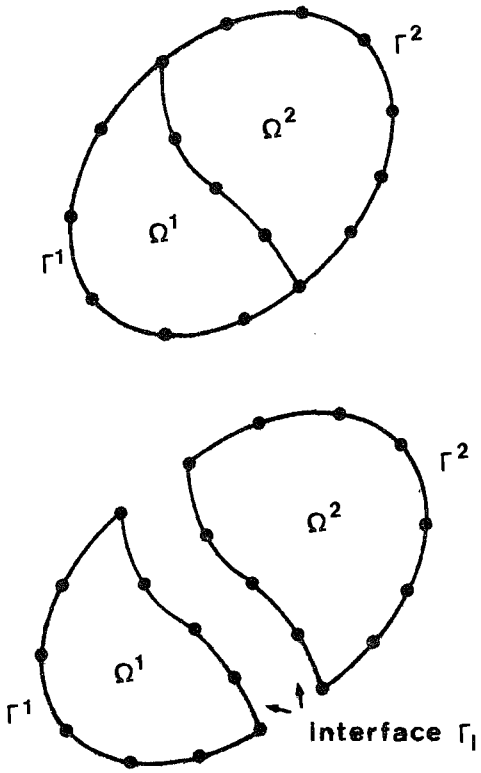

Figure 3.4.1 - Domain divided into two sub-regions

The system of equations (3.1.8) corresponding to sub-region Ω^1 can be written as,

$$\left[\underset{\sim}{H}^1 \; \underset{\sim}{H}_I^1\right] \begin{Bmatrix} \underset{\sim}{U}^1 \\ \underset{\sim}{U}_I^1 \end{Bmatrix} = \left[\underset{\sim}{G}^1 \; \underset{\sim}{G}_I^1\right] \begin{Bmatrix} \underset{\sim}{Q}^1 \\ \underset{\sim}{Q}_I^1 \end{Bmatrix} \tag{3.4.1}$$

where, assuming that there are N_1 and N_I boundary nodes over surfaces Γ^1 and Γ_I, respectively, the dimensions of matrices $\underset{\sim}{H}^1$ and $\underset{\sim}{G}^1$ are $(N_1 + N_I) \times N_1$ and of matrices $\underset{\sim}{H}_I^1$ and $\underset{\sim}{G}_I^1$ are $(N_1 + N_I) \times N_I$.

For sub-region Ω^2, we have

$$\left[\underset{\sim}{H}^2 \; \underset{\sim}{H}_I^2\right] \begin{Bmatrix} \underset{\sim}{U}^2 \\ \underset{\sim}{U}_I^2 \end{Bmatrix} = \left[\underset{\sim}{G}^2 \; \underset{\sim}{G}_I^2\right] \begin{Bmatrix} \underset{\sim}{Q}^2 \\ \underset{\sim}{Q}_I^2 \end{Bmatrix} \tag{3.4.2}$$

where the dimensions of matrices $\underset{\sim}{H}^2$ and $\underset{\sim}{G}^2$ are $(N_2 + N_I) \times N_2$ and of matrices $\underset{\sim}{H}_I^2$ and $\underset{\sim}{G}_I^2$ are $(N_2 + N_I) \times N_I$.

The compatibility and equilibrium conditions to be applied at the interface Γ_I between Ω^1 and Ω^2 are, respectively,

$$\begin{aligned} \underset{\sim}{U}_I^1 &= \underset{\sim}{U}_I^2 = \underset{\sim}{U}_I \\ \underset{\sim}{Q}_I^1 &= -\underset{\sim}{Q}_I^2 = \underset{\sim}{Q}_I \end{aligned} \tag{3.4.3}$$

Equations (3.4.1) to (3.4.3) can be combined to form the system,

$$\begin{bmatrix} \underset{\sim}{H}^1 & \underset{\sim}{H}_I^1 & \underset{\sim}{0} \\ \underset{\sim}{0} & \underset{\sim}{H}_I^2 & \underset{\sim}{H}^2 \end{bmatrix} \begin{Bmatrix} \underset{\sim}{U}^1 \\ \underset{\sim}{U}_I \\ \underset{\sim}{U}^2 \end{Bmatrix} = \begin{bmatrix} \underset{\sim}{G}^1 & \underset{\sim}{G}_I^1 & \underset{\sim}{0} \\ \underset{\sim}{0} & -\underset{\sim}{G}_I^2 & \underset{\sim}{G}^2 \end{bmatrix} \begin{Bmatrix} \underset{\sim}{Q}^1 \\ \underset{\sim}{Q}_I \\ \underset{\sim}{Q}^2 \end{Bmatrix} \tag{3.4.4}$$

or, more simply,

$$\underset{\sim}{H}\ \underset{\sim}{U} = \underset{\sim}{G}\ \underset{\sim}{Q} \tag{3.4.5}$$

This system of equations is formally similar to (3.1.8) except that the matrices $\underset{\sim}{H}$ and $\underset{\sim}{G}$ are now banded. By imposing the boundary conditions of the problem and remembering that both the potentials and fluxes at the interface are considered as unknowns, the system (3.4.4) can be reordered as,

$$\begin{bmatrix} \underset{\sim}{H}^1 & \underset{\sim}{H}_I^1 & -\underset{\sim}{G}_I^1 & \underset{\sim}{0} \\ \underset{\sim}{0} & \underset{\sim}{H}_I^2 & \underset{\sim}{G}_I^2 & \underset{\sim}{H}^2 \end{bmatrix} \begin{Bmatrix} \underset{\sim}{U}^1 \\ \underset{\sim}{U}_I \\ \underset{\sim}{Q}_I \\ \underset{\sim}{U}^2 \end{Bmatrix} = \begin{bmatrix} \underset{\sim}{G}^1 & \underset{\sim}{0} \\ \underset{\sim}{0} & \underset{\sim}{G}^2 \end{bmatrix} \begin{Bmatrix} \underset{\sim}{Q}^1 \\ \underset{\sim}{Q}^2 \end{Bmatrix} \tag{3.4.6}$$

According to the prescribed boundary conditions, the sub-matrices corresponding to Γ^1 (and Γ^2) may interchange their positions. Notice that the final system matrix in (3.4.6) is also banded.

Detailed explanations of the computer implementation of the above procedures, including numerical results, can be found in [26], [67], [68].

3.5 Orthotropy and Anisotropy

Let us now assume that the medium over which the problem is defined is orthotropic (see figure 3.5.1). The governing equation in the

directions of orthotropy can be written as,

$$k_1 \frac{\partial^2 u}{\partial y_1^2} + k_2 \frac{\partial^2 u}{\partial y_2^2} = 0 \qquad (3.5.1)$$

for the two-dimensional case, being k_i the medium property coefficient in the direction of orthotropy i.

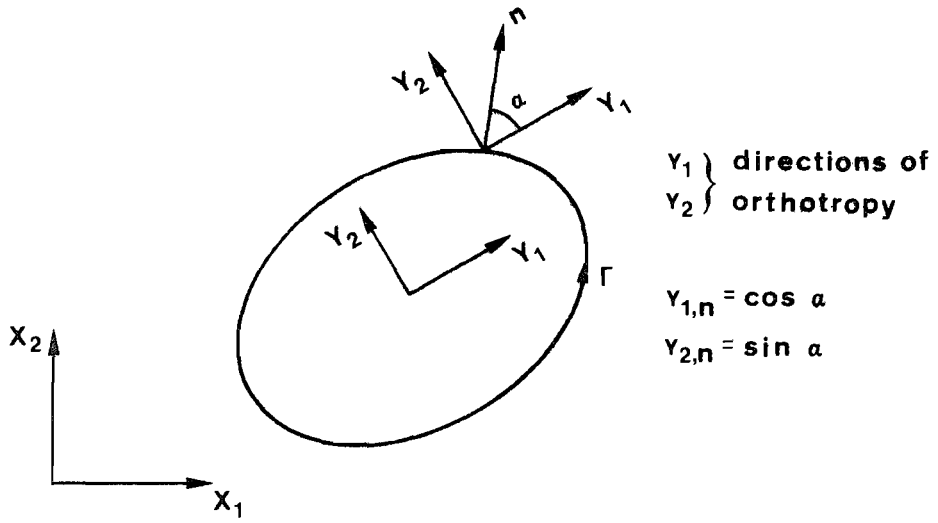

Figure 3.5.1 - Orthotropic medium

The fundamental solution to this equation is [2] (see also chapter 2, section 2.1),

$$u^*(p,s) = \frac{1}{(k_1 k_2)^{\frac{1}{2}}} \log \frac{1}{r(p,s)} \qquad (3.5.2)$$

where

$$r(p,s) = \left\{ \frac{1}{k_1} [y_1(p) - y_1(s)]^2 + \frac{1}{k_2} [y_2(p) - y_2(s)]^2 \right\}^{\frac{1}{2}} \qquad (3.5.3)$$

Applying the divergence theorem [13] to the terms of equation (3.5.1) yields,

$$\int_\Omega \left(k_1 \frac{\partial^2 u}{\partial y_1^2} + k_2 \frac{\partial^2 u}{\partial y_2^2} \right) d\Omega = \int_\Gamma \left(k_1 \frac{\partial u}{\partial y_1} y_{1,n} + k_2 \frac{\partial u}{\partial y_2} y_{2,n} \right) d\Gamma \qquad (3.5.4)$$

where $y_{1,n}$ and $y_{2,n}$ are the direction cosines of the outward normal n to surface Γ (figure 3.5.1). The term enclosed in brackets in the

right-hand side integral is the normal boundary flux q. Analogously, we can define

$$q^*(p,S) = k_1 \frac{\partial u^*(p,S)}{\partial y_1(S)} y_{1,n}(S) + k_2 \frac{\partial u^*(p,S)}{\partial y_2(S)} y_{2,n}(S) \tag{3.5.5}$$

The problem can then be solved in the same way as for isotropic problems, i.e. by transforming the governing equation (3.5.1) plus boundary conditions into a boundary integral equation similar to (3.1).

For fully anisotropic media, the governing equation becomes,

$$k_{11} \frac{\partial^2 u}{\partial x_1^2} + 2k_{12} \frac{\partial^2 u}{\partial x_1 \partial x_2} + k_{22} \frac{\partial^2 u}{\partial x_2^2} = 0 \tag{3.5.6}$$

for two-dimensional problems, the coefficients k_{ij} defining the medium properties. This equation has the following fundamental solution [27],

$$u^*(p,s) = \frac{1}{|k_{ij}|^{\frac{1}{2}}} \log \frac{1}{r(p,s)} \tag{3.5.7}$$

where $|k_{ij}|$ is the determinant of the medium property coefficients matrix and

$$r(p,s) = \left\{ \frac{1}{k_{11}} [x_1(p) - x_1(s)]^2 + \frac{2}{k_{12}} [x_1(p) - x_1(s)] [x_2(p) - x_2(s)] + \frac{1}{k_{22}} [x_2(p) - x_2(s)]^2 \right\}^{\frac{1}{2}} \tag{3.5.8}$$

The normal boundary flux q is now given by,

$$q = (k_{11} \frac{\partial u}{\partial x_1} + k_{12} \frac{\partial u}{\partial x_2}) x_{1,n} + (k_{12} \frac{\partial u}{\partial x_1} + k_{22} \frac{\partial u}{\partial x_2}) x_{2,n} \tag{3.5.9}$$

Analogously, we have

$$q^*(p,S) = (k_{11} \frac{\partial u^*(p,S)}{\partial x_1(S)} + k_{12} \frac{\partial u^*(p,S)}{\partial x_2(S)}) x_{1,n}(S) + (k_{12} \frac{\partial u^*(p,S)}{\partial x_1(S)} + k_{22} \frac{\partial u^*(p,S)}{\partial x_2(S)}) x_{2,n}(S) \tag{3.5.10}$$

and the problem can now be solved as previously.

Numerical results for orthotropic problems are presented in [26], [68] and for anisotropic problems in [27].

3.6 Infinite Regions

Although the boundary integral equation (3.1) has been derived considering that the region Ω is bounded, all concepts presented thus far are also valid for infinite regular regions in the sense defined by Kellogg [13], i.e. regions bounded by a regular surface (hence a bounded surface) and containing all sufficiently distant points. However, for this extension to be valid, certain regularity conditions concerning the behaviour of the functions in equation (3.1) on a surface which is infinitely remote from the origin must be fulfilled.

Let $\overline{\Gamma}$ be the surface of a circle (or a sphere if the problem is three-dimensional) of radius R surrounding the surface Γ and centred at the point P (figure 3.6.1). A boundary integral equation similar to (3.1) for the finite region Ω enclosed by the actual surface Γ and the fictitious surface $\overline{\Gamma}$ can be written as,

$$c(P)\, u(P) + \int_{\Gamma} u(S)\, q^*(P,S)\, d\Gamma(S) + \int_{\overline{\Gamma}} u(S)\, q^*(P,S)\, d\Gamma(S)$$

$$= \int_{\Gamma} q(S)\, u^*(P,S)\, d\Gamma(S) + \int_{\overline{\Gamma}} q(S)\, u^*(P,S)\, d\Gamma(S) \qquad (3.6.1)$$

If we let the radius $R \to \infty$, equation (3.6.1) will only be valid for points in Γ (and Ω) if

$$\lim_{R\to\infty} \int_{\overline{\Gamma}} \left[q(S)\, u^*(P,S) - u(S)\, q^*(P,S)\right] d\Gamma(S) = 0 \qquad (3.6.2)$$

For three-dimensional problems, since

$$\begin{aligned} &d\Gamma(S) = |J|\, d\phi\, d\Phi \quad , \quad |J| = O(R^2) \\ &u^*(P,S) = O(R^{-1}) \quad , \quad S \in \overline{\Gamma} \\ &q^*(P,S) = O(R^{-2}) \end{aligned} \qquad (3.6.3)$$

where $O(\ )$ represents the asymptotic behaviour of the functions as $R \to \infty$, the condition of equation (3.6.2) is satisfied if the function $u(S)$ behaves at most as $O(R^{-1})$, such that its derivative $q(S) = O(R^{-2})$

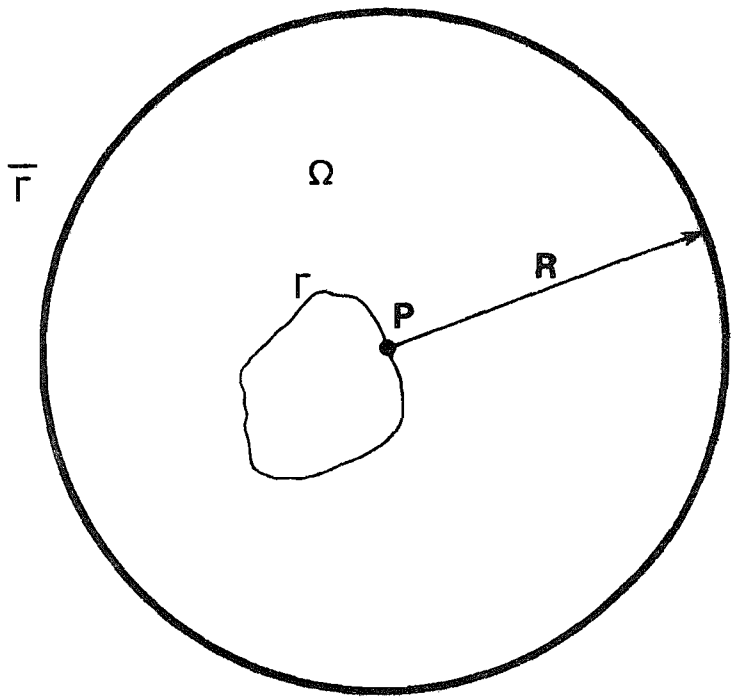

Figure 3.6.1 - Infinite region with cavity

in the worst case. These are the regularity conditions at infinity [13], [40] and they ensure that each term in the integral in equation (3.6.2) behaves at most as $O(R^{-1})$, i.e. they approach zero as $R\to\infty$.

For two-dimensional problems, we have that the function $u^*(P,S)$ behaves as the logarithm of R and its derivative $q^*(P,S) = O(R^{-1})$ as $R\to\infty$. The regularity conditions at infinity for this case imply that $u(S)$ behaves at most as log R such that $q(S) = O(R^{-1})$ in the worst case. Note that now the terms in the integral in equation (3.6.2) do not approach zero separately as $R\to\infty$ since $d\Gamma(S) = |J|d\xi$ and $|J| = O(R)$, but they cancel each other thus fulfilling condition (3.6.2).

Therefore, applying condition (3.6.2) into equation (3.6.1) yields,

$$c(P)\ u(P) + \int_\Gamma u(S)\ q^*(P,S)\ d\Gamma(S) = \int_\Gamma q(S)\ u^*(P,S)\ d\Gamma(S) \qquad (3.6.4)$$

that is, the boundary integral equation obtained for points on the internal surface Γ of the infinite regular region Ω is of the same form as equation (3.1) for finite regions. The same is also valid for the integral equation for points inside the infinite region Ω.

Consider a three-dimensional Neumann problem defined over the infinite region Ω. Unlike the case of finite regions (see section 2.2), equation (3.6.4) has a unique solution for arbitrary continuous values of q prescribed over the internal boundary Γ. Moreover, the Gauss condition (2.2.6) need not be satisfied by q since the integral of q around Γ is balanced by a compensating flux at infinity. As the region Ω enclosed by Γ and $\overline{\Gamma}$ is solenoidal, we can write

$$\int_{\Gamma} q(S)\, d\Gamma(S) + \int_{\overline{\Gamma}} q(S)\, d\overline{\Gamma}(S) = 0 \qquad (3.6.5)$$

where

$$\int_{\overline{\Gamma}} q(S)\, d\overline{\Gamma}(S) = O(1) \qquad (3.6.6)$$

since $u(S) = O(R^{-1})$ as $R \to \infty$. If u(S) behaves as $O(R^{-2})$ the flux over $\overline{\Gamma}$ vanishes and so equation (3.6.5) becomes the Gauss condition

$$\int_{\Gamma} q(S)\, d\Gamma(S) = 0 \qquad (3.6.7)$$

Conversely, if condition (3.6.7) is fulfilled, it follows that u(S) behaves as $O(R^{-2})$ as $R \to \infty$.

By analogous considerations we can state that, for two-dimensional Neumann problems, satisfaction of the Gauss condition (3.6.7) ensures that u(S) behaves at most as $O(R^{-1})$ as $R \to \infty$.

If the function q tends towards a non-zero limiting value at infinity, this value can be included in the analysis through a particular solution as will be shown in a following example.

A final remark concerning infinite regions is that although it is possible to evaluate the diagonal coefficients of matrix $\underset{\sim}{H}$ through condition (3.1.9) (see section 3.1), care must be taken because the regularity conditions at infinity are violated as the function u is now assumed to be constant everywhere in Ω. Since it can easily be shown that,

$$\lim_{R\to\infty} \int_{\bar{\Gamma}} q^*(P,S)\, d\Gamma(S) = -2\alpha\pi \tag{3.6.8}$$

for both two and three-dimensional problems (α = 1 or 2, respectively), being the surface $\bar{\Gamma}$ defined as previously, we have (see equation (3.1.10)),

$$H_{ii} = -\sum_{\substack{j=1 \\ (j\neq i)}}^{N} H_{ij} + 2\alpha\pi \tag{3.6.9}$$

Example 3.6.1

Let us consider the problem of a circular cavity of unit radius in an infinite two-dimensional region with Neumann boundary conditions, i.e. a constant radial influx of 31.21^{o}C/cm specified along the cavity surface.

Since the Gauss condition (3.6.7) is not satisfied, the solution will have a logarithmic potential behaviour at infinity. The exact solution of this problem is,

$$u = -31.21 \log R$$

which shows the expected behaviour.

Results for the temperature at points on the boundary Γ and inside the region Ω are given in table 3.6.1 and for the radial flux at points in Ω in table 3.6.2, compared to the exact solution. Taking symmetry into account, only one quarter of the cavity surface was subdivided using constant elements.

R	BEM (N=4)	BEM (N=8)	EXACT
1.0	0.48	0.12	0.00
1.5	12.57	12.63	12.65
2.0	21.49	21.60	21.63
3.0	34.07	34.23	34.28
5.0	49.91	50.15	50.22
10.0	71.40	71.75	71.86
100.0	142.81	143.50	143.72
1000.0	214.21	215.24	215.58

Table 3.6.1 - Temperature (-) at points on infinite region

R	BEM (N=4)	BEM (N=8)	EXACT
1.5	20.68	20.77	20.81
2.0	15.51	15.58	15.61
3.0	10.34	10.39	10.40
5.0	6.20	6.23	6.24
10.0	3.10	3.12	3.12
100.0	0.31	0.31	0.31
1000.0	0.03	0.03	0.03

Table 3.6.2 - Radial flux at points on infinite region

Example 3.6.2

The previously discussed formulation for infinite regions can be readily applied to practical problems such as potential fluid flow past obstacles.

As an example, we study a two-dimensional potential flow with uniform onset velocity U in the x_1 direction around a NACA 0018 aerofoil, whose shape is shown in figure 3.6.2. For the solution of this problem, we employ a stream function ψ as defined in example 3.3.2.

It is now convenient to separate the stream function ψ into two parts,

$$\psi = \psi_1 + \psi_2$$

where $\psi_1 = Ux_2$ defines the steady onset flow and ψ_2 is a perturbation stream function. Since the perturbation decays at infinity, we require that $\psi_2 = O(R^{-1})$ at most as $R \to \infty$. Furthermore, as $\nabla^2\psi = 0$, we also have that $\nabla^2\psi_2 = 0$ and the problem can now be solved in terms of the perturbation ψ_2.

Considering the surface of the aerofoil as the streamline $\psi = 0$, the boundary conditions of the problem are

$$\psi_2 = -\psi_1 = -Ux_2 \qquad \text{on} \quad \Gamma$$

As the problem is anti-symmetric with respect to the x_1-axis, only one half of the aerofoil needed to be analysed. The linear boundary elements discretisation employed for the solution is shown in figure 3.6.2. Results for the tangential velocity presented in the same figure are in good agreement with analytical results given in [88].

3.7 Special Fundamental Solutions

The fundamental solution we have employed in all problems studied so far can be immediately recognised as the Green's function

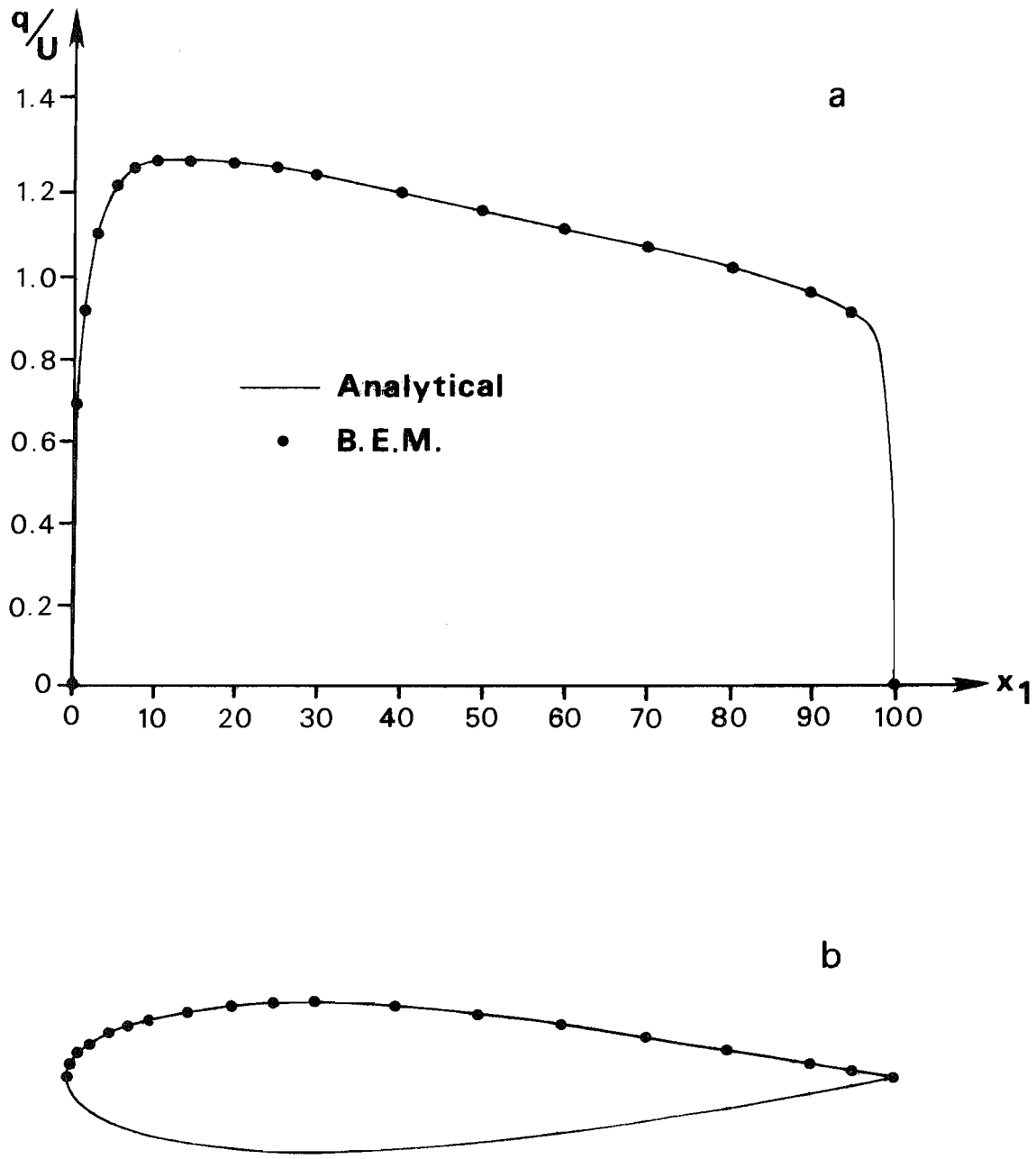

Figure 3.6.2 - NACA 0018 aerofoil: a) Results;
b) Discretisation

for an infinite region. Since it was derived without any proper attention to boundary conditions (see chapter 2), the boundary conditions of the actual problem are introduced by requiring that the function or its normal derivative (or a linear relation between both) satisfies prescribed values at points on the boundary, which was previously discretised. In some problems, the problem region may be confined in some regular way and it may be more convenient to find a fundamental solution specific to the region [3].

As an example, let us derive the fundamental solution for a semi-infinite region such as occurs in fluid mechanics or geotechnical problems. Figure 3.7.1 represents a problem of groundwater flow round a tunnel which runs under a river. In a problem of this nature, it is preferable to remove the infinite boundary $\overline{\Gamma}$. By choosing a fundamental solution which identically satisfies the boundary condition on the surface $\overline{\Gamma}$ we shall not need to discretise this surface, thus considerably reducing the amount of numerical work involved in the solution of the problem.

Consider a source of intensity $\sigma(S)$ at a point $S \in \Gamma$ (figure 3.7.1). The potential generated by this source will somehow be reflected at the surface $\overline{\Gamma}$, depending on the boundary condition applied there. In order to represent this reflection, we shall introduce an image source of intensity $\sigma(S')$ at a point S' symmetrically located with respect to $\overline{\Gamma}$. Thus, the potential at any field point p will be the superposition of the ones generated by both sources, i.e. (see chapter 2),

$$u(p) = \sigma(S)\, u^*(p,S) + \sigma(S')\, u^*(p,S') \qquad (3.7.1)$$

where u^* is the infinite space fundamental solution.

Applying the boundary condition $u = 0$ at the surface $\overline{\Gamma}$, we obtain

$$\sigma(S)\ u^*(p,S) + \sigma(S')\ u^*(p,S') = 0 \qquad \text{on } x_2(p) = 0 \qquad (3.7.2)$$

Taking for instance the two-dimensional Laplace's equation, condition (3.7.2) implies that

$$\sigma(S)\ \log \frac{1}{\{[x_1(p)-x_1(S)]^2 + [-x_2(S)]^2\}^{\frac{1}{2}}}$$

$$+ \sigma(S')\ \log \frac{1}{\{[x_1(p)-x_1(S)]^2 + [x_2(S)]^2\}^{\frac{1}{2}}} = 0 \qquad (3.7.3)$$

which gives

$$\sigma(S) = -\sigma(S') \qquad (3.7.4)$$

Since, by definition, the fundamental solution is equivalent to the potential generated by unit sources, the fundamental solution for the semi-infinite region with zero potential at the interface is simply

$$u^*(p,s) = \log \left\{ \frac{[x_1(p)-x_1(s)]^2 + [x_2(p)-x_2(s)]^2}{[x_1(p)-x_1(s)]^2 + [x_2(p)+x_2(s)]^2} \right\}^{\frac{1}{2}} \qquad (3.7.5)$$

If the boundary condition at the interface $\overline{\Gamma}$ is that of zero normal flux, i.e.

$$\sigma(S)\ q^*(p,S) + \sigma(S')\ q^*(p,S') = 0 \qquad \text{on } x_2(p) = 0 \qquad (3.7.6)$$

implying the condition

$$-\sigma(S) \frac{x_2(S)}{[x_1(p)-x_1(S)]^2 + [-x_2(S)]^2} + \sigma(S') \frac{x_2(S)}{[x_1(p)-x_1(S)]^2 + [x_2(S)]^2} = 0 \qquad (3.7.7)$$

which gives,

$$\sigma(S) = \sigma(S') \qquad (3.7.8)$$

then the fundamental solution of the problem is

$$u^*(p,s) = \log(\{[x_1(p)-x_1(s)]^2 + [x_2(p)-x_2(s)]^2\}^{\frac{1}{2}}\ \{[x_1(p)-x_1(s)]^2 + [x_2(p)+x_2(s)]^2\}^{\frac{1}{2}}) \qquad (3.7.9)$$

Fundamental solutions for other problems such as parallel layered regions can be constructed in the same way, as well as three-dimensional fundamental solutions.

Example 3.7.1

The problem represented in figure 3.7.1, that is, a two-dimensional problem of groundwater flow round a tunnel with permeable invert was studied in order to illustrate the ideas developed in this section. As seen in section 3.2, if the medium is homogeneous and isotropic the problem is reduced to that of Laplace's equation for the groundwater pressure u. The boundary conditions of the problem are,

$$u = d \qquad \text{on } \bar{\Gamma}$$

$$u = 0 \qquad \text{on } \Gamma_1$$

$$q = -\cos\theta \qquad \text{on } \Gamma_2$$

where d is the depth of the river and θ is the angle measured from the vertical (see figure 3.7.1). The surface Γ_1 is the permeable invert of the tunnel where we assume that water flows in freely and Γ_2 is the impermeable part of the tunnel lining, where the condition of no flow across the surface holds. Notice that for a point at infinity we have the condition $u = d-x_2$.

The problem can be reformulated by subtracting out the solution at infinity. The groundwater pressure u is divided into two parts,

$$u = u_1 + u_2$$

where $u_1 = d-x_2$ satisfies the infinity condition. Then we have that u_2 tends to zero at infinity and furthermore, that $\nabla^2 u_2 = 0$ such that the problem can now be solved in terms of u_2. The boundary conditions for u_2 become then,

$$\begin{aligned} u_2 &= 0 && \text{on } \bar{\Gamma} \\ u_2 &= -(d+a-r_t\cos\theta) && \text{on } \Gamma_1 \\ q_2 &= 0 && \text{on } \Gamma_2 \end{aligned} \qquad (3.7.10)$$

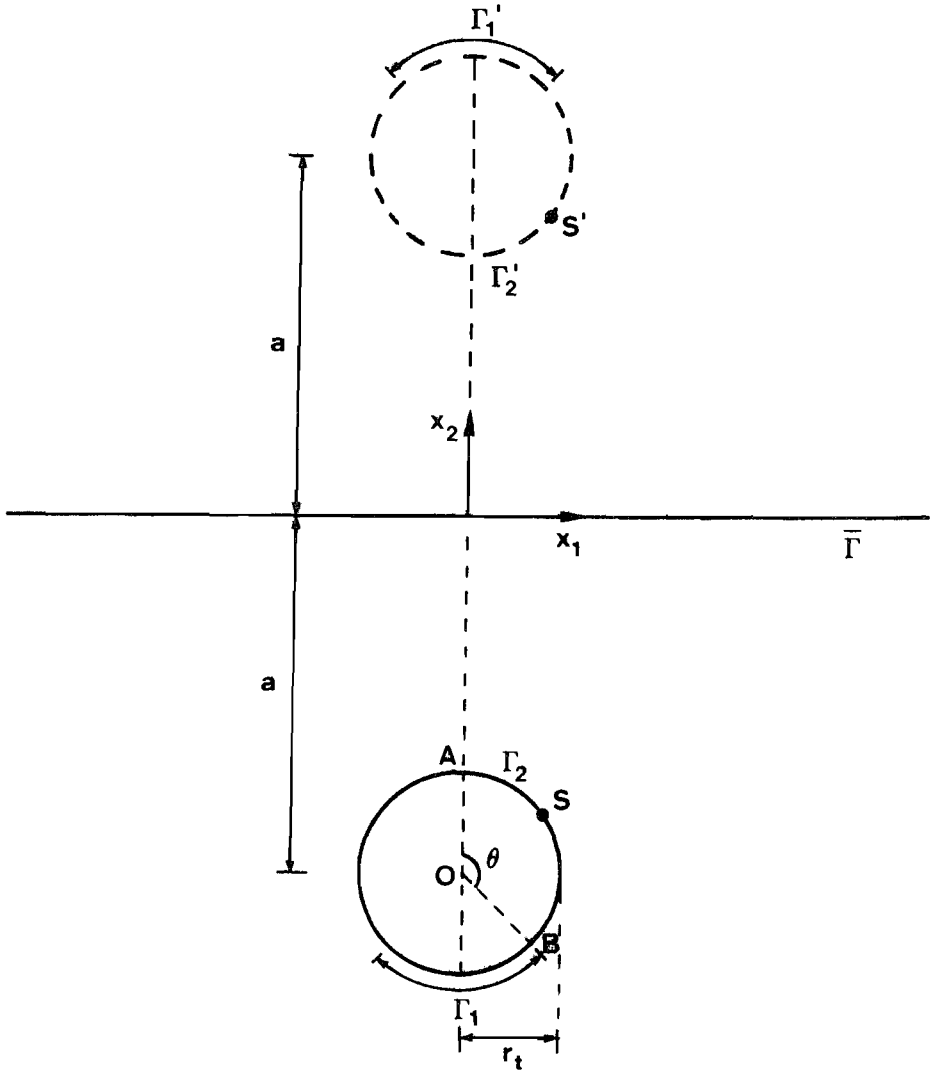

Figure 3.7.1 - Groundwater flow round a tunnel

θ	BEM (N=8)	BEM (N=16)	BEM (N=32)	FEM
0	30.51	29.08	28.87	33.44
π/8	31.52	30.03	29.83	34.51
π/4	34.60	32.87	32.73	37.76
3π/8	39.96	38.05	37.85	43.46
π/2	48.24	45.96	45.72	52.34
5π/8	61.43	58.42	58.10	66.46

Table 3.7.1 - Values of u_2 (-) on tunnel surface

where r_t is the radius of the tunnel and a is the distance of the centre of the tunnel below the bottom of the river. The numerical values adopted for the parameters are d = 60, a = 30, r_t = 3.5 and $\hat{AOB} = 3\pi/4$.

The same computer program developed using the infinite space fundamental solution can be applied to this problem by specifying anti-symmetry with respect to the x_1-axis, thus also satisfying condition (3.7.4). The solution of the new problem, i.e. Laplace's equation in the infinite domain bounded internally by Γ and its image Γ', with boundary conditions $u_2 = -u_1$ on Γ_1, $u_2 = u_1$ on Γ_1', $q_2 = 0$ on Γ_2 and Γ_2', is identical in the lower half-space to the solution of the original problem with boundary conditions (3.7.10). By taking into account the symmetry with respect to the x_2-axis, only one half of the tunnel surface needs to be discretised.

Results for the function u_2 at some boundary points are presented in table 3.7.1 for three different discretisations using linear boundary elements and compared to a finite element solution [69] obtained by discretising the whole semi-infinite region into 152 triangular finite elements plus some infinite elements (see figure 3.7.2). The discrepancy between both solutions is due to the coarseness of the finite element mesh around the tunnel (see figure 3.7.2), which does not take into account properly the discontinuity on the radial flux at the point B.

Example 3.7.2

This example studies the steady-state heat conduction problem of a semi-infinite medium bounded internally by two parallel and equal cylinders, as shown in figure 3.7.3. The interface $\bar{\Gamma}$ is at zero temperature, the temperature at infinity is also zero and the surfaces of the cylinders are isotherms.

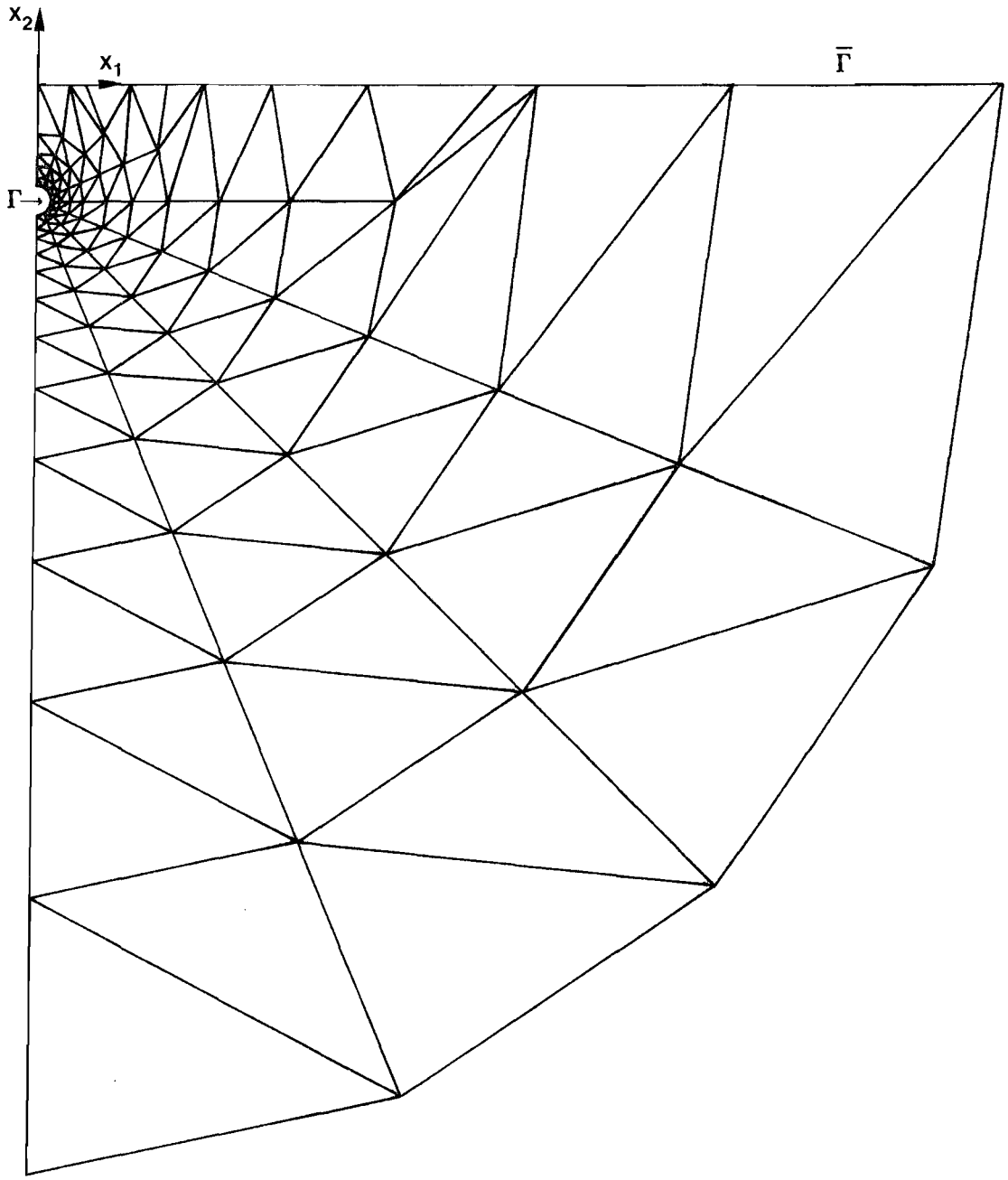

Figure 3.7.2 - Finite element mesh for groundwater flow round a tunnel

If the depth d is much greater than the cylinder radius a, this problem can be seen as an approximation to the more practical one of two equally loaded electricity cables laid direct in the ground in horizontal formation. Of interest in this kind of problem is the determination of the external thermal resistance of each cable.

The thermal resistance G per unit length between the surface Γ at a temperature c and the surface $\bar{\Gamma}$ at zero temperature, through a medium with thermal conductivity k, is given by

$$G = - \frac{c}{k \int_{\Gamma} q \, d\Gamma}$$

Results for the non-dimensional ratio Gk are presented in table 3.7.2 for several values of d/a, for a unit cylinder surface temperature c. Two different cases were considered, i.e. when the cables are touching (b = 0) and when the cable spacing equals one diameter (b = a). These results were obtained by sub-dividing the surface of one cylinder into 32 linear elements and considering symmetry with respect to the x_2-axis and anti-symmetry with respect to the x_1-axis, using the infinite space Green's function. Also shown in the table are the results obtained through an approximate analytical solution [70]; the agreement between both solutions is very good.

Since anti-symmetry was considered the Gauss condition (3.6.7) is automatically satisfied, thus fulfilling the condition of zero temperature at infinity.

3.8 Three-Dimensional Problems

The solution of the boundary integral equation (3.1) for three-dimensional problems can be attempted following basically the same steps as discussed in section 3.1 for two-dimensions. The boundary Γ, now a two-dimensional curve, can be modelled by using flat or curved

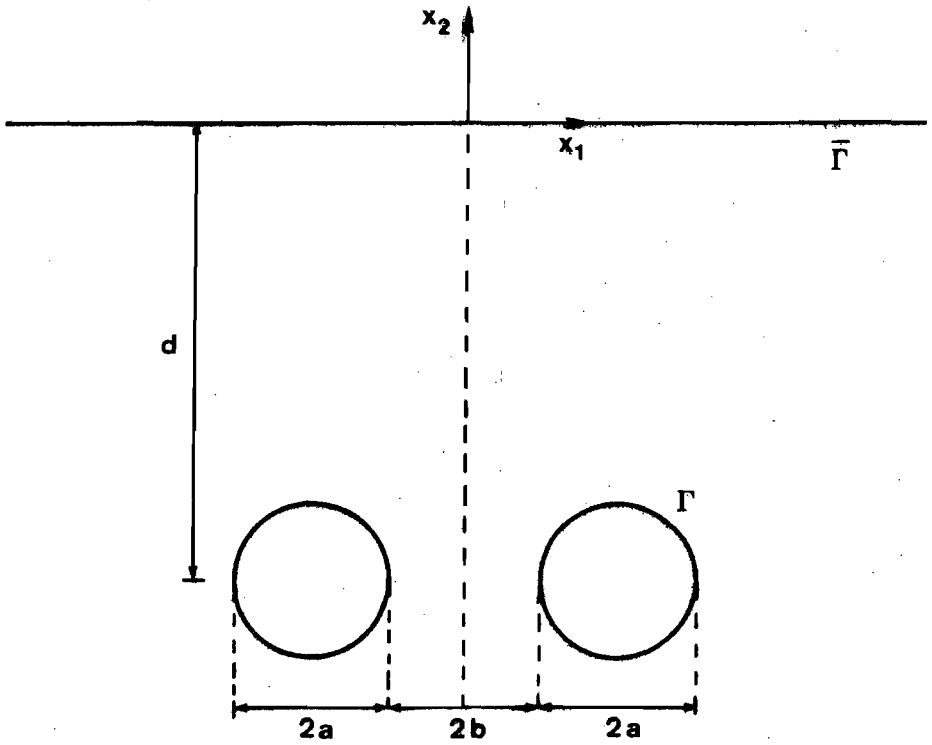

Figure 3.7.3 - Semi-infinite region bounded internally by two equal cylinders

b	d/a	BEM	ANALYTICAL
b = 0	10	0.810	0.810
	25	1.102	1.102
	50	1.322	1.322
	100	1.543	1.543
b = a	10	0.726	0.724
	25	1.016	1.014
	50	1.236	1.235
	100	1.457	1.456

Table 3.7.2 - Values of ratio Gk

triangles or quadrilaterals and the potentials and normal derivatives over it assumed to be piecewise constant, linear, quadratic, etc. The interpolation functions adopted are generally the same as employed for two-dimensional finite element analyses.

In what follows, the numerical procedures necessary for the computer implementation of a simple element, namely a flat triangle with constant potential and normal derivative will be described in detail. Numerical results are included at the end of the section in order to show the validity of these procedures and a description of the computer program developed is given in chapter 6. As for the two-dimensional case, extension to high order interpolation functions presents no further theoretical difficulties.

For the discretisation of equation (3.1), the boundary is modelled by using flat triangles such that the cartesian coordinates $\underset{\sim}{x}$ of points within each element are expressed by equation (3.1.1), being now

$$\underset{\sim}{x} = \begin{Bmatrix} x_1 \\ x_2 \\ x_3 \end{Bmatrix} \qquad \underset{\sim}{\psi}^T = \begin{bmatrix} \underset{\sim}{\psi}^T & \underset{\sim}{0} & \underset{\sim}{0} \\ \underset{\sim}{0} & \underset{\sim}{\psi}^T & \underset{\sim}{0} \\ \underset{\sim}{0} & \underset{\sim}{0} & \underset{\sim}{\psi}^T \end{bmatrix} \qquad \underset{\sim}{X}^m = \begin{Bmatrix} \underset{\sim}{X}_1^m \\ \underset{\sim}{X}_2^m \\ \underset{\sim}{X}_3^m \end{Bmatrix} \tag{3.8.1}$$

where the index m = 1,2,3 is associated to points at the vertices of each triangle and

$$\underset{\sim}{\psi} = \begin{Bmatrix} \xi_1 \\ \xi_2 \\ \xi_3 \end{Bmatrix} \qquad \underset{\sim}{X}_i^m = \begin{Bmatrix} X_i^1 \\ X_i^2 \\ X_i^3 \end{Bmatrix} \tag{3.8.2}$$

in which ξ_i are the intrinsic triangular coordinates (figure 3.8.1).

The functions u and q are assumed to be constant within each element and associated to their nodal values at the centroid of the element (figure 3.8.1), i.e. equation (3.1.3) becomes simply,

$$\begin{aligned} u &= U \\ q &= Q \end{aligned} \tag{3.8.3}$$

If the boundary Γ is discretised into S elements and N nodes, the substitution of equation (3.8.3) into (3.1) yields

$$c_i U^i + \sum_{s=1}^{S} \left(\int_{\Gamma_s} q^* \, d\Gamma \right) \underset{\sim}{U}^n = \sum_{s=1}^{S} \left(\int_{\Gamma_s} u^* \, d\Gamma \right) \underset{\sim}{Q}^n \qquad (3.8.4)$$

The transformation of the element of surface $d\Gamma$ from the global cartesian system of coordinates to the intrinsic system of coordinates now gives,

$$d\Gamma = |J| \, d\xi_1 \, d\xi_2 \qquad (3.8.5)$$

where the Jacobian J equals twice the area of the triangle [60]. The unit normal vector, necessary for the evaluation of the function q^*, can be calculated by considering the cross-product between the vectors (2-1) and (3-1) shown in figure 3.8.1.

The integrals to be calculated in equation (3.8.4) are of the type

$$\begin{aligned} \int_{\Gamma_s} q^*(\underset{\sim}{x}) \, d\Gamma &= |J| \int_0^1 \left[\int_0^{1-\xi_2} q^*(\underset{\sim}{\xi}) \, d\xi_1 \right] d\xi_2 \\ \int_{\Gamma_s} u^*(\underset{\sim}{x}) \, d\Gamma &= |J| \int_0^1 \left[\int_0^{1-\xi_2} u^*(\underset{\sim}{\xi}) \, d\xi_1 \right] d\xi_2 \end{aligned} \qquad (3.8.6)$$

For the cases when $i \notin \Gamma_s$, these integrals are computed numerically using Hammer's quadrature scheme [65]. Thus the off-diagonal coefficients of matrices $\underset{\sim}{H}$ and $\underset{\sim}{G}$ in equation (3.1.8) are given by summations of the form,

$$\begin{aligned} H_{ij} &= 2A_j \, d_{ij} \sum_{k=1}^{7} \frac{1}{r_{ik}^3} W_k \\ G_{ij} &= 2A_j \sum_{k=1}^{7} \frac{1}{r_{ik}} W_k \end{aligned} \qquad (3.8.7)$$

in which A_j and d_{ij} refer to the element containing node j, being A_j its area and

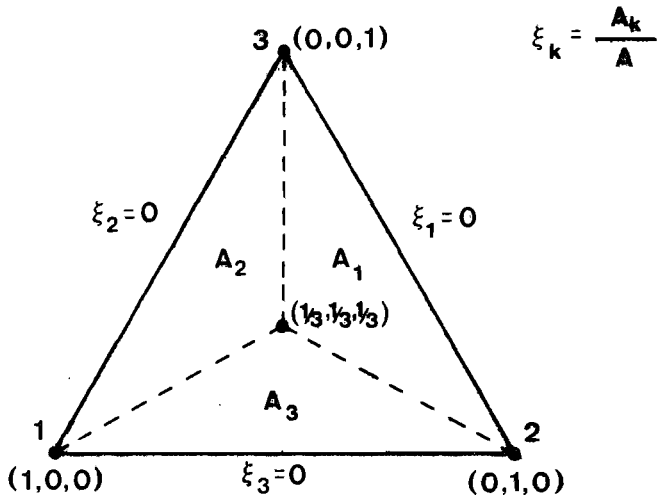

Figure 3.8.1 - Intrinsic triangular coordinates

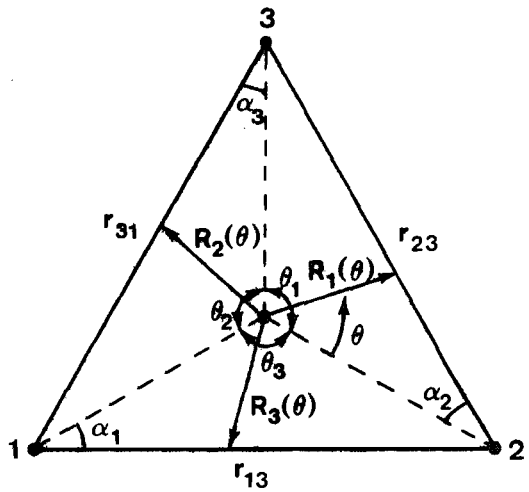

Figure 3.8.2 - Geometrical definitions for analytical integration

$$d_{ij} = \frac{(X_1^i - X_1^1)Z_1 + (X_2^i - X_2^1)Z_2 + (X_3^i - X_3^1)Z_3}{(Z_1^2 + Z_2^2 + Z_3^2)^{\frac{1}{2}}} \tag{3.8.8}$$

where

$$Z_a = Y_b^2 \, Y_c^3 - Y_b^3 \, Y_c^2 \tag{3.8.9}$$

being a = 1,2,3 for b = 2,3,1 and c = 3,1,2, and

$$\begin{aligned} Y_m^2 &= X_m^3 - X_m^1 \\ Y_m^3 &= Y_m^3 - X_m^1 \end{aligned} \tag{3.8.10}$$

for m = 1,2,3. Notice that seven integration points (quintic scheme) are employed for the numerical evaluation of the integrals in equation (3.8.6).

The H_{ii} coefficients may again be calculated by using equation (3.1.10) for finite regions or equation (3.6.9) for infinite regions. The G_{ii} coefficients, which contain integrable singularities, can be evaluated analytically by employing polar coordinates (see figure 3.8.2),

$$G_{ii} = \int_0^{\theta_1} \int_0^{R_1(\theta)} dR \, d\theta + \int_{\theta_1}^{\theta_1+\theta_2} \int_0^{R_2(\theta)} dR \, d\theta + \int_{\theta_1+\theta_2}^{2\pi} \int_0^{R_3(\theta)} dR \, d\theta \tag{3.8.11}$$

where

$$\begin{aligned} R_j(\theta) &= \frac{2A_i}{3(b_\ell \cos\theta' + a_k \sin\theta')} \\ b_j &= (r_{\ell j}^2 - a_\ell^2)^{\frac{1}{2}} \\ a_j &= \frac{Z_1^j + Z_2^j + Z_3^j}{r_{ij}} \\ Z_m^j &= (X_m^i - X_m^j)Y_m^\ell \\ Y_m^j &= X_m^\ell - X_m^k \end{aligned} \tag{3.8.12}$$

in which m = 1,2,3 and j = 1,2,3 for k = 2,3,1 and ℓ = 3,1,2. The angle θ' equals θ for j = 1, $\theta' = \theta - \theta_1$ for j = 2 and $\theta' = \theta - (\theta_1 + \theta_2)$ for

j = 3. Evaluating the integrals in equation (3.8.11) finally yields,

$$G_{ii} = \frac{2A_i}{3}\left\{\frac{1}{r_{23}}\log\left(\frac{\tan\left[(\theta_1+\alpha_2)/2\right]}{\tan\left[\alpha_2/2\right]}\right) + \frac{1}{r_{31}}\log\left(\frac{\tan\left[(\theta_2+\alpha_3)/2\right]}{\tan\left[\alpha_3/2\right]}\right)\right.$$

$$\left. + \frac{1}{r_{12}}\log\left(\frac{\tan\left[(\theta_3+\alpha_1)/2\right]}{\tan\left[\alpha_1/2\right]}\right)\right\} \qquad (3.8.13)$$

Example 3.8.1

The first three-dimensional example studies the temperature distribution over a unit cube with Dirichlet boundary conditions as follows (see figure 3.8.3),

$u = 1.$ at $x_1 = +0.5$

$u = 2.$ at $x_1 = -0.5$

$u = 0.$ at $x_2 = \pm 0.5$

$u = 0.$ at $x_3 = \pm 0.5$

Due to symmetry with respect to the planes x_1-x_2 and x_1-x_3, only one quarter of the actual cube needed to be analysed. Two different meshes were employed, the finer of which is shown in figure 3.8.3. Results for the temperature at some internal points are presented in table 3.8.1 and compared with an available analytical solution [16].

Example 3.8.2

In this example, we seek the temperature distribution over a rectangular parallelepiped with the following mixed boundary conditions (figure 3.8.4),

$u = 10.$ at $x_1 = -0.5$

$\frac{\partial u}{\partial n} + 5u = 0.$ at $x_1 = +0.5$

$\frac{\partial u}{\partial n} + 5u = 0.$ at $x_2 = \pm 1.$

$\frac{\partial u}{\partial n} + 5u = 0.$ at $x_3 = \pm 1.$

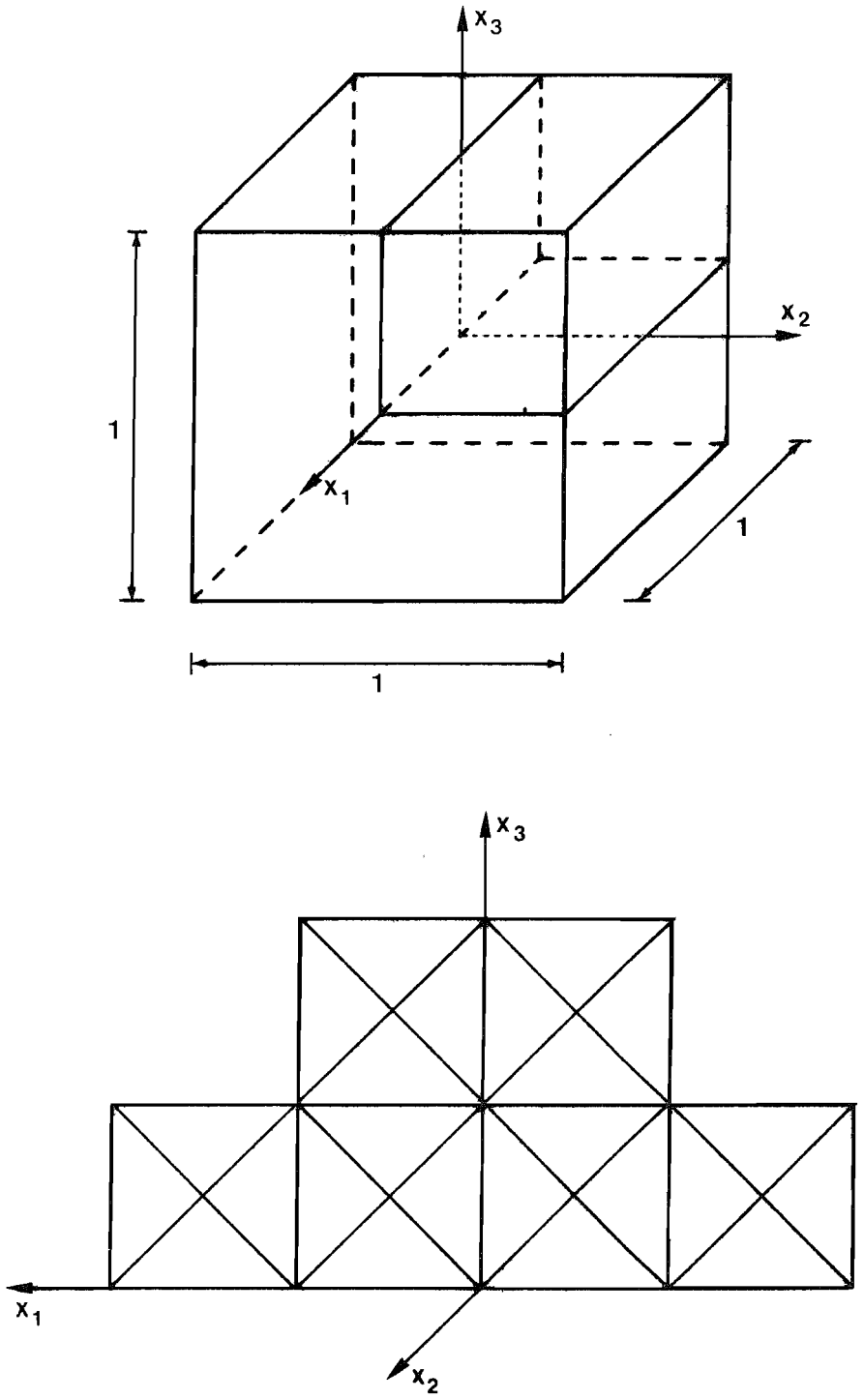

Figure 3.8.3 - Unit cube: a) Geometry; b) Discretisation

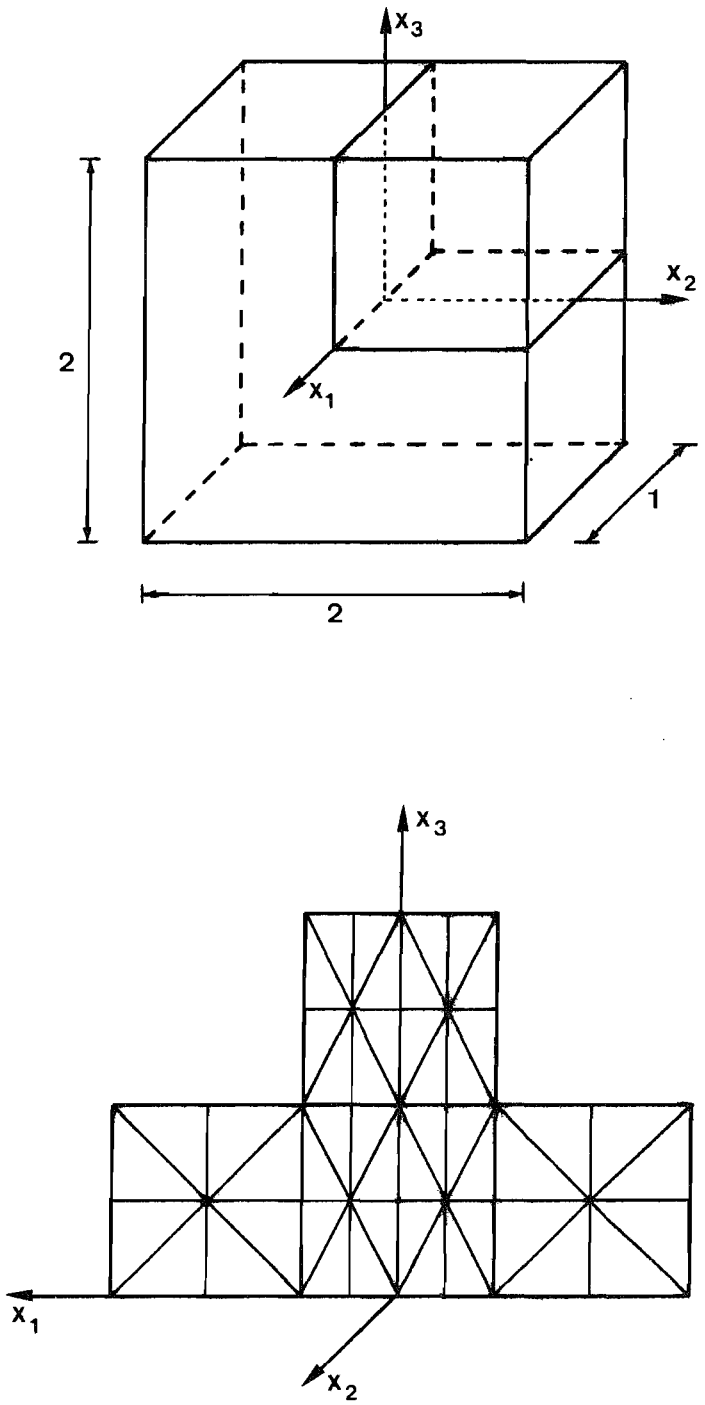

Figure 3.8.4 - Rectangular parallelepiped: a) Geometry; b) Discretisation

x_1	BEM (N=12)	BEM (N=24)	ANALYTICAL
-0.375	1.637	1.472	1.430
-0.250	1.044	0.979	0.967
-0.125	0.678	0.661	0.659
0.	0.500	0.500	0.500
0.125	0.478	0.472	0.472
0.250	0.597	0.566	0.560
0.375	0.855	0.770	0.748

Table 3.8.1 - Temperature along the x_1-axis

x_1	x_2	x_3	BEM (N=24)	BEM (N=48)	ANALYTICAL
-0.25	0.	0.	7.387	7.282	7.259
0.	0.	0.	4.827	4.840	4.837
0.	0.50	0.50	3.745	3.843	3.843
0.25	0.	0.	2.816	2.843	2.844
0.25	0.25	0.25	2.612	2.658	2.658
0.25	0.50	0.50	2.000	2.073	2.089
0.25	0.75	0.75	1.050	1.144	1.180

Table 3.8.2 - Temperature at internal points

As in the previous example, we take advantage of the symmetry of the problem with respect to the planes x_1-x_2 and x_1-x_3. The finer mesh employed in this analysis (48 elements) is shown in figure 3.8.4 and the numerical results at some internal points are compared with the ones obtained through an analytical solution [16] in table 3.8.2.

Example 3.8.3

Let us now study the problem of a spherical cavity of unit radius in an infinite region with a constant radial influx of 10^{o}C/cm prescribed along the cavity surface.

The exact solution of this problem is simply,

$$u = \frac{10}{R}$$

which shows that the expected solution behaves as $O(R^{-1})$ as $R \to \infty$ since the Gauss condition (3.6.7) is not satisfied.

By taking symmetry into account, only one eighth of the cavity surface needed to be analysed. Results for the averaged surface temperature and for the temperature at some points inside the domain Ω are shown in table 3.8.3, compared to the exact solution. The slow convergence of the numerical solution on and near the cavity surface are attributed to the geometrical approximation of the sphere using flat elements.

3.9 Axisymmetric Problems

In chapter 2, it was pointed out that the fundamental solution to the two-dimensional Laplace's equation (the logarithmic potential) can be derived by integrating the three-dimensional one (the Newtonian potential) for a line source at a point s. The same idea can be applied in order to derive the fundamental solution for Laplace's equation over an axisymmetric domain, which is equivalent to a ring source.

R	BEM (N=7)	BEM (N=16)	EXACT
1.0	9.676	9.727	10.000
1.5	6.505	6.569	6.667
2.0	4.899	4.922	5.000
3.0	3.274	3.281	3.333
6.0	1.639	1.640	1.667
10.0	0.983	0.984	1.000
100.0	0.098	0.098	0.100
1000.0	0.010	0.010	0.010

Table 3.8.3 - Temperature at points on infinite region

Assuming that all boundary values have axial symmetry (and consequently all domain values are also axisymmetric), equation (3.1) can be written in cylindrical polar coordinates (R,θ,Z) as

$$c(P)\ u(P) + \int_{\bar{\Gamma}} u(S) \int_0^{2\pi} q^*(P,S)\ d\theta(S)\ R(S)\ d\bar{\Gamma}(S)$$

$$= \int_{\bar{\Gamma}} q(S) \int_0^{2\pi} u^*(P,S)\ d\theta(S)\ R(S)\ d\bar{\Gamma}(S) \qquad (3.9.1)$$

since

$$d\Gamma = dx_1\ dx_2\ dx_3 = R\ d\theta\ dR\ dZ = R\ d\theta\ d\bar{\Gamma} \qquad (3.9.2)$$

Note that $\bar{\Gamma}$ is the generating boundary contour which is the projection of Γ in the R^+-Z semi-plane (figure 3.9.1).

Writing the three-dimensional fundamental solution in cylindrical polar coordinates,

$$u^*(P,S) = \frac{1}{r(P,S)} = \frac{1}{\{R^2(P)+R^2(S)-2R(P)R(S)\cos[\theta(P)-\theta(S)]+[Z(P)-Z(S)]^2\}^{\frac{1}{2}}}$$

(3.9.3)

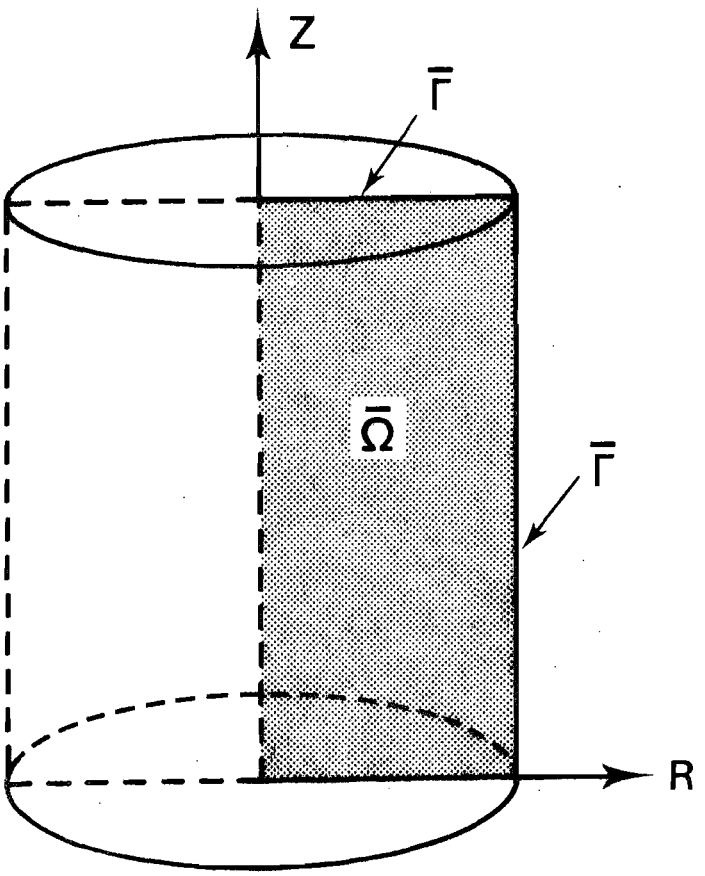

Figure 3.9.1 - Generating area and boundary contour of solid of revolution

the axisymmetric one can be calculated explicitly in terms of the complete elliptic integral of the first kind K(m) as,

$$\bar{u}^*(P,S) = \int_0^{2\pi} u^*(P,S)\, d\theta(S) = \frac{4\,K(m)}{(a+b)^{\frac{1}{2}}} \tag{3.9.4}$$

where

$$\begin{aligned} m &= \frac{2b}{a+b} \\ a &= R^2(P)+R^2(S)+\left[Z(P)-Z(S)\right]^2 \\ b &= 2\,R(P)\,R(S) \end{aligned} \tag{3.9.5}$$

The range of variation of the parameter m is $0 \leq m \leq 1$. Unlike the two and three-dimensional cases, the axisymmetric fundamental solution cannot be written as simply a function of the distance between two points, but it also depends on the distance of the points to the axis of revolution.

The normal derivative of the fundamental solution along the boundary contour $\bar{\Gamma}$ is given by,

$$\bar{q}^*(P,S) = \frac{4}{(a+b)^{\frac{1}{2}}} \left\{ \frac{1}{2R(S)} \left[\frac{R^2(P)-R^2(S)+\left[Z(P)-Z(S)\right]^2}{a-b} \right] E(m)-K(m) \Big] R,_n(S) + \frac{Z(P)-Z(S)}{a-b}\, E(m)\, Z,_n(S) \right\} \tag{3.9.6}$$

where E(m) is the complete elliptic integral of the second kind.

From expressions (3.9.4) to (3.9.6), it can be seen that as $R(P) \to 0$ we have that $m \to 0$, $K(m) \to \pi/2$, $E(m) \to \pi/2$, so that the ring source tends to a point source with intensity 2π over the axis of revolution.

Substituting (3.9.4) and (3.9.6) into equation (3.9.1) yields the following boundary integral equation,

$$c(P)\, u(P) + \int_{\bar{\Gamma}} u(S)\, \bar{q}^*(P,S)\, R(S)\, d\bar{\Gamma}(S) = \int_{\bar{\Gamma}} q(S)\, \bar{u}^*(P,S)\, r(S)\, d\bar{\Gamma}(S) \tag{3.9.7}$$

The solution of the above equation can be attempted by using the same basic calculation procedures as discussed in section 3.1 for two-

dimensional problems. Again, constant and linear elements were derived and a description of the computer program developed is given in chapter 6.

For convenience of the numerical computation, the complete elliptic integrals are approximated by polynomial expressions [46] which are given in appendix A.

After discretising equation (3.9.7) and summing the contributions from all boundary elements, a system of equations of the form (3.1.8) is obtained. The terms H_{ij} and G_{ij} $(i \neq j)$ of this system are evaluated numerically using a standard Gaussian quadrature with four integration points. The diagonal terms H_{ii} and G_{ii} however, are the result of evaluating singular integrals for which standard quadratures cannot be applied.

In order to facilitate the evaluation of these integrals, the fundamental solution and its normal derivative can be written in terms of Legendre functions of the second kind as,

$$\bar{u}^*(P,S) = \frac{8^{\frac{1}{2}} \; Q_{-\frac{1}{2}}(\gamma)}{b^{\frac{1}{2}}} \tag{3.9.8}$$

$$\bar{q}^*(P,S) = -\frac{8^{\frac{1}{2}}}{R(S)\, b^{\frac{1}{2}}} \left\{ \left[\frac{Q_{-\frac{1}{2}}(\gamma)}{2} + \frac{R^2(P)-R^2(S)+[Z(P)-Z(S)]^2}{b} \frac{dQ_{-\frac{1}{2}}(\gamma)}{d\gamma} \right] R,_n(S) \right.$$

$$\left. + \frac{Z(P)-Z(S)}{R(P)} \; \frac{dQ_{-\frac{1}{2}}(\gamma)}{d\gamma} \, Z,_n(S) \right\} \tag{3.9.9}$$

where

$$\gamma = 1 + \frac{a-b}{b} \qquad 1 \leq \gamma \leq \infty \tag{3.9.10}$$

This form of the fundamental solution is the same as given by Snow [71].

This Legendre function can be expanded, for small values of γ, as [72]

$$Q_{-\frac{1}{2}}(\gamma) = -\frac{1}{2} \ln \left(\frac{\gamma-1}{32}\right) \tag{3.9.11}$$

$$\frac{dQ_{-\frac{1}{2}}(\gamma)}{d\gamma} = -\frac{1}{2(\gamma-1)} \qquad (3.9.12)$$

The substitution of expressions (3.9.11) and (3.9.12) into (3.9.8) and (3.9.9) permits the explicit evaluation of the singular integrals. As previously, the H_{ii} coefficients may be calculated by using equation (3.1.10) for finite regions or equation (3.6.9) for infinite regions (with $\alpha=2$) while formulas for G_{ii} obtained through analytical integration are given in appendix B, for both constant and linear elements.

For higher order elements, the complexity of the integrals makes almost impractical their closed form evaluation. To overcome this problem, we can integrate in closed form over a short straight line segment near the singularity and numerically integrate the rest of the element. Alternatively, the kernels in these integrals can be expanded in order to isolate the leading singular term which can then be integrated in closed form, being the remainder of the kernel numerically integrated.

Notice that for elements located near the axis of revolution (so with small R(P)) it is not always possible to integrate the whole element analytically in the way above described, since the value of the parameter γ will be large for points far from the singularity and therefore, approximations (3.9.11) and (3.9.12) are no longer valid for these points. Thus, the scheme adopted for these cases was to integrate analytically over a short segment near the singularity and numerically integrate the rest of the element using a standard Gaussian quadrature, as if these parts were separate elements. For computational purposes, the length L of the analytically integrated part of the element was assumed to be [73],

$$\frac{L}{2} \leq \left[\frac{R(P)\ R(S)}{50}\right]^{\frac{1}{2}} \leq \frac{\ell}{2} \qquad (3.9.13)$$

where ℓ is the total length of the element and R(S) is the distance from the nearest point of that part to the axis of revolution.

Example 3.9.1

The first example studied was that of a finite hollow cylinder $a<R<b$, $-\ell<Z<\ell$, subjected to a discontinuous heat influx on the inner face as follows,

$u = 0$ at $R = b$ and $Z = \pm\ell$

$q = 0$ at $R = a$, $-\ell<Z<-L$

$q = 0$ at $R = a$, $L<Z<\ell$

$q = V$ at $R = a$, $-L<Z<L$

This is a rough approximation to the arrangement in a tube furnace; an analytical solution of this problem can be found by employing an infinite series expansion in terms of Bessel functions [16].

Results are presented in tables 3.9.1 and 3.9.2, compared to the analytical solution. Both constant and linear elements were employed and due to the symmetry with respect to the R-axis only one half of the cylinder was discretised into 14 equal elements (figure 3.9.2). The numerical values adopted for this analysis were $a=2, b=6, \ell=5, L=2$ and $V=1$.

Example 3.9.2

This application considers a finite solid cylinder $0\leq R<a$, $0<Z<\ell$, over one face of which the 'radiation' boundary condition is prescribed. The total boundary conditions of the problem are,

$u = 0$ at $Z = \ell$

$u = V$ at $Z = 0$

$q + hu = 0$ at $R = a$

Again constant and linear boundary elements were employed and the cylinder surface discretised into 20 equal elements, in both cases (figure 3.9.3). Notice that there is no need for elements over the axis of revolution, which is not part of the generating contour. The numerical values assumed for these analyses were $a = 1$, $\ell = 3$, $h = 0.1$,

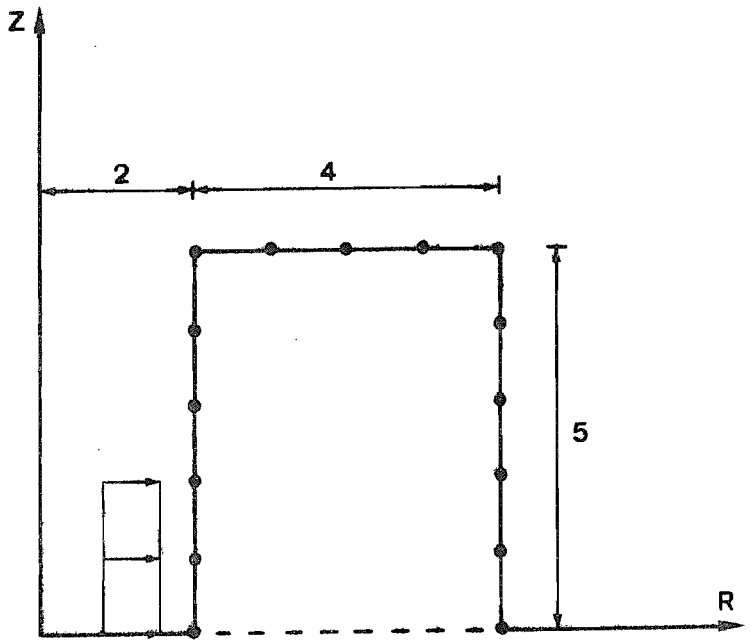

Figure 3.9.2 - Discretisation of hollow cylinder

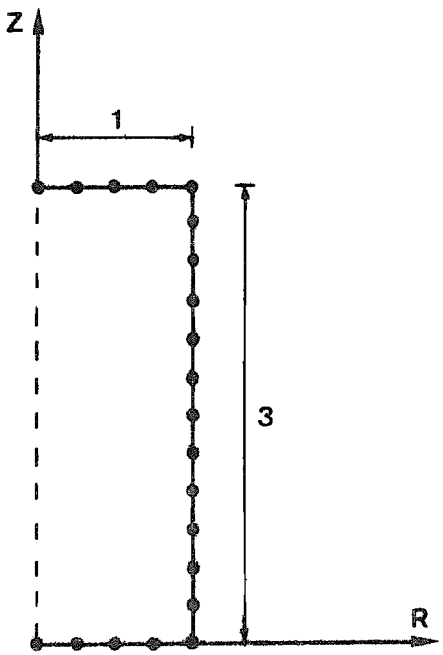

Figure 3.9.3 - Discretisation of solid cylinder

R	Z	BEM (constant)	BEM (linear)	Analytical
3.0	4.0	0.140	0.141	0.141
3.0	3.0	0.317	0.320	0.319
3.0	2.0	0.556	0.556	0.556
3.0	1.0	0.762	0.760	0.761
3.0	0.0	0.832	0.831	0.831
5.0	4.0	0.043	0.043	0.043
5.0	3.0	0.088	0.088	0.088
5.0	2.0	0.133	0.133	0.133
5.0	1.0	0.167	0.167	0.167
5.0	0.0	0.180	0.180	0.180

Table 3.9.1 - Temperature at internal points

R	BEM (constant)	BEM (Linear)	Analytical
2.0	-	0.148	0.155
2.5	0.155	-	0.149
3.0	-	0.141	0.134
3.5	0.112	-	0.113
4.0	-	0.089	0.090
4.5	0.066	-	0.066
5.0	-	0.043	0.042
5.5	0.017	-	0.020
6.0	-	0.000	0.000

Table 3.9.2 - Normal flux at $Z = \pm \ell$

Z	BEM (constant)	BEM (linear)	Analytical
0.5	0.782	0.781	0.781
1.0	0.587	0.585	0.585
1.5	0.417	0.416	0.416
2.0	0.267	0.267	0.267
2.5	0.130	0.130	0.130

Table 3.9.3 - Temperature at R = 0.25

Z	BEM (constant)	BEM (linear)	Analytical
0.375	0.807	-	0.805
0.500	-	0.751	0.751
0.875	0.606	-	0.604
1.000	-	0.560	0.560
1.375	0.437	-	0.436
1.500	-	0.397	0.397
1.875	0.289	-	0.289
2.000	-	0.254	0.254
2.375	0.155	-	0.156
2.500	-	0.124	0.124

Table 3.9.4 - Temperature at R = 1.00

V = 1. Results are compared in tables 3.9.3 and 3.9.4 with an available analytical solution [16].

Example 3.9.3

The problem of a spherical cavity of unit radius in an infinite medium already studied with three-dimensional elements in example 3.8.3 is now re-studied with axisymmetric constant elements in order to assess a comparison between both types of approximations.

Results are presented in table 3.9.5 for two different discretisations of one half of the generating contour of the sphere, taking symmetry into account. This provides a better geometrical representation of the cavity surface and the improvement of the results reflects this fact.

R	BEM (N=4)	BEM (N=8)	EXACT
1.0	9.961	9.991	10.000
1.5	6.539	6.634	6.667
2.0	4.904	4.976	5.000
3.0	3.269	3.317	3.333
6.0	1.635	1.659	1.667
10.0	0.981	0.995	1.000
100.0	0.098	0.100	0.100
1000.0	0.010	0.010	0.010

Table 3.9.5 - Temperature at points on infinite region

Example 3.9.4

Finally, a more practical application is the analysis of a prototype nuclear reactor pressure vessel subjected to an increase of temperature applied on the inside. This problem was studied using 96 triangular

finite elements in [74] and the results, as well as the mesh employed, are reproduced in figure 3.9.4.

Results for a linear boundary elements analysis employing 31 elements and taking into account the symmetry with respect to the R-axis are plotted in figure 3.9.5, and compare well with the finite elements solution.

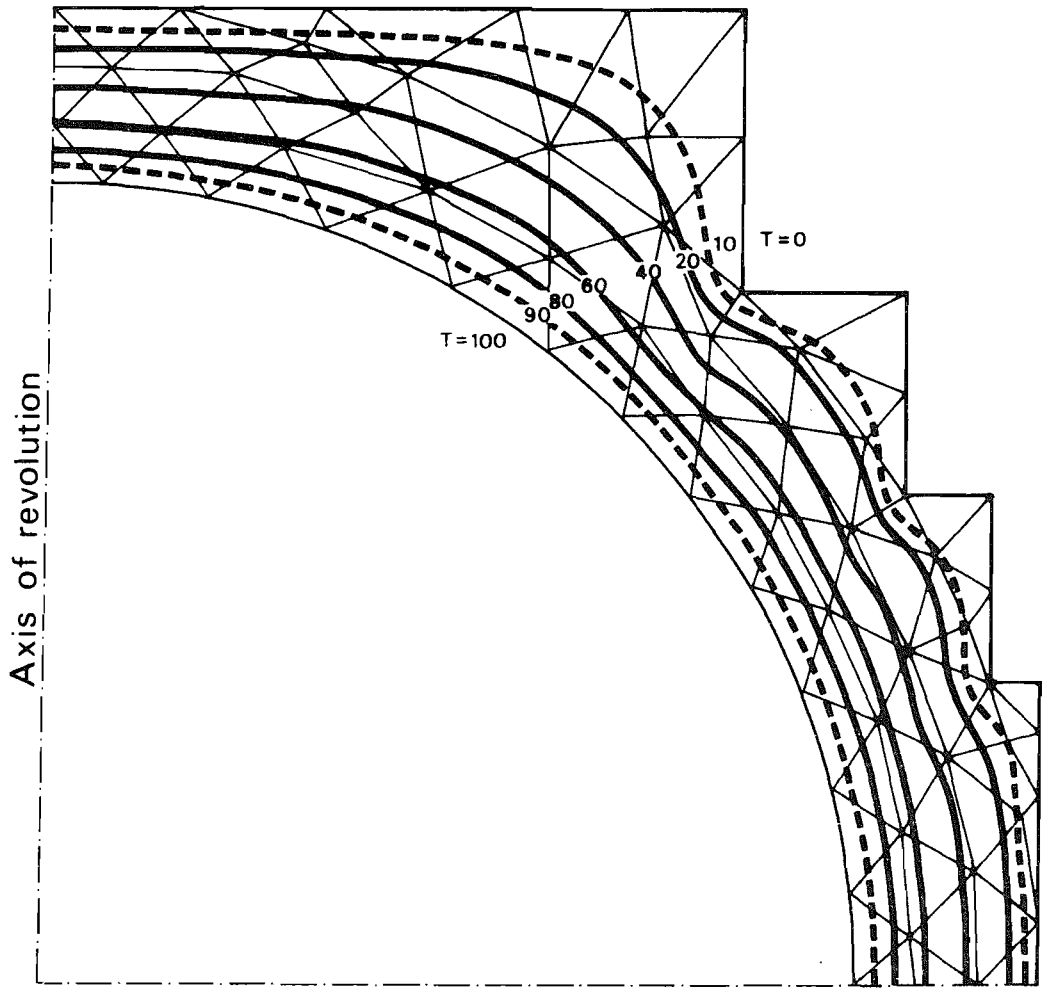

Figure 3.9.4 - F.E.M. mesh and isotherms

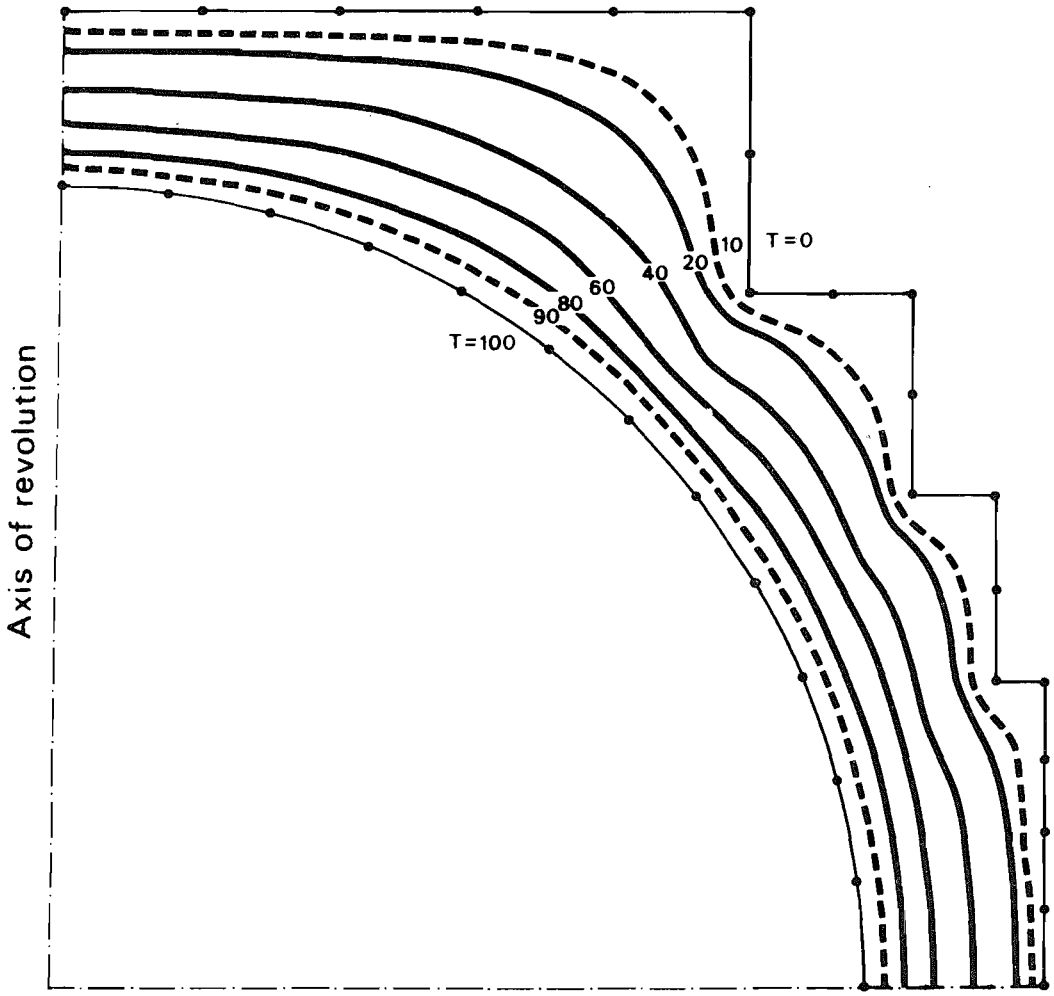

Figure 3.9.5 - Linear B.E.M. discretisation and isotherms

4. TRANSIENT POTENTIAL PROBLEMS

This chapter studies numerical solutions to the time-dependent boundary integral equation (2.8.11), repeated here for convenience, which is equivalent to the diffusion equation (2.5.1) with boundary conditions (2.5.2) and initial conditions (2.5.3),

$$c(P)\, u(P,t_F) + k \int_{t_0}^{t_F} \int_{\Gamma} u(S,t)\, q^*(P,S,t_F,t)\, d\Gamma(S)\, dt$$

$$= k \int_{t_0}^{t_F} \int_{\Gamma} q(S,t)\, u^*(P,S,t_F,t)\, d\Gamma(S)\, dt + \int_{\Omega} u_0(s,t_0)\, u^*(P,s,t_F,t_0)\, d\Omega(s) \tag{4.1}$$

Two different time-marching schemes can be employed on these numerical solutions. Both adopt a time-stepping technique where the functions u and q are assumed to vary within each time step according to interpolation functions which can be constant or of higher orders. This assumption makes it possible for the time integrals in equation (4.1) to be carried out analytically. For the first scheme, which treats each time step as a new problem, the result is a boundary integral equation similar to (3.1) but including a domain integral that accounts for the initial conditions at the beginning of each step. For the second, where the time integration process always starts at time t_0, it is a summation of boundary integrals corresponding to the time variation of functions u and q since the initial time t_0 plus a domain integral accounting for the initial conditions at t_0, which vanishes if the prescribed initial conditions of the problem are $u_0 = 0$ or can be transformed into equivalent boundary integrals, if u_0 satisfies Laplace's equation.

The basic procedures for numerical implementation of both time-marching schemes in connection with two-dimensional problems are presented in the following section. Although they are only discussed

for problems defined over finite regions of homogeneous, isotropic media, several other features such as internal sources, piecewise homogeneous regions, orthotropy and anisotropy, infinite or semi-infinite regions, can be included in the analysis in a similar way as it has been done in chapter 3 for steady-state problems.

Specific numerical and computational procedures for each time-marching scheme are then described and their accuracy and computer efficiency compared.

Next, boundary conditions of the Robin-type are introduced into the formulation. For transient heat conduction problems the assumption of (say) stepwise linear variation for both the heat transfer coefficient h and the temperature of the surrounding medium u_s (see example 3.2.1) gives rise to a quasi-quadratic variation for the flux q, and it is shown how the higher order terms can be properly accounted for.

Finally, transient axisymmetric problems are discussed, the time-dependent axisymmetric fundamental solution derived and a numerical formulation for the solution of equation (4.1) over an axisymmetric domain is presented. The complexity of the fundamental solution requires the introduction of series expansions in order to enable the time integrals in the equation to be carried out analytically.

Computer programs incorporating several features discussed in this chapter were developed and are described in chapter 6. Results of applications of such programs are presented in sections 4.4 to 4.6.

4.1 Two-Dimensional Problems

For the numerical solution of equation (4.1), the boundary Γ is discretised into a series of elements. The geometry of these elements can be modelled by straight lines, circular arcs, parabolas, etc., as discussed in section 3.1. Furthermore, functions u and q are assumed to vary within each element and each time step according to space and time interpolation functions as,

$$u = \underset{\sim}{\phi}^T \; \underset{\sim}{\chi} \; U^n_m$$
$$q = \underset{\sim}{\phi}^T \; \underset{\sim}{\chi} \; Q^n_m \qquad (4.1.1)$$

where $\underset{\sim}{\phi}$ and $\underset{\sim}{\chi}$ are the space and the time interpolation functions, respectively. The index n refers to the number of boundary nodes within each element to which nodal values of u and q are associated and the index m refers to the degree of variation of function $\underset{\sim}{\chi}$, i.e. m = 1 if $\underset{\sim}{\chi}$ is constant, m = 1,2 if $\underset{\sim}{\chi}$ is linear, etc. Let us also assume that the domain Ω is divided into cells, as discussed in section 3.3.

For two-dimensional problems, the fundamental solution and its normal derivative are given by (see equation (2.8.3)),

$$u^*(p,S,t_F,t) = \frac{1}{4\pi k\tau} \exp\left[-\frac{r^2(p,S)}{4k\tau}\right] \qquad (4.1.2)$$

$$q^*(p,S,t_F,t) = \frac{d(p,S)}{8\pi k^2\tau^2} \exp\left[-\frac{r^2(p,S)}{4k\tau}\right] \qquad (4.1.3)$$

in which $\tau = t_F - t$ and $d(p,S) = \left[X_1(p)-X_1(S)\right] x_{1,n}(S) + \left[X_2(p) - X_2(S)\right] x_{2,n}(S)$.

If the boundary Γ is discretised into S elements and N nodes, the domain Ω sub-divided into L cells and the time dimension sub-divided into F time steps, the substitution of equations (4.1.1) into equation (4.1) yields, for scheme 1, the following equation,

$$c_i \, U^i_F + k \sum_{s=1}^{S} \left(\int\int_{\Gamma_s} \underset{\sim}{\phi}^T \int_{t_{F-1}}^{t_F} q^* \, \underset{\sim}{\chi} \, dt \, d\Gamma \right) \underset{\sim}{U}^n$$

$$= k \sum_{s=1}^{S} \left(\int\int_{\Gamma_s} \underset{\sim}{\phi}^T \int_{t_{F-1}}^{t_F} u^* \, \underset{\sim}{\chi} \, dt \, d\Gamma \right) \underset{\sim}{Q}^n + \sum_{\ell=1}^{L} \int_{\Omega_\ell} u^* \, \underset{\sim}{u}_{F-1} \, d\Omega \qquad (4.1.4)$$

and for scheme 2 the equation,

$$c_i \, U^i_F + k \sum_{s=1}^{S} \sum_{f=1}^{F} \left(\int\int_{\Gamma_s} \underset{\sim}{\phi}^T \int_{t_{f-1}}^{t_f} q^* \, \underset{\sim}{\chi} \, dt \, d\Gamma \right) \underset{\sim}{U}^n$$

$$= k \sum_{s=1}^{S} \sum_{f=1}^{F} \left(\int\int_{\Gamma_s} \underset{\sim}{\phi}^T \int_{t_{f-1}}^{t_f} u^* \, \underset{\sim}{\chi} dt \, d\Gamma \right) \underset{\sim}{Q}^n + \sum_{\ell=1}^{L} \int_{\Omega_\ell} u^* \, \underset{\sim}{u}_0 \, d\Omega \qquad (4.1.5)$$

4.1.1 Constant Time Interpolation

Assuming that functions u and q remain constant on time over each time step, i.e. the interpolation function χ is unity, applying equation (4.1.4) to all N boundary nodes yields the following system of equations (see equation (3.1.8)),

$$\underset{\sim}{H}\ \underset{\sim}{U}_F = \underset{\sim}{G}\ \underset{\sim}{Q}_F + \underset{\sim}{B}\ \underset{\sim}{\overline{U}}_{F-1} \tag{4.1.6}$$

The coefficients of matrices $\underset{\sim}{\hat{H}}$, $\underset{\sim}{G}$ and $\underset{\sim}{B}$ are constituted of terms, or combination of terms, of the form (see equations (3.1.15), (3.1.18), (3.1.24)),

$$\begin{aligned}
h^m_{ij} &= k \int_{\Gamma_s} \phi^m \int_{t_{F-1}}^{t_F} q^*(i,S,t_F,t)\ dt\ d\Gamma(S) \\
g^m_{ij} &= k \int_{\Gamma_s} \phi^m \int_{t_{F-1}}^{t_F} u^*(i,S,t_F,t)\ dt\ d\Gamma(S) \\
B_{ij} &= \int_{\Omega_\ell} u^*(i,s,t_F,t_{F-1})\ d\Omega(s)
\end{aligned} \tag{4.1.7}$$

where the index m refers to the degree of variation of the interpolation function $\underset{\sim}{\phi}$. Note that $H_{ij} = \hat{H}_{ij} + c_i\ \delta_{ij}$, where δ_{ij} is the Kronecker delta.

For scheme 2, the application of equation (4.1.5) to all N boundary nodes gives,

$$\sum_{f=1}^{F} \underset{\sim}{H}_{fF}\ \underset{\sim}{U}_f = \sum_{f=1}^{F} \underset{\sim}{G}_{fF}\ \underset{\sim}{Q}_f + \underset{\sim}{B}_0\ \underset{\sim}{\overline{U}}_0 \tag{4.1.8}$$

where

$$\begin{aligned}
h^m_{fFij} &= k \int_{\Gamma_s} \phi^m \int_{t_{f-1}}^{t_f} q^*(i,S,t_F,t)\ dt\ d\Gamma(S) \\
g^m_{fFij} &= k \int_{\Gamma_s} \phi^m \int_{t_{f-1}}^{t_f} u^*(i,S,t_F,t)\ dt\ d\Gamma(S) \\
B_{0ij} &= \int_{\Omega_\ell} u^*(i,s,t_F,t_0)\ d\Omega(s)
\end{aligned} \tag{4.1.9}$$

being $H_{fFij} = \hat{H}_{fFij} + c_i \delta_{fF} \delta_{ij}$ now. The values of $\underset{\sim}{U}_f$ and $\underset{\sim}{Q}_f$ for $f = 1,\ldots,F-1$ are known from calculations at previous steps.

From (4.1.7) and (4.1.9), it follows that the time integrals can be carried out analytically. The integral in q^* gives,

$$\int_{t_{f-1}}^{t_f} q^*(i,S,t_F,t)\, dt = \frac{d}{2\pi k r^2} \int_{t_{f-1}}^{t_f} \frac{r^2}{4k\tau^2} \exp\left(-\frac{r^2}{4k\tau}\right) dt$$

$$= \frac{d}{2\pi k r^2} \left[\exp(-a_{f-1}) - \exp(-a_f)\right] \qquad (4.1.10)$$

where

$$a_f = \frac{r^2}{4k(t_F - t_f)} \qquad (4.1.11)$$

In order to perform the integral in u^*, we need to make an appropriate change of variables. Calling

$$x = \frac{r^2}{4k\tau} \qquad (4.1.12)$$

the integral becomes [75],

$$\int_{t_{f-1}}^{t_f} u^*(i,S,t_F,t)\, dt = \frac{1}{\pi r^2} \int_{t_{f-1}}^{t_f} \frac{r^2}{4k\tau} \exp\left(-\frac{r^2}{4k\tau}\right) dt$$

$$= \frac{1}{4\pi k} \int_{a_{f-1}}^{a_f} \frac{e^{-x}}{x}\, dx = \frac{1}{4\pi k} \left[E_1(a_{f-1}) - E_1(a_f)\right] \qquad (4.1.13)$$

where E_1 is the exponential-integral function. From definition (4.1.11), we note that $\exp(-a_F) = 0$ in (4.1.10) and $E_1(a_F) = 0$ in (4.1.13).

4.1.2 Linear Time Interpolation

Let us now assume a linear variation on time for functions u and q within each time step according to the following interpolation functions,

$$\chi_1 = \frac{t_f - t}{\Delta t_f} \quad ; \quad \chi_2 = \frac{t - t_{f-1}}{\Delta t_f} \qquad (4.1.14)$$

where $\Delta t_f = t_f - t_{f-1}$.

The system of equations obtained from the application of equation (4.1.4) to all boundary nodes is now of the form,

$$\underset{\sim}{H}^1 \underset{\sim}{U}_{F-1} + \underset{\sim}{H}^2 \underset{\sim}{U}_F = \underset{\sim}{G}^1 \underset{\sim}{Q}_{F-1} + \underset{\sim}{G}^2 \underset{\sim}{Q}_F + \underset{\sim}{B} \underset{\sim}{U}_{F-1} \tag{4.1.15}$$

where the coefficients of the matrices involved are constituted of terms such as,

$$h_{ij}^{1,m} = \frac{k}{\Delta t_F} \int_{\Gamma_s} \phi^m \int_{t_{F-1}}^{t_F} (t_F - t)\, q^*(i,S,t_F,t)\, dt\, d\Gamma(S)$$

$$h_{ij}^{2,m} = \frac{k}{\Delta t_F} \int_{\Gamma_s} \phi^m \int_{t_{F-1}}^{t_F} (t - t_{F-1})\, q^*(i,S,t_F,t)\, dt\, d\Gamma(S)$$

$$g_{ij}^{1,m} = \frac{k}{\Delta t_F} \int_{\Gamma_s} \phi^m \int_{t_{F-1}}^{t_F} (t_F - t)\, u^*(i,S,t_F,t)\, dt\, d\Gamma(S) \tag{4.1.16}$$

$$g_{ij}^{2,m} = \frac{k}{\Delta t_F} \int_{\Gamma_s} \phi^m \int_{t_{F-1}}^{t_F} (t - t_{F-1})\, u^*(i,S,t_F,t)\, dt\, d\Gamma(S)$$

with B_{ij} being calculated as in (4.1.7) and $H_{ij}^2 = \hat{H}_{ij}^2 + c_i \delta_{ij}$.

Analogously, the application of (4.1.5) to all boundary nodes gives,

$$\sum_{f=1}^{F} (\underset{\sim}{H}_{fF}^1 \underset{\sim}{U}_{f-1} + \underset{\sim}{H}_{fF}^2 \underset{\sim}{U}_f) = \sum_{f=1}^{F} (\underset{\sim}{G}_{fF}^1 \underset{\sim}{Q}_{f-1} + \underset{\sim}{G}_{fF}^2 \underset{\sim}{Q}_f) + \underset{\sim}{B}_0 \underset{\sim}{\overline{U}}_0 \tag{4.1.17}$$

where

$$h_{fFij}^{1,m} = \frac{k}{\Delta t_f} \int_{\Gamma_s} \phi^m \int_{t_{f-1}}^{t_f} (t_f - t)\, q^*(i,S,t_F,t)\, dt\, d\Gamma(S)$$

$$h_{fFij}^{2,m} = \frac{k}{\Delta t_f} \int_{\Gamma_s} \phi^m \int_{t_{f-1}}^{t_f} (t - t_{f-1})\, q^*(i,S,t_F,t)\, dt\, d\Gamma(S)$$

$$g_{fFij}^{1,m} = \frac{k}{\Delta t_f} \int_{\Gamma_s} \phi^m \int_{t_{f-1}}^{t_f} (t_f - t)\, u^*(i,S,t_F,t)\, dt\, d\Gamma(S) \tag{4.1.18}$$

$$g_{fFij}^{2,m} = \frac{k}{\Delta t_f} \int_{\Gamma_s} \phi^m \int_{t_{f-1}}^{t_f} (t - t_{f-1})\, u^*(i,S,t_F,t)\, dt\, d\Gamma(S)$$

with B_{0ij} computed as in (4.1.9) and $H^2_{fFij} = \hat{H}^2_{fFij} + c_i \delta_{fF} \delta_{ij}$.

The time integrals can now be divided into integrals of the same form as previously (equations (4.1.10) and (4.1.13)) plus integrals of the form,

$$\int_{t_{f-1}}^{t_f} t\, q^*(i,S,t_F,t)\, dt = \frac{d}{2\pi k} \int_{t_{f-1}}^{t_f} \frac{t}{4k\tau^2} \exp\left(-\frac{r^2}{4k\tau}\right) dt$$

$$= \frac{d}{2\pi k} \left[\frac{t_F}{r^2} \int_{a_{f-1}}^{a_f} e^{-x}\, dx - \frac{1}{4k} \int_{a_{f-1}}^{a_f} \frac{e^{-x}}{x}\, dx\right] \qquad (4.1.19)$$

$$\int_{t_{f-1}}^{t_f} t\, u^*(i,S,t_F,t)\, dt = \frac{1}{4\pi k} \int_{t_{f-1}}^{t_f} \frac{t}{\tau} \exp\left(-\frac{r^2}{4k\tau}\right) dt$$

$$= \frac{1}{4\pi k} \left[t_F \int_{a_{f-1}}^{a_f} \frac{e^{-x}}{x}\, dx - \frac{r^2}{4k} \int_{a_{f-1}}^{a_f} \frac{e^{-x}}{x^2}\, dx\right] \qquad (4.1.20)$$

The integrals in the above equations are of the same type as the ones in equations (4.1.10) and (4.1.13) apart from the last one in (4.1.20), which gives [75]

$$\int_{a_{f-1}}^{a_f} \frac{e^{-x}}{x^2}\, dx = \Gamma(-1,a_{f-1}) - \Gamma(-1,a_f) \qquad (4.1.21)$$

where Γ is the incomplete Gamma function.

Thus, adding up all terms and taking into account the relation between Γ and E_1, i.e. [46]

$$\Gamma(-n,a) = \frac{(-1)^n}{n!} \left[E_1(a) - e^{-a} \sum_{i=0}^{n-1} \frac{(-1)^i\, i!}{a^{i+1}}\right] \qquad n=1,2,\ldots \qquad (4.1.22)$$

the time integrals in (4.1.16) and (4.1.18) finally give,

$$\int_{t_{f-1}}^{t_f} (t_f-t)\, u^*(i,S,t_F,t)\, dt = -\frac{1}{4\pi k}\left\{\left[(t_F-t_f)+\frac{r^2}{4k}\right]\left[E_1(a_{f-1})-E_1(a_f)\right]\right.$$

$$\left. -\frac{r^2}{4k}\left[\frac{1}{a_{f-1}}\exp(-a_{f-1})-\frac{1}{a_f}\exp(-a_f)\right]\right\}$$

$$\int_{t_{f-1}}^{t_f} (t-t_{f-1})\, u^*(i,S,t_F,t)\, dt = \frac{1}{4\pi k}\left\{\left[(t_F-t_{f-1})+\frac{r^2}{4k}\right]\left[E_1(a_{f-1})-E_1(a_f)\right]\right.$$

$$\left. -\frac{r^2}{4k}\left[\frac{1}{a_{f-1}}\exp(-a_{f-1})-\frac{1}{a_f}\exp(-a_f)\right]\right\} \qquad (4.1.23)$$

$$\int_{t_{f-1}}^{t_f} (t_f-t)\, q^*(i,S,t_F,t)\, dt = -\frac{d}{2\pi k}\left\{\frac{(t_F-t_f)}{r^2}\left[\exp(-a_{f-1})-\exp(-a_f)\right]\right.$$

$$\left. -\frac{1}{4k}\left[E_1(a_{f-1})-E_1(a_f)\right]\right\}$$

$$\int_{t_{f-1}}^{t_f} (t-t_{f-1})\, q^*(i,S,t_F,t)\, dt = \frac{d}{2\pi k}\left\{\frac{(t_F-t_{f-1})}{r^2}\left[\exp(-a_{f-1})-\exp(-a_f)\right]\right.$$

$$\left. -\frac{1}{4k}\left[E_1(a_{f-1})-E_1(a_f)\right]\right\}$$

4.1.3 Quadratic Time Interpolation

Although the computer programs described in chapter 6 only make use of stepwise constant or linear time variations, it is interesting to investigate the difficulties associated with the use of higher order time interpolation functions.

Consider, for instance, that functions u and q have a quadratic variation within each time step according to the following interpolation functions,

$$\chi_1 = 2\bar{t}^2 - 3\bar{t} + 1$$

$$\chi_2 = 4\bar{t}(1-\bar{t}) \qquad ; \qquad \chi_3 = \bar{t}(2\bar{t}-1) \qquad (4.1.24)$$

where $\bar{t} = (t-t_{f-1})/(t_f-t_{f-1})$ and the time stations are t_{f-1}, $t_{f-\frac{1}{2}}$ and t_f, being $t_{f-\frac{1}{2}} = (t_{f-1}+t_f)/2$.

For simplicity, only time-marching scheme 1 will be considered in what follows, extension to scheme 2 being straightforward. In this case, the application of equation (4.1.4) to all N boundary nodes gives,

$$\underset{\sim}{H}^1 \underset{\sim}{U}_{F-1} + \underset{\sim}{H}^2 \underset{\sim}{U}_{F-\frac{1}{2}} + \underset{\sim}{H}^3 \underset{\sim}{U}_F = \underset{\sim}{G}^1 \underset{\sim}{Q}_{F-1} + \underset{\sim}{G}^2 \underset{\sim}{Q}_{F-\frac{1}{2}} + \underset{\sim}{G}^3 \underset{\sim}{Q}_F + \underset{\sim}{B}\, \underset{\sim}{\bar{U}}_{F-1} \qquad (4.1.25)$$

in which the coefficients of the matrices are constituted of terms such as,

$$h_{ij}^{1,m} = \frac{k}{\Delta t_F^2} \int_{\Gamma_s} \phi^m \int_{t_{F-1}}^{t_F} \left[(t-t_F)(2t-t_F-t_{F-1})\right] q^*(i,S,t_F,t)\, dt\, d\Gamma(S)$$

$$h_{ij}^{2,m} = \frac{k}{\Delta t_F^2} \int_{\Gamma_s} \phi^m \int_{t_{F-1}}^{t_F} \left[4(t-t_{F-1})(t_F-t)\right] q^*(i,S,t_F,t)\, dt\, d\Gamma(S)$$

$$h_{ij}^{3,m} = \frac{k}{\Delta t_F^2} \int_{\Gamma_s} \phi^m \int_{t_{F-1}}^{t_F} \left[(t-t_{F-1})(2t-t_F-t_{F-1})\right] q^*(i,S,t_F,t)\, dt\, d\Gamma(S)$$

(4.1.26)

$$g_{ij}^{1,m} = \frac{k}{\Delta t_F^2} \int_{\Gamma_s} \phi^m \int_{t_{F-1}}^{t_F} \left[(t-t_F)(2t-t_F-t_{F-1})\right] u^*(i,S,t_F,t)\, dt\, d\Gamma(S)$$

$$g_{ij}^{2,m} = \frac{k}{\Delta t_F^2} \int_{\Gamma_s} \phi^m \int_{t_{F-1}}^{t_F} \left[4(t-t_{F-1})(t_F-t)\right] u^*(i,S,t_F,t)\, dt\, d\Gamma(S)$$

$$g_{ij}^{3,m} = \frac{k}{\Delta t_F^2} \int_{\Gamma_s} \phi^m \int_{t_{F-1}}^{t_F} \left[(t-t_{F-1})(2t-t_F-t_{F-1})\right] u^*(i,S,t_F,t)\, dt\, d\Gamma(S)$$

with B_{ij} being calculated as in (4.1.7) and $H_{ij}^3 = \hat{H}_{ij}^3 + c_i\, \delta_{ij}$.

Expanding the terms in brackets in (4.1.26), we note that all the integrals involved have been previously calculated in (4.1.10), (4.1.13) and (4.1.21), apart from the following,

$$\int_{t_{F-1}}^{t_F} t^2\, q^*(i,S,t_F,t)\, dt = \frac{d}{2\pi k} \int_{t_{F-1}}^{t_F} \frac{t^2}{4k\tau^2} \exp\left(-\frac{r^2}{4k\tau}\right) dt$$

$$= \frac{d}{2\pi k}\left[\frac{t_F^2}{r^2}\int_{a_{F-1}}^{\infty} e^{-x}\, dx - \frac{t_F}{2k}\int_{a_{F-1}}^{\infty} \frac{e^{-x}}{x}\, dx + \frac{r^2}{16k^2}\int_{a_{F-1}}^{\infty} \frac{e^{-x}}{x^2}\, dx\right] \tag{4.1.27}$$

$$\int_{t_{F-1}}^{t_F} t^2\, u^*(i,S,t_F,t)\, dt = \frac{1}{4\pi k} \int_{t_{F-1}}^{t_F} \frac{t^2}{\tau} \exp\left(-\frac{r^2}{4k\tau}\right) dt$$

$$= \frac{1}{4\pi k}\left[t_F^2\int_{a_{F-1}}^{\infty} \frac{e^{-x}}{x}\, dx - \frac{t_F r^2}{2k}\int_{a_{F-1}}^{\infty} \frac{e^{-x}}{x^2}\, dx + \frac{r^4}{16k^2}\int_{a_{F-1}}^{\infty} \frac{e^{-x}}{x^3}\, dx\right] \tag{4.1.28}$$

Again, the integrals in the above equations are of the same type as the ones in equations (4.1.10), (4.1.13) and (4.1.21) except the term [75],

$$\int_{a_{F-1}}^{\infty} \frac{e^{-x}}{x^3}\, dx = \Gamma(-2, a_{F-1}) \tag{4.1.29}$$

The final expressions for the time integrals in equations (4.1.26) can now be easily written by combining the appropriate terms explicitly calculated in (4.1.10), (4.1.13), (4.1.21) and (4.1.29), taking into account relation (4.1.22).

After introducing the boundary conditions of the problem (4.1.25) becomes a system of N equations with 2N unknowns, since all values of $\underset{\sim}{U}_{F-1}$ and $\underset{\sim}{Q}_{F-1}$ are prescribed (or have been previously calculated) but only half the boundary values at times $t_{F-\frac{1}{2}}$ and t_F are known. This means that for the problem to be well-posed we need to double the total number of simultaneous equations involved in solving a single

time step. This can be achieved by writing a boundary integral equation similar to (4.1) for the time $t=t_{F-\frac{1}{2}}$,

$$c(P)\ u(P,t_{F-\frac{1}{2}}) + k \int_{t_0}^{t_{F-\frac{1}{2}}} \int_{\Gamma} u(S,t)\ q^*(P,S,t_{F-\frac{1}{2}},t)\ d\Gamma(S)\ dt$$

$$= k \int_{t_0}^{t_{F-\frac{1}{2}}} \int_{\Gamma} q(S,t)\ u^*(P,S,t_{F-\frac{1}{2}},t)\ d\Gamma(S)\ dt + \int_{\Omega} u_0(s,t_0)\ u^*(P,s,t_{F-\frac{1}{2}},t_0)\ d\Omega(s) \tag{4.1.30}$$

The upper limit of the time integrals was taken as $t_{F-\frac{1}{2}}$ because of the causality condition (see section 2.8) which specifies that u^* and q^* are identically zero for $t>t_{F-\frac{1}{2}}$.

Discretising the above equation and applying it to all N boundary nodes yields the system of equations,

$$\underset{\sim}{\bar{H}}^1\ \underset{\sim}{U}_{F-1} + \underset{\sim}{\bar{H}}^2\ \underset{\sim}{U}_{F-\frac{1}{2}} + \underset{\sim}{\bar{H}}^3\ \underset{\sim}{U}_F = \underset{\sim}{\bar{G}}^1\ \underset{\sim}{Q}_{F-1} + \underset{\sim}{\bar{G}}^2\ \underset{\sim}{Q}_{F-\frac{1}{2}} + \underset{\sim}{\bar{G}}^3\ \underset{\sim}{Q}_F + \underset{\sim}{\bar{B}}\ \underset{\sim}{\bar{U}}_{F-1} \tag{4.1.31}$$

in which the coefficients of the matrices can be calculated by using expressions similar to (4.1.26).

The simultaneous solution of equations (4.1.25) and (4.1.31) now permits determining the unknown boundary values of $\underset{\sim}{U}$ and $\underset{\sim}{Q}$ at times $t_{F-\frac{1}{2}}$ and t_F from the knowledge of the initial conditions at t_{F-1} and prescribed boundary conditions at $t_{F-\frac{1}{2}}$ and t_F.

This procedure can be extended to time functions of higher orders, noting that the total number of simultaneous equations to be stepwise solved will be further increased.

4.1.4 Space Integration

The remaining step in the numerical solution of equation (4.1) is the computation of the space integrals. Although the space interpolation functions $\underset{\sim}{\phi}$ in equation (4.1.1) can be taken as constant,

linear, quadratic, etc., as discussed in the previous chapter, only linear elements were implemented in the computer programs developed, following the results obtained for steady-state problems. Extension to higher order elements should involve the same degree of difficulty as for Laplace's equation and can be done by following the same procedures as described in section 3.1.

The terms H_{fFij} and G_{fFij} (excluding the singular terms f=F, i=j) in equation (4.1.8) for linear elements can be computed as,

$$\begin{aligned} H_{fFij} &= h^2_{fFip} + h^1_{fFiq} \\ G_{fFij} &= g^2_{fFip} + g^1_{fFiq} \end{aligned} \tag{4.1.32}$$

where the indices p and q refer to the element at the intersection of which node j is located. In general, we can evaluate these terms by using a six-points Gauss quadrature rule,

$$\begin{aligned} h^m_{fFip} &= \frac{d_{ip}}{4\pi} \sum_{k=1}^{6} \frac{1}{r^2_{ik}} \left[\exp(-a_{f-1}) - \exp(-a_f)\right]_K \phi^m_K W_K \\ g^m_{fFip} &= \frac{\ell_p}{8\pi} \sum_{k=1}^{6} \left[E_1(a_{f-1}) - E_1(a_f)\right]_K \phi^m_K W_K \end{aligned} \tag{4.1.33}$$

where $d_{ip} = (X^i_1-X^1_1)(X^2_2-X^1_2) + (X^i_2-X^1_2)(X^1_1-X^2_1)$, m=1,2 and ϕ is given in equation (3.1.17). For convenience of the numerical computation, the exponential-integral function is approximated by rational and polynomial expansions [46] which are given in appendix A. Note that the coefficients H_{ij} and G_{ij} (i≠j) in equation (4.1.6) can be computed through the same formulae, with f=F.

For linear time interpolation functions, the terms that form the coefficients H^2_{fFij}, G^2_{fFij} (excluding the singular coefficients, f=F, i=j), H^1_{fFij} and G^1_{fFij} (which have no singular coefficients) in equations (4.1.15) and (4.1.17) can be evaluated as,

$$h^{1,m}_{fFip} = -\frac{d_{ip}}{4\pi\Delta t_f}\sum_{K=1}^{6}\left\{\frac{(t_F-t_f)}{r^2_{iK}}\left[\exp(-a_{f-1}) - \exp(-a_f)\right]\right.$$

$$\left. - \frac{1}{4k}\left[E_1(a_{f-1}) - E_1(a_f)\right]\right\}_K \phi^m_K W_K$$

$$h^{2,m}_{fFip} = \frac{d_{ip}}{4\pi\Delta t_f}\sum_{K=1}^{6}\left\{\frac{(t_F-t_{f-1})}{r^2_{iK}}\left[\exp(-a_{f-1}) - \exp(-a_f)\right]\right.$$

$$\left. - \frac{1}{4k}\left[E_1(a_{f-1}) - E_1(a_f)\right]\right\}_K \phi^m_K W_K \qquad (4.1.34)$$

$$g^{1,m}_{fFip} = -\frac{\ell_p}{8\pi\Delta t_f}\sum_{K=1}^{6}\left\{\left[t_F-t_f + \frac{r^2_{iK}}{4k}\right]\left[E_1(a_{f-1}) - E_1(a_f)\right]\right.$$

$$\left. - \frac{r^2_{iK}}{4k}\left[\frac{1}{a_{f-1}}\exp(-a_{f-1}) - \frac{1}{a_f}\exp(-a_f)\right]\right\}_K \phi^m_K W_K$$

$$g^{2,m}_{fFip} = \frac{\ell_p}{8\pi\Delta t_f}\sum_{K=1}^{6}\left\{\left[t_F-t_{f-1} + \frac{r^2_{iK}}{4k}\right]\left[E_1(a_{f-1}) - E_1(a_f)\right]\right.$$

$$\left. - \frac{r^2_{iK}}{4k}\left[\frac{1}{a_{f-1}}\exp(-a_{f-1}) - \frac{1}{a_f}\exp(-a_f)\right]\right\}_K \phi^m_K W_K$$

The coefficients G_{ii} in (4.1.6), G_{FFii} in (4.1.8), G^2_{ii} in (4.1.15) and G^2_{FFii} in (4.1.17) all contain integrals with a logarithmic (integrable) singularity. For the first and second of these terms we can write, with reference to figure 3.1.3,

$$G_{ii} = G_{FFii} = \frac{1}{4\pi}\left\{\frac{\ell_p}{4}\int_{-1}^{1} E_1\left[\frac{\alpha_p(1-\xi_p)^2}{4}\right](1+\xi_p)\,d\xi\right.$$

$$\left. + \frac{\ell_q}{4}\int_{-1}^{1} E_1\left[\frac{\alpha_q(1+\xi_q)^2}{4}\right](1-\xi_q)\,d\xi\right\} \qquad (4.1.35)$$

where

$$\alpha_p = \frac{\ell^2_p}{4k\Delta t_F} \qquad (4.1.36)$$

Expanding the exponential-integral in series [46],

$$E_1(x) = -C - \log x + \sum_{n=1}^{\infty}(-1)^{n-1}\frac{x^n}{nn!} \qquad (4.1.37)$$

in which C is the Euler's constant, C = 0.57721566..., the integrals in equation (4.1.35) can be evaluated in closed form as,

$$G_{ii} = G_{FFii} = \frac{1}{8\pi} \left[\ell_p \, F(\alpha_p) + \ell_q \, F(\alpha_q) \right] \tag{4.1.38}$$

where

$$F(\alpha_p) = 3 - C - \log \alpha_p + \sum_{n=1}^{\infty} (-1)^{n-1} \frac{\alpha_p^n}{n(2n+1)(n+1)!} \tag{4.1.39}$$

The series that appears in (4.1.39) converges very quickly for small values of α but slowly as α increases. To overcome this problem, we can integrate analytically over a segment near the singularity thus ensuring that the coefficient α is always less or equal one and numerically integrate the rest of the element using a standard Gaussian quadrature, as if these parts were separate elements. The length L of the analytically integrated part of the element is calculated through (4.1.36),

$$L_p \leqslant 2(k\Delta t_F)^{\frac{1}{2}} \leqslant \ell_p \tag{4.1.40}$$

For computer efficiency, it is more convenient to relate each term of the series in equation (4.1.39) to the previous one,

$$S_n = \frac{(1-n)(2n-1)\alpha_p}{n(2n+1)(n+1)} S_{n-1} \qquad n = 2,3,\ldots$$
$$S_1 = \frac{\alpha_p}{6} \tag{4.1.41}$$

For the coefficients G^2_{ii} in (4.1.15) and G^2_{FFii} in (4.1.17) we have,

$$G^2_{ii} = G^2_{FFii} = \frac{1}{4\pi} \left\{ \frac{\ell_p}{4} \int_{-1}^{1} \left[(1+\beta_p) \, E_1(\beta_p) - \exp(-\beta_p) \right] (1+\xi_p) \, d\xi \right.$$
$$\left. + \frac{\ell_q}{4} \int_{-1}^{1} \left[(1+\beta_q) \, E_1(\beta_q) - \exp(-\beta_q) \right] (1-\xi_q) \, d\xi \right\} \tag{4.1.42}$$

where

$$\beta_p = \frac{\alpha_p (1-\xi_p)^2}{4} \quad , \quad \beta_q = \frac{\alpha_q (1+\xi_q)^2}{4} \tag{4.1.43}$$

Separating the first integral in equation (4.1.42) as,

$$\int_{-1}^{1} E_1(\beta_p)(1+\xi_p)\ d\xi + \int_{-1}^{1} \beta_p\ E_1(\beta_p)(1+\xi_p)\ d\xi - \int_{-1}^{1} \exp(-\beta_p)(1+\xi_p)\ d\xi \tag{4.1.44}$$

we note that only the first integral above is singular and that this integral is the same as the first integral in equation (4.1.35). Thus it can be evaluated in closed form as previously (see equation (4.1.38)) and the remaining integrals, which are non-singular, are computed by using a standard Gaussian quadrature. The same is valid for the second integral in equation (4.1.42).

The coefficients H_{ii} in (4.1.6), H_{FFii} in (4.1.8), H^2_{ii} in (4.1.15) and H^2_{FFii} in (4.1.17) all contain integrals with a stronger singularity which are only integrable in the Cauchy principal value sense. The same procedures previously applied for Laplace's equation can again be employed to calculate these coefficients (which include the free terms c_i).

The application of a constant potential over the whole body now gives, for instance, for H_{ii} in (4.1.6),

$$H_{ii} = -\sum_{\substack{j=1 \\ (j\neq i)}}^{N} H_{ij} + \sum_{k=1}^{M} B_{ik} \tag{4.1.45}$$

where N is the number of boundary nodes and M is the number of internal points adopted for the domain integration (as will be explained in the following section). This procedure has the obvious disadvantage that the whole domain always needs to be discretised, since $\underset{\sim}{U}$ is now a constant potential. For scheme 2, it can be noted from equation (4.1.5) that no domain integration is needed if the initial conditions of the problem are $u_0 = 0$ everywhere. Thus, the use of equation (4.1.45) implies an extra (and unnecessary) computational effort.

The alternative procedure is to compute the diagonal coefficients of the matrices by employing the relation $H_{ii} = \hat{H}_{ii} + c_i$. The value of

the coefficients c_i can be obtained in the same way as for Laplace's equation (see equation (2.4.7)),

$$c_i = 1 + \lim_{\varepsilon \to 0} k \int_{\Gamma_\varepsilon} \int_{t_0}^{t_F} q^* \, dt \, d\Gamma \qquad (4.1.46)$$

which, with reference to figure 2.4.1, reduces to

$$c_i = 1 - \frac{1}{2\pi} \lim_{\varepsilon \to 0} \int_{\theta_1}^{\theta_2} \frac{1}{\varepsilon} \exp \left[- \frac{\varepsilon^2}{4k(t_F - t_0)} \right] \varepsilon \, d\theta = \frac{\pi + \alpha_1 - \alpha_2}{2\pi} \qquad (4.1.47)$$

For linear elements, the terms $\hat{H}_{ii}$ are identically zero due to the orthogonality between r and n, which makes d = 0 in (4.1.3). This is not so for higher order elements, and the integrals must then be carried out in closed form (at least over a short straight line segment around the singularity) in order to properly account for their principal values.

It should be pointed out that, for a certain space interpolation function, refining the order of the time approximation introduces only additional regular terms into the boundary integrals. This means that for linear elements, for instance, the only singular integral to be evaluated is the one appearing in equation (4.1.35), irrespective of the order of the time interpolation function.

4.2 Scheme 1 (Step-by-Step)

At the beginning of the process (time $t = t_0$), initial values u_0 of function u over $\Omega + \Gamma$ are specified. The domain is subdivided into L (triangular) cells, N_I internal points being used to define the cells (figure 4.2.1). The initial conditions are taken into account through a numerical integration over the domain and their values at a number M of points considered.

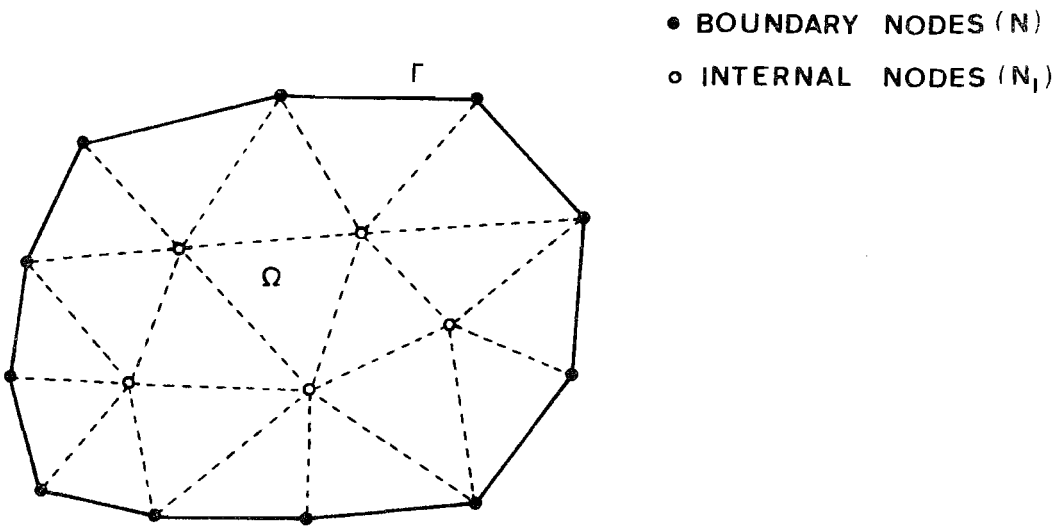

Figure 4.2.1 - Region Ω + Γ discretised into S boundary elements and L cells

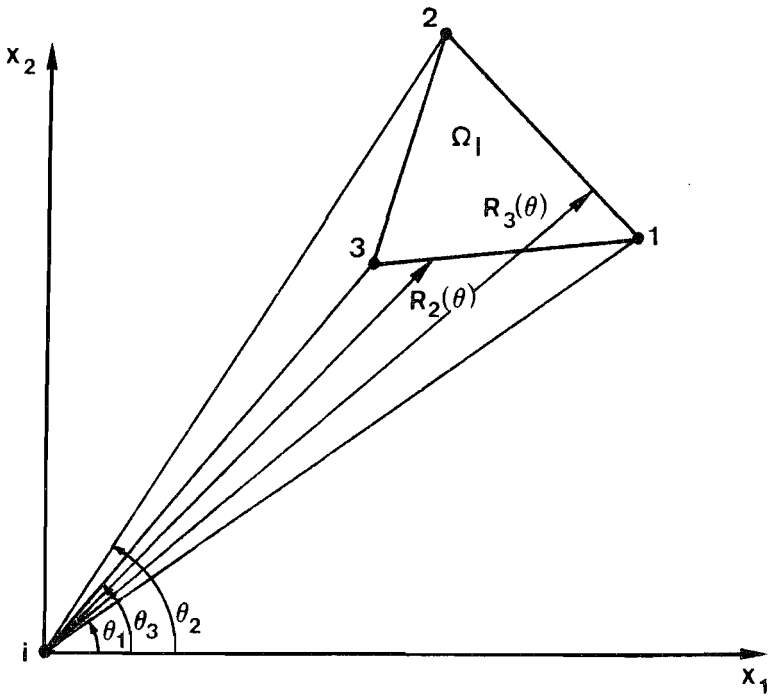

Figure 4.2.2 - Polar coordinates for semi-analytical integration

Since half the boundary values of u and q are prescribed, equation (4.1.6) can then be employed to compute the remaining boundary data for the first time step (F=1). Note that if linear (or higher orders) time interpolation functions are adopted, initial values of function q along Γ must also be given (equation (4.1.15)).

At the end of the time step (time $t = t_1$), the values of u at the previously selected M points are recomputed to be used as initial values for the next step. This can be done by using equation (2.8.6) which, in matricial form, becomes (for the constant case),

$$\underset{\sim}{\overline{U}}_F = \underset{\sim}{G}' \underset{\sim}{Q}_F - \underset{\sim}{H}' \underset{\sim}{U}_F + \underset{\sim}{B}' \underset{\sim}{\overline{U}}_{F-1} \tag{4.2.1}$$

and for the linear case,

$$\underset{\sim}{\overline{U}}_F = \underset{\sim}{G}'^1 \underset{\sim}{Q}_{F-1} + \underset{\sim}{G}'^2 \underset{\sim}{Q}_F - \underset{\sim}{H}'^1 \underset{\sim}{U}_{F-1} - \underset{\sim}{H}'^2 \underset{\sim}{U}_F + \underset{\sim}{B}' \underset{\sim}{\overline{U}}_{F-1} \tag{4.2.2}$$

where the dimensions of matrices $\underset{\sim}{G}'$ and $\underset{\sim}{H}'$ are M x N and of matrix $\underset{\sim}{B}'$ are M x M.

The coefficients of matrices $\underset{\sim}{G}$, $\underset{\sim}{H}$, $\underset{\sim}{G}'$ and $\underset{\sim}{H}'$ in equations (4.1.6), (4.1.15), (4.2.1) and (4.2.2) depend on geometrical data, properties of the medium and the time step (see (4.1.33), (4.1.34), (4.1.38) and (4.1.42)). Thus, adopting a constant time step throughout the analysis, they can all be computed only once and stored.

The same also applies to the coefficients of matrices $\underset{\sim}{B}$ and $\underset{\sim}{B}'$ (see equation (4.1.7)), which result from integrals over the cells. Two different kinds of approximations for the variation of u within each cell were tested, as well as two different numerical integration schemes.

Calling

$$\sum_{\ell=1}^{L} \int_{\Omega_\ell} u^* \, \underset{\sim}{u}_{F-1} \, d\Omega = \sum_{j=1}^{M} B_{ij} \, \overline{U}_{(F-1)j} \tag{4.2.3}$$

and applying Hammer's quintic quadrature scheme to numerically integrate

the cells, assuming that the values of $\overline{\underset{\sim}{U}}$ are calculated directly at each integration point, gives

$$\sum_{\ell=1}^{L} \int_0^1 \left[\int_0^{1-\xi_2} \underset{\sim}{u^*}(\xi)\ \underset{\sim}{u}_{F-1}(\xi)\ |J(\xi)|\ d\xi_1 \right] d\xi_2$$

$$= \sum_{\ell=1}^{L} \sum_{K=1}^{7} u^*_K\ |J|_K\ W_K\ u_{(f-1)K} \qquad (4.2.4)$$

so the coefficients of matrix $\underset{\sim}{B}$ are of the form

$$B_{ij} = \frac{1}{4\pi k\Delta t} \exp\left(-\frac{r^2_{ij}}{4k\Delta t}\right) |J|_j\ W_j \qquad (4.2.5)$$

and the number of initial-value points is M = 7L.

Alternatively, assuming that function u varies linearly within each cell, we have

$$\sum_{\ell=1}^{L} \sum_{m=1}^{3} \int_{\Omega_\ell} u^*\ \Psi_m\ d\Omega\ u_{(F-1)m} = \sum_{j=1}^{M} B_{ij}\ \overline{U}_{(F-1)j} \qquad (4.2.6)$$

where the interpolation functions $\underset{\sim}{\Psi}$ are given in (3.8.2).

Transforming the above integral to polar coordinates (R,θ) gives, with reference to figure 4.2.2 [76],

$$\int_{\Omega_\ell} u^*\ \Psi_m\ d\Omega = \frac{1}{4\pi k\Delta t} \int_{\Omega_\ell} \Psi_m \exp\left(-\frac{r^2}{4k\Delta t}\right) d\Omega$$

$$= \frac{1}{4\pi k\Delta t} \left\{ \int_{\theta_1}^{\theta_3} \int_{R_2(\theta)}^{R_3(\theta)} \Psi_m(R,\theta) \exp\left(-\frac{R^2}{4k\Delta t}\right) R\ dR\ d\theta \right.$$

$$\left. + \int_{\theta_3}^{\theta_2} \int_{R_1(\theta)}^{R_3(\theta)} \Psi_m(R,\theta) \exp\left(-\frac{R^2}{4k\Delta t}\right) R\ dR\ d\theta \right\} \qquad (4.2.7)$$

where:

$$R_m(\theta) = -\frac{2A_\ell \xi_m^\ell(i)}{b_m \cos\theta + a_m \sin\theta}$$

$$\Psi_m(R,\theta) = \xi_m^\ell(i) + \frac{R}{2A_\ell}(b_m \cos\theta + a_m \sin\theta) \qquad (4.2.8)$$

$$a_m = X_1^p - X_1^n$$

$$b_m = X_2^n - X_2^p$$

in which m = 1,2,3 for n = 2,3,1 and p = 3,1,2, A_ℓ is the area of cell ℓ and $\xi_m^\ell(i)$ are the triangular coordinates of point i relative to cell ℓ.

The integration with respect to R can be performed analytically as follows,

$$\int_{\Omega_\ell} u^* \Psi_m \, d\Omega = \frac{1}{2\pi} \left\{ \int_{\theta_1}^{\theta_3} \left\{ \xi_m^\ell(i) \left[\exp\left[-\frac{R_2^2(\theta)}{4k\Delta t}\right] - \exp\left[-\frac{R_3^2(\theta)}{4k\Delta t}\right] \right] \right.\right.$$

$$\left.\left. + \frac{(k\Delta t)^{\frac{1}{2}}}{A_\ell} (b_m \cos\theta + a_m \sin\theta) \left[\gamma\left[\frac{3}{2}, \frac{R_3^2(\theta)}{4k\Delta t}\right] - \gamma\left[\frac{3}{2}, \frac{R_2^2(\theta)}{4k\Delta t}\right] \right] \right\} d\theta \right.$$

$$+ \int_{\theta_3}^{\theta_2} \left\{ \xi_m^\ell(i) \left[\exp\left[-\frac{R_1^2(\theta)}{4k\Delta t}\right] - \exp\left[-\frac{R_3^2(\theta)}{4k\Delta t}\right] \right] \right.$$

$$\left. \left. + \frac{(k\Delta t)^{\frac{1}{2}}}{A_\ell} (b_m \cos\theta + a_m \sin\theta) \left[\gamma\left[\frac{3}{2}, \frac{R_3^2(\theta)}{4k\Delta t}\right] - \gamma\left[\frac{3}{2}, \frac{R_1^2(\theta)}{4k\Delta t}\right] \right] \right\} d\theta \right| \qquad (4.2.9)$$

where γ is the incomplete Gamma function normalized. The integration with respect to θ can be carried out numerically using a standard Gaussian quadrature with four integration points. To effect this, a new variable η is introduced such that its value, for instance, for θ in the range $\theta_1 < \theta < \theta_3$, is

$$\eta = \frac{2\theta - \theta_1 - \theta_3}{\theta_3 - \theta_1} \quad , -1 \leq \eta \leq 1 \qquad (4.2.10)$$

Thus, the coefficients of matrix B for this case are of

the form,

$$B_{ij} = \frac{1}{2\pi} \sum_{\ell=1}^{L} \sum_{m=1}^{3} \left\{ \frac{\theta_3-\theta_1}{2} \int_{-1}^{1} \ldots \, d\eta + \frac{\theta_2-\theta_3}{2} \int_{-1}^{1} \ldots \, d\eta \right\} \qquad (4.2.11)$$

and the number of initial-value points is now $M=N+N_I$. Note that since the values of u at the N boundary points have already been computed through the solution of the boundary integral equation, there remain only the values of u at N_I internal points to be calculated.

For computer efficiency, the incomplete Gamma function normalized can be related to the error function as [46] , [75]

$$\gamma\left(\frac{3}{2}, x\right) = \Gamma\left(\frac{3}{2}\right) - \Gamma\left(\frac{3}{2}, x\right) = \Gamma\left(\frac{3}{2}\right) - \frac{1}{2}\Gamma\left(\frac{1}{2}, x\right) - x^{\frac{1}{2}} e^{-x}$$

$$= \frac{1}{2} \pi^{\frac{1}{2}} \operatorname{erf}\left(x^{\frac{1}{2}}\right) - x^{\frac{1}{2}} e^{-x} \qquad (4.2.12)$$

being the error function evaluated by means of a rational approximation [46] which is given in appendix A.

The procedures to solve, for example, a problem with time-independent boundary conditions (e.g. prescribed values of q) using constant time interpolation functions can then be summarized as follows:

a) Discretise the boundary Γ into S elements and N boundary nodes and the domain Ω into L cells, with N_I internal points defining the cells;

b) Compute the coefficients of matrices $\underset{\sim}{G}$, $\underset{\sim}{H}$, $\underset{\sim}{B}$ in equation (4.1.6) and $\underset{\sim}{G}'$, $\underset{\sim}{H}'$, $\underset{\sim}{B}'$ in (4.2.1) using the specified values of geometrical data, properties of the medium and time step. Matrices $\underset{\sim}{H}$ (N x N) , $\underset{\sim}{H}'$ (M x N), $\underset{\sim}{B}$ (N x M) and $\underset{\sim}{B}'$ (M x M) are formed, being $\underset{\sim}{H}$ (the system matrix) then inverted. Introduce the boundary conditions, multiplying them by the $\underset{\sim}{G}$ and $\underset{\sim}{G}'$ coefficients to form the vectors of independent terms $\underset{\sim}{F}(N)$ and $\underset{\sim}{F}'(M)$, respectively. Store the four matrices and two vectors;

c) Multiply matrix $\underset{\sim}{B}$ by the initial conditions, add to vector $\underset{\sim}{F}$ and pre-multiply the result by $\underset{\sim}{H}^{-1}$ to find the unknown boundary values of u;

d) Compare the actual values of u with their previous values to verify if a steady-state is reached, i.e. if their difference is less than a prescribed tolerance;

e) Multiply $\underset{\sim}{B}'$ by the initial conditions, add to $\underset{\sim}{F}'$ and subtract from the total the result of the product of $\underset{\sim}{H}'$ by the computed boundary values of u to find the initial conditions for next step;

f) Return to c).

4.3 Scheme 2 (Time Process Starting at t_0)

The main difference between this scheme and the previous one is that the time variation of functions u and q is now taken into account through boundary integrals in such a way that values of u at internal points need not be computed at the end of each time step. A domain integral (accounting for the initial conditions at t_0) is required only if $u_0 \neq 0$. Furthermore, if $\nabla^2 u_0 = 0$ the domain integral can be transformed into equivalent boundary integrals. As this is the case in many practical problems a reduction in the dimensionality of the problem is effectively achieved. But since the number of boundary integrals to be evaluated increases as the time progresses, a selective numerical integration scheme has to be employed for computer efficiency.

In order to clarify the ideas, let us return to equation (4.1.8). From this equation,we note that computing the unknown boundary data at a time $t = t_F$ requires the evaluation of matrices $\underset{\sim}{G}_{fF}$ and $\underset{\sim}{H}_{fF}$ for $f = 1,2,\ldots, F$, a total of 2F matrices. The matrices $\underset{\sim}{G}_{FF}$ and $\underset{\sim}{H}_{FF}$ are computed as in the previous scheme, i.e. six Gaussian points are

employed to numerically integrate the corresponding boundary integrals (see equation (4.1.33)). But using six Gaussian points to evaluate all matrices would require a great computational effort for large values of F.

The matrices $\underset{\sim}{G}_{1F}$ to $\underset{\sim}{G}_{(F-1)F}$, $\underset{\sim}{H}_{1F}$ to $\underset{\sim}{H}_{(F-1)F}$ will accordingly multiply the prescribed or calculated values of q and u at previous time steps to form the vector $\underset{\sim}{F}$ of independent coefficients. Because of the variation of the integrands with time (see equation (4.1.33)), it is obvious that the contribution of the matrices corresponding to the initial steps will be smaller than those corresponding to the final steps. Thus, it is reasonable to use fewer Gaussian integration points to compute the boundary integrals corresponding to these matrices, without loss of accuracy. Various tests were carried out in order to find the optimum integration scheme and it was concluded that only two Gaussian points are necessary to evaluate matrices $\underset{\sim}{G}_{1F}$ to $\underset{\sim}{G}_{(F-1)F}$, $\underset{\sim}{H}_{1F}$ to $\underset{\sim}{H}_{(F-1)F}$ with an accuracy that is sufficient for our calculations.

A selective integration scheme could also be employed for the space integrals, i.e. fewer Gaussian points adopted for elements located far from the singularity. In fact, such a scheme was tested but the computational savings were not significant. However, the fast variation of the integrands in (4.1.33) with r results in the matrices being sparse, since $E_1(a)$ and $\exp(-a)$ quickly tend to zero as $a \to \infty$. In the computer program developed, a maximum value of a above which the corresponding coefficients in matrices $\underset{\sim}{G}$ and $\underset{\sim}{H}$ are taken as zero was then fixed (see chapter 6).

Note that if a constant time step is adopted throughout the analysis only two new matrices need to be evaluated for each step. But this also implies storing two matrices for each step, which would amount in an unreasonable computer core allocation requirement (since all matrices are kept in-core) if the number of boundary elements and

time steps is great. Thus, only matrices $\underset{\sim}{G}_{FF}$ and $\underset{\sim}{H}_{FF}$ are stored since their evaluation employ a larger number of integration points, being all the other matrices recomputed.

The transformation of the domain integral into equivalent boundary integrals for the case when u_0 is harmonic can be carried out byapplying Green's second identity (equation (2.3.4)) as follows,

$$\int_{\Omega} u_0 \ \nabla^2 U \ d\Omega = \int_{\Gamma} (u_0 \frac{\partial U}{\partial n} - U \frac{\partial u_0}{\partial n}) \ d\Gamma \qquad (4.3.1)$$

Since the domain integral to be evaluated is of the form (equation (4.1)),

$$\int_{\Omega} u_0 \ u^* \ d\Omega \qquad (4.3.2)$$

we have to determine a function U such that $\nabla^2 U = u^*$. One such function can be easily found by,

$$U = \int \frac{1}{r} \left(\int r \ u^* \ dr \right) dr = \frac{1}{4\pi} \ E_1 \left(\frac{r^2}{4k\tau}\right) \qquad (4.3.3)$$

and (4.3.1) becomes,

$$\int_{\Omega} u_0 \ u^* \ d\Omega = \frac{1}{2\pi} \int_{\Gamma} \left\{ \frac{d}{r^2} \ \exp\left[- \frac{r^2}{4k(t_F - t_0)} \right] u_0 \right.$$

$$\left. - \frac{1}{2} E_1 \left[\frac{r^2}{4k(t_F - t_0)} \right] q_0 \right\} d\Gamma = \underset{\sim}{\bar{H}} \ \underset{\sim}{U}_0 + \underset{\sim}{\bar{G}} \ \underset{\sim}{Q}_0 \qquad (4.3.4)$$

where $q_0 = \partial u_0 / \partial n$ and d is defined in (4.1.3). The above integrals can be evaluated numerically in the same way as the ones in equation (4.1.33) (see also discussion on the computation of the singular terms in section 4.1.1).

For the sake of comparison, the procedures to solve the same problem as proposed at the end of the previous section (assuming that the initial conditions are harmonic) can be summarized as follows:

a) Discretise the boundary Γ into S elements and N boundary nodes;

b) Compute the coefficients of matrices $\underset{\sim}{G}_{FF}$ and $\underset{\sim}{H}_{FF}$ in equation (4.1.8) using the specified values of geometrical data, properties of the medium and time step. Matrix $\underset{\sim}{H}_{FF}$ (the system matrix) is formed and inverted. Introduce the boundary conditions, multiplying them by the $\underset{\sim}{G}_{FF}$ coefficients to form the vector $\underset{\sim}{F}$ of independent terms. Store matrix $\underset{\sim}{H}_{FF}$ and vector $\underset{\sim}{F}$;

c) Compute the coefficients of matrices $\underset{\sim}{\overline{G}}$ and $\underset{\sim}{\overline{H}}$ in equation (4.3.4), multiplying them by the initial conditions (q_0 and u_0), add to vector $\underset{\sim}{F}$ and pre-multiply the results by $\underset{\sim}{H}_{FF}^{-1}$ to find the unknown boundary data (which are also stored);

d) Compare the actual values of u with their previous values to verify if a steady-state is reached, i.e. if their difference is less than a prescribed tolerance;

e) Compute the coefficients of matrices $\underset{\sim}{G}_{fF}$ and $\underset{\sim}{H}_{fF}$ for f = 1,2,..., F-1. Multiply them accordingly by the prescribed or calculated boundary values of q and u at the corresponding time steps and add to vector $\underset{\sim}{F}$;

f) Return to c).

4.4 Examples of Application

This section presents results of some examples analysed with the computer programs described in chapter 6, employing the theory and numerical procedures discussed in this chapter. In all cases, the boundary was discretised by using linear elements and whenever necessary, triangular cells were used to discretise the domain. Both constant and linear time interpolation functions were adopted to approximate the variation of functions u and q within each time step. Also, both

previously discussed time-marching schemes were tested, the results obtained with scheme 1 being labelled BEM1 and with scheme 2, BEM2. For time-marching scheme 1 we also tested two different ways of calculating the domain integral, namely using Hammer's (quintic) quadrature scheme and computing the potential values at each integration point (hereafter referred to as BEM1A) or assuming a linear variation for the potentials within each cell with a semi-analytical integration scheme (BEM1B).

When employing linear time interpolation functions it can be noted from equations (4.1.15) and (4.1.17) that, apart from the initial conditions u_0 at time t_0 (that form vector $\overline{U}_0$ in these equations), initial boundary values of u and q at time t_0^+ must also be prescribed (vectors U_0 and Q_0). Examples 4.4.1, 4.4.3, 4.4.4, 4.4.6 and 4.4.8 present as a common feature a discontinuity between the values of u_0 and the prescribed boundary values of u, which makes the values of q_0 unbounded at t_0^+. This problem can be overcome by simply applying the boundary conditions linearly over the first step thus making the fluxes equal zero at t_0^+. The validity of such approximation is verified in some of these examples.

All problems analysed have zero initial conditions, except example 4.4.6. This example was selected in order to verify the transformation of the domain integral into equivalent boundary integrals as described in section 4.3. Thus, no domain discretisation is required when employing scheme 2 and the dimensionality of the problems is effectively reduced by one.

Where symmetry exists, it is taken into account as for the steady-state case (see chapter 3), i.e. only one half or one quarter of the actual region is considered (according to the type of symmetry) with no discretisation of the symmetry axes (see chapter 6).

The results of examples 4.4.1 to 4.4.5 are compared with available analytical solutions, while examples 4.4.6 to 4.4.8 are also compared against solutions obtained through the Finite Element Method in order to assess the accuracy of both methods.

Example 4.4.1

The first example studied was that of a rectangular region $-L<x_1<L$, $-\ell<x_2<\ell$ with zero initial conditions, subjected to the Dirichlet boundary condition u=1 along Γ for any $t > t_0$. The numerical values adopted for the analysis were $\ell=4$, L=5 for the cross-section and k=1 for the material constant.

Initially, a comparison was carried out between the results obtained with schemes BEM1A, BEM1B and BEM2 for coarse discretisations of one quarter of the region, as shown in the left column of figure 4.4.1. The results for u at the point $x_1=x_2=0$, for a time step $\Delta t=1.0$ are summarized in table 4.4.1, together with an analytical solution of the problem [16].

It can be seen from the table that schemes BEM1A and BEM2 present the same level of accuracy, which indicates that the initial conditions are properly taken into account with BEM1A. Their calculation implies computing values of u at internal points located very near the boundary but a check on these values showed no loss of precision. The results obtained with BEM1B are much less accurate; since the boundary discretisation is the same as for the other schemes, the problem is caused by the assumed linear variation of u within each cell.

The influence of the time step value, which was arbitrarily chosen, was verified by running the problem with the same discretisations as previously and a time step $\Delta t=0.5$. Results are given in table 4.4.2 and they show that the numerical solution converges to the exact one

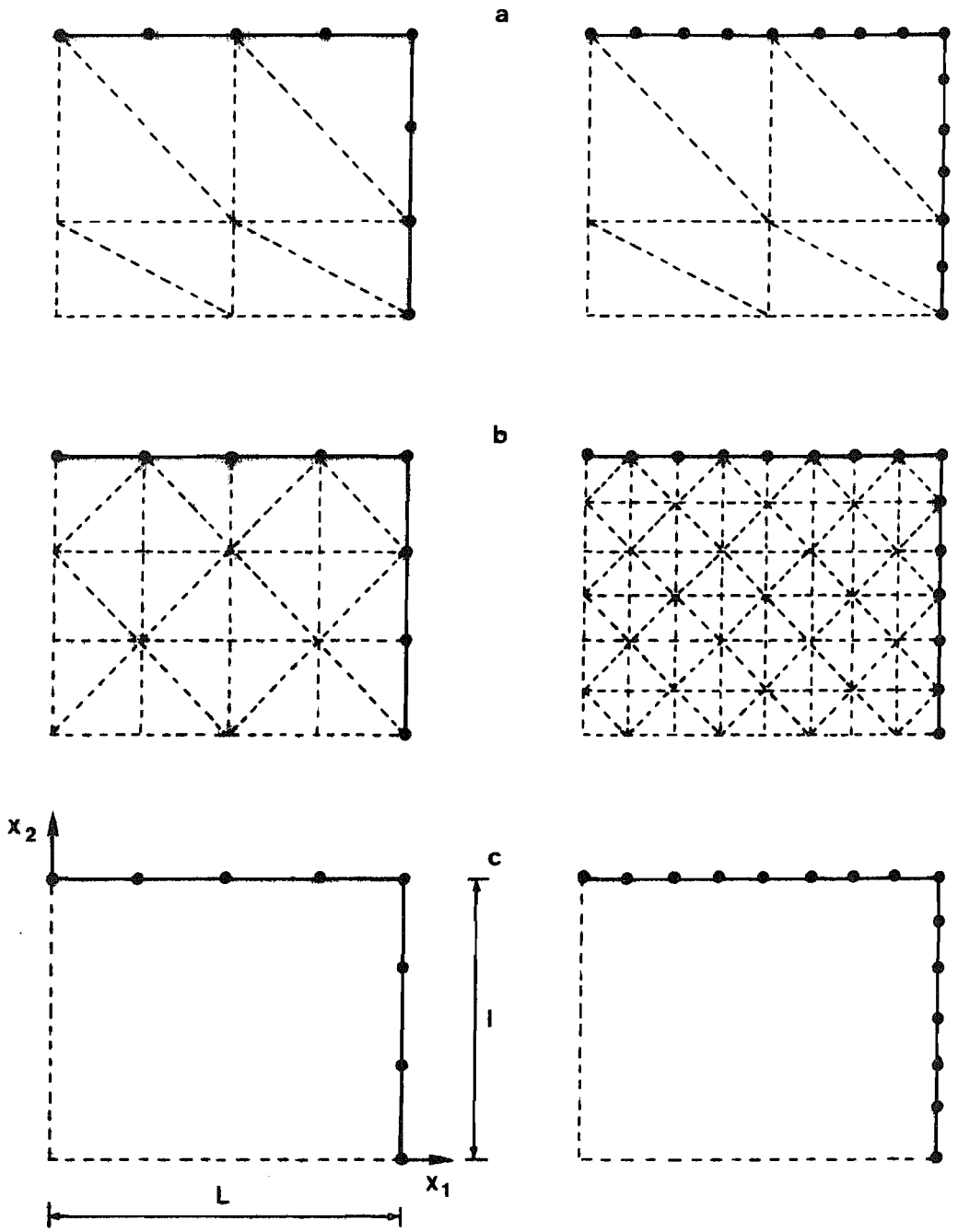

Figure 4.4.1 - Discretisations of one quarter of rectangular region: a) BEM1A; b) BEM1B; c) BEM2

for schemes BEM1A and BEM2 but failed to do so for BEM1B. The convergence of BEM1A and BEM2 was then further tested by adopting a time step $\Delta t=0.25$; although the solution is still convergent for the second scheme, the first one does not converge any longer (see table 4.4.3).

Since the numerical problems for BEM1A are related to the domain integration (and consequently to the domain discretisation), we refined it by sub-dividing the domain into 12 equal cells. The results obtained for the time steps $\Delta t=1.0$ and $\Delta t=0.5$ showed no significant changes from the previous ones, but the results for $\Delta t=0.25$ are now clearly convergent, as can be seen in table 4.4.3. Further refining the domain discretisation with 24 cells, however, caused a different sort of numerical problem: some domain integration points are now located so close to the boundary that accuracy is lost in the computation of the potential value at them. This problem can be overcome by either refining the boundary discretisation or increasing the number of integration points adopted for the computation of the boundary integrals. The latter was employed here, the number of Gaussian points being increased from six to twelve. Results for a time step value $\Delta t=0.25$ are shown in table 4.4.3.

Another test was carried out with the more refined discretisations shown in the right column of figure 4.4.1. Results are given in table 4.4.4 for $\Delta t=1.0$; they are virtually coincident with that of table 4.4.1 for schemes BEM1A and BEM2 but much improved for BEM1B. However, employing a time step $\Delta t=0.5$ again produced poor results for BEM1B and no changes for BEM1A and BEM2.

Example 4.4.2

A comparison between the use of constant and linear time interpolation functions was carried out in this example of a circular region of unit radius with zero initial conditions, subjected to the

TIME	BEM1A	BEM1B	BEM2	ANALYT.
2	0.093	0.112	0.092	0.114
4	0.390	0.450	0.389	0.420
6	0.623	0.686	0.621	0.646
8	0.770	0.822	0.769	0.786
10	0.860	0.899	0.860	0.871
12	0.915	0.943	0.915	0.922
14	0.948	0.968	0.948	0.953
16	0.968	0.982	0.968	0.972
18	0.981	0.990	0.981	0.983
20	0.988	0.994	0.988	0.990
CPU(s)	1.4	2.0	10.7	-
Core Storage	4096	400	224	-
Data Cards	33	57	21	-

Table 4.4.1 - Results at $x_1=x_2=0$ for $\Delta t=1.0$ (coarse discretisation)

TIME	BEM1A	BEM1B	BEM2	ANALYT.
2	0.101	0.166	0.101	0.114
4	0.404	0.534	0.404	0.420
6	0.634	0.754	0.633	0.646
8	0.778	0.871	0.778	0.786
10	0.865	0.932	0.865	0.871
12	0.919	0.965	0.919	0.922
14	0.951	0.981	0.951	0.953
16	0.970	0.990	0.970	0.972
18	0.982	0.995	0.982	0.983
20	0.989	0.997	0.989	0.990
CPU(s)	1.4	2.2	42.5	-
Core Storage	4096	400	384	-
Data Cards	33	57	21	-

Table 4.4.2 - Results at $x_1=x_2=0$ for $\Delta t=0.5$ (coarse discretisation)

TIME	BEM1A (8 cells)	BEM1A (12 cells)	BEM1A (24 cells)	BEM2	ANALYT.
2	0.106	0.106	0.107	0.106	0.114
4	0.414	0.411	0.412	0.412	0.420
6	0.651	0.638	0.639	0.639	0.646
8	0.801	0.781	0.781	0.782	0.786
10	0.895	0.868	0.867	0.868	0.871
12	0.953	0.921	0.920	0.920	0.922
14	0.989	0.953	0.951	0.952	0.953
16	1.010	0.972	0.970	0.971	0.972
18	1.024	0.983	0.981	0.982	0.983
20	1.032	0.990	0.988	0.989	0.990
CPU(s)	1.5	1.9	4.8	234.9	-
Core Stor.	4096	8464	30976	704	-
Data Cards	33	39	57	21	-

Table 4.4.3 - Results at $x_1=x_2=0$ for $\Delta t=0.25$
(coarse discretisation)

TIME	BEM1A	BEM1B	BEM2	ANALYT.
2	0.093	0.097	0.092	0.114
4	0.390	0.406	0.389	0.420
6	0.623	0.640	0.621	0.646
8	0.770	0.784	0.769	0.786
10	0.861	0.871	0.860	0.871
12	0.915	0.923	0.915	0.922
14	0.949	0.954	0.948	0.953
16	0.969	0.973	0.969	0.972
18	0.981	0.984	0.981	0.983
20	0.989	0.990	0.988	0.990
CPU(s)	2.5	21.0	33.2	-
Core Storage	5041	3969	525	-
Data Cards	47	179	35	-

Table 4.4.4 - Results at $x_1=x_2=0$ for $\Delta t=1.0$ (fine discretisation)

Neumann boundary condition q=5 along Γ for any $t > t_0$. For simplicity, the value of the material parameter k was taken to be unity.

Table 4.4.5 presents numerical results for u at a point with radius r=0.6 for the discretisations shown in the left column of figure 4.4.2 and a time step Δt=0.01. Note that only 6 boundary elements were employed in these discretisations. It can be seen that better results are obtained with stepwise linear functions for all three schemes, although the results for BEM1B are quite poor.

Further numerical results are given in tables 4.4.6 to 4.4.8 for the previous discretisations with a time step Δt=0.005 and for finer discretisations (shown in the right column of figure 4.4.2) with Δt=0.01 and Δt=0.005, respectively. These results corroborate the ones from example 4.4.1 for the stepwise constant cases: for scheme BEM2, convergence was always achieved; for BEM1A convergence was achieved when the discretisation was refined but not when the time step was decreased; scheme BEM1B presented the poorest results even with the fine discretisations employed, and they became meaningless when the time step value was decreased.

The use of stepwise linear functions, in general, improves the accuracy of the solution but it appears to aggravate the numerical problems inherent in scheme BEM1A. However, this example seems to be particularly sensitive to a precise evaluation of the domain integral and in order to assess this, we tested a numerical integration scheme other than Hammer's, namely the one recently proposed by Reddy and Shippy [77], which the authors claim to be very accurate even for integrals with singularities. The results obtained with seven integration points are summarized in table 4.4.9.

Example 4.4.3

A problem with mixed boundary conditions, i.e. u=1 prescribed along the faces $x_1 = \pm L$ and q=0 along the faces $x_2 = \pm \ell$ of a rectangular

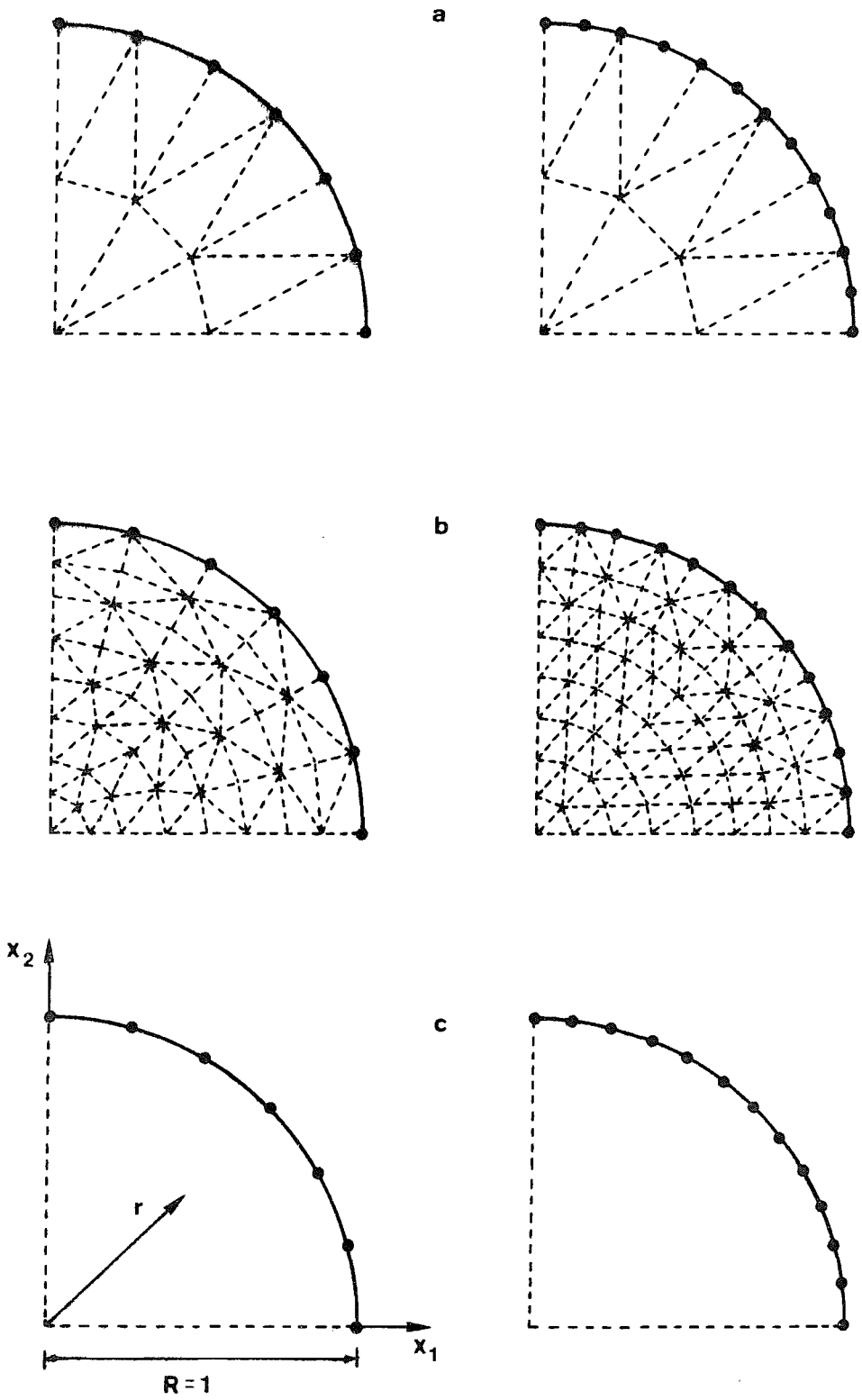

Figure 4.4.2 - Discretisations of one quarter of circular region:
a) BEM1A; b) BEM1B; c) BEM2

TIME	BEM1AC	BEM1AL	BEM1BC	BEM1BL	BEM2C	BEM2L	ANALYT.
0.02	0.033	0.022	0.040	0.028	0.033	0.022	0.023
0.04	0.173	0.145	0.208	0.182	0.166	0.145	0.139
0.06	0.358	0.318	0.430	0.392	0.341	0.315	0.303
0.08	0.559	0.508	0.668	0.621	0.531	0.503	0.484
0.10	0.766	0.706	0.913	0.859	0.727	0.698	0.674
0.12	0.975	0.908	1.162	1.100	0.926	0.896	0.867
0.14	1.186	1.110	1.412	1.345	1.126	1.095	1.062
0.16	1.397	1.315	1.664	1.590	1.328	1.296	1.259
0.18	1.608	1.519	1.916	1.836	1.530	1.497	1.457
0.20	1.819	1.725	2.168	2.084	1.732	1.698	1.655
CPU(s)	1.7	1.8	7.7	7.7	8.7	9.8	-
Core Storage	8281	8918	2304	2640	189	238	-
Data Cards	36	43	132	139	19	26	-

Table 4.4.5 - Results at r=0.6 for Δt=0.01
(coarse discretisation)

TIME	BEM1AC	BEM1AL	BEM2C	BEM2L	ANALYT.
0.02	0.030	0.025	0.029	0.025	0.023
0.04	0.165	0.153	0.158	0.150	0.139
0.06	0.346	0.331	0.330	0.323	0.303
0.08	0.543	0.528	0.518	0.512	0.484
0.10	0.746	0.733	0.713	0.707	0.674
0.12	0.951	0.940	0.911	0.906	0.867
0.14	1.157	1.149	1.111	1.107	1.062
0.16	1.363	1.359	1.312	1.308	1.259
0.18	1.570	1.569	1.513	1.510	1.457
0.20	1.776	1.779	1.715	1.712	1.655
CPU(s)	1.8	2.0	32.9	38.1	-
Core Storage	8281	8918	329	378	-
Data Cards	36	43	19	26	-

Table 4.4.6 - Results at r=0.6 for Δt=0.005
(coarse discretisation)

TIME	BEM1AC	BEM1AL	BEM1BC	BEM1BL	BEM2C	BEM2L	ANALYT.
0.02	0.031	0.020	0.036	0.025	0.031	0.021	0.023
0.04	0.160	0.133	0.191	0.164	0.159	0.137	0.139
0.06	0.329	0.289	0.393	0.353	0.329	0.303	0.303
0.08	0.508	0.459	0.611	0.561	0.516	0.486	0.484
0.10	0.690	0.632	0.835	0.775	0.709	0.677	0.674
0.12	0.872	0.807	1.061	0.992	0.905	0.871	0.867
0.14	1.052	0.980	1.288	1.212	1.103	1.067	1.062
0.16	1.230	1.152	1.516	1.432	1.302	1.265	1.259
0.18	1.405	1.322	1.745	1.653	1.501	1.464	1.457
0.20	1.579	1.491	1.973	1.875	1.701	1.662	1.655
CPU(s)	2.1	2.4	16.4	16.4	25.0	28.2	-
Core Storage	9409	10670	5625	6600	429	598	-
Data Cards	48	61	226	239	31	44	-

Table 4.4.7 - Results at r=0.6 for Δt=0.01
(fine discretisation)

TIME	BEM1AC	BEM1AL	BEM2C	BEM2L	ANALYT.
0.02	0.027	0.021	0.027	0.022	0.023
0.04	0.143	0.127	0.151	0.140	0.139
0.06	0.298	0.274	0.318	0.305	0.303
0.08	0.468	0.437	0.503	0.488	0.484
0.10	0.642	0.606	0.695	0.679	0.674
0.12	0.818	0.777	0.890	0.873	0.867
0.14	0.996	0.950	1.087	1.069	1.062
0.16	1.174	1.124	1.285	1.267	1.259
0.18	1.353	1.300	1.484	1.465	1.457
0.20	1.533	1.475	1.683	1.663	1.655
CPU(s)	2.4	3.4	100.0	104.6	-
Core Storage	9409	10670	689	858	-
Data Cards	48	61	31	44	-

Table 4.4.8 - Results at r=0.6 for Δt=0.005
(fine discretisation)

TIME	BEM1AC (Δt=0.01)	BEM1AL (Δt=0.01)	BEM1AC (Δt=0.005)	BEM1AL (Δt=0.005)	ANALYT.
0.02	0.035	0.023	0.029	0.024	0.023
0.04	0.171	0.144	0.168	0.155	0.139
0.06	0.349	0.309	0.360	0.344	0.303
0.08	0.543	0.492	0.574	0.557	0.484
0.10	0.745	0.684	0.797	0.781	0.674
0.12	0.951	0.881	1.025	1.010	0.867
0.14	1.160	1.082	1.256	1.244	1.062
0.16	1.371	1.285	1.490	1.480	1.259
0.18	1.583	1.491	1.726	1.720	1.457
0.20	1.797	1.698	1.965	1.962	1.655

Table 4.4.9 - Results at r=0.6 for Reddy and Shippy's integration scheme (coarse discretisation)

region with zero initial conditions was the object of this example. The numerical values adopted for the cross-section and the material constant were the same as for example 4.4.1. The no-flux condition reduces the problem to the one-dimensional one of a infinite slab over both faces of which a constant potential is specified.

Several analyses were carried out using the discretisations shown in figure 4.4.1, the results of which are presented in tables 4.4.10 to 4.4.13. Note that double nodes had to be introduced at each corner in order to properly account for the boundary conditions there.

As can be seen from the tables, the results followed basically the same pattern as the ones for example 4.4.1 regarding convergence and accuracy of the time-marching schemes. For the stepwise linear cases, the boundary conditions were applied linearly over the first time step (instead of suddenly). The effects of this approximation tend to decay rapidly over few steps and to decrease as smaller values of time steps are adopted.

Discussion of Results

A mathematical proof of convergence of the Boundary Element Method as applied to transient potential problems was recently reported in [78], where it was demonstrated the second order convergence in Δt and $\Delta\Gamma$ of BEM solutions. Only a scheme of the type BEM2 was considered in [78] and although no numerical results were produced, convergence for this scheme was clearly achieved in the examples studied herein.

The numerical problems presented by BEM1A are mainly associated to errors introduced in the computation of the domain integral. As $\Delta t \to 0$, the integrand in equation (4.2.3) (the fundamental solution u^*) becomes less and less smooth, being its limit a Dirac delta function (see figure 4.4.3). Thus, the relative sizes of geometrical data and time step have to be carefully chosen if accurate results are to be expected with BEM1A. Furthermore, attention should be paid to the

TIME	BEM1AC	BEM1AL	BEM1BC	BEM1BL	BEM2C	BEM2L	ANALYT.
2	0.292	0.250	0.311	0.279	0.291	0.250	0.317
4	0.476	0.454	0.499	0.481	0.473	0.453	0.484
6	0.583	0.564	0.609	0.592	0.579	0.563	0.587
8	0.662	0.645	0.690	0.675	0.657	0.644	0.660
10	0.726	0.709	0.754	0.740	0.719	0.708	0.721
15	0.837	0.823	0.862	0.851	0.828	0.822	0.830
20	0.902	0.892	0.922	0.915	0.895	0.891	0.896
25	0.941	0.934	0.956	0.951	0.936	0.934	0.937
30	0.964	0.959	0.975	0.971	0.960	0.959	0.961
CPU(s)	1.8	1.9	3.0	3.3	30.8	32.0	-
Core Storage	4225	4810	441	630	351	432	-
Data Cards	35	44	59	68	23	32	-

Table 4.4.10 - Results at $x_1=3$ for $\Delta t=1.0$
(coarse discretisation)

TIME	BEM1AC	BEM1AL	BEM1BC	BEM1BL	BEM2C	BEM2L	ANALYT.
2	0.305	0.284	0.353	0.338	0.304	0.285	0.317
4	0.481	0.470	0.532	0.523	0.480	0.470	0.484
6	0.586	0.576	0.640	0.632	0.582	0.574	0.584
8	0.665	0.654	0.721	0.714	0.659	0.652	0.660
10	0.728	0.717	0.784	0.777	0.721	0.715	0.721
15	0.837	0.829	0.885	0.880	0.830	0.826	0.830
20	0.902	0.896	0.939	0.935	0.896	0.894	0.896
25	0.941	0.936	0.967	0.965	0.937	0.936	0.937
30	0.964	0.961	0.982	0.981	0.961	0.961	0.961
CPU(s)	2.0	2.1	2.8	2.9	116.7	122.0	-
Core Stor.	4225	4810	441	630	621	702	-
Data Cards	35	44	59	68	23	32	-

Table 4.4.11 - Results at $x_1=3$ for $\Delta t=0.5$
(coarse discretisation)

TIME	BEM1AC (8 cells)	BEM1AL (8 cells)	BEM1AC (12 cells)	BEM1AL (12 cells)	BEM1AC (24 cells)	BEM1AL (24 cells)	BEM2C	BEM2L	ANALYT.
2	0.313	0.303	0.312	0.301	0.312	0.302	0.311	0.301	0.317
4	0.490	0.483	0.487	0.479	0.486	0.479	0.483	0.477	0.484
6	0.598	0.590	0.591	0.584	0.589	0.583	0.584	0.579	0.584
8	0.680	0.673	0.670	0.663	0.667	0.660	0.660	0.656	0.660
10	0.748	0.740	0.733	0.726	0.730	0.723	0.721	0.718	0.721
15	0.871	0.864	0.864	0.840	0.839	0.833	0.830	0.828	0.830
20	0.949	0.943	0.915	0.909	0.903	0.899	0.896	0.895	0.896
25	0.998	0.994	0.956	0.952	0.942	0.938	0.937	0.937	0.937
30	1.030	1.026	0.981	0.978	0.964	0.962	0.961	0.961	0.961
CPU(s)	2.0	2.4	2.6	3.4	6.4	7.2	600.0	620.0	-
Core Stor.	4225	4810	8649	9486	31329	32922	1161	1242	-
Data Cards	35	44	41	50	57	66	23	32	-

Table 4.4.12 - Results at x_1=0.3 for Δt=0.25 (coarse discretisation)

TIME	BEM1AC	BEM1AL	BEM1BC	BEM1BL	BEM2C	BEM2L	ANALYT.
2	0.292	0.250	0.297	0.257	0.291	0.249	0.317
4	0.475	0.453	0.482	0.461	0.472	0.453	0.484
6	0.582	0.563	0.590	0.571	0.577	0.562	0.584
8	0.661	0.643	0.670	0.653	0.655	0.643	0.660
10	0.724	0.708	0.733	0.717	0.718	0.707	0.721
15	0.835	0.822	0.843	0.830	0.828	0.821	0.830
20	0.902	0.892	0.907	0.897	0.895	0.891	0.896
25	0.941	0.934	0.944	0.937	0.935	0.933	0.937
30	0.965	0.960	0.966	0.961	0.960	0.959	0.961
CPU(s)	2.6	3.2	23.3	24.0	87.6	90.0	-
Core Storage	5184	6336	4096	5120	736	992	-
Data Cards	49	65	181	197	37	53	-

Table 4.4.13 - Results at $x_1=3$ for $\Delta t=1.0$
(fine discretisation)

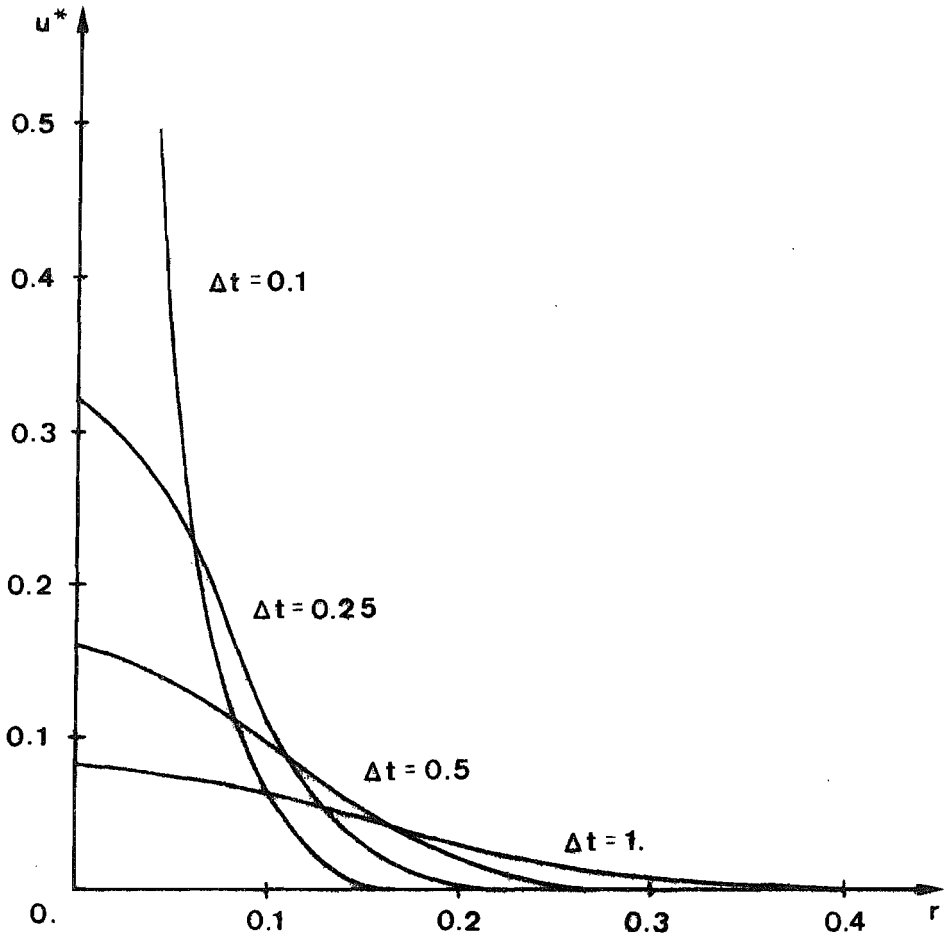

Figure 4.4.3 - Variation of u^* with r for several values of time steps

fact that the more refined the domain discretisation employed, the closer to the boundary cells integration points become, and that this also implies refining the boundary integration (or discretisation).

The above mentioned numerical problems were also noticed in [79] where some one-dimensional transient potential problems were analysed with a scheme of the type BEM1. But the reasons for the non-convergence with decreasing values of time steps were wrongly attributed to the use of stepwise constant approximations for u and q (which does not seem to affect convergence, as can be seen from the results for BEM2) and to truncation errors inherent in Simpson's rule, which was employed for the domain integration.

For problems with unbounded initial fluxes at time t_0^+, as is the case for examples 4.4.1 and 4.4.3, it was reported in [79] that the computed values of u were very accurate for points far from the boundary but the accuracy decreased as the points became closer to it. No problems of that kind were detected herein (apart from the previously discussed), and the accuracy of the results presented can be assumed to be typical of any internal point.

Note that the semi-analytical integration scheme associated with BEM1B does not present the previous problem since the integration with respect to r is performed analytically (equation (4.2.9)). Thus, the errors obtained with this scheme are basically related to the piecewise linear variation adopted for u over the domain. This approximation is similar to the one for linear finite elements and, as in that case, accurate results are produced only if very refined discretisations are employed. But even so convergence with decreasing time steps was not achieved.

An empirical formula to determine the critical value of the time step (with respect to accuracy) was suggested in [78] as,

$$\Delta t_{crit} = \frac{\Delta\Gamma^2}{2k} \qquad (4.4.1)$$

where $\Delta\Gamma$ is the dimension of the largest boundary element employed in the discretisation. This formula explores the similarity between the fundamental solution to the diffusion equation and the probability density function of a bivariate normal distribution in mathematical statistics.

Applying the above formula to the previous examples gives critical time steps of 0.88 and 0.22 for problems 4.4.1 and 4.4.3 and 0.034 and 0.0085 for 4.4.2, for the coarses and fines discretisations, respectively. These values appear to underestimate the accuracy of the numerical solutions, since larger time steps than the ones predicted were employed with the fine discretisation in examples 4.4.1 and 4.4.3 with no deterioration of results. However, the formula is useful in providing an estimate of the magnitude of the time step to be adopted for each problem, and further checks will be effected on following examples.

Regarding the computer efficiency of the time-marching schemes, we note that the last three rows of each table compare CPU time, core storage and number of data cards required for each analysis. These numbers should not be seen as definite since the computer programs developed can be improved much further. For simplicity, a fixed basic structure was adopted for all programs and the matrices kept in-core (see chapter 6). The main purpose of this comparison is to give an idea of the programming difficulties associated with each scheme. The row corresponding to core storage refers to the number of positions needed to store only the relevant matrices in the actual computation, which are as follows: NxN+2(NxM)+MxM for schemes BEM1 (see section 4.2) and NxN+FxN for BEM2 (section 4.3), being F the number of time steps. For stepwise linear

functions, we should add NxN+NxM to the first case and NxN to the second.

It can be seen that scheme BEM1A is by far the fastest one. This appears to be contradictory since scheme BEM1B is a simplified version of BEM1A. The difference between both lies in the domain integration: the semi-analytical scheme employed in conjunction with BEM1B requires a great deal of computer time for the evaluation of the numerous terms that appear in equation (4.2.11), and this operation is repeated several times at each integration point. An alternative procedure for computing the domain integral in BEM1B is by directly applying Hammer's quadrature scheme to equation (4.2.6). Although the savings in computer time are enormous, numerical problems become even more severe.

Another advantage of BEM1A is that the domain discretisation can be dissociated from the boundary discretisation as opposed to BEM1B where they are directly related. This permits using very large cells, as can be seen in figures 4.4.1 and 4.4.2, with no loss of accuracy and making data preparation easier.

Since the system of equations to be solved in all examples is always very small, the CPU times reported are almost entirely spent on computing the coefficients of the matrices. As discussed in section 4.2, all matrices that appear in the formulation of BEM1A and BEM1B are calculated only once and stored. For BEM2, however, we have decided to always recompute matrices $\underset{\sim}{G}_{FF}$ and $\underset{\sim}{H}_{FF}$ (see section 4.3), but this strategy led to very large CPU times being required for this scheme.

Consider, for instance, example 3: table 4.4.10 shows that 30.8 s are needed to solve the problem for 30 time steps. If we assume that 1 s is spent in input-output, solution of the systems of equations and computation of matrices $\underset{\sim}{G}_{FF}$ and $\underset{\sim}{H}_{FF}$ (which is a reasonable assumption,

judging from the CPU times reported for BEM1A), this gives approximately 0.0343 s for the computation of each matrix $\underset{\sim}{G}_{fF}$ or $\underset{\sim}{H}_{fF}$ (a total of 870 matrices). For 60 and 120 time steps, the number of matrices to be computed throughout the process is 3540 and 14280, respectively. Thus, the large CPU times presented in tables 4.4.11 and 4.4.12 are to be expected.

If, on the other hand, the matrices calculated for each step are all stored in such a way that only two new matrices need to be computed for each new step, the total number of matrices $\underset{\sim}{G}_{fF}$ and $\underset{\sim}{H}_{fF}$ ($f \neq F$) to be evaluated throughout the process would be 58, 118 and 238 for 30, 60 and 120 time steps, respectively. The expected CPU times and core storage requirements for the problem can then be summarized as follows,

Number of time steps	30	60	120
CPU (s)	3.0	5.0	9.2
Core storage	2700	5400	10800

Table 4.4.14 - Expected CPU times and core storage requirements for example 3 with scheme BEM2C (modified program)

Note that for problems involving a large number of boundary elements and time steps the use of disc files appears to be necessary since the number of coefficients to be stored grows very rapidly.

In what follows several more examples are considered, including problems with time-dependent boundary conditions and comparisons with available finite element solutions. Due to the poor performance of scheme BEM1B in the previous examples, we concentrate our attention only on BEM1A and BEM2. Further suggestions for improving the computer efficiency of the time-marching schemes are discussed in chapter 7.

Example 4.4.4

Lachat and Combescure reported in [47] some results for a transient heat conduction problem with time-dependent boundary conditions using the Boundary Element Method in conjunction with Laplace transforms. The problem studied was that of a circular region of unit radius, initially at zero temprerature, subjected to sudden thermal shocks applied at times t_0=0 and t_1. They obtained very good results for the case of only one thermal shock imposed at the initial time (t_1=0) but the results deteriorated as the value of t_1 was increased (see figures 4.4.5 to 4.4.7). This behaviour was attributed to the numerical inversion of the Laplace transform and they concluded that step-by-step methods should be preferred for this kind of problem.

In order to verify the accuracy of the formulation developed in this work for problems with time-dependent boundary conditions, we analysed the above problem assuming, for simplicity, a unit value for the thermal diffusivity k (as was done in [47]). The discretisation employed for BEM1A is shown in figure 4.4.4, together with the variation with respect to time of the boundary temperature. The same boundary discretisation (6 elements) as shown in the figure was also adopted for BEM2 and the results obtained with both time-marching schemes were practically equal. These results are plotted in figures 4.4.5 to 4.4.7 for different values of t_1 and compared with analytical solutions [47]. The accuracy of the BEM solutions is very good for all values of t_1. It should be pointed out that the values of time steps employed were Δt=0.05 for t_1=0 and t_1=0.5 and Δt=0.10 for t_1=1, compared with a critical value Δt_{crit}=0.034 given by equation (4.4.1).

Example 4.4.5

In this example, we study the same problem as before but assuming now a linear time variation for the boundary temperature as indicated in

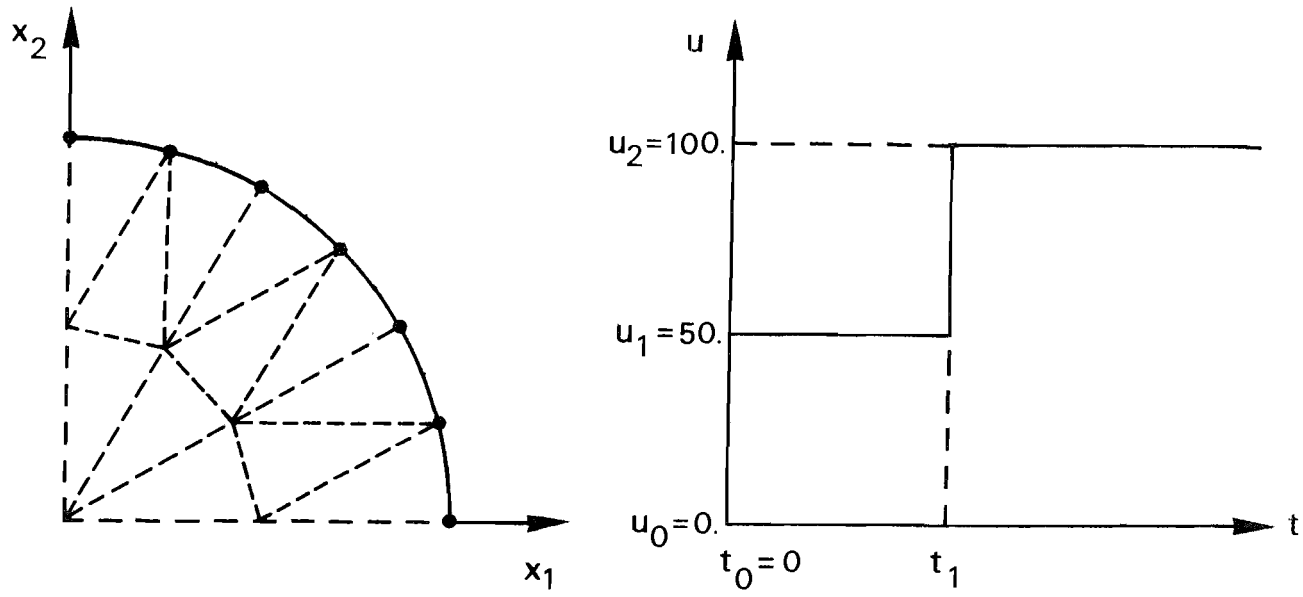

Figure 4.4.4 - Circular region with thermal shocks: a) Discretisation; b) Time variation of surface temperature

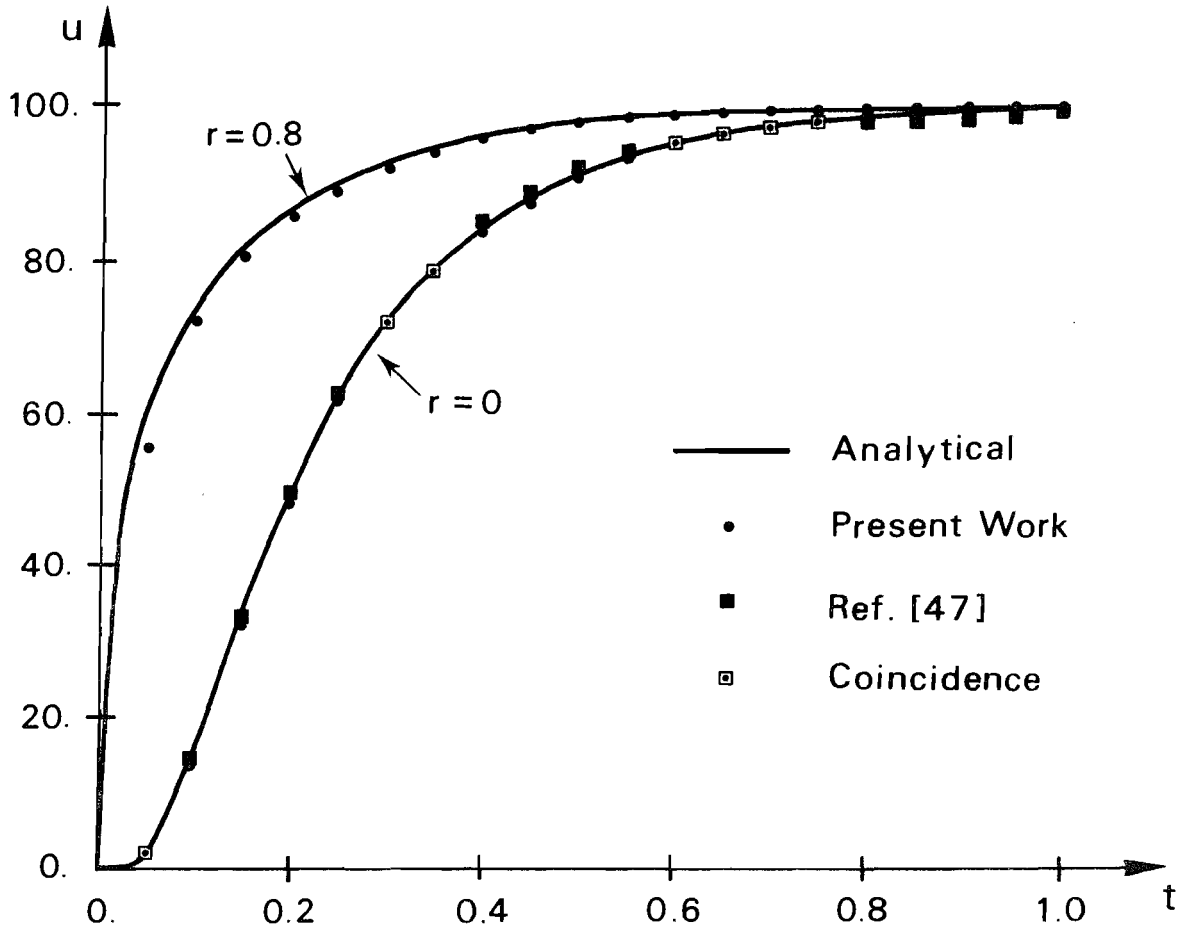

Figure 4.4.5 - Temperature at internal points for thermal shock applied at $t_0=t_1=0$.

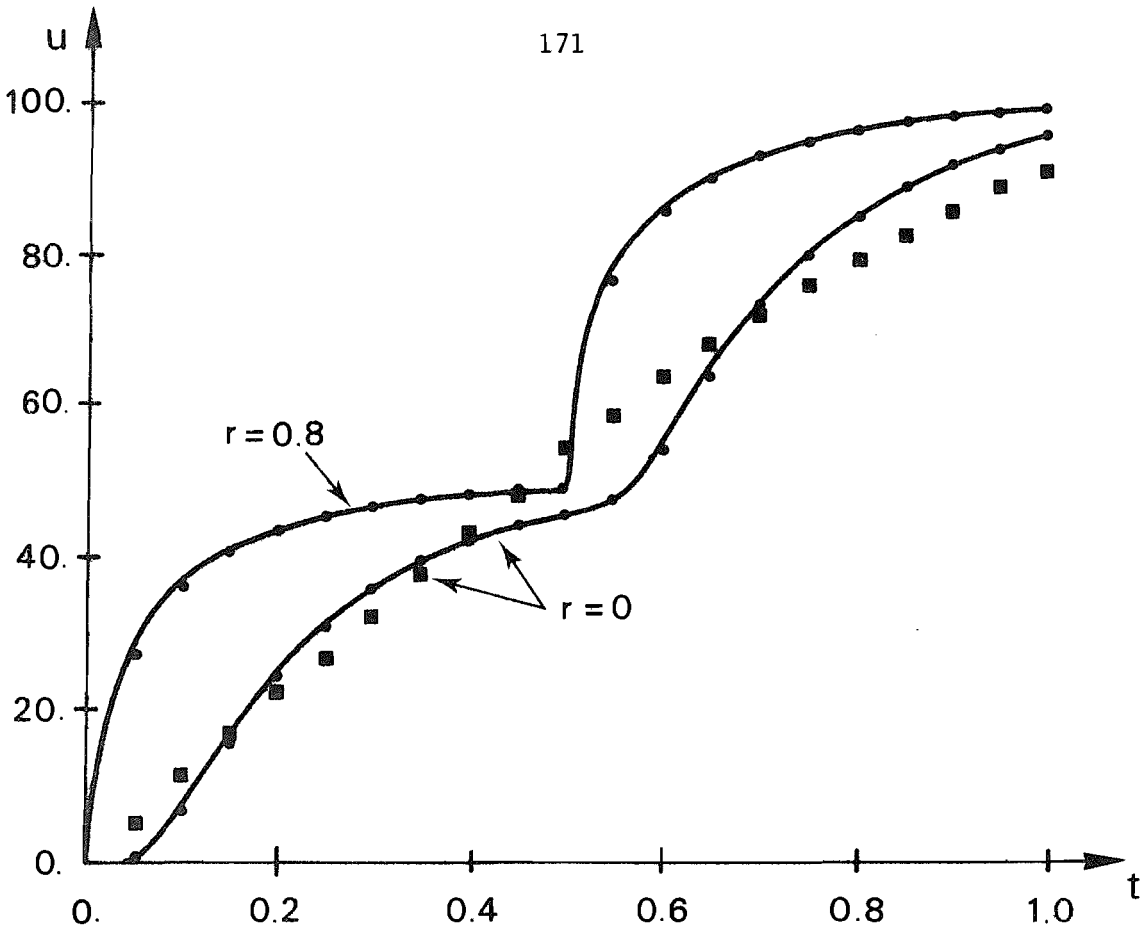

Figure 4.4.6 - Temperature at internal points for thermal shocks applied at t_0=0. and t_1=0.5

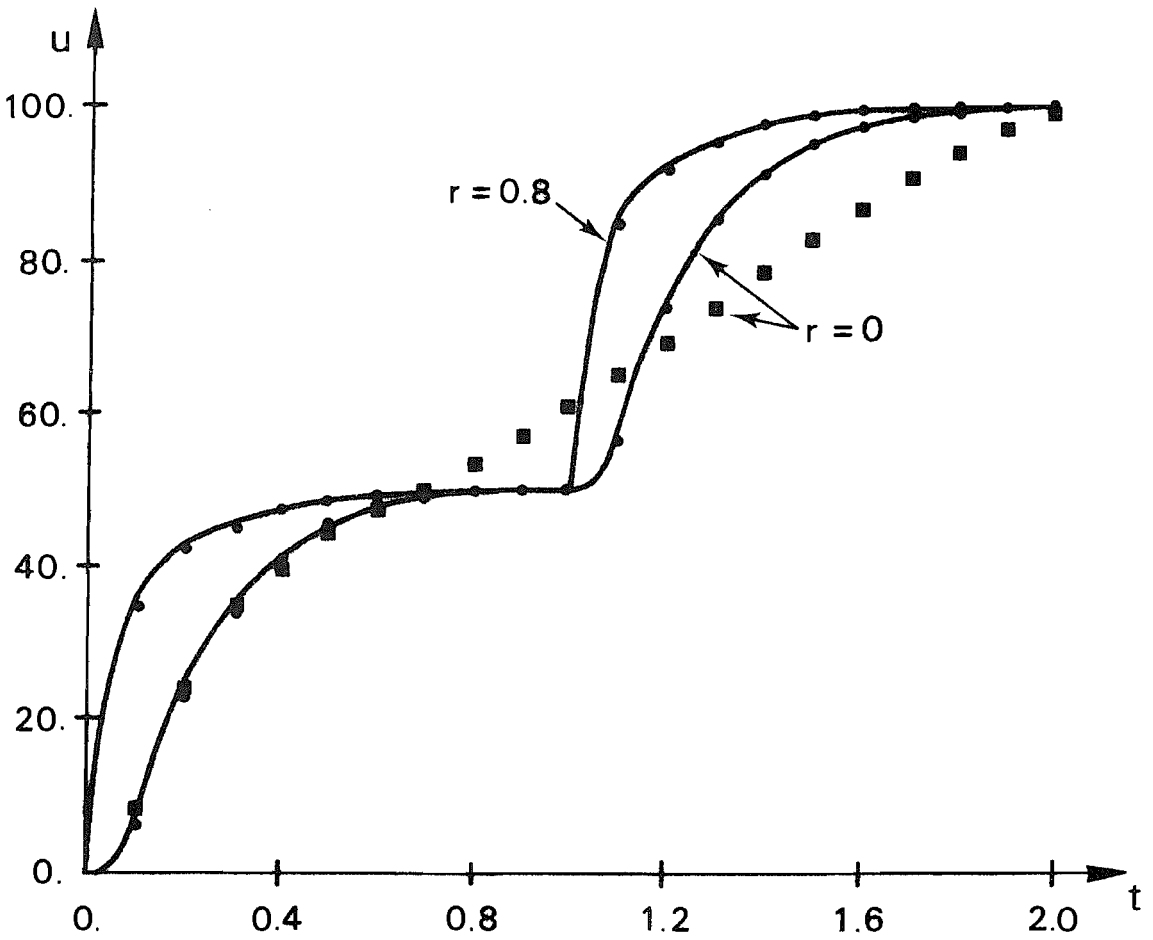

Figure 4.4.7 - Temperature at internal points for thermal shocks applied at t_0=0. and t_1=1

figure 4.4.8 and a value k=5 for the thermal diffusivity.

Initially, a solution was attempted by adopting stepwise constant variations for functions u and q such that the prescribed values of u are equal to their average within each time step. The results obtained for schemes BEM1A and BEM2 with the same discretisations as previously (see figure 4.4.4) were coincident and are plotted in figure 4.4.9.

The problem was then re-studied using stepwise linear variations for u and q and, in this way, the specified boundary temperature within each time step can be exactly accounted for. Again, the discretisations shown in figure 4.4.4 were employed. The results for both schemes agreed with the analytical solution given by [16] to three significant figures even for the first time step,and are also plotted in figure 4.4.9.

All numerical analyses adopted a time step value $\Delta t=0.02$ compared with a much lower critical value $\Delta t_{crit}=0.0068$ predicted by equation (4.4.1).

Example 4.4.6

The object of the present investigation is a 3x3 m square region with initial temperature $u_0=30^oF$ and thermal diffusivity k=1.25 Btu/h m^oF, subjected to the Dirichlet boundary condition u=0 along Γ for any $t > t_0$. This problem is similar to the one considered in example 4.4.1 and the actual numerical values were chosen as to allow the results to be compared with an available finite element solution [80].

Since the initial conditions satisfy Laplace's equation, we can apply equation (4.3.4) in order to transform the domain integral of scheme BEM2 into equivalent boundary integrals, as discussed in section 4.3. The results obtained for this analysis, together with the ones for BEM1A, the finite element solution [80] and an analytical solution [80] are presented in tables 4.4.15 and 4.4.16 for two different values of time steps, with the discretisations shown in figure 4.4.10. It can

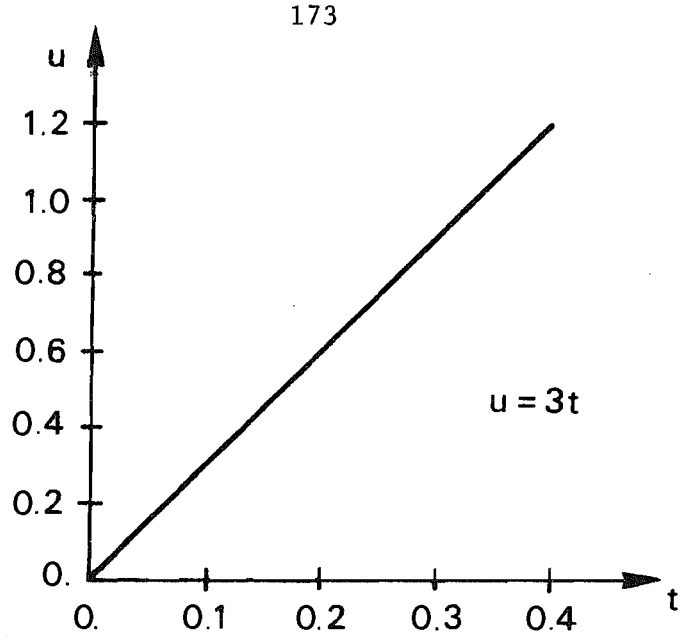

Figure 4.4.8 - Time variation of surface temperature

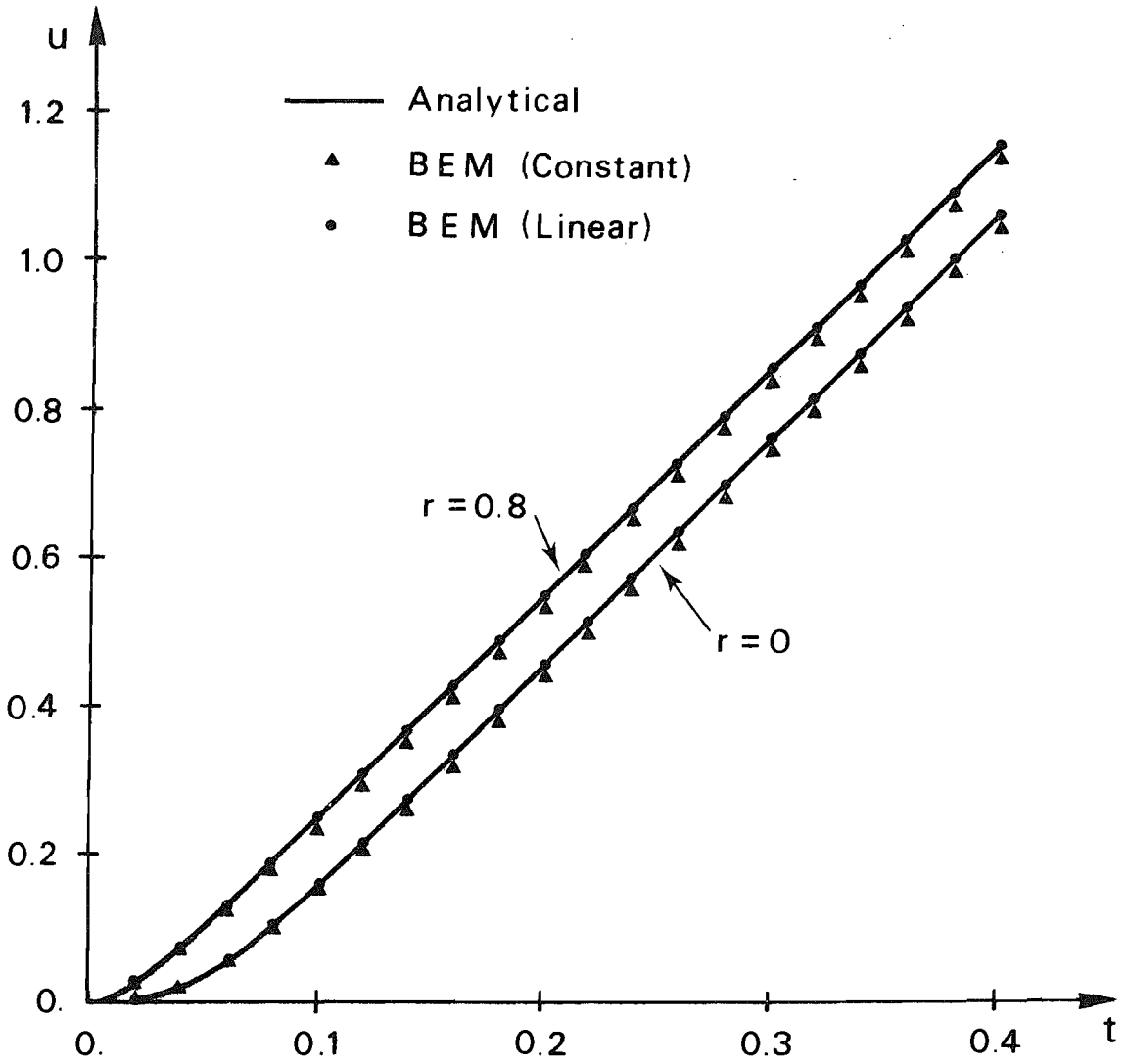

Figure 4.4.9 - Temperature at internal points

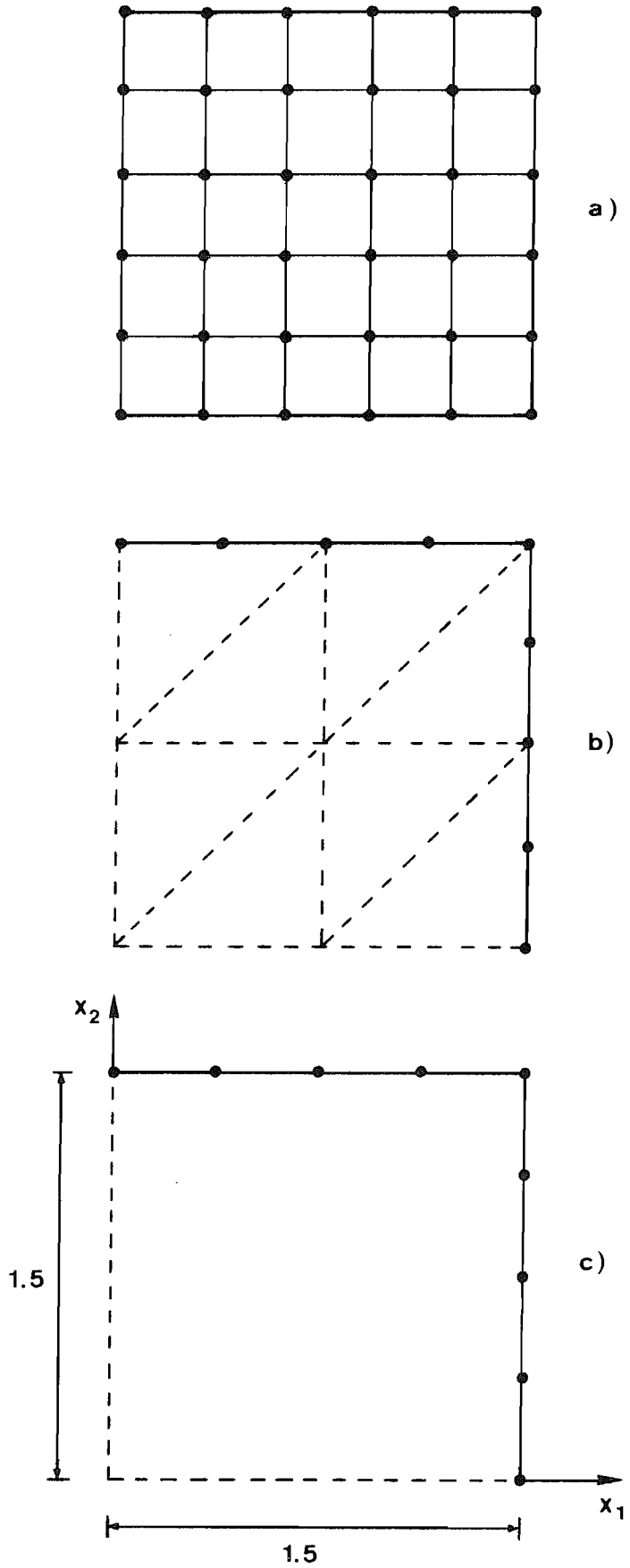

Figure 4.4.10 - Discretisations of one quarter of square region:
a) FEM; b) BEM1A; c) BEM2

x_1	x_2	BEM1A	BEM2	FEM	ANALYT.
0.	0.	1.988	2.009	2.108	1.812
0.3	0.	1.893	1.913	2.005	1.723
0.6	0.	1.614	1.632	1.706	1.466
0.9	0.	1.180	1.194	1.239	1.065
1.2	0.	0.630	0.639	0.652	0.560
0.3	0.3	1.802	1.821	1.907	1.639
0.6	0.6	1.310	1.325	1.380	1.186
0.9	0.9	0.700	0.710	0.728	0.626
1.2	1.2	0.199	0.201	0.201	0.173

Table 4.4.15 - Temperature values at t=1.2h for a time step Δt=0.10h

x_1	x_2	BEM1A	BEM2	FEM	ANALYT.
0.	0.	1.887	1.902	1.938	1.812
0.3	0.	1.798	1.809	1.843	1.723
0.6	0.	1.534	1.541	1.568	1.466
0.9	0.	1.114	1.122	1.139	1.065
1.2	0.	0.589	0.595	0.599	0.560
0.3	0.3	1.713	1.721	1.753	1.639
0.6	0.6	1.214	1.248	1.269	1.186
0.9	0.9	0.657	0.663	0.670	0.626
1.2	1.2	0.184	0.185	0.185	0.173

Table 4.4.16 - Temperature values at t=1.2h for a time step Δt=0.05h

be seen that the BEM solutions are of the same level of accuracy and that they are superior to the finite element one at all points, for both time steps, despite employing coarser discretisations.

To verify if the use of equation (4.3.4) was introducing additional numerical errors, we re-studied the problem by subtracting out a constant temperature of $30^{o}F$ so as to make the initial conditions equal to zero. This constant value is afterwards added to the new solution. Results obtained in this way agreed to the previous ones to the significant figures shown in the tables.

Finally, analyses were carried out using stepwise linear functions and applying the boundary conditions as described in example 4.4.3. Again, results of the same order of accuracy as shown in the tables were obtained with both time-marching schemes.

Example 4.4.7

This example studies the one-dimensional problem of constant heat flux applied to a semi-infinite solid. The material properties of the solid are assumed to be unit as well as the applied heat flux per unit time, in order for the results to be compared with a finite element solution presented in [62]. This FEM analysis considered a linear variation for the temperature between time steps and produced results for the surface temperature versus time for two different values of time steps as shown in figure 4.4.12, but did not comment on the space discretisation adopted.

Four BEM analyses were carried out using the discretisations shown in figure 4.4.11 and employing stepwise constant or linear variations for the functions. The results obtained agreed with the exact solution given in [16] to three significant figures for scheme BEM2 with stepwise linear u and q and were slightly less accurate for the other analyses, being the maximum relative errors 0.7% for

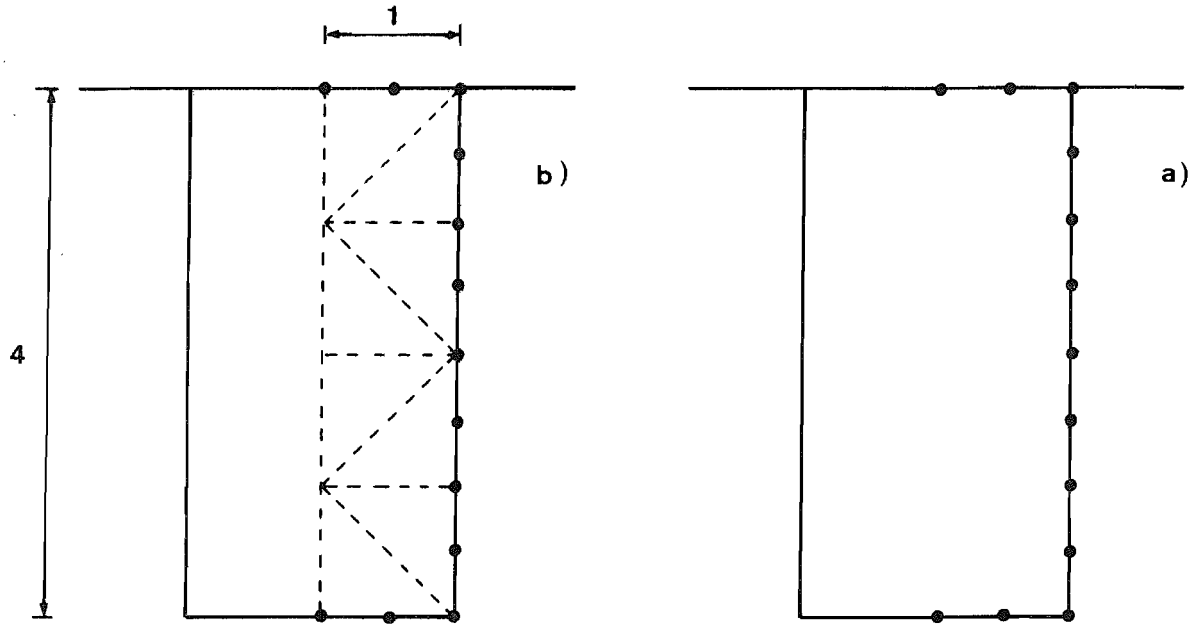

Figure 4.4.11 - Discretisation of semi-infinite solid:
a) BEM1A; b) BEM2

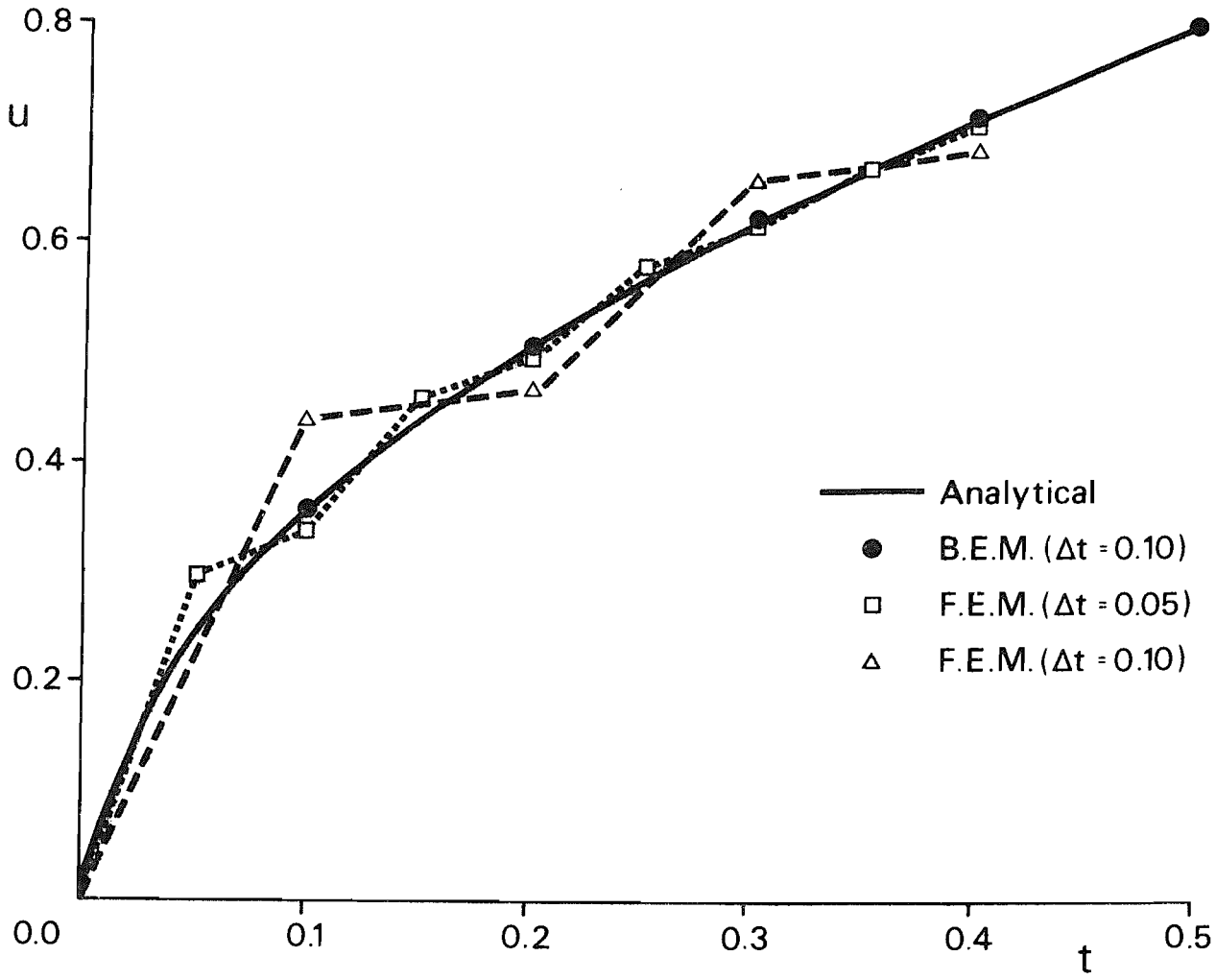

Figure 4.4.12 - Surface temperature of semi-infinite solid

BEM1A (linear), 2% for BEM2 (constant) and 5% for BEM1A (constant). No oscillations about the exact solution were observed for the BEM, as opposed to the FEM results (figure 4.4.12).

Example 4.4.8

Another comparison between BEM and FEM solutions was effected in this example of a bar with unit material properties, at zero initial temperature. We assume that for any time $t > t_0$ a unit temperature is applied at $x_1=0$, all other surfaces being insulated. The problem is essentially one-dimensional because of the symmetry imposed by the non-conducting boundaries.

This problem was analysed with the FEM in [81] where the space domain was discretised into four linear, quadratic or cubic isoparametric elements and the variation with time approximated by the Crank-Nicholson method. The finite element mesh, together with the BEM discretisations, is shown in figure 4.4.13.

Again, four BEM analyses of the problem were carried out, the results for scheme BEM2 being plotted in figure 4.4.14. Notice that for the stepwise linear case the unit temperature at $x_1=0$ was applied linearly over the first time step. The results for scheme BEM1A also behaved as depicted in the figure and were of the same order of accuracy for the linear case and slightly less accurate for the constant one (8% maximum relative error compared to 3.6% for BEM2).

Since a rather large value of time step was employed for the problem the FEM solutions presented severe oscillations about the exact solution given in [16] (see figure 4.4.14). This was not the case for the BEM solutions despite this value being much larger than the critical value ($\Delta t_{crit}=0.125$) predicted by equation (4.4.1).

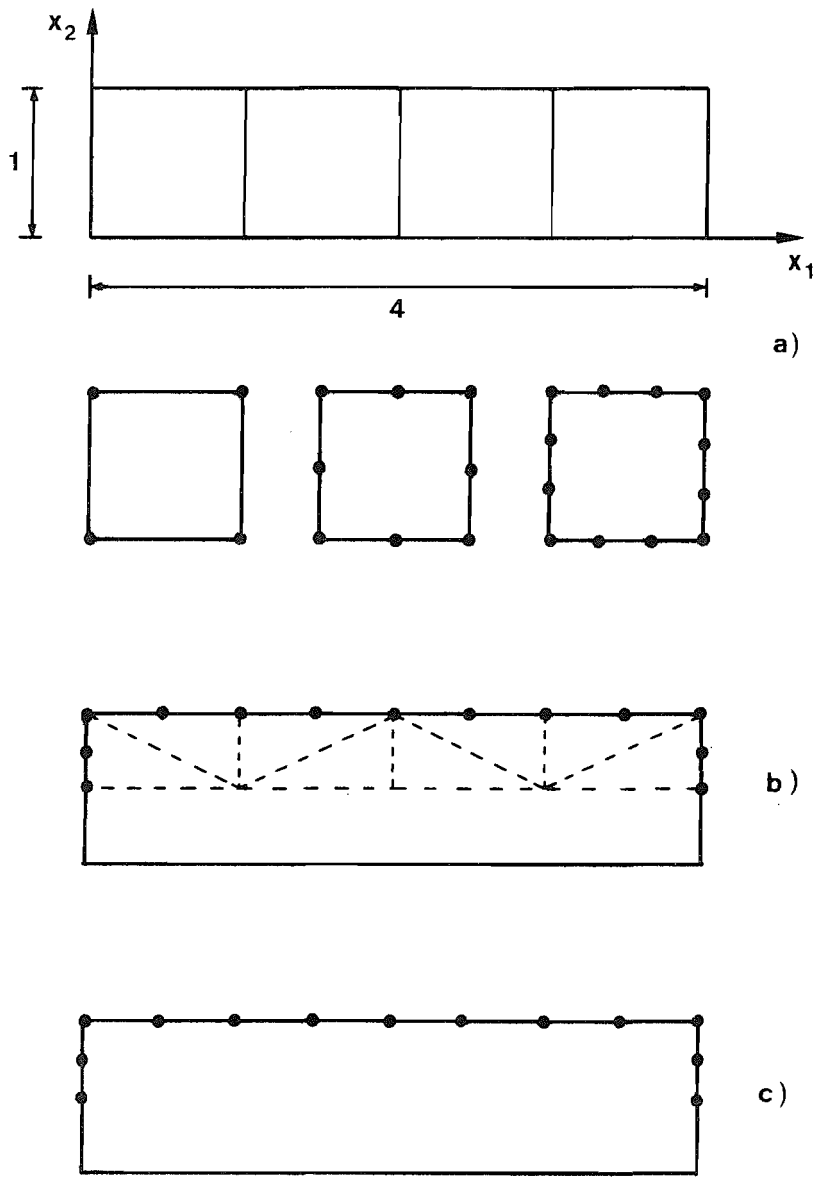

Figure 4.4.13 - One-dimensional bar: a) Geometry and FEM mesh;
b) BEM1A discretisation; c) BEM2 discretisation

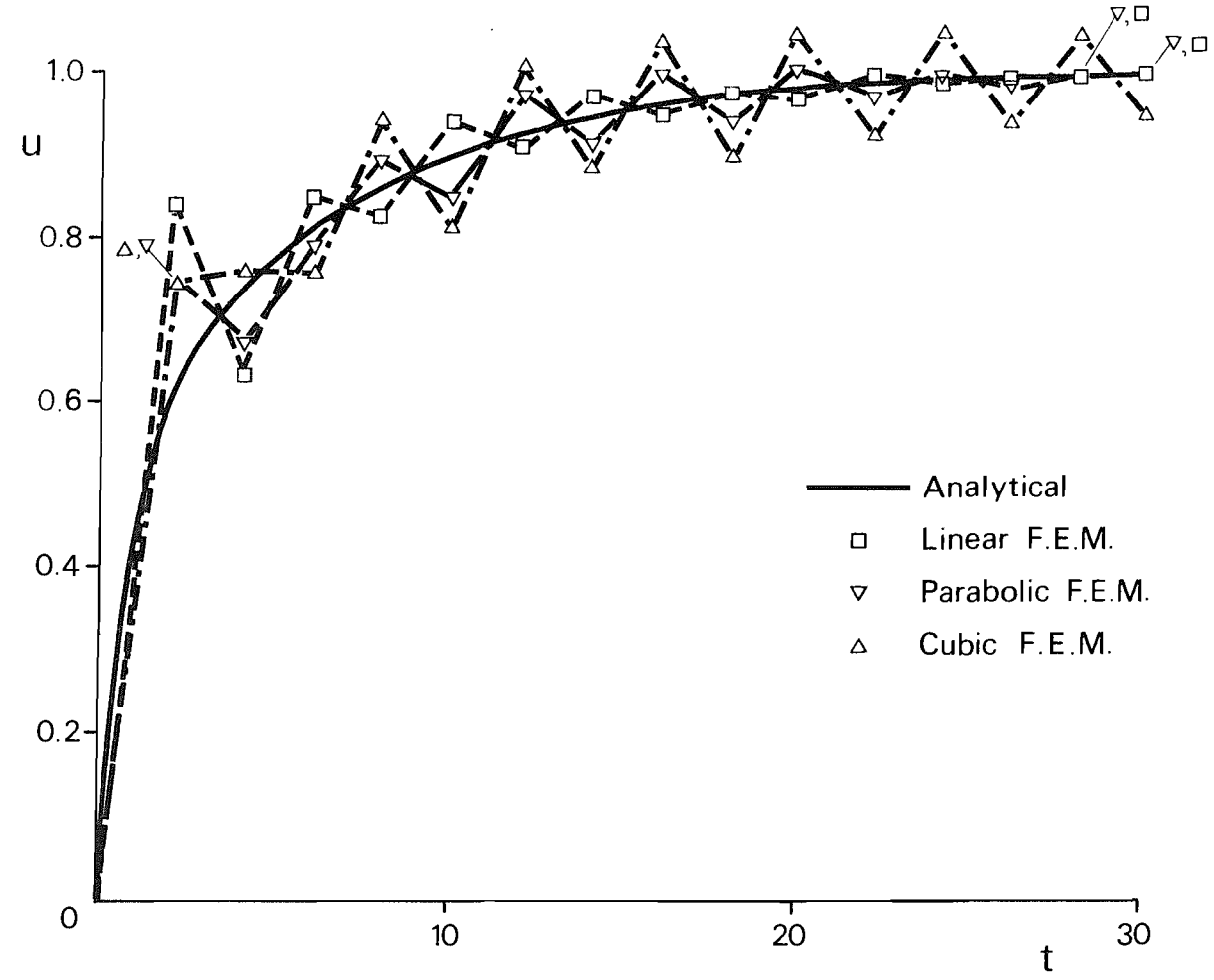

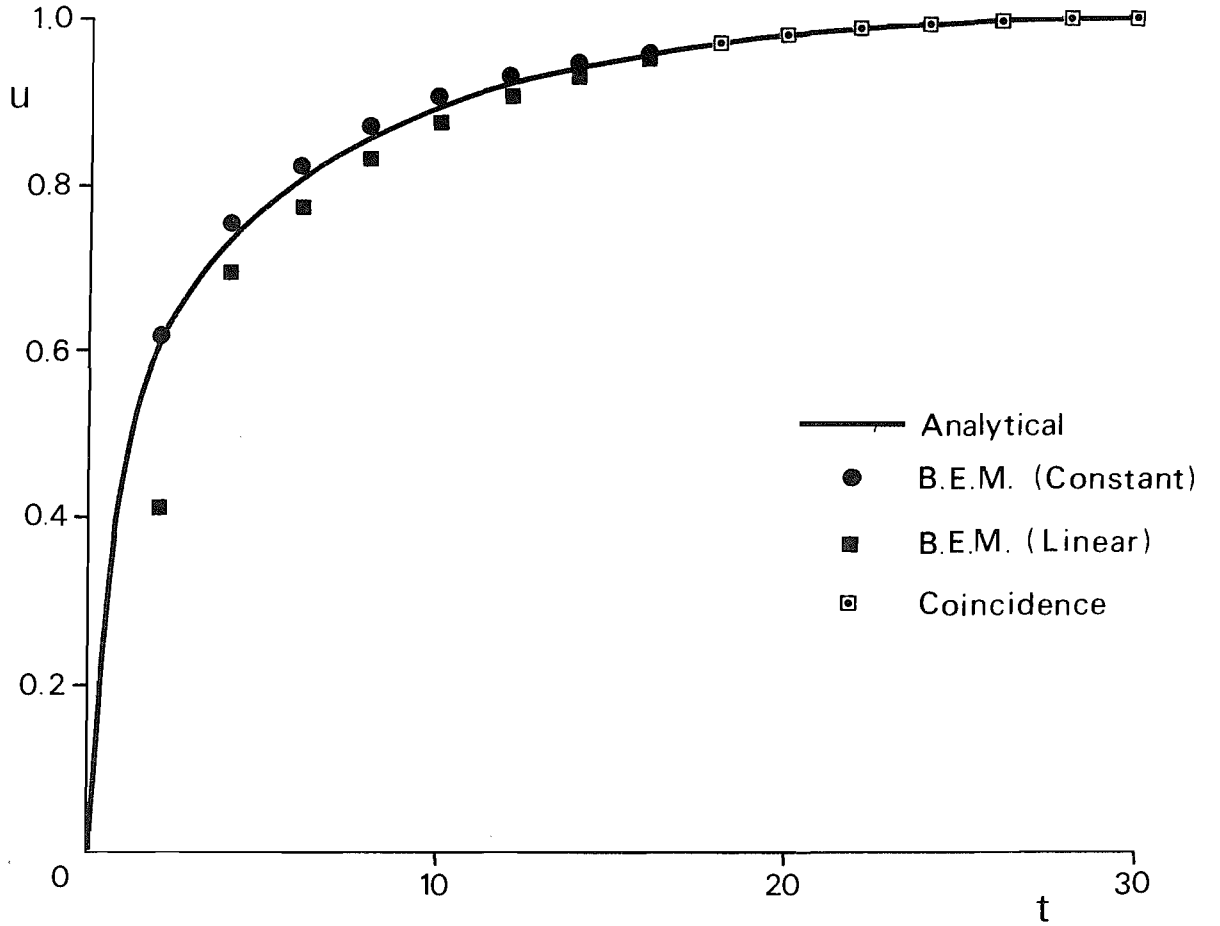

Figure 4.4.14 - Temperature variation of bar, at x_1=1, for Δt=2

4.5 Robin-Type Boundary Conditions

As discussed in section 3.2, many problems of interest present boundary conditions of the Robin-type,

$$a\ u + b\ q = d \tag{4.5.1}$$

where a, b and d are functions of the position, being the condition valid at any instant in time. If this equation is applied to all boundary nodes we can write, in matricial form (see equation (3.2.2)),

$$\underset{\sim}{Q} = \underset{\sim}{D} - \underset{\sim}{A}\ \underset{\sim}{U} \tag{4.5.2}$$

which, substituted into (say) (4.1.8) gives,

$$\sum_{f=1}^{F} (\underset{\sim}{H}_{fF} + \underset{\sim}{G}_{fF})\ \underset{\sim}{A}\ \underset{\sim}{U}_f = \sum_{f=1}^{F} \underset{\sim}{G}_{fF}\ \underset{\sim}{D} + \underset{\sim}{B}_0\ \underset{\sim}{\overline{U}}_0 \tag{4.5.3}$$

The above recurrence relation can then be employed to advance the boundary (and internal) values of u in time.

A well-known such condition is the convection or 'radiation' boundary condition of heat conduction problems (see example 3.2.1),

$$q + h\ u = h\ u_s \tag{4.5.4}$$

It may occur, in many practical situations, that functions h and u_s are also time-dependent. Assuming at first that u and u_s have stepwise linear variations while h is only stepwise constant, condition (4.5.4) gives,

$$q = h(u_s - u) = \frac{h}{\Delta t_f}\left[(t-t_{f-1})(u_{s,f}-u_f) + (t_f-t)(u_{s,f-1}-u_{f-1})\right] \tag{4.5.5}$$

Equation (4.1.17) can then be rearranged for our numerical solution as,

$$\sum_{f=1}^{F}\left[(\underset{\sim}{H}^1_{fF} + \underset{\sim}{G}^1_{fF}\ \underset{\sim}{A})\ \underset{\sim}{U}_{f-1} + (\underset{\sim}{H}^2_{fF} + \underset{\sim}{G}^2_{fF}\ \underset{\sim}{A})\ \underset{\sim}{U}_f\right]$$

$$= \sum_{f=1}^{F} (\underset{\sim}{G}^1_{fF}\ \underset{\sim}{A}\ \underset{\sim}{D}_{f-1} + \underset{\sim}{G}^2_{fF}\ \underset{\sim}{A}\ \underset{\sim}{D}_f) + \underset{\sim}{B}_0\ \underset{\sim}{\overline{U}}_0 \tag{4.5.6}$$

where the diagonal matrix $\underset{\sim}{A}$ and the vector $\underset{\sim}{D}$ now contain the values

of h and u_s, respectively.

Consider now that the heat transfer coefficient h is also stepwise linear, its variation being prescribed by functions (4.1.14). Applying condition (4.5.4) then yields [82] ,

$$q = \frac{1}{\Delta t_f^2} \Big\{ (t-t_{f-1})^2 \, h_f \, (u_{s,f}-u_f) + (t-t_{f-1})(t_f-t) \Big[h_f \, (u_{s,f-1} - u_{f-1}) + h_{f-1} \, (u_{s,f} - u_f) \Big] + (t_f-t)^2 \, h_{f-1} \, (u_{s,f-1} - u_{f-1}) \Big\} \tag{4.5.7}$$

which implies a quasi-quadratic variation for function q.

The application of equation (4.1.5) to all boundary nodes gives, for this kind of problems,

$$\sum_{f=1}^{F} \Big[(H^1_{\sim fF} + G^1_{\sim fF} \, A_{\sim f-1} + G^2_{\sim fF} \, A_{\sim f}) \, U_{\sim f-1} + (H^2_{\sim fF} + G^2_{\sim fF} \, A_{\sim f-1} + G^3_{\sim fF} \, A_{\sim f}) \, U_{\sim f} \Big] = \sum_{f=1}^{F} \Big[(G^1_{\sim fF} \, A_{\sim f-1} + G^2_{\sim fF} \, A_{\sim f}) \, D_{\sim f-1} + (G^2_{\sim fF} \, A_{\sim f-1} + G^3_{\sim fF} \, A_{\sim f}) \, D_{\sim f} \Big] + B_{\sim 0} \, \overline{U}_{\sim 0} \tag{4.5.8}$$

where the coefficients of matrices $\underset{\sim}{H}$ are computed as in (4.1.18), of matrix $B_{\sim 0}$ as in (4.1.9) and of matrices $\underset{\sim}{G}$ as follows

$$g^{1,m}_{fFij} = \frac{k}{\Delta t_f^{\,2}} \int_{\Gamma_s} \phi^m \int_{t_{f-1}}^{t_f} (t_f-t)^2 \, u^*(i,S,t_F,t) \, dt \, d\Gamma(S)$$

$$g^{2,m}_{fFij} = \frac{k}{\Delta t_f^{\,2}} \int_{\Gamma_s} \phi^m \int_{t_{f-1}}^{t_f} (t_f-t)(t-t_{f-1}) \, u^*(i,S,t_F,t) \, dt \, d\Gamma(S) \tag{4.5.9}$$

$$g^{3,m}_{fFij} = \frac{k}{\Delta t_f^{\,2}} \int_{\Gamma_s} \phi^m \int_{t_{f-1}}^{t_f} (t-t_{f-1})^2 \, u^*(i,S,t_F,t) \, dt \, d\Gamma(S)$$

The analytical evaluation of the time integrals in (4.5.9) gives

(see equations (4.1.13), (4.1.21) and (4.1.29)),

$$\int_{t_{f-1}}^{t_f} (t_f-t)^2\, u^*(i,S,t_F,t)\, dt = \frac{1}{4\pi k}\left\{\left[(t_f-t_F)^2 - \frac{r^2}{2k}\left((t_f-t_F) - \frac{r^2}{16k}\right)\right]\left[E_1(a_{f-1}) - E_1(a_f)\right] + \frac{r^2}{2k}\left[(t_f-t_F) - \frac{r^2}{16k}\right]\left[\frac{1}{a_{f-1}}\exp(-a_{f-1}) - \frac{1}{a_f}\exp(-a_f)\right] + \frac{r^4}{32k^2}\left[\frac{1}{a_{f-1}^2}\exp(-a_{f-1}) - \frac{1}{a_f^2}\exp(-a_f)\right]\right\} \tag{4.5.10}$$

$$\int_{t_{f-1}}^{t_f} (t_f-t)\,(t-t_{f-1})\, u^*(i,S,t_F,t)\, dt = \frac{1}{4\pi k}\left\{\left[(t_f-t_F)\,(t_F-t_{f-1}) + \frac{r^2}{4k}\left((t_f-t_F) - (t_F-t_{f-1}) - \frac{r^2}{8k}\right)\right]\left[E_1(a_{f-1}) - E_1(a_f)\right] - \frac{r^2}{4k}\left[(t_f-t_F) - (t_F-t_{f-1}) - \frac{r^2}{8k}\right]\left[\frac{1}{a_{f-1}}\exp(-a_{f-1}) - \frac{1}{a_f}\exp(-a_f)\right] - \frac{r^4}{32k^2}\left[\frac{1}{a_{f-1}^2}\exp(-a_{f-1}) - \frac{1}{a_f^2}\exp(-a_f)\right]\right\}$$

$$\int_{t_{f-1}}^{t_f} (t-t_{f-1})^2\, u^*(i,S,t_F,t)\, dt = \frac{1}{4\pi k}\left\{\left[(t_F-t_{f-1})^2 + \frac{r^2}{2k}\left((t_F-t_{f-1}) + \frac{r^2}{16k}\right)\right]\left[E_1(a_{f-1}) - E_1(a_f)\right] - \frac{r^2}{2k}\left[(t_F-t_{f-1}) + \frac{r^2}{16k}\right]\left[\frac{1}{a_{f-1}}\exp(-a_{f-1}) - \frac{1}{a_f}\exp(-a_f)\right] + \frac{r^4}{32k^2}\left[\frac{1}{a_{f-1}^2}\exp(-a_{f-1}) - \frac{1}{a_f}\exp(-a_f)\right]\right\}$$

Example 4.5.1

This example studies a square region at unit initial temperature 'radiating' into a surrounding medium at zero temperature. The heat transfer coefficient is constant all over the surface and equal to 2 and the thermal diffusivity assumed to be unity.

Boundary elements analyses were carried out for schemes BEM1A and BEM2 with stepwise constant or linear variations for u and q, with the discretisation shown in figure 4.5.2. Note that for the BEM2 cases only the boundary is discretisated into 8 elements and the domain integral evaluated using equation (4.3.4). Coincident results were obtained for both schemes and they are plotted in figures 4.5.1 and 4.5.2 for the constant case, compared with an analytical solution [16].

As can be seen in figure 4.5.1, the maximum error occurs at the corner $x_1=x_2=1$, at the time t=0.10 (7.5% relative error). Using stepwise linear functions, this error is reduced to 2%.

Example 4.5.2

Another comparison with the Finite Element Method is effected in this example of a plane plate, initially at 0^oC, surrounded by a medium at 100^oC. Its cross-section has 0.1 x 0.1 m and the values of thermal conductivity, heat capacity and heat transfer coefficient are 18 kcal/h m^oC, 912 kcal/m^3 ^oC and 5000 kcal/h m^2 ^oC, respectively.

Again, four BEM analyses were carried out with the same discretisations adopted for the previous example (see figure 4.5.2) and coincident results obtained for both time-marching schemes. The averaged surface temperature of the plate is plotted in figure 4.5.3. The FEM analyses employed 5 parabolic isoparametric elements in space and linear, parabolic and cubic elements in time [83]. Results using a central finite difference scheme are also presented in the same reference.

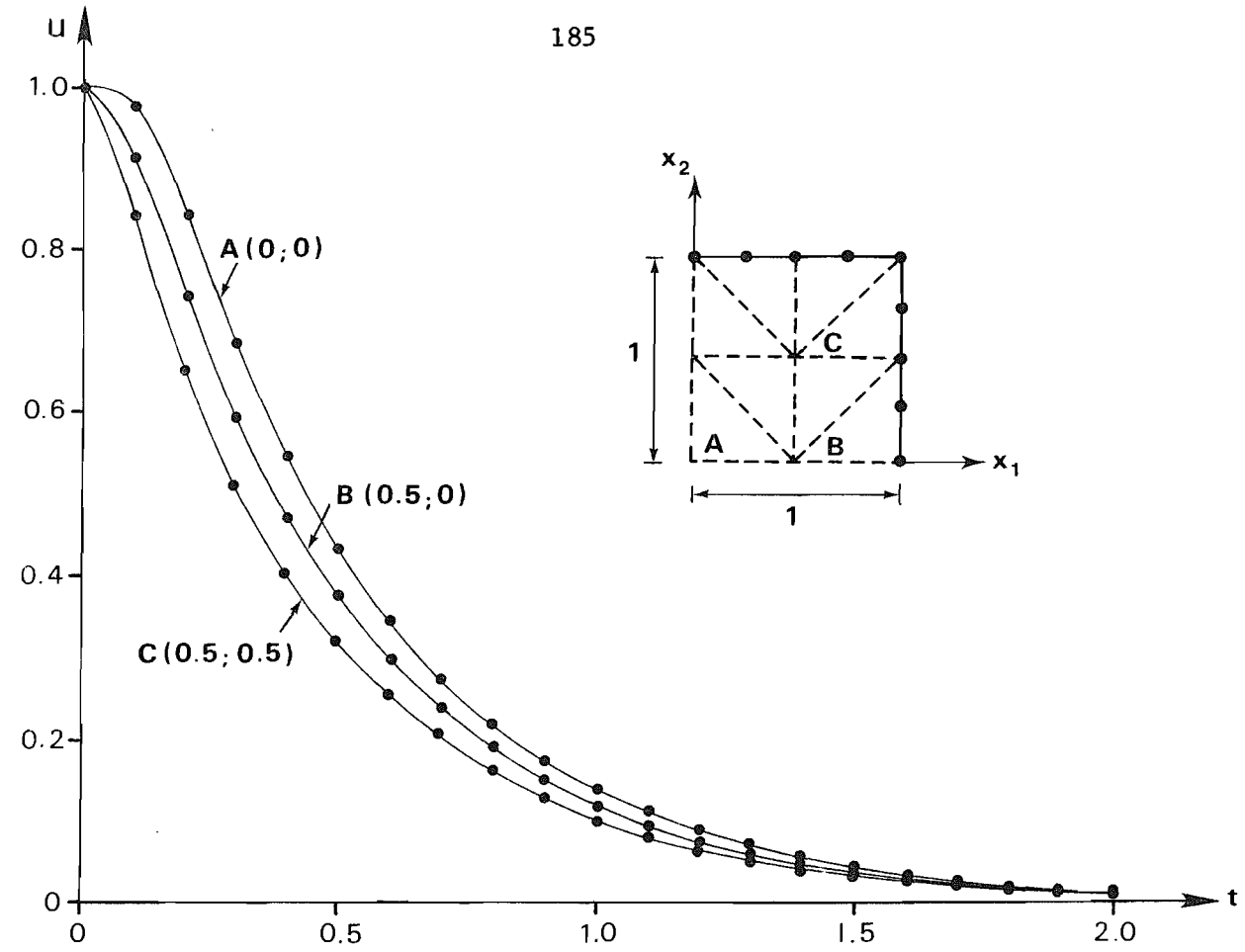

Figure 4.5.1 - Temperature values along the face $x_1=1$

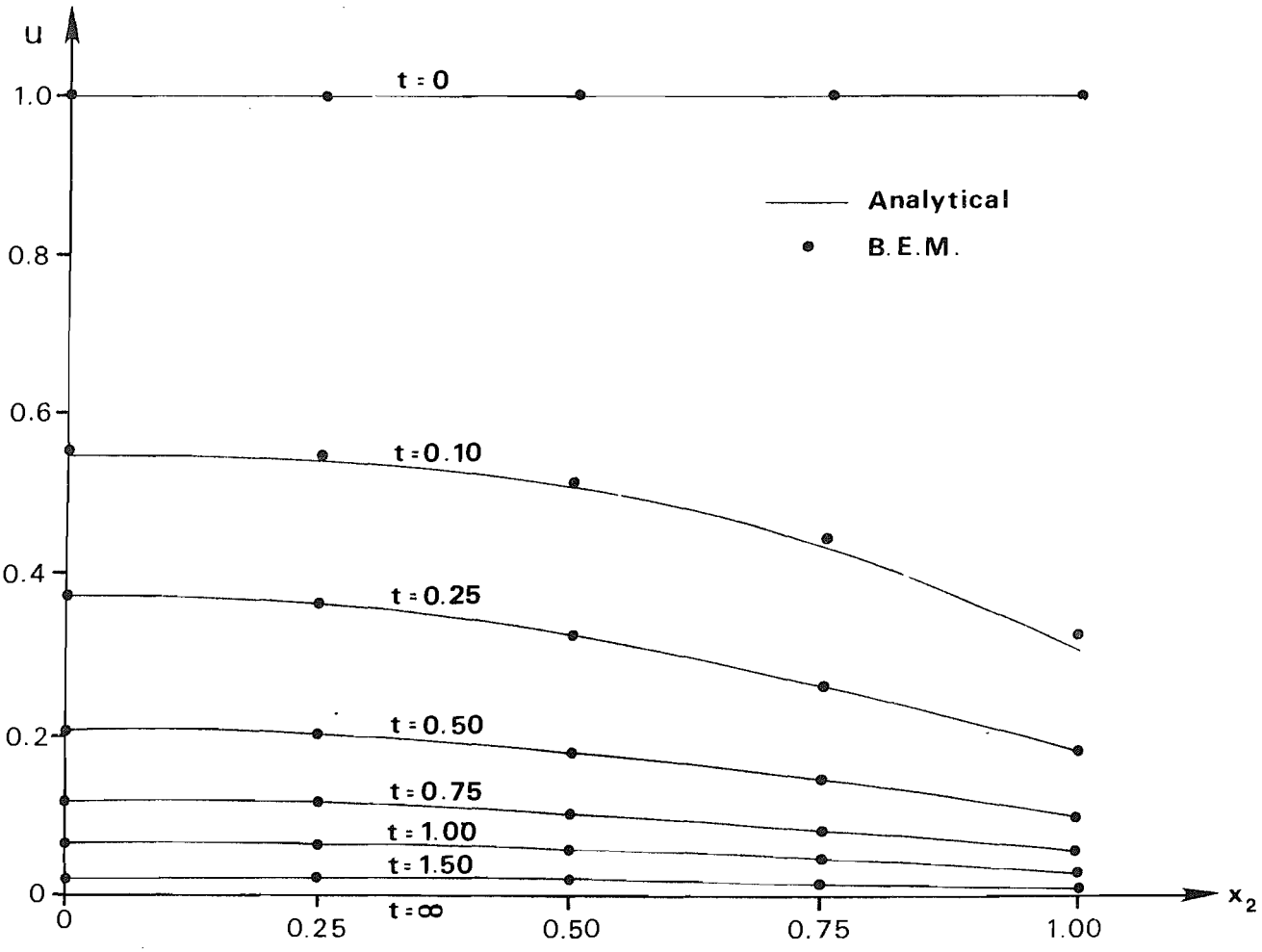

Figure 4.5.2 - Temperature at internal points

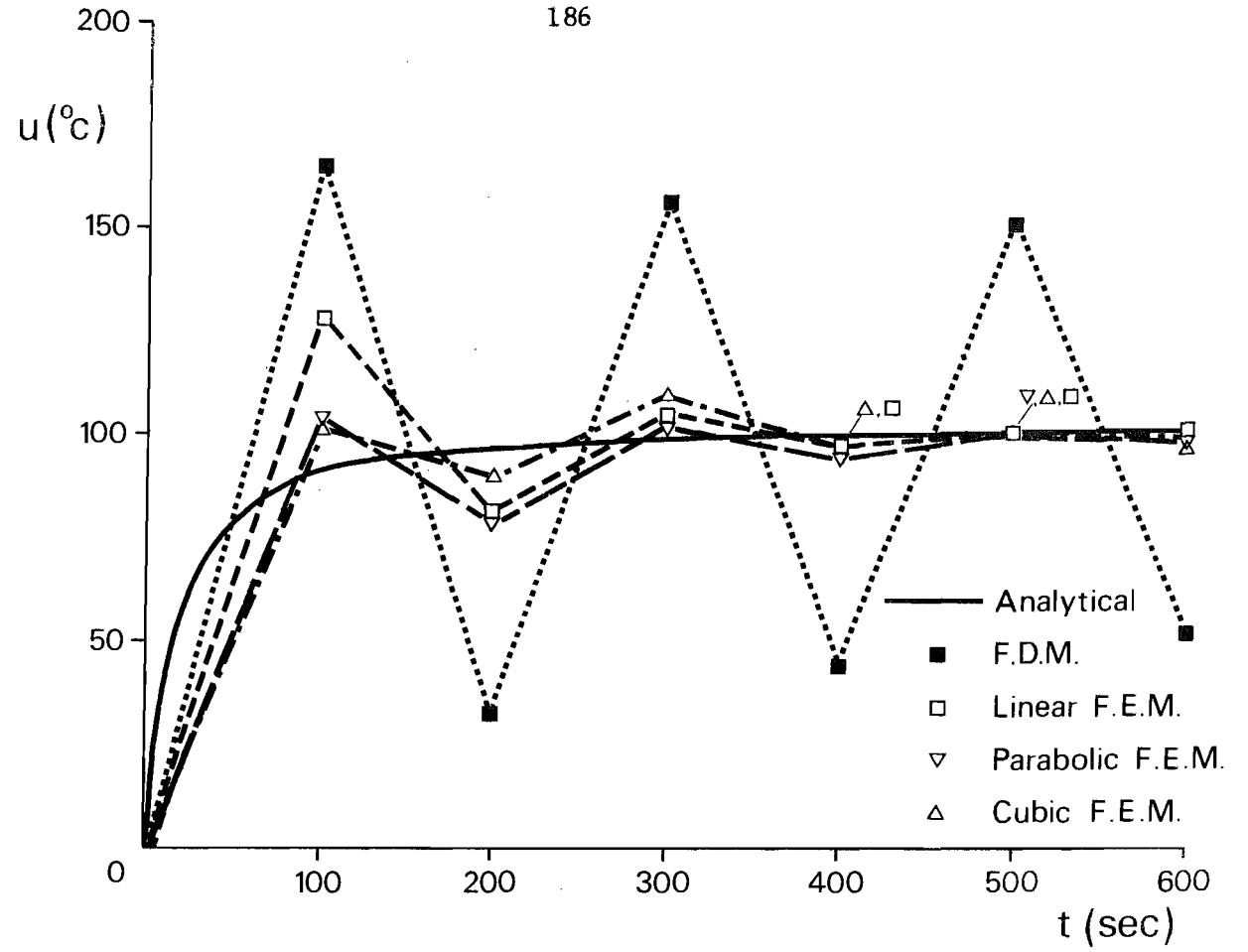

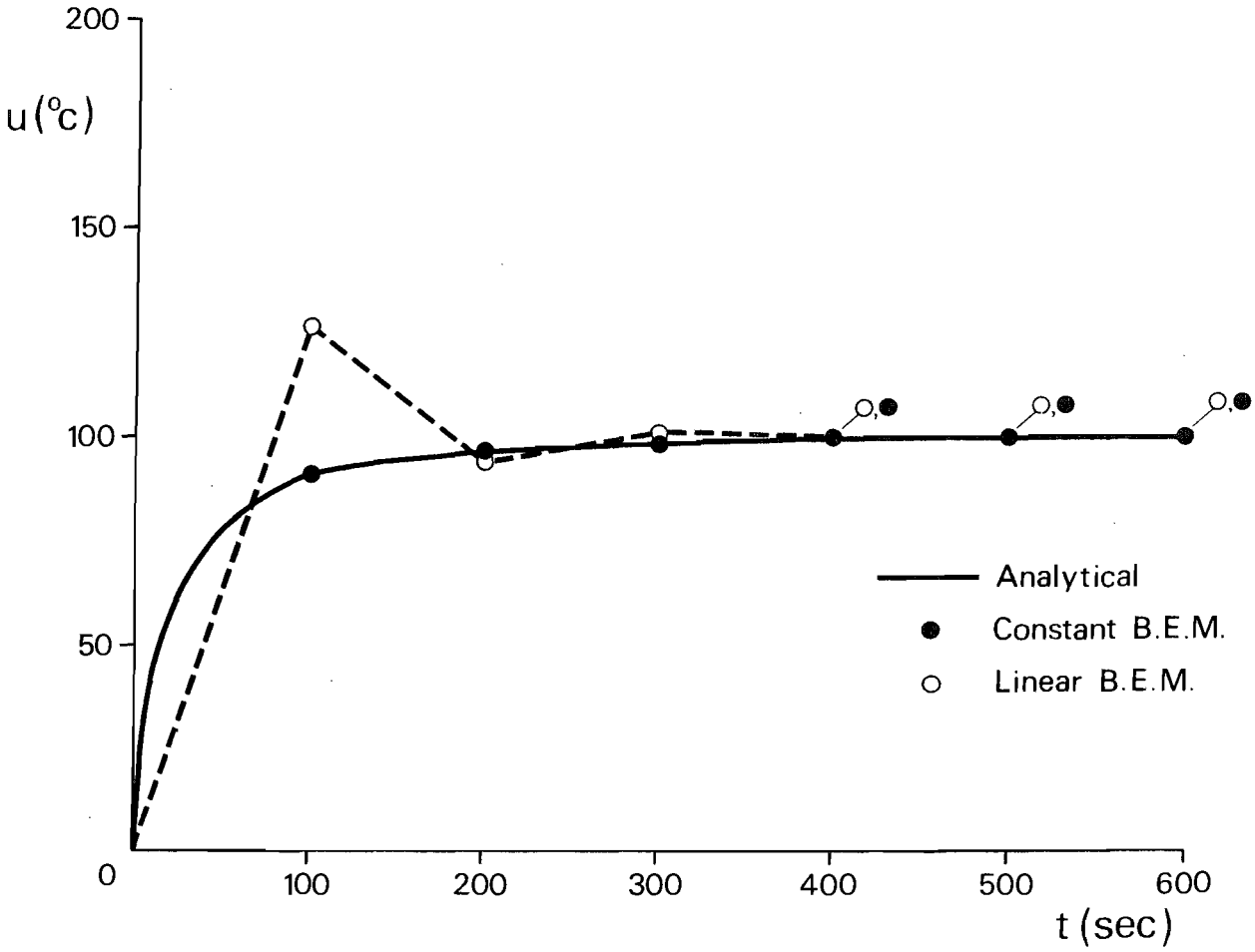

Figure 4.5.3 - Surface temperature of plane plate

As pointed out in [83], the time step value Δt=100 s adopted from the problem is extremely large (the critical value predicted by equation (4.4.1) is only Δt_{crit}=14 s). The solution goes from the initial-state to the steady-state almost in one increment. Because of this, the linear BEM solution produced oscillations which are, however, much smaller than the FDM and FEM ones. The constant BEM seems to be remarkably stable and produced no oscillation at all.

Example 4.5.3

For problems involving regions extending to infinity, BEM solutions with scheme BEM2 are much more economical than FEM ones. In order to demonstrate this, we study in this example a circular opening in an infinite plane region with initial conditions u_0=10. The radius of the hole is unity, its ambient temperature equals zero and the material properties of the medium are also assumed to be unity, for simplicity.

The variation of the surface temperature with time is presented in figure 4.5.5 for various values of the heat transfer coefficient, compared to an analytical solution given in [16]. The agreement between the two solutions is very good. A time step value Δt=0.5 was adopted and the analyses carried out until the surface temperature began to drop significantly. The BEM results were obtained with stepwise constant functions and, due to symmetry, only one quarter of the interface between hole and medium was discretised into 6 boundary elements (figure 4.5.4).

This problem was also studied with the FEM in [84] but since the FEM is a domain-type technique, the infinite region has to be limited by a finite, non-conducting boundary. In order to achieve the same level of accuracy, a time step ten times smaller (Δt=0.05) was adopted and the domain discretised using 70 triangular elements or 3 cubic

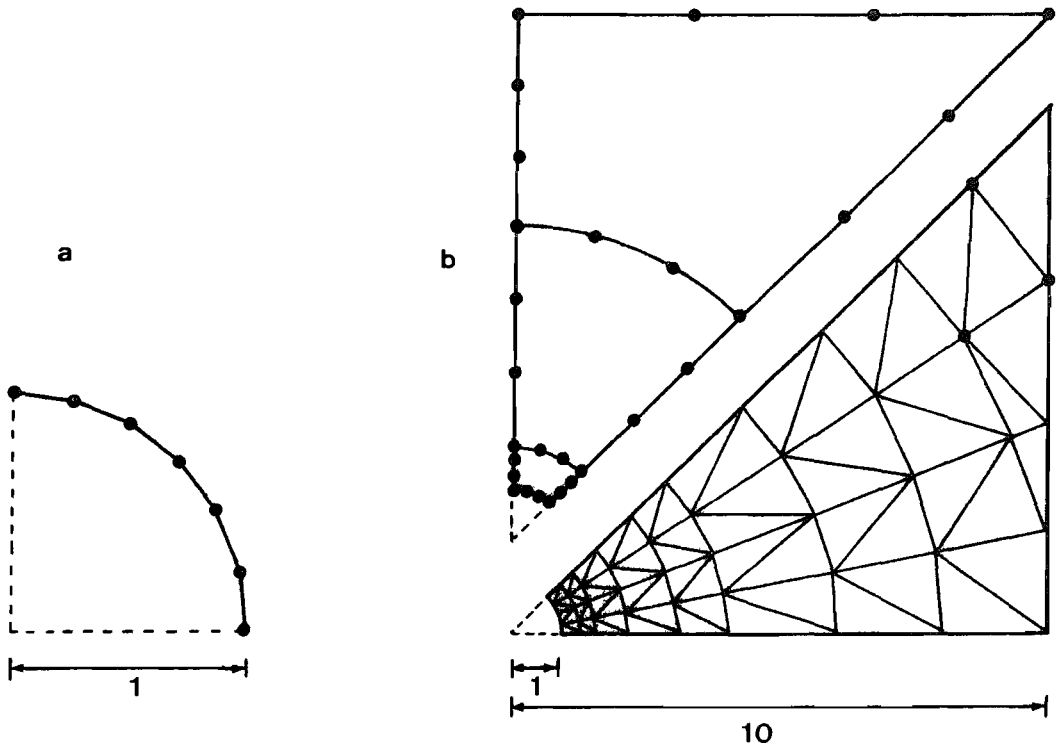

Figure 4.5.4 - Discretisation of hole in infinite region:
a) BEM; b) FEM

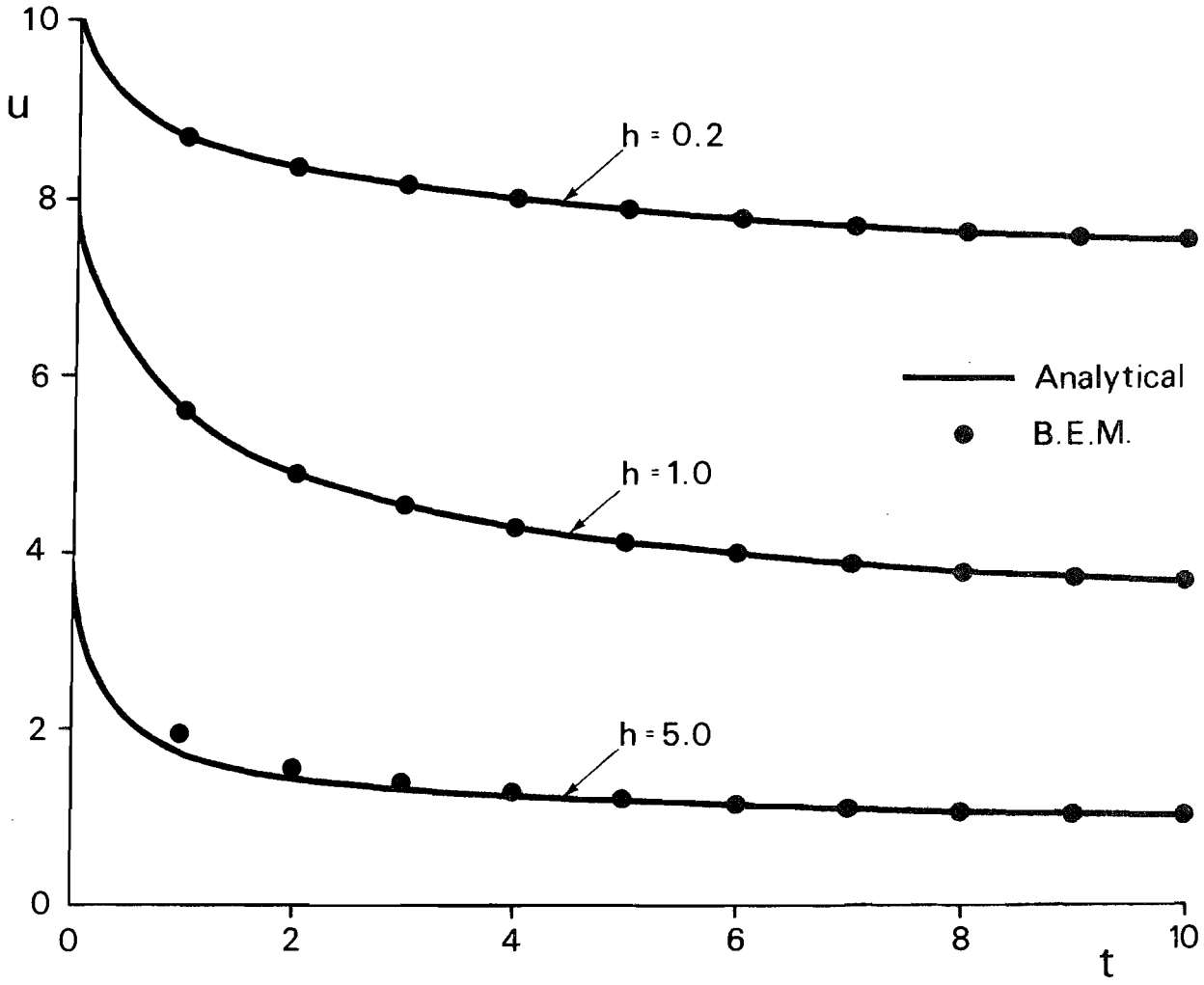

Figure 4.5.5 - Surface temperature of cooling hole in an infinite medium

isoparametric elements (see figure 4.5.4). Note that a similar kind of approximation has to be introduced for the BEM if time-marching scheme BEM1A is utilised: although boundary elements are still restricted only to the hole-medium interface, cells have to be employed to integrate over the (infinite) domain.

Example 4.5.4

A more practical problem with complex time-dependent boundary conditions is studied in this example, where the temperature distribution inside an actual turbine disc is sought. Although the real structure is axisymmetric, a two-dimensional FEM analysis was carried out for comparison purposes [85], employing 85 quadratic isoparametric elements and 348 nodes (figure 4.5.7a).

The initial temperature of the turbine disc is 295.1^{o}K and the values of the thermal conductivity, density and specific heat of the material are 15 W/m^{o}K, 8221 kg/m^{3} and 550 J/kg^{o}K, respectively. There are 18 different zones along the boundary, each of which with a different set of prescribed values for the heat transfer coefficient and the temperature of the surrounding gas. Their time variation at one of such boundary zones is shown in figure 4.5.6.

The BEM discretisation employed 90 elements and 106 nodes (there are 16 double nodes at the intersections of boundary zones). A stepwise linear variation was prescribed for the boundary temperature. For the boundary flux, it was assumed to be linear or quasi-quadratic, according to the variation of h and u_s within each time step.

The first BEM analysis was carried out with a step-by-step time-marching scheme. However, due to core storage limitations of the computer utilised, a full analysis was only possible with scheme BEM1B. Previous experiences with such scheme have shown that a refined domain discretisation is necessary for accurate results to be obtained. So,

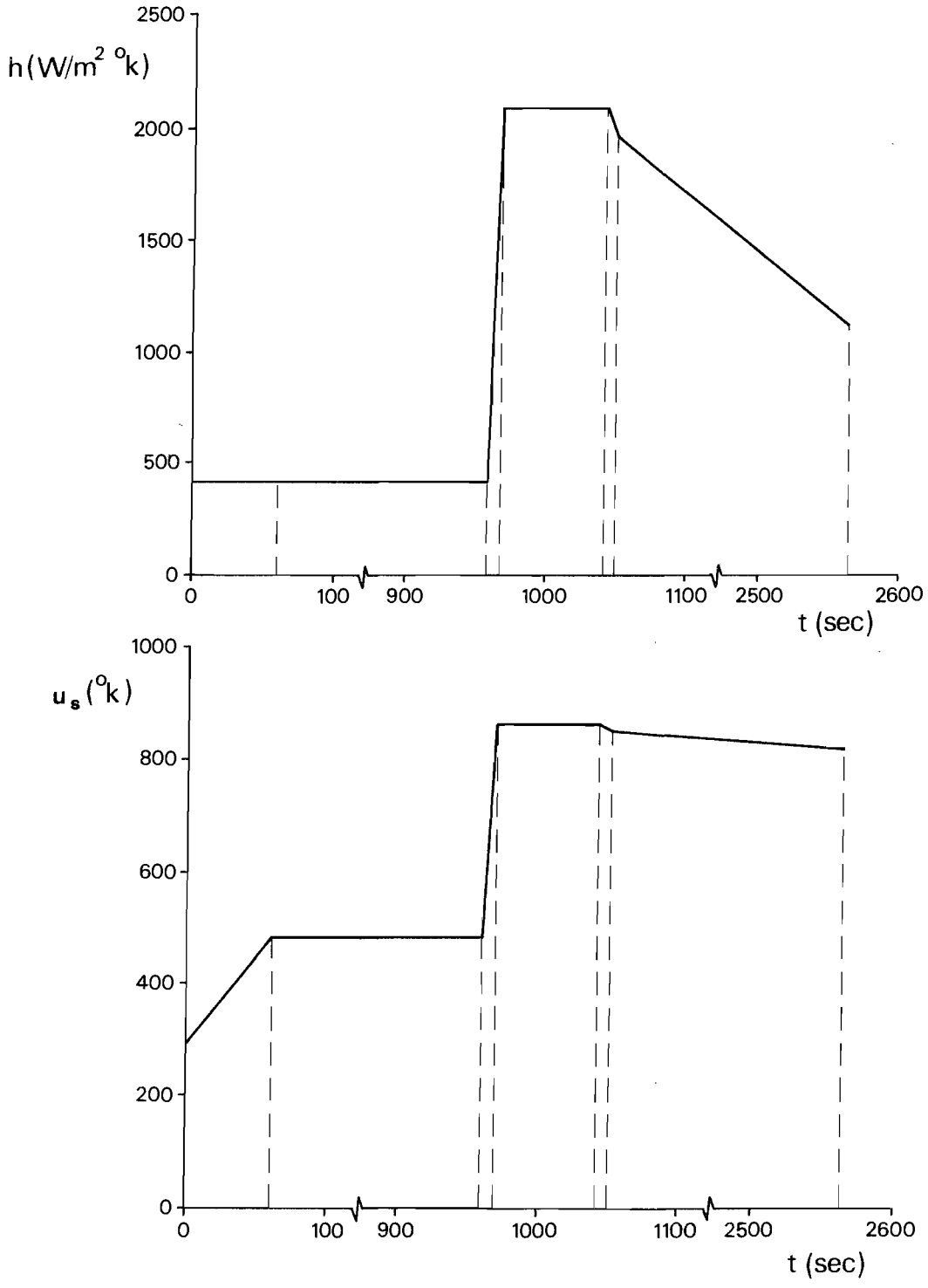

Figure 4.5.6 - Time variation of heat transfer coefficient and temperature of the surrounding gas for a typical boundary zone

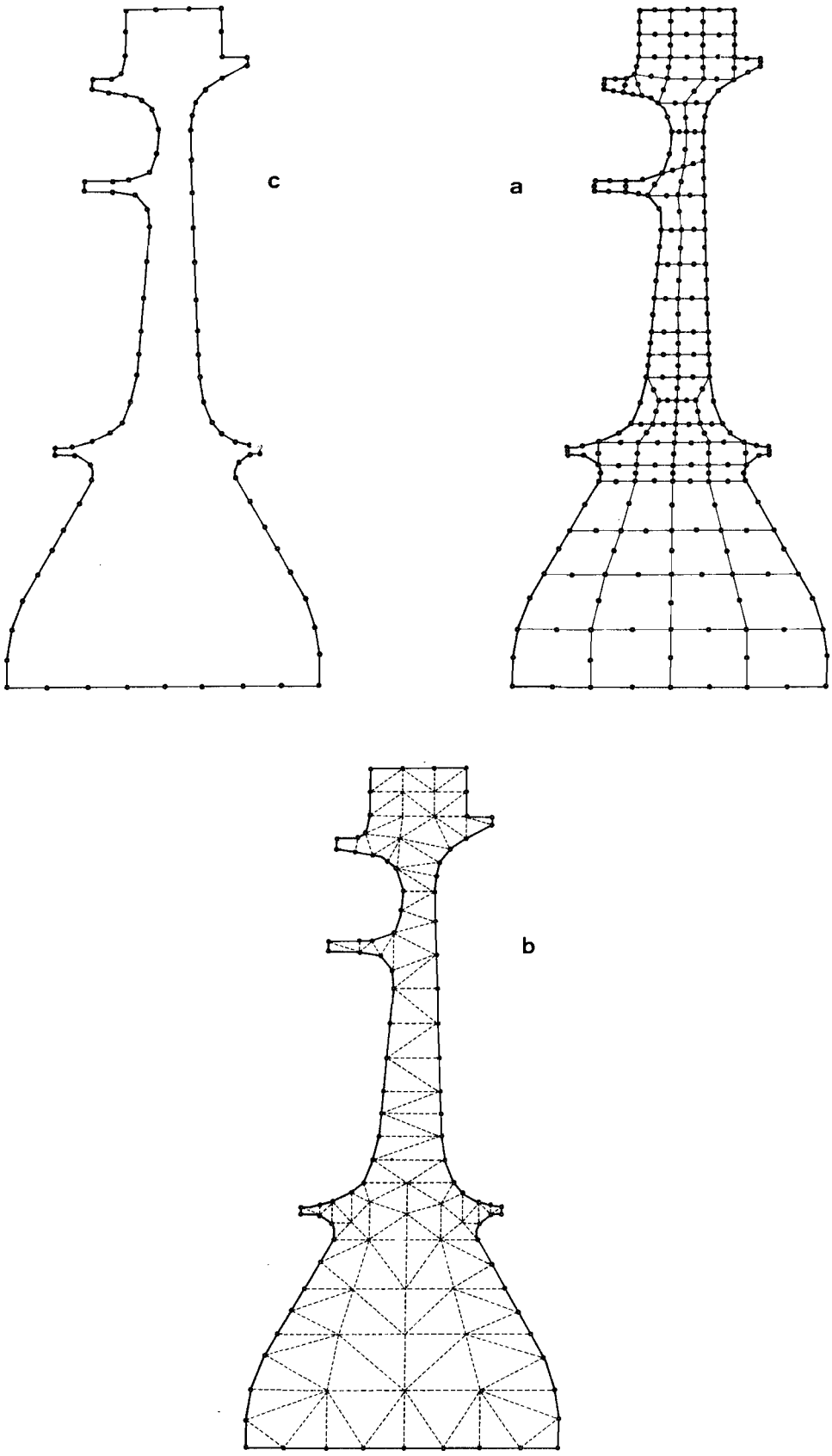

Figure 4.5.7 - Discretisations of turbine disc: a) FEM; b) BEM1B; c) BEM2

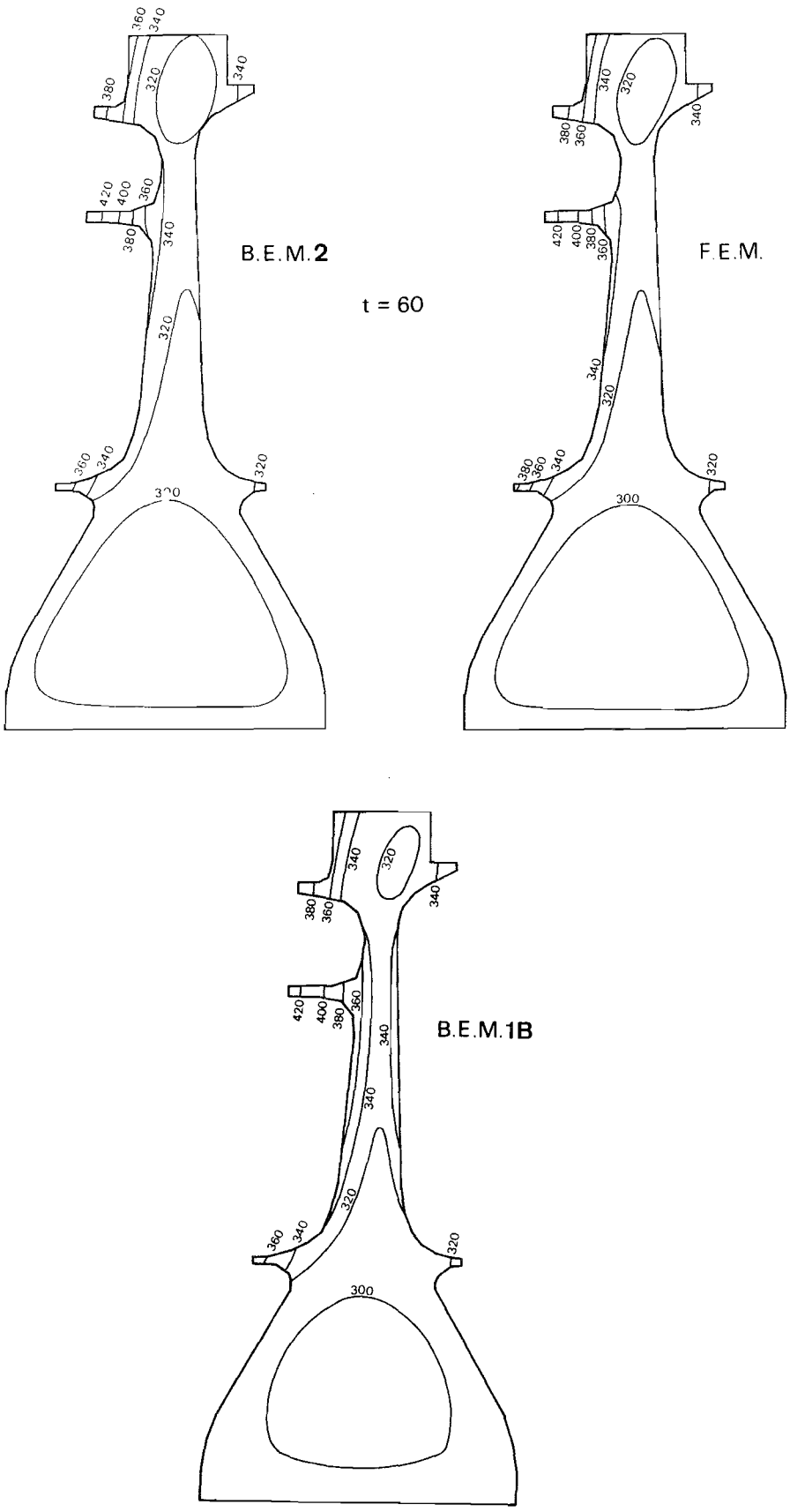

Figure 4.5.8a - Isotherms at t=60

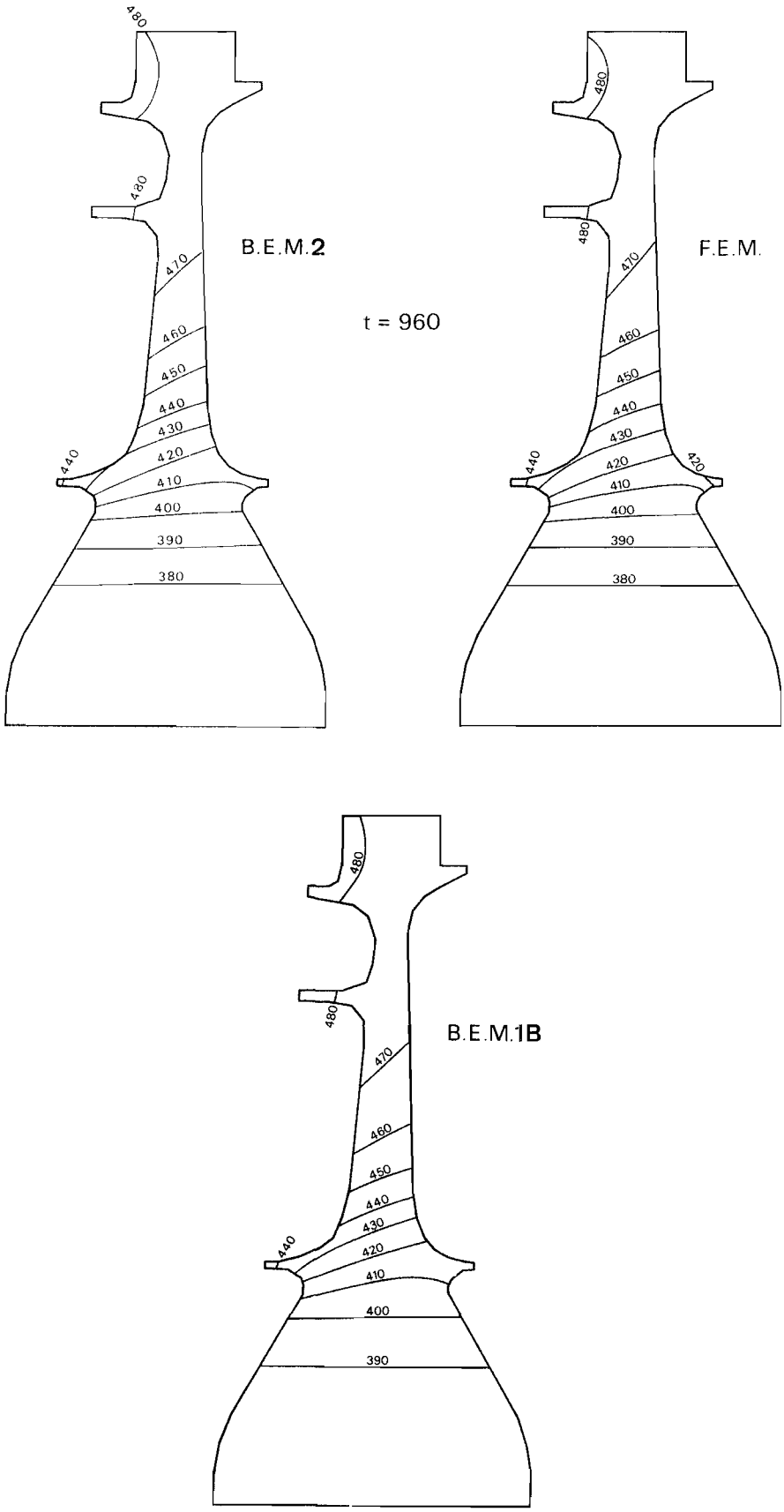

Figure 4.5.8b - Isotherms at t=960

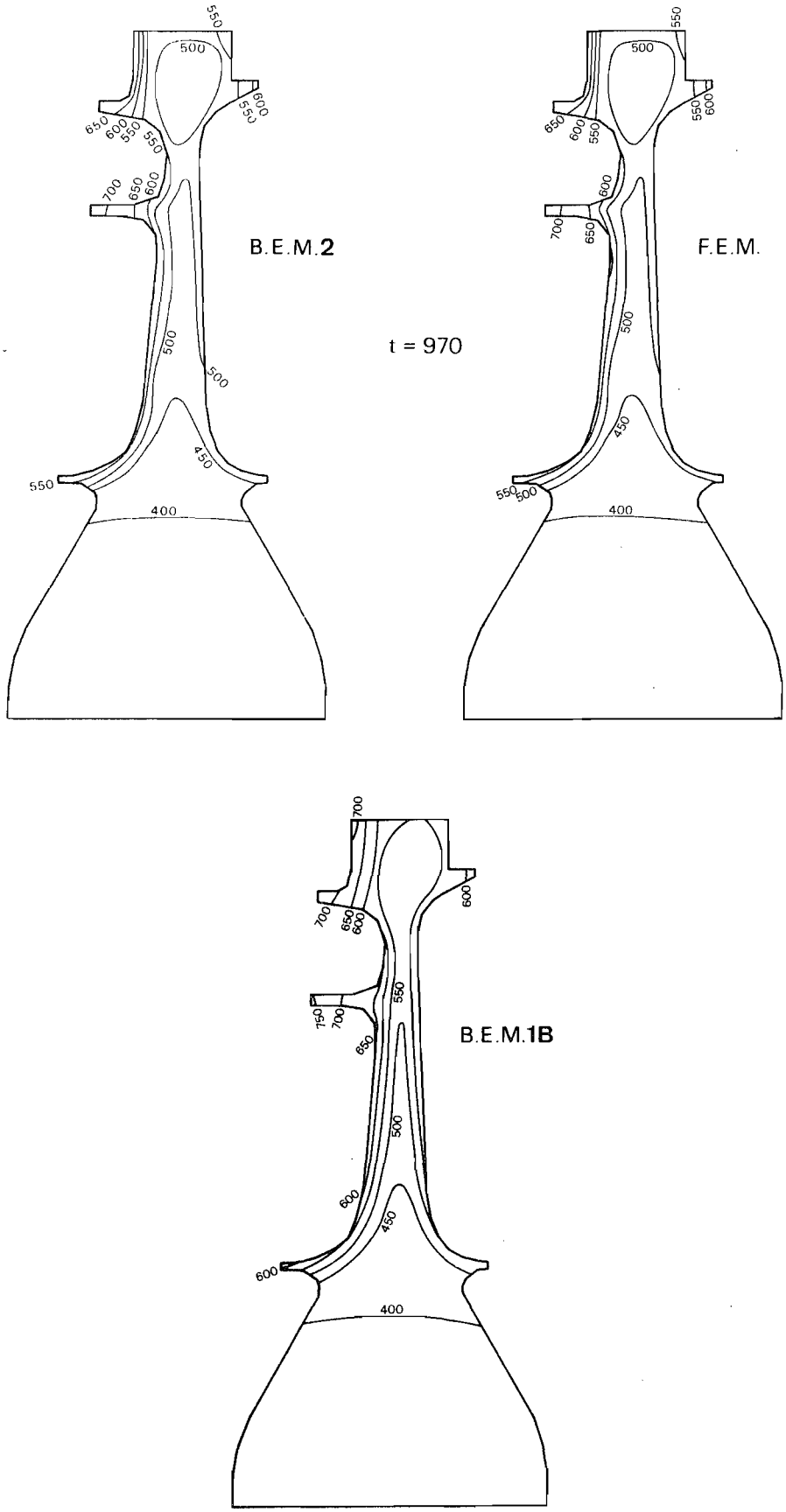

Figure 4.5.8c - Isotherms at t=970

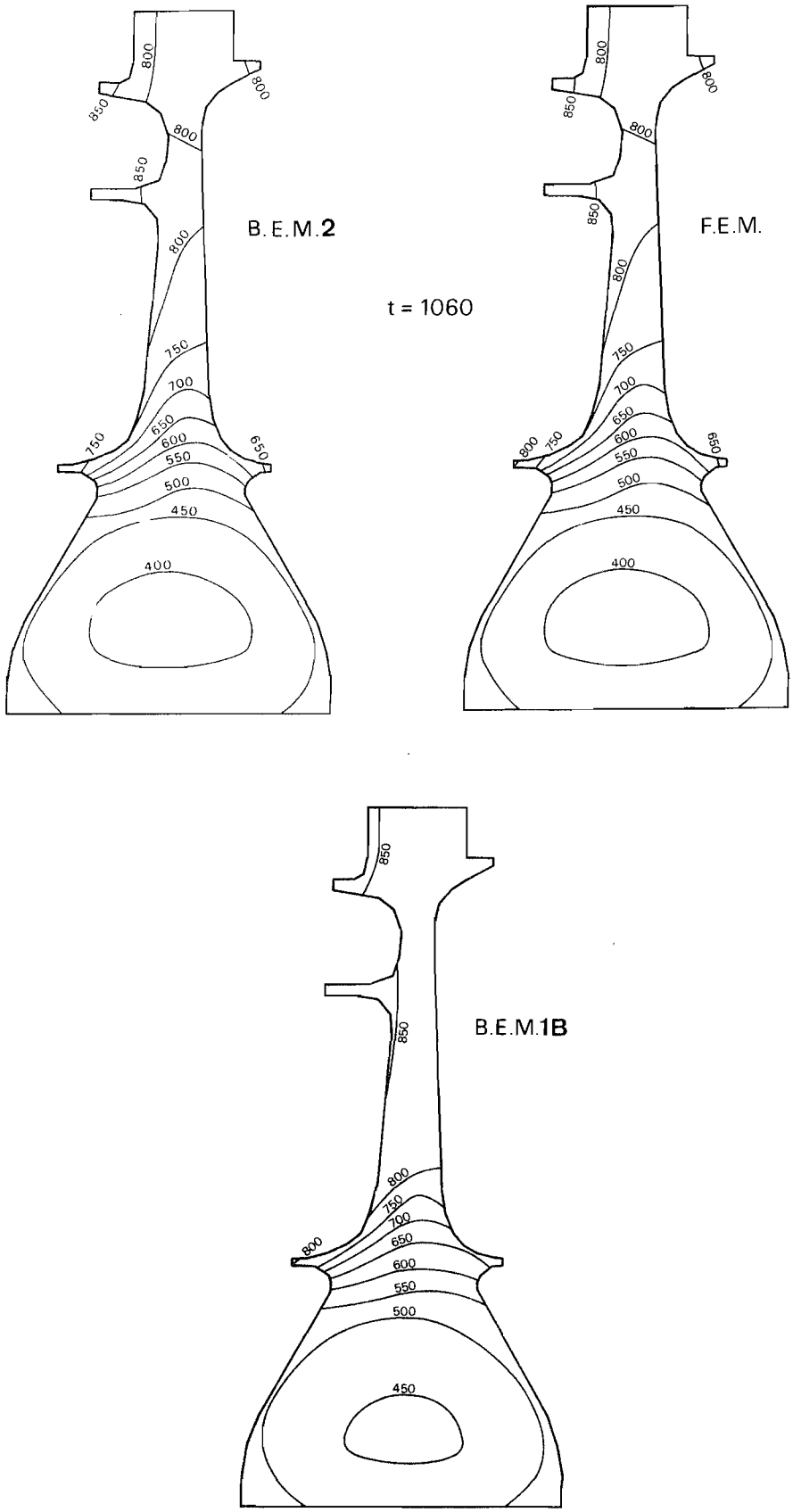

Figure 4.5.8d - Isotherms at time t=1060

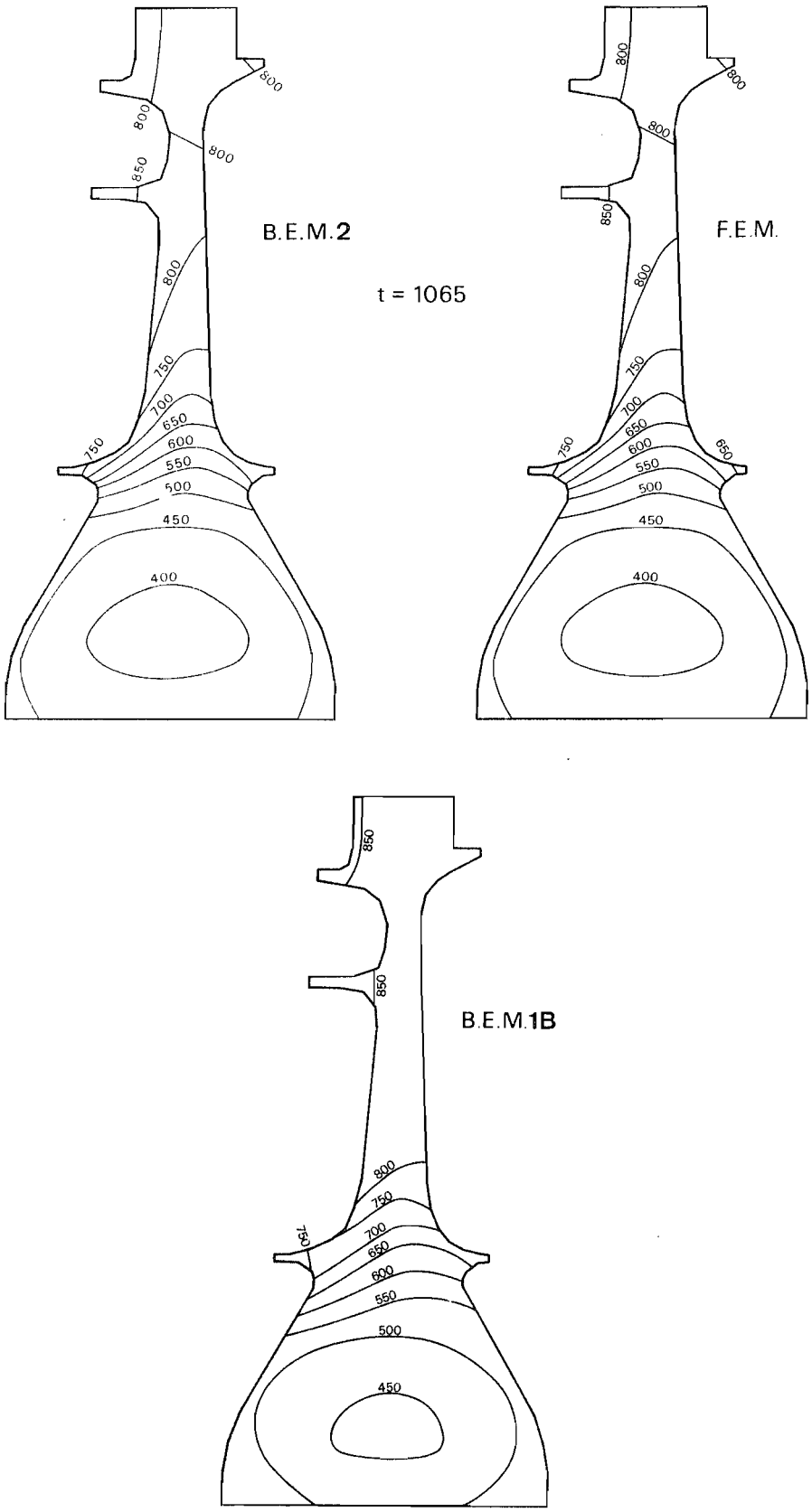

Figure 4.5.8e - Isotherms at time t=1065

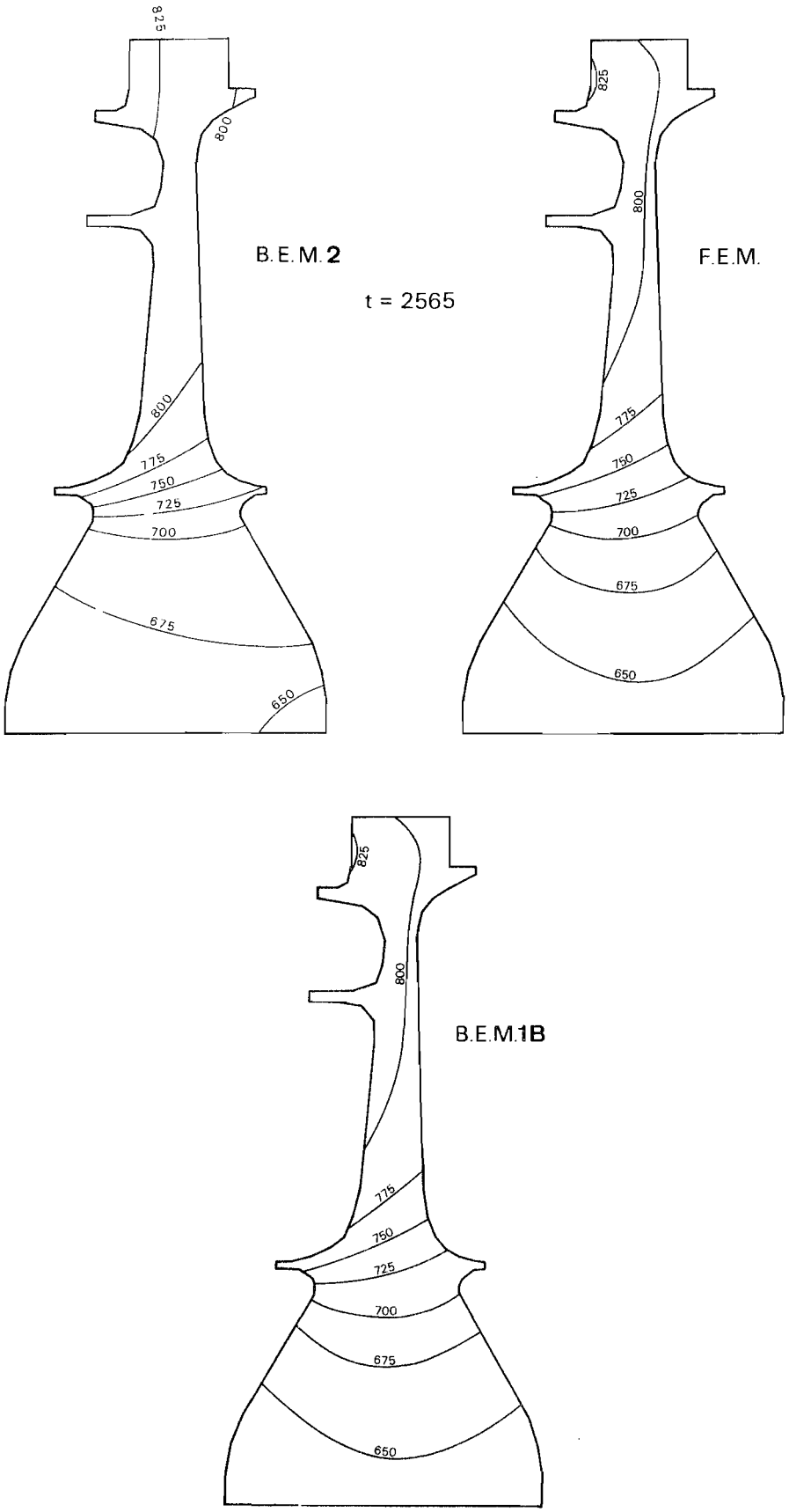

Figure 4.5.8f - Isotherms at time t=2565

we sub-divided the domain into 134 triangular cells with 23 internal points (figure 4.5.7b). Results (isotherms) at several times are plotted in figure 4.5.8 and compared to the FEM results, showing good agreement.

Finally, the problem was studied with scheme BEM2 and, in this case, no domain discretisation is needed (figure 4.5.7c). Results for this analysis are also plotted in figure 4.5.8 and agreed extremely well with the refined finite element solution. Due to the structure of the computer program developed, that recomputes the matrices instead of storing them, this analysis proved to be rather time-consuming, since a large number of boundary elements and time steps is involved. Note, however, that this problem is a characteristic of the actual computer program and not of the time-marching scheme: it was estimated that storing all matrices in disc files would reduce the total CPU computer time to the same order of the one required by the BEM1B analysis, i.e. 3 min.

4.6 Axisymmetric Problems

Assuming that all boundary and internal values have axial symmetry, equation (4.1) can be written in cylindrical polar coordinates (R,θ,Z) as,

$$c(P)\ u(P,t_F) + k \int_{t_0}^{t_F} \int_{\bar{\Gamma}} u(S,t) \int_0^{2\pi} q^*(P,S,t_F,t)\ d\theta(S)\ R(S)\ d\bar{\Gamma}(S)\ dt$$

$$= k \int_{t_0}^{t_F} \int_{\bar{\Gamma}} q(S,t) \int_0^{2\pi} u^*(P,S,t_F,t)\ d\theta(S)\ R(S)\ d\bar{\Gamma}(S)\ dt$$

$$+ \int_{\bar{\Omega}} u_0(s,t_0) \int_0^{2\pi} u^*(P,s,t_F,t_0)\ d\theta(s)\ R(s)\ d\bar{\Omega}(s) \qquad (4.6.1)$$

where $\bar{\Omega}$ and $\bar{\Gamma}$ are the generating area and boundary contour of the solid of revolution, i.e. the projections of Ω and Γ, respectively, in the R^+-Z semi-plane (see figure 3.9.1).

Writing the three-dimensional fundamental solution (equation (2.8.3)) in cylindrical polar coordinates and integrating over a ring of radius R(S) at the plane Z=Z(S) we have,

$$\bar{u}^*(P,S,t_F,t) = \int_0^{2\pi} u^*(P,S,t_F,t)\, d\theta(S)$$

$$= \frac{1}{(4\pi k\tau)^{3/2}} \exp\left(-\frac{d}{4k\tau}\right) \int_0^{2\pi} \exp\left[\frac{R(P)\, R(S)\, \cos[\theta(P)-\theta(S)]}{2k\tau}\right] d\theta(S) \tag{4.6.2}$$

where $\tau=t_F-t$ and $d=R^2(P)+R^2(S)+[Z(P)-Z(S)]^2$.

The axisymmetric fundamental solution then becomes [86],

$$\bar{u}^*(P,S,t_F,t) = \frac{2\pi}{(4\pi k\tau)^{3/2}} \exp\left(-\frac{d}{4k\tau}\right) I_0\left(\frac{\ell}{2k\tau}\right) \tag{4.6.3}$$

where $\ell=R(P)\, R(S)$ and I_0 is the modified Bessel function of the first kind of order zero. The normal derivative of the fundamental solution along the boundary contour can be obtained by differentiating expression (4.6.3),

$$\bar{q}^*(P,S,t_F,t) = -\frac{1}{8\pi^{\frac{1}{2}}(k\tau)^{5/2}} \exp\left(-\frac{d}{4k\tau}\right)\left\{\left[R(S)\, I_0\left(\frac{\ell}{2k\tau}\right) - R(P)\, I_1\left(\frac{\ell}{2k\tau}\right)\right] R_{,n}(S) - [Z(P)-Z(S)]\, I_0\left(\frac{\ell}{2k\tau}\right) Z_{,n}(S)\right\} \tag{4.6.4}$$

where I_1 is the modified Bessel function of the first kind of order one.

From the above expressions, it can be seen that as $R(P)\to 0$ we have that $\ell\to 0$, $I_0(\ell/2k\tau)\to 1$, $I_1(\ell/2k\tau)\to 0$, so that the ring source tends to a point source with intensity 2π over the axis of revolution.

Substituting (4.6.3) and (4.6.4) into equation (4.6.1) yields the following time-dependent boundary integral equation,

$$c(P)\, u(P,t_F) + k \int_{t_0}^{t_F} \int_{\bar{\Gamma}} u(S,t)\, \bar{q}^*(P,S,t_F,t)\, R(S)\, d\bar{\Gamma}(S)\, dt$$

$$= k \int_{t_0}^{t_F} \int_{\bar{\Gamma}} q(S,t)\, \bar{u}^*(P,S,t_F,t)\, R(S)\, d\bar{\Gamma}(S)\, dt$$

$$+ \int_{\bar{\Omega}} u(s,t_0)\, \bar{u}^*(P,s,t_F,t_0)\, R(s)\, d\bar{\Omega}(s) \tag{4.6.5}$$

The solution of equation (4.6.5) can be attempted by using the same calculation procedures as discussed in the previous sections. For simplicity, only time-marching scheme BEM1A with stepwise constant variation for the functions u and q will be considered in what follows.

After discretising the surface and interior of the actual domain into boundary elements and cells, respectively, an equation similar to(4.1.6)is obtained, the coefficients of the matrices involved being computed as in (4.1.7). In order to perform the time integrals analytically, an appropriate change of variables is needed. Calling,

$$c = \frac{\ell}{d} \; ; \quad x = \frac{d}{4k\tau} \; ; \quad a = \frac{d}{4k\Delta t_F} \tag{4.6.6}$$

the integral in $\bar{u}^*$ becomes,

$$\int_{t_{F-1}}^{t_F} \bar{u}^*(i,S,t_F,t)\, dt = \frac{1}{2k(\pi d)^{\frac{1}{2}}} \int_a^{\infty} I_0(2cx)\, x^{-\frac{1}{2}}\, e^{-x}\, dx \tag{4.6.7}$$

The Bessel function I_0 can be expanded in series as [46],

$$I_0(2cx) = \sum_{n=0}^{\infty} \frac{(cx)^{2n}}{n!^2} \tag{4.6.8}$$

and the integration in (4.6.7) is then performed term-by-term, giving

$$\int_{t_{F-1}}^{t_F} \bar{u}^*(i,S,t_F,t)\, dt = \frac{1}{2k(\pi d)^{\frac{1}{2}}} \sum_{n=0}^{\infty} \frac{c^{2n}}{n!^2}\, \Gamma(2n + \tfrac{1}{2}, a) \tag{4.6.9}$$

For the integral in $\bar{q}^*$, we have

$$\int_{t_{F-1}}^{t_F} \bar{q}^*(i,S,t_F,t)\, dt = -\frac{1}{kd(\pi d)^{\frac{1}{2}}} \left\{ \left[R(S)\, R,_n(S) - \left[Z(P) - Z(S)\right] Z,_n(S) \right] \int_a^{\infty} I_0(2cx)\, x^{\frac{1}{2}}\, e^{-x}\, dx \right.$$
$$\left. - R(P)\, R,_n(S) \int_a^{\infty} I_1(2cx)\, x^{\frac{1}{2}}\, e^{-x}\, dx \right\} \tag{4.6.10}$$

Expanding the Bessel function I_1 as [46],

$$I_1(2cx) = \sum_{n=0}^{\infty} \frac{(cx)^{2n+1}}{n!^2(n+1)} \tag{4.6.11}$$

the integral becomes,

$$\int_{t_{F-1}}^{t_F} \bar{q}^*(i,S,t_F,t)\, dt = -\frac{1}{kd(\pi d)^{\frac{1}{2}}}\left\{\left[R(S)\, R_{,n}(S) - [Z(P) - Z(S)]\, Z_{,n}(S)\right] \sum_{n=0}^{\infty} \frac{c^{2n}}{n!^2}\, \Gamma(2n + \tfrac{3}{2}, a) - R(P)\, R_{,n}(S) \sum_{n=0}^{\infty} \frac{c^{2n+1}}{n!^2(n+1)}\, \Gamma(2n + \tfrac{5}{2}, a)\right\} \tag{4.6.12}$$

All the incomplete Gamma functions that appear in the above series can be evaluated in terms of $\Gamma(\frac{1}{2},a)$ by using the following recurrence relation [75],

$$\Gamma(n+1, a) = n\Gamma(n, a) + a^n e^{-a} \tag{4.6.13}$$

and, for computational purposes, $\Gamma(\frac{1}{2},a)$ can be related to the error function by [46], [75],

$$\Gamma(\tfrac{1}{2},a) = \pi^{\frac{1}{2}}\, \mathrm{erfc}(a^{\frac{1}{2}}) \tag{4.6.14}$$

being the complementary error function computed through a rational approximation [46] which is given in appendix A.

From definition (4.6.6) we notice that the value of c varies between 0 (for R(P) or R(S)=0 or for $d\to\infty$) and 0.5 (for P=S). All the series that appear in expressions (4.6.9) and (4.6.12) converge very quickly for small values of c but slowly as $c\to 0.5$. In fact, they do not converge for c=0.5 due to the singularity at P=S. So, from the computational point of view, it is not convenient to use expansions (4.6.8) and (4.6.11) for values of c in the vicinity of c=0.5.

To overcome this problem, we can use asymptotic expansions of the Bessel functions that are valid for large values of their arguments. Thus, whenever x is large we can write [46],

$$I_0(2cx) = \frac{e^{2cx}}{2(\pi cx)^{\frac{1}{2}}}\left[1 + \sum_{n=1}^{\infty} \frac{f_1(n)}{n!(16cx)^n}\right] \tag{4.6.15}$$

$$I_1(2cx) = \frac{e^{2cx}}{2(\pi cx)^{\frac{1}{2}}}\left[1 + \sum_{n=1}^{\infty} \frac{f_2(n)}{n!(16cx)^n}\right] \tag{4.6.16}$$

$$f_1(n) = (2n-1)^2\,(2n-3)^2 \ldots 1 \tag{4.6.17}$$

$$f_2(n) = (-1)^n\,[4-(2n-1)^2]\;\;[4-(2n-3)^2]\;\ldots[4-1]$$

The time integrals can then be carried out as follows,

$$\int_{t_{F-1}}^{t_F} \bar{u}^*(i,S,t_F,t)\,dt = \frac{1}{4\pi k\ell^{\frac{1}{2}}}\left[E_1(B) + \sum_{n=1}^{\infty} \frac{f_1(n)b^n}{n!(16c)^n}\,\Gamma(-n,B)\right] \tag{4.6.18}$$

$$\int_{t_{F-1}}^{t_F} \bar{q}^*(i,S,t_F,t)\,dt = -\frac{1}{2\pi kd\ell^{\frac{1}{2}}}\left\{-\frac{1}{b}\,e^{-B}\right.$$

$$\times\left[[R(P)-R(S)]R_{,n}(S) + [Z(P)-Z(S)]\,Z_{,n}(S)\right]$$

$$+\left[R(S)\,R_{,n}(S) - [Z(P)-Z(S)]\,Z_{,n}(S)\right]\sum_{n=1}^{\infty}\frac{f_1(n)b^{n-1}}{n!(16c)^n}\,\Gamma(1-n,B)$$

$$\left. - R(P)\,R_{,n}(S)\sum_{n=1}^{\infty}\frac{f_2(n)b^{n-1}}{n!(16c)^n}\,\Gamma(1-n,B)\right\} \tag{4.6.19}$$

where b=1-2c and B=ab. The incomplete Gamma functions can now be computed from $\Gamma(0,B)$ through the recurrence relation [46],

$$\Gamma(-n,B) = -\frac{1}{n}\left[\Gamma(1-n,B) - \frac{e^{-B}}{B^n}\right] \tag{4.6.20}$$

$$\Gamma(0,B) = E_1(B)$$

When the value of c tends to 0.5 but x is small over part of the integration interval (a,∞) we cannot apply expansions (4.6.15) and (4.6.16) directly. Alternatively, equation (4.6.7) may be written as,

$$\int_{t_{F-1}}^{t_F} \bar{u}^*(i,S,t_F,t)\,dt = \frac{1}{2k(\pi d)^{\frac{1}{2}}} \left[\int_a^{a'} I_0(2cx)\, x^{-\frac{1}{2}}\, e^{-x}\, dx + \int_{a'}^{\infty} I_0(2cx)\, x^{-\frac{1}{2}}\, e^{-x}\, dx \right] \qquad (4.6.21)$$

where x is sufficiently large in the interval (a',∞). Thus

$$\int_a^{a'} I_0(2cx)\, x^{-\frac{1}{2}}\, e^{-x}\, dx = \sum_{n=0}^{\infty} \frac{c^{2n}}{n!^2} \left[\Gamma(2n+\tfrac{1}{2},a') - \Gamma(2n+\tfrac{1}{2},a) \right] \qquad (4.6.22)$$

and expansion (4.6 15) is now used to evaluate the second integral in (4.6.21). The same idea can be applied on calculating the time integral in $\bar{q}^*$.

The remaining step in the numerical solution of the boundary integral equation (4.6.5) is the computation of the space integrals. As for the two-dimensional case, the program developed employs only linear boundary elements with triangular cells. The terms H_{ij} and $G_{ij}(i\neq j)$ of the final system of equations (similar to (4.1.6)) can be calculated using a six-points Gauss quadrature rule (see section 4.1.4). The diagonal terms H_{ii} and G_{ii} however, need to be investigated more carefully since their calculation involves the evaluation of singular integrals.

The coefficients G_{ii} contain an integral with a logarithmic (integrable) singularity. Expanding the exponential-integral in equation (4.6.18), we can isolate the logarithmic term and integrate it analytically (see appendix C). All the remainder is non-singular and can be computed by using a standard Gaussian quadrature.

The coefficients $\hat{H}_{ii}$ contain a logarithmic plus a 1/b singularity. The first one is directly integrable but the second is only integrable in the Cauchy principal value sense. For the present case (linear elements) however, we can write with reference to figure 4.6.1,

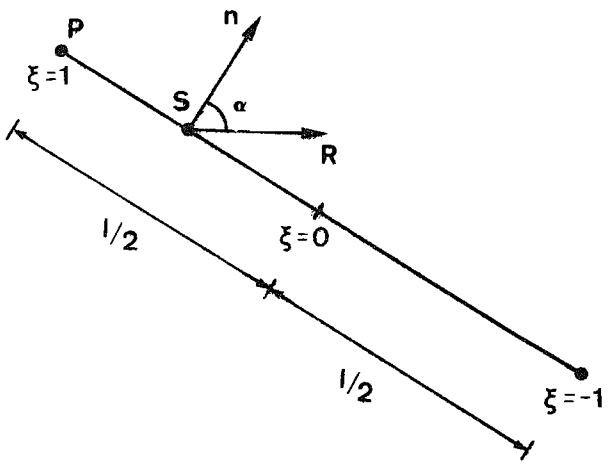

Figure 4.6.1 - Definitions for linear element

$$R,_n(S) = \cos\alpha \quad ; \quad Z,_n(S) = \sin\alpha$$
$$R(P) - R(S) = -\xi\frac{\ell}{2}\sin\alpha \qquad (4.6.23)$$
$$Z(P) - Z(S) = \xi\frac{\ell}{2}\cos\alpha$$

such that the first term in the right-hand side of (4.6.19), which is the Cauchy singular one, becomes identically zero. Expanding the first term of each series in (4.6.19) in order to isolate the logarithmic singularity, we can then evaluate it analytically (see appendix C) and all the remainder, which is non-singular, using a standard Gaussian quadrature.

The free coefficients c_i account for the jump that the integral in q^* experiences as it approaches the boundary Γ from the internal domain Ω. Their values are the same if the limit is taken for the steady-state or the time-integrated transient fundamental solutions, as shown in equations (2.4.8) and (4.1.47) for two-dimensional problems, a result to be expected following the discussion in section 2.8 (see equation (2.8.7)). For three-dimensional problems, we have

$$c_i = 1 - \frac{1}{4\pi}\lim_{\varepsilon\to 0}\int_{\Gamma_\varepsilon}\frac{1}{\varepsilon^2}\,d\Gamma = \frac{\beta}{4\pi} \qquad (4.6.24)$$

where β is the solid angle of the boundary at i and $d\Gamma = \varepsilon^2 \; d\phi \; d\Phi$. For the actual (axisymmetric) case, $\beta = 2(\pi + \alpha_1 - \alpha_2)$ (see figure 2.4.1) and the values of c_i become the same as for two-dimensional problems, equation (4.1.47).

A computer program using time-marching scheme BEM1A with stepwise constant variations for functions u and q and incorporating the numerical procedures derived in this section was developed. Its structure follows the ideas discussed in section 4.2 and again Hammer's quintic quadrature rule was employed for the domain integral. The program is described in detail in chapter 6.

Example 4.6.1

The first example analysed was that of a solid cylinder with unit initial conditions, subjected to the following boundary conditions,

$u = 0$ at $R = a$

$q = 2u$ at $Z = \pm \ell$

The discretisation adopted is shown in figure 4.6.3. Note that due to the symmetry with respect to the R-axis, only one half of the cross-section needed to be discretised. The numerical values assumed for the cross-section were a=1, ℓ=1 and for simplicity, the material coefficient k was also taken to be unity.

Results are compared in figures 4.6.2 and 4.6.3 with an available analytical solution [16], showing good agreement. The analysis was performed with a time step Δt=0.025 and took about 4s of CPU time to converge to a steady-state (20 time intervals).

Example 4.6.2

This example studies the heat conduction problem of a prolate spheroid initially at zero temperature and subjected to a unit surface temperature at t=0. A parametric representation of points

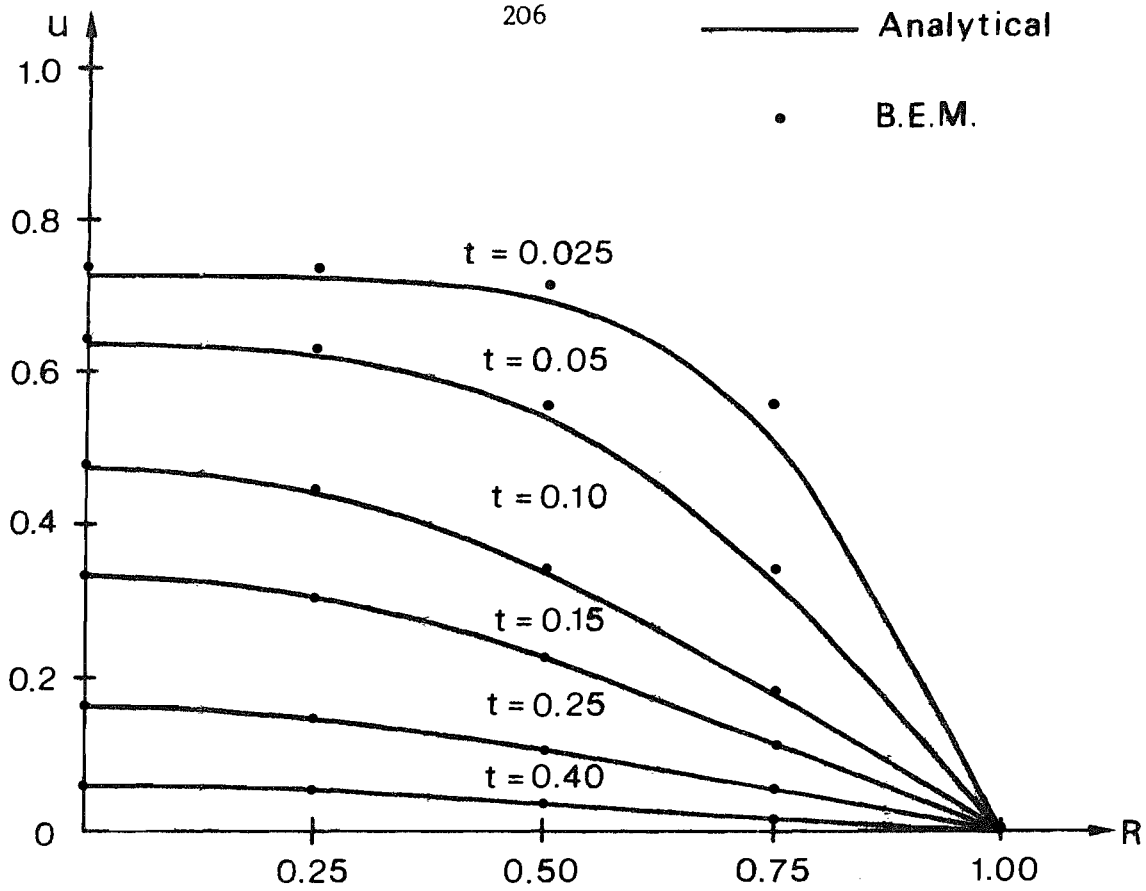

Figure 4.6.2 - Values of u along the faces Z=±ℓ

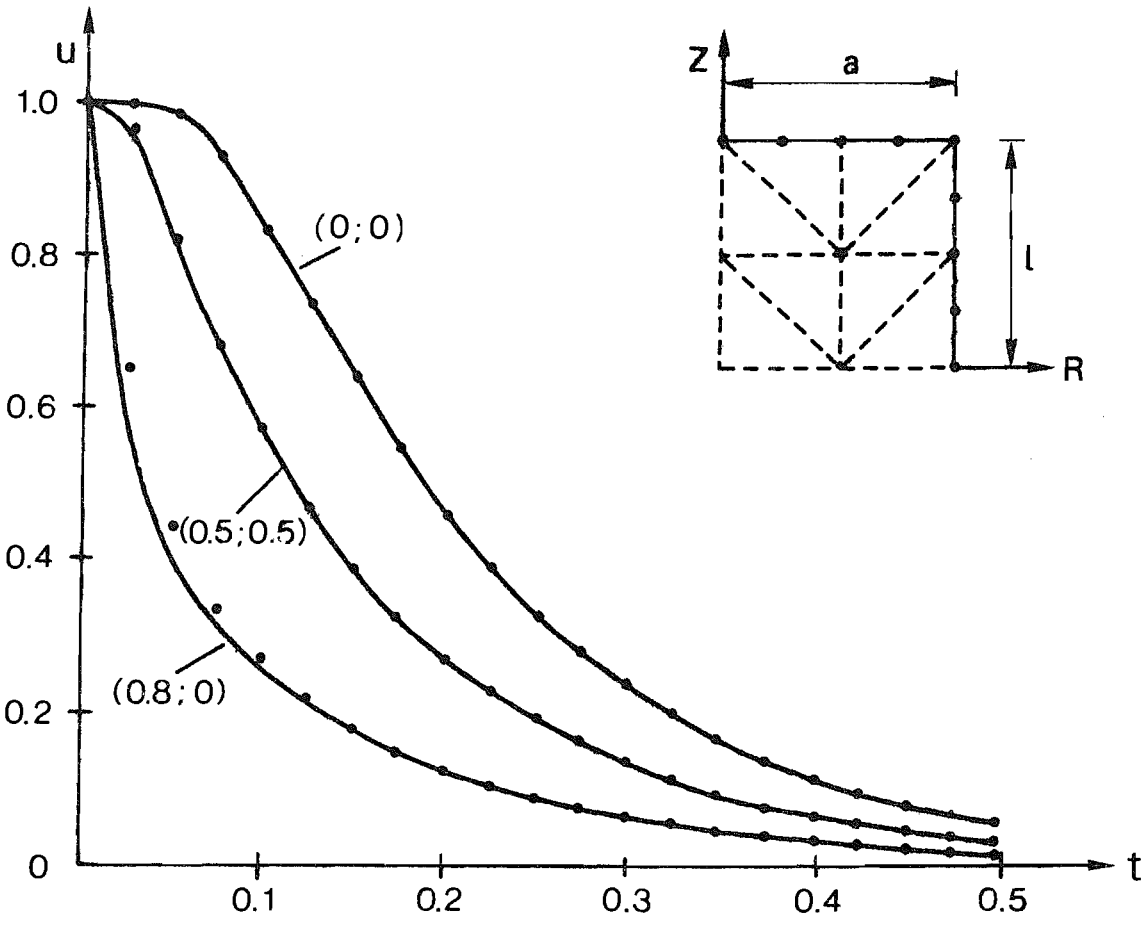

Figure 4.6.3 - Values of u at internal points

on its surface, in the R-Z plane, may be written as

$$R = L_1 \cos \phi$$

$$Z = L_2 \sin \phi$$

where the ϕ angle is indicated in figure 4.6.4.

The discretisation adopted is also shown in the figure and the numerical values assumed for this analysis were k=1, L_1=1, L_2=2. Results for the temperature at the centre point (R=Z=0) are compared in figure 4.6.4 with an analytical solution [87] and a finite element solution [84] obtained with parabolic three-dimensional isoparametric elements. The finite element analysis was performed with a time step value Δt=0.025 whereas the boundary element solution employed a Δt=0.050. The total CPU time for 20 time steps was 4.5 s.

Example 4.6.3

A problem similar to the one studied in example 4.4.4 was considered in this example of a sphere of unit radius, initially at zero temperature, subjected to sudden thermal shocks applied at times t_0=0 and t_1. The discretisation and numerical values adopted here were the same as for example 4.4.4 (see figure 4.4.4).

Results are plotted in figures 4.6.5 to 4.6.7 for different values of t_1 and compared with analytical solutions [16]. The agreement between the two solutions is of the same order as for the two-dimensional cases, and uniform for all values of t_1. It is interesting to note that the CPU time required for each analysis was about 4 s compared with 2 s for example 4.4.4.

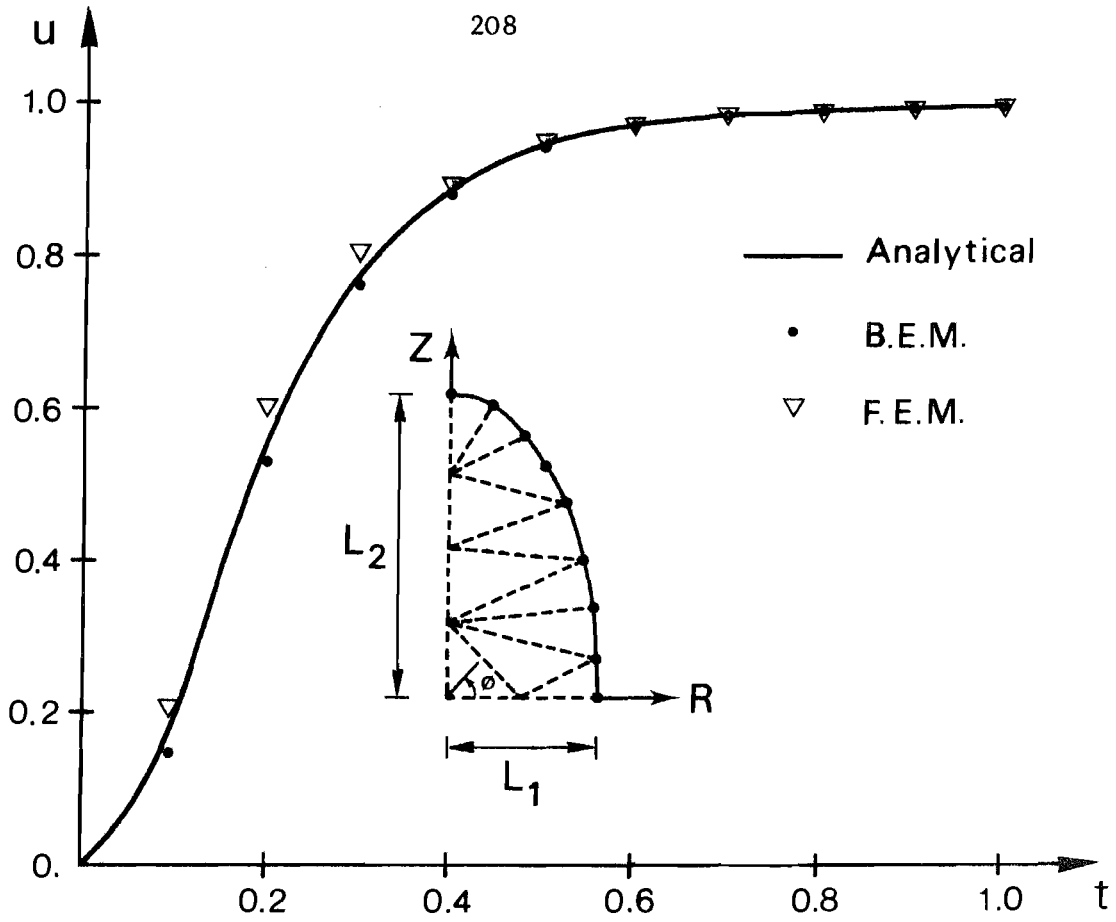

Figure 4.6.4 - Temperature at centre of prolate spheroid

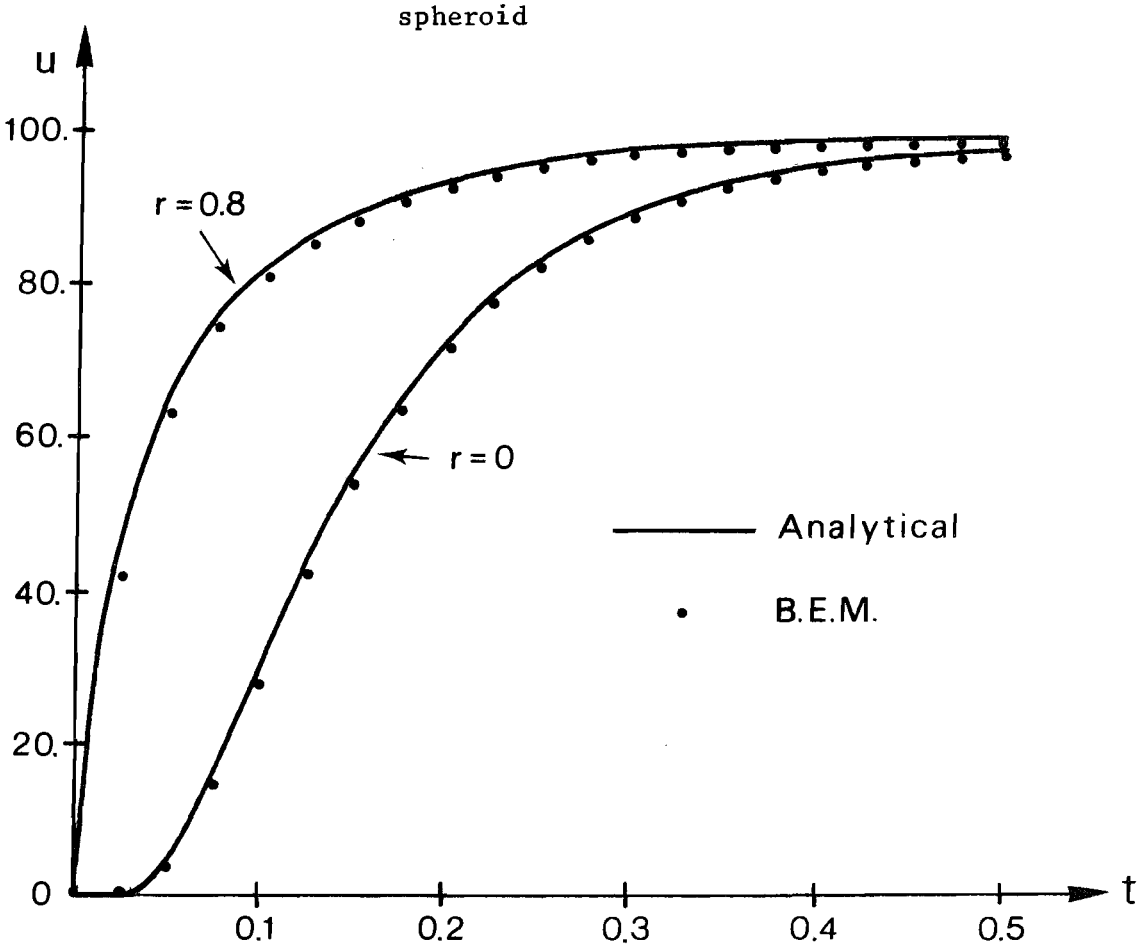

Figure 4.6.5 - Temperature at internal points for thermal shock applied at $t_0=t_1=0$.

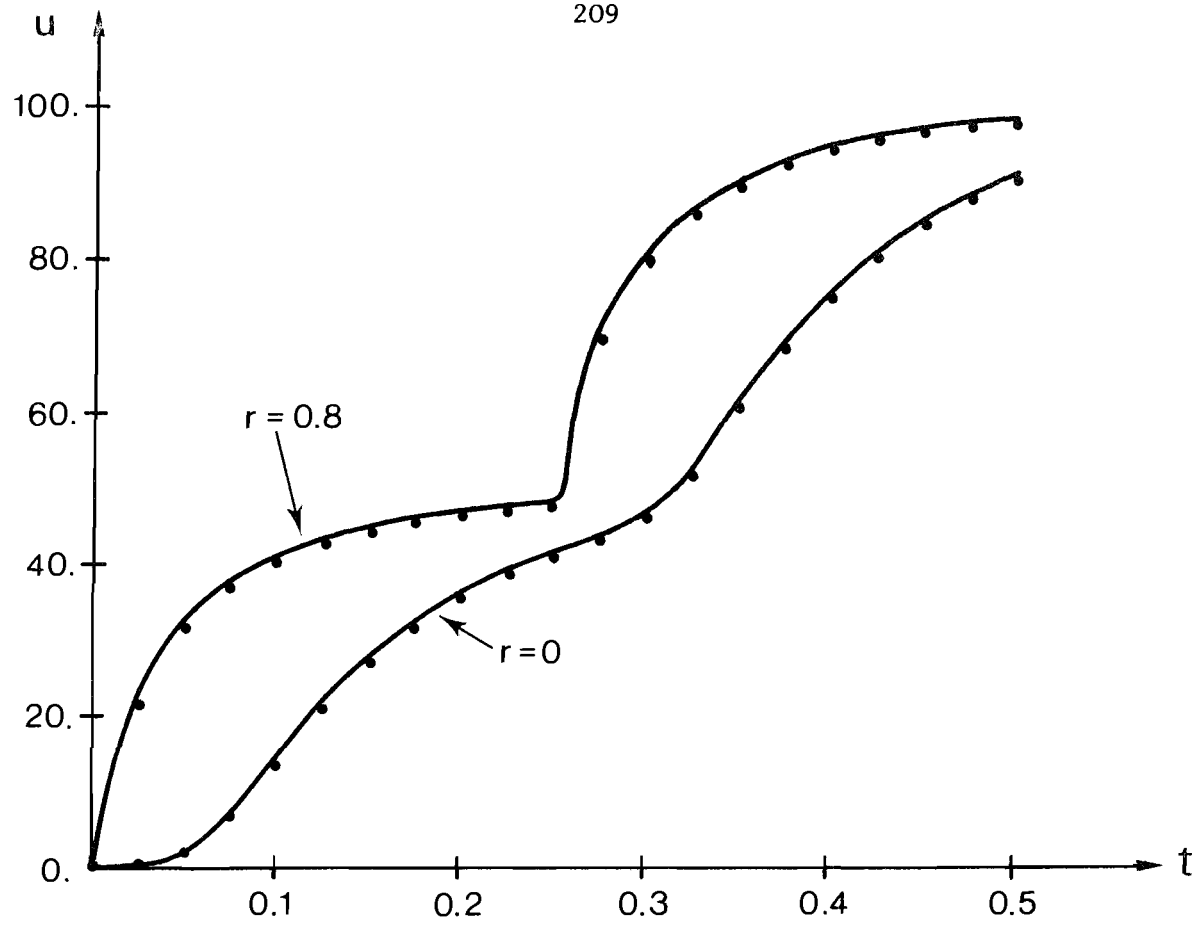

Figure 4.6.6 - Temperature at internal points for thermal shocks applied at t_0=0. and t_1=0.25

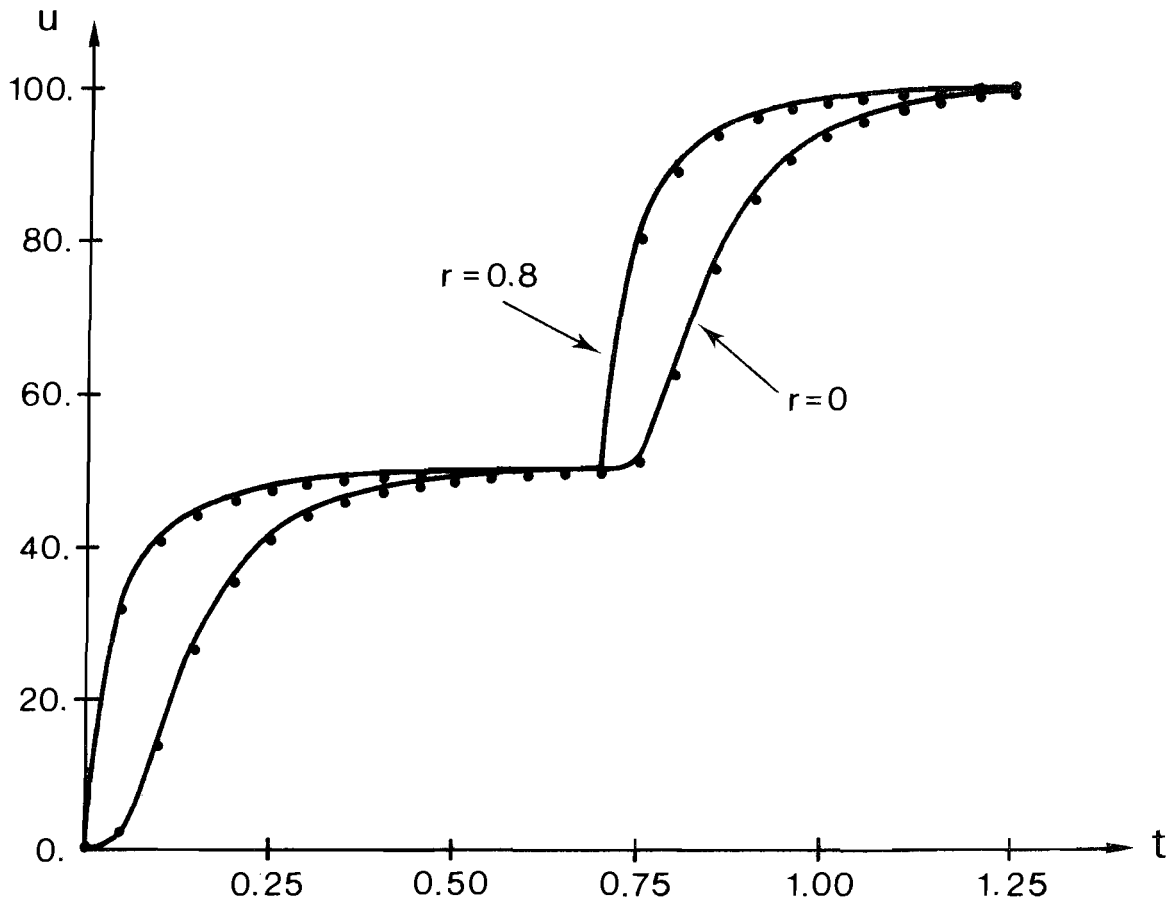

Figure 4.6.7 - Temperature at internal points for thermal shocks applied at t_0=0. and t_1=0.7

5. VISCOUS FLOW PROBLEMS

This chapter considers problems of incompressible viscous fluid motion, governed by the Navier-Stokes equations together with the continuity equation. Following the concepts developed by Lighthill [31], the vorticity-velocity formulation is employed and the flow problem is partitioned into its kinetic aspect, expressed as a transport equation describing the rate of change of vorticity through convection and diffusion, and its kinematic part, which determines the velocity distribution at any instant of time from the (known) vorticity distribution at that instant ([32] to [35]).

The prevailing Finite Difference and Finite Element methods of solution treat the above equations in differential form. The major difficulty experienced by these methods is associated with the fact that implicit numerical procedures are necessary for the kinematic part of the computation. As a consequence, the solution field must comprise the entire flowfield, inclusive of the viscous and the inviscid regions. Furthermore, for problems of external flow past finite bodies, satisfaction of boundary conditions prescribed at infinity implies the truncation of the infinite region at a finite distance.

Earlier works ([32] to [35]) employing Lighthill's formulation recast the kinematic part of the problem into an integral equation for the velocity in terms of the vorticity. The main advantage of doing so is that it permits the explicit, point-by-point, computation of the velocity, in much the same way as the potential in Laplace's equation is computed through (2.4.5). Since only the vorticity distribution in the viscous region contributes to the calculation of the velocity anywhere in the flow, the solution field can be confined to the viscous region of the flow. Moreover, the imposed boundary conditions at infinity are implicitly contained in this integral equation, therefore there is no need of specifying them at a (truncated) finite

distance from the body. The kinetic part of the problem,however, was kept in the differential form.

In the next section, we review the vorticity-velocity formulation of the Navier-Stokes equations, showing how the problem can be partitioned into its kinetic and kinematic aspects, and how the kinematic part can be recast into a convenient integral equation.

Then, steady-state problems are discussed and the kinetic part of the problem also transformed into an integral equation. An iterative scheme for the solution of the resulting set of (non-linear) equations is discussed, following basically the numerical procedures derived in chapter 3.

Finally, transient problems are considered and, again, it is shown how the kinetic part of the problem can be recast into an integral equation. Since the vorticity transport equation can be interpreted as a non-homogeneous diffusion equation with a (non-linear) convective term, the numerical procedures derived in chapter 4 are directly applicable to this case.

5.1 Navier-Stokes Equations

Three-dimensional problems of incompressible viscous fluid motion are governed by the following set of partial differential equations [66],

$$\frac{\partial \underset{\sim}{\omega}}{\partial t} = \underset{\sim}{\nabla} \times (\underset{\sim}{v} \times \underset{\sim}{\omega}) + \nu \nabla^2 \underset{\sim}{\omega} \qquad (5.1.1)$$

$$\underset{\sim}{\nabla} \cdot \underset{\sim}{v} = 0 \qquad (5.1.2)$$

$$\underset{\sim}{\nabla} \times \underset{\sim}{v} = \underset{\sim}{\omega} \qquad (5.1.3)$$

where $\underset{\sim}{v}$ and $\underset{\sim}{\omega}$ are the velocity and vorticity vectors, respectively, and ν is the kinematic viscosity of the fluid. In the above equations, "$\nabla \times$" means curl, "$\nabla \cdot$" stands for divergence and the gradient vector $\underset{\sim}{\nabla}$ is defined as,

$$\underset{\sim}{\nabla} = \left\{ \frac{\partial}{\partial x_1} \quad \frac{\partial}{\partial x_2} \quad \frac{\partial}{\partial x_3} \right\} \tag{5.1.4}$$

Equation (5.1.1) can be readily recognised as the vorticity transport equation, describing the rate of change of the vorticity field through convection (as stated by the first term in the right-hand side) and diffusion (second term in the right-hand side). Equations (5.1.2) and (5.1.3) are the continuity equation and the definition of vorticity, respectively.

The kinematic relation between $\underset{\sim}{v}$ and $\underset{\sim}{\omega}$ is described by equations (5.1.2) and (5.1.3). For a given distribution of $\underset{\sim}{\omega}$, the velocity distribution throughout the flowfield is usually evaluated by using a vector Poisson's equation obtained by taking the curl of (5.1.3), accounting for (5.1.2),

$$\nabla^2 \underset{\sim}{v} = -\underset{\sim}{\nabla} \times \underset{\sim}{\omega} \tag{5.1.5}$$

Comparing this equation with equation (3.3.1) in chapter 3 and reminding the derivation of equation (2.4.5) in chapter 2, we can write the following integral equation as equivalent to (5.1.5),

$$4\pi \underset{\sim}{v}(p) + \int_\Gamma \underset{\sim}{v}(S) \frac{\partial u^*(p,S)}{\partial \underset{\sim}{n}(S)} \, d\Gamma(S)$$

$$= \int_\Gamma \frac{\partial \underset{\sim}{v}(S)}{\partial \underset{\sim}{n}(S)} u^*(p,S) \, d\Gamma(S) + \int_\Omega \left[\underset{\sim}{\nabla} \times \underset{\sim}{\omega}(s)\right] u^*(p,s) \, d\Omega(s) \tag{5.1.6}$$

where $u^*(p,s)$ is the fundamental solution to Laplace's equation defined in section 2.2 and $\underset{\sim}{n}(S)$ is the unit normal vector.

The correct boundary conditions for the physical problem are prescribed velocities. Therefore, prior to calculate the values of $\underset{\sim}{v}$ throughout the flowfield (for a known vorticity distribution), it is necessary to take the above equation to the boundary (employing the same limiting process as described in chapter 2), thus yielding a boundary integral equation whose solution produces the values of

$\partial \underset{\sim}{v}/\partial n$ along Γ. These values are then placed in equation (5.1.6) to allow the prediction of the velocity distribution in Ω.

Wu and Thompson [33] contested the validity of the use of equation (5.1.5) to represent the kinematics of the flow. They pointed out that the solution of equations (5.1.2) and (5.1.3) for $\underset{\sim}{v}$ is unique if either v_t (the tangential component of $\underset{\sim}{v}$) or v_n (its normal component) is prescribed over the boundary Γ, but the solution of (5.1.5) for $\underset{\sim}{v}$ is unique only if both v_t and v_n are prescribed over Γ. Thus, while solutions of (5.1.2) and (5.1.3) with prescribed v_t or v_n also satisfy (5.1.5) the converse is not necessarily true, i.e. solutions of (5.1.5) for prescribed v_t and v_n may not satisfy (5.1.2) and (5.1.3).

A more convenient integral representation for the kinematic part of the flow was then derived by Wu and Thompson [33] directly from equations (5.1.2) and (5.1.3). It follows from an application of Green's theorem for vectors, which can be written as [15],

$$\int_\Omega (\underset{\sim}{E} \cdot \nabla^2 \underset{\sim}{F} - \underset{\sim}{F} \cdot \nabla^2 \underset{\sim}{E})\, d\Omega = \int_\Gamma [\underset{\sim}{E} \times (\nabla \times \underset{\sim}{F}) + \underset{\sim}{E}(\nabla \cdot \underset{\sim}{F}) - \underset{\sim}{F} \times (\nabla \times \underset{\sim}{E}) - \underset{\sim}{F}(\nabla \cdot \underset{\sim}{E})] \cdot \underset{\sim}{n}\, d\Gamma \qquad (5.1.7)$$

where

$$\nabla^2 \underset{\sim}{F} = \nabla(\nabla \cdot \underset{\sim}{F}) - \nabla \times \nabla \times \underset{\sim}{F} \qquad (5.1.8)$$

being equation (5.1.7) the vector analogue to equation (2.3.4).

Let $\underset{\sim}{v}^*(p,s)$ be a vector fundamental solution to the vector Laplace's equation $\nabla^2 \underset{\sim}{F} = \underset{\sim}{0}$, given by

$$\underset{\sim}{v}^*(p,s) = \nabla [u^*(p,s)] \times \underset{\sim}{a} \qquad (5.1.9)$$

where $\underset{\sim}{a}$ is a constant unit vector. By direct substitution, it can be seen that

$$\nabla \cdot \underset{\sim}{v}^* = 0 \qquad (5.1.10)$$

$$\nabla \times \underset{\sim}{v}^* = \nabla (\underset{\sim}{a} \cdot \nabla \underset{\sim}{u}^*) \qquad \text{,for } p \neq s \tag{5.1.11}$$

By virtue of equation (5.1.2), there exists a vector potential $\underset{\sim}{\Psi}$ such that [66]

$$\nabla \times \underset{\sim}{\Psi} = \underset{\sim}{v} \tag{5.1.12}$$

$$\nabla \cdot \underset{\sim}{\Psi} = 0 \tag{5.1.13}$$

Thus, considering $\underset{\sim}{F}$ in equation (5.1.7) to be the fundamental solution $\underset{\sim}{v}^*$ and $\underset{\sim}{E}$ to be the vector potential $\underset{\sim}{\Psi}$, accounting for equations (5.1.3) and (5.1.9) to (5.1.13) and assuming, as in section 2.1, that a small sphere of radius ε surrounding the point p, with surface Γ_ε, is excluded from the domain Ω of integration, equation (5.1.7) becomes,

$$\int_\Omega (\nabla \underset{\sim}{u}^* \times \underset{\sim}{a}) \cdot \underset{\sim}{\omega} \, d\Omega = \int_{\Gamma+\Gamma_\varepsilon} \underset{\sim}{\Psi} \times \nabla (\underset{\sim}{a} \cdot \nabla \underset{\sim}{u}^*) \cdot \underset{\sim}{n} \, d\Gamma$$

$$- \int_{\Gamma+\Gamma_\varepsilon} (\nabla \underset{\sim}{u}^* \times \underset{\sim}{a}) \times \underset{\sim}{v} \cdot \underset{\sim}{n} \, d\Gamma \tag{5.1.14}$$

The above equation may be rewritten as

$$\int_\Omega \underset{\sim}{a} \cdot (\underset{\sim}{\omega} \times \nabla \underset{\sim}{u}^*) \, d\Omega = \int_{\Gamma+\Gamma_\varepsilon} (\underset{\sim}{a} \cdot \nabla \underset{\sim}{u}^*)(\underset{\sim}{v} \cdot \underset{\sim}{n}) \, d\Gamma$$

$$- \int_{\Gamma+\Gamma_\varepsilon} \underset{\sim}{a} \cdot [(\underset{\sim}{v} \times \underset{\sim}{n}) \times \nabla \underset{\sim}{u}^*] \, d\Gamma \tag{5.1.15}$$

Taking the limit as $\varepsilon \to 0$, the volume Ω in the integral in the left-hand side of (5.1.15) becomes the entire volume bounded by Γ, since the volume integral over the interior of Γ_ε goes to zero as $\varepsilon \to 0$. The integrals over Γ_ε in the right-hand side of equation (5.1.15) give,

$$\lim_{\varepsilon \to 0} \left\{ \int_{\Gamma_\varepsilon} (\underset{\sim}{a} \cdot \nabla \underset{\sim}{u}^*)(\underset{\sim}{v} \cdot \underset{\sim}{n}) \, d\Gamma - \int_{\Gamma_\varepsilon} \underset{\sim}{a} \cdot [(\underset{\sim}{v} \times \underset{\sim}{n}) \times \nabla \underset{\sim}{u}^*] \, d\Gamma \right\}$$

$$= \lim_{\varepsilon \to 0} \left\{ \frac{1}{\varepsilon^2} \int_{\Gamma_\varepsilon} \left[(\underset{\sim}{a} \cdot \underset{\sim}{n})(\underset{\sim}{v} \cdot \underset{\sim}{n}) - \underset{\sim}{a} \cdot [(\underset{\sim}{v} \times \underset{\sim}{n}) \times \underset{\sim}{n}] \right] d\Gamma \right\}$$

$$= 4\pi \underset{\sim}{a} \cdot \underset{\sim}{v}(p) \tag{5.1.16}$$

Inserting the above result into equation (5.1.15) and noting that the direction of the vector $\underset{\sim}{a}$ is arbitrary, we obtain the following equation

$$4\pi \underset{\sim}{v}(p) + \int_\Gamma (\underset{\sim}{v} \cdot \underset{\sim}{n})\, \nabla u^* \, d\Gamma = \int_\Gamma (\underset{\sim}{v} \times \underset{\sim}{n}) \times \nabla u^* \, d\Gamma$$

$$+ \int_\Omega \underset{\sim}{\omega} \times \nabla u^* \, d\Omega \qquad (5.1.17)$$

A similar expression for two-dimensional flow problems can be obtained by taking $u^*(p,s)$ to be the two-dimensional fundamental solution defined in section 2.2, for which case the result of the limit (5.1.16) is $(2\pi \underset{\sim}{a} \cdot \underset{\sim}{v}(p))$. Thus, the general expression for the velocity $\underset{\sim}{v}$ is of the form [33],

$$\underset{\sim}{v}(p) = \frac{1}{2\alpha\pi} \left\{ \int_\Omega \frac{\underset{\sim}{\omega}(s) \times \underset{\sim}{r}(p,s)}{r^d(p,s)} \, d\Omega(s) \right.$$

$$\left. + \int_\Gamma \frac{[\underset{\sim}{v}(S) \times \underset{\sim}{n}(S)] \times \underset{\sim}{r}(p,S)}{r^d(p,S)} \, d\Gamma(S) - \int_\Gamma \frac{[\underset{\sim}{v}(S) \cdot \underset{\sim}{n}(S)]\, \underset{\sim}{r}(p,S)}{r^d(p,S)} \, d\Gamma(S) \right\} \qquad (5.1.18)$$

where $\alpha = 2$, $d = 3$ and

$$\underset{\sim}{r}(p,s) = \left\{ X_1(p) - X_1(s) \quad X_2(p) - X_2(s) \quad X_3(p) - X_3(s) \right\}$$

for three-dimensional problems, $\alpha = 1$, $d = 2$ and

$$\underset{\sim}{r}(p,s) = \left\{ X_1(p) - X_1(s) \quad X_2(p) - X_2(s) \right\}$$

for two-dimensional problems.

Note that the use of equation (5.1.18) for the evaluation of $\underset{\sim}{v}$ throughout the flowfield requires the knowledge of both v_t and v_n over Γ. Provided that these values are compatible with each other, i.e. one of them is identical to the value obtained from the solution of (5.1.2) and (5.1.3) using the other as the prescribed boundary condition, the specification of both in (5.1.18) is admissible, and

does not overspecify the problem.

For problems of external flow past finite bodies, we can consider the region Ω in equation (5.1.18) to be the entire (infinite) region occupied by the fluid. Then, following section 3.6, the boundary Γ is divided into two parts: the fluid-solid interface on which the no-slip condition ($\underset{\sim}{v} = \underset{\sim}{0}$) applies and a surface infinitely remote from (and enclosing) the body on which the freestream velocity boundary condition ($\underset{\sim}{v} = \underset{\sim}{v}_\infty$) applies. The surface integrals in (5.1.18) can then be evaluated, giving

$$\underset{\sim}{v}(p) = \frac{1}{2\alpha\pi} \int_\Omega \frac{\underset{\sim}{\omega}(s) \times \underset{\sim}{r}(p,s)}{r^d(p,s)} \, d\Omega(s) + \underset{\sim}{v}_\infty \qquad (5.1.19)$$

The above equation can be recognised as the Biot-Savart law of induced velocities [36], [66]. Thus we can consider the integral equation (5.1.18) to be an extension of the Biot-Savart law to a region bounded by Γ.

With prescribed values of $\underset{\sim}{v}$ in Γ and known values of $\underset{\sim}{\omega}$ in Ω, equation (5.1.18) permits the explicit, point-by-point, computation of the velocity anywhere in the flowfield. Since only the vorticity distribution in the viscous region of the flow contributes to the calculation of the velocity, as the integrand in the domain integral vanishes for $\underset{\sim}{\omega} = \underset{\sim}{0}$, the solution field can be confined to the viscous region of the flow. Furthermore, the prescribed boundary conditions at infinity are now implicitly contained in equation (5.1.18), as can be seen in (5.1.19).

5.2 Steady Problems

Before proceeding to the solution of the transient Navier-Stokes equations as depicted in (5.1.1), it is convenient to discuss the numerical procedures related to the solution of steady incompressible viscous flow problems. Although many numerical studies of steady flow problems employ the time-dependent equations to obtain the desired

steady-state asymptotically, this approach introduces an additional dependent variable (the time) into the solution procedure and consequently additional numerical complexities.

As discussed earlier, the kinematic aspect of the flow is described by equation (5.1.18). The kinetic aspect of the flow is represented by the Navier-Stokes equations which, for a steady motion, can be written in the form [66],

$$\nabla \times \omega = \frac{1}{\nu} (v \times \omega - \nabla h) \tag{5.2.1}$$

where h is the total head defined by,

$$h = \frac{p}{\rho} + \frac{v^2}{2} \tag{5.2.2}$$

being p the pressure, ρ the density of the fluid and $v^2 = v \cdot v$.

From the definition of vorticity (equation (5.1.3)), it is clear that

$$\nabla \cdot \omega = 0 \tag{5.2.3}$$

Thus, the differential equations (5.2.1) and (5.2.3) for the vorticity are analogous to the set of equations (5.1.2) and (5.1.3) for the velocity. Therefore, an integral equation for the kinetic part of the flow can be obtained by simply replacing v by ω and ω by the term $(v \times \omega - \nabla h)/\nu$ in equation (5.1.18). This gives,

$$\omega(p) = \frac{1}{2\alpha\pi} \left\{ \frac{1}{\nu} \int_\Omega \frac{[v(s) \times \omega(s) - \nabla h(s)] \times r(p,s)}{r^d(p,s)} \, d\Omega(s) \right.$$

$$\left. + \int_\Gamma \frac{[\omega(S) \times n(S)] \times r(p,S)}{r^d(p,S)} \, d\Gamma(S) - \int_\Gamma \frac{[\omega(S) \cdot n(S)] \, r(p,S)}{r^d(p,S)} \, d\Gamma(S) \right\} \tag{5.2.4}$$

By applying the divergence theorem [13] to the term in h,

$$\int_\Omega \frac{\nabla h(s) \times r(p,s)}{r^d(p,s)} \, d\Omega(s) = \int_\Gamma \frac{[h(S) \, n(S)] \times r(p,S)}{r^d(p,S)} \, d\Gamma(S) \tag{5.2.5}$$

equation (5.2.4) can be rewritten as,

$$\underset{\sim}{\omega}(p) = \frac{1}{2\alpha\pi}\left\{\frac{1}{\nu}\int_{\Omega}\frac{[\underset{\sim}{v}(s)\times\underset{\sim}{\omega}(s)]\times\underset{\sim}{r}(p,s)}{r^{d}(p,s)}\,d\Omega(s)\right.$$

$$+\int_{\Gamma}\frac{[\underset{\sim}{\omega}(S)\times\underset{\sim}{n}(S)]\times\underset{\sim}{r}(p,S)-[\underset{\sim}{\omega}(S)\cdot\underset{\sim}{n}(S)]\,\underset{\sim}{r}(p,S)}{r^{d}(p,S)}\,d\Gamma(S)$$

$$\left.-\frac{1}{\nu}\int_{\Gamma}\frac{[h(S)\underset{\sim}{n}(S)]\times\underset{\sim}{r}(p,S)}{r^{d}(p,S)}\,d\Gamma(S)\right\} \qquad (5.2.6)$$

The calculation of $\underset{\sim}{\omega}$ throughout the flowfield can be carried out iteratively using the above equation, for known values of $\underset{\sim}{v}$ in Ω and $\underset{\sim}{\omega}$ and h in Γ. The contribution of the inviscid part of the flow to the computation of $\underset{\sim}{\omega}$ anywhere in the flow is zero (as it was in the calculation of $\underset{\sim}{v}$). Thus, only the values of $\underset{\sim}{v}$ in Γ (which are the prescribed boundary conditions) and in the viscous region of the flow are needed in the calculation of $\underset{\sim}{\omega}$.

We can now devise a numerical formulation for the solution of steady incompressible viscous flow problems using equations (5.1.18) and (5.2.6), employing basically the same procedures as derived in chapter 3. For simplicity, only the two-dimensional case is considered, being extension to three-dimensional and axisymmetric problems carried out by using the concepts outlined in sections 3.8 and 3.9, respectively. The present formulation is based on the one discussed in [93].

For the present case, the flow motion is described by the following set of scalar equations, obtained by specialising equations (5.1.18) and (5.2.6) for two-dimensions,

$$v_1(p) = -\frac{1}{2\pi}\left\{\int_{\Omega}\frac{\omega(s)\,Y_2(p,s)}{r^2(p,s)}\,d\Omega(s)\right.$$

$$\left.+\int_{\Gamma}\frac{k_1(S)\,Y_1(p,S)+k_2(S)\,Y_2(p,S)}{r^2(p,S)}\,d\Gamma(S)\right\} \qquad (5.2.7)$$

$$v_2(p) = \frac{1}{2\pi}\left\{\int_\Omega \frac{\omega(s)\ Y_1(p,s)}{r^2(p,s)}\, d\Omega(s)\right.$$

$$\left. - \int_\Gamma \frac{k_1(S)\ Y_2(p,S) - k_2(S)\ Y_1(p,S)}{r^2(p,S)}\, d\Gamma(S)\right\} \qquad (5.2.8)$$

$$\omega(p) = \frac{1}{2\pi}\left\{\frac{1}{\nu}\int_\Omega \frac{v_1(s)\ \omega(S)\ Y_1(p,s) + v_2(s)\ \omega(s)\ Y_2(p,s)}{r^2(p,s)}\, d\Omega(s)\right.$$

$$- \int_\Gamma \frac{\omega(S)\left[\ n_1(S)\ Y_1(p,S) + n_2(S)\ Y_2(p,S)\ \right]}{r^2(p,S)}\, d\Gamma(S)$$

$$\left. - \frac{1}{\nu}\int_\Gamma \frac{h(S)\left[n_1(S)\ Y_2(p,S) - n_2(S)\ Y_1(p,S)\ \right]}{r^2(p,S)}\, d\Gamma(S)\right\} \qquad (5.2.9)$$

where:

$$Y_i(p,s) = X_i(p) - X_i(s) \qquad , i = 1,2$$

$$k_1(S) = v_1(S)\ n_1(S) + v_2(S)\ n_2(S)$$

$$k_2(S) = v_1(S)\ n_2(S) - v_2(S)\ n_1(S)$$

The surface Γ is discretised into S boundary elements, with N_b boundary nodes, and the domain Ω into L cells, with N_ℓ cells nodes. Let us also assume that the values of the variables within each boundary element and cell are related to their nodal values through suitable interpolation functions, which are at least linear. This assumption is important since it permits us to obtain a relation between boundary and internal vorticities using equation (5.1.18), as will be shown in what follows.

The N_ℓ cells nodes may be divided into N_i internal nodes in Ω but not in Γ and the remaining N_b nodes in Γ, which coincide with the boundary nodes. Applying equations (5.2.7) to (5.2.9) at the N_i internal nodes, replacing the integrals in these equations by summations of

integrals over individual boundary elements and cells and employing numerical integration schemes to evaluate these integrals (see sections 3.1 and 3.3), we obtain matricial equations of the form,

$$\underset{\sim}{v}_{ki} = \underset{\sim}{F}_{kii}\ \underset{\sim}{\omega}_i + \underset{\sim}{G}_{kib}\ \underset{\sim}{\omega}_b + \underset{\sim}{H}_{kib}\ \underset{\sim}{v}_{1b} + \underset{\sim}{P}_{kib}\ \underset{\sim}{v}_{2b} \qquad (5.2.10)$$

$$\underset{\sim}{\omega}_i = \underset{\sim}{A}_{i\ell}\ (\underset{\sim}{v}_1\omega)_\ell + \underset{\sim}{B}_{i\ell}\ (\underset{\sim}{v}_2\omega)_\ell + \underset{\sim}{D}_{ib}\ \underset{\sim}{h}_b + \underset{\sim}{E}_{ib}\ \underset{\sim}{\omega}_b \qquad (5.2.11)$$

where k = 1,2 and the subscripts b and i stand for boundary and internal quantities, respectively, being ℓ = b+i. The notation adopted implies that the matrix $\underset{\sim}{E}_{ib}$, for instance, relates the contribution of the boundary values of ω ($\underset{\sim}{\omega}_b$) to the internal values of ω ($\underset{\sim}{\omega}_i$). All matrices in the above equations depend only on geometrical data and physical properties of the fluid, thus they need to be computed only once during the whole iteration process.

Note that the result of the domain integral in (5.2.7) and (5.2.8) was separated into two parts in (5.2.10), being the first term in the right-hand side representative of the contribution of the internal nodes and the second term that of the boundary nodes.

The first two terms in the right-hand side in equation (5.2.11) involve the field variables $v_1\omega$ and $v_2\omega$. The use of these two variables (instead of v_1, v_2 and ω) was suggested in [93] because they lead to coefficient matrices $\underset{\sim}{A}$ and $\underset{\sim}{B}$ that are proportional to the coefficient matrices $\underset{\sim}{F}_k$ and $\underset{\sim}{G}_k$ in equation (5.2.10), as can be seen from (5.2.7) to (5.2.9). As a consequence, it is not necessary to evaluate and store $\underset{\sim}{A}$ and $\underset{\sim}{B}$; since these matrices are usually large, this feature leads to a significant reduction in computer time and storage requirements.

Equation (5.2.10) gives a set of $2N_i$ algebraic equations which relates the values of v_1 and v_2 at the N_i internal nodes to the N_ℓ values of ω in Ω and the N_b boundary values of v_1 and v_2. A similar set of equations can be obtained by applying equations (5.2.7) and (5.2.8) to the N_b boundary nodes,

$$\underset{\sim}{C}_k \underset{\sim}{v}_{kb} = \underset{\sim}{F}_{kbi} \underset{\sim}{\omega}_i + \underset{\sim}{G}_{kbb} \underset{\sim}{\omega}_b + \underset{\sim}{H}_{kbb} \underset{\sim}{v}_{1b} + \underset{\sim}{P}_{kbb} \underset{\sim}{v}_{2b} \qquad (5.2.12)$$

where the coefficients of the diagonal matrix $\underset{\sim}{C}_k$ can be determined through a limiting process (see equations (2.4.8) and (5.1.16)).

Since the appropriate boundary conditions of the problem are prescribed velocities, equation (5.2.12) gives a set of $2N_b$ algebraic equations in which $\underset{\sim}{\omega}_i$ and $\underset{\sim}{\omega}_b$ are the only unknowns. Reminding, however, that the prescribed velocities are linked through equations (5.1.2) and (5.1.3), in the sense that for a given distribution of $\underset{\sim}{\omega}$ and the specification of (say) v_n there is one and only one value of v_t which satisfies (5.1.2) and (5.1.3), we note that only N_b equations of the above set are independent of one another. These N_b equations can be written in the form,

$$\underset{\sim}{\omega}_b = \underset{\sim}{Q}_{bi} \underset{\sim}{\omega}_i + \underset{\sim}{R}_b \qquad (5.2.13)$$

where, assuming that the boundary values of $\underset{\sim}{v}_1$ are used to evaluate the $\underset{\sim}{\omega}_b$ values, we have

$$\underset{\sim}{Q}_{bi} = - \underset{\sim}{G}_{1bb}^{-1} \underset{\sim}{F}_{1bi} \qquad (5.2.14)$$

$$\underset{\sim}{R}_b = \left[\underset{\sim}{G}_{1bb}^{-1} (\underset{\sim}{C}_1 - \underset{\sim}{H}_{1bb}) \right] \underset{\sim}{v}_{1b} - (\underset{\sim}{G}_{1bb}^{-1} \underset{\sim}{P}_{1bb}) \underset{\sim}{v}_{2b} \qquad (5.2.15)$$

Analogously to (5.2.10), equation (5.2.11) gives a set of N_i algebraic equations relating the values of ω at the N_i internal nodes to the N_ℓ values of $v_1\omega$ and $v_2\omega$ in Ω and the N_b boundary values of ω and h. Applying equation (5.2.9) to the N_b boundary nodes gives,

$$\underset{\sim}{C} \underset{\sim}{\omega}_b = \underset{\sim}{A}_{b\ell} (\underset{\sim}{v_1}\omega)_\ell + \underset{\sim}{B}_{b\ell} (\underset{\sim}{v_2}\omega)_\ell + \underset{\sim}{D}_{bb} \underset{\sim}{h}_b + \underset{\sim}{E}_{bb} \underset{\sim}{\omega}_b \qquad (5.2.16)$$

This equation may be rearranged as,

$$\underset{\sim}{h}_b = \left[\underset{\sim}{D}_{bb}^{-1} (\underset{\sim}{C} - \underset{\sim}{E}_{bb}) \right] \underset{\sim}{\omega}_b - (\underset{\sim}{D}_{bb}^{-1} \underset{\sim}{A}_{b\ell}) (\underset{\sim}{v_1}\omega)_\ell - (\underset{\sim}{D}_{bb}^{-1} \underset{\sim}{B}_{b\ell}) (\underset{\sim}{v_2}\omega)_\ell \qquad (5.2.17)$$

Since $\underset{\sim}{\omega}_b$, $\underset{\sim}{v}_1$ and $\underset{\sim}{v}_2$ are all expressible in terms of $\underset{\sim}{\omega}_i$ (see equations

(5.2.10) and (5.2.13)), the above set of N_b equations can ultimately be seen as an expression of the $\underset{\sim}{h}_b$ values in terms of non-linear functions of $\underset{\sim}{\omega}_i$.

The previous development demonstrates that, with properly specified velocity boundary conditions, all the unknowns in equations (5.2.7) to (5.2.9) (which are equivalent to (5.1.2), (5.1.3) and (5.2.1)) are expressible in terms of $\underset{\sim}{\omega}_i$. Consequently, steady incompressible viscous flow problems can be solved using an iterative procedure involving equations (5.2.7) to (5.2.9), starting with a set of assumed values of $\underset{\sim}{\omega}_i$. This iterative procedure can be summarised as follows:

a) Discretise the boundary Γ into S elements and N_b boundary nodes and the domain Ω into L cells, with N_ℓ (= N_b + N_i) cells nodes;

b) Compute the coefficients of matrices $\underset{\sim}{C}$, $\underset{\sim}{D}$, $\underset{\sim}{E}$, $\underset{\sim}{F}$, $\underset{\sim}{G}$, $\underset{\sim}{H}$ and $\underset{\sim}{P}$ in equations (5.2.10) to (5.2.12) and (5.2.16) using the specified values of geometrical data and physical properties of the fluid. Of these, matrices $\underset{\sim}{D}(N_i \times N_b)$, $\underset{\sim}{E}(N_i \times N_b)$, $\underset{\sim}{F}(N_i \times N_i)$ and $\underset{\sim}{G}(N_i \times N_b)$ are stored for subsequent use; the matrices appearing in equation (5.2.17) (dimensions: $N_b \times N_b + 2(N_b \times N_\ell)$) are computed and stored, together with matrix $\underset{\sim}{Q}(N_b \times N_i)$ in (5.2.13). Introduce the prescribed velocity boundary conditions to calculate vector $\underset{\sim}{T}(N_i)$, corresponding to the sum of the last two terms in equation (5.2.10), and vector $\underset{\sim}{R}(N_b)$ in (5.2.13), all of which are also stored;

c) Multiply matrix $\underset{\sim}{Q}$ by the assumed (or previously calculated) values of $\underset{\sim}{\omega}_i$ and add to vector $\underset{\sim}{T}$ to find the vorticity boundary values $\underset{\sim}{\omega}_b$ (equation (5.2.13));

d) Multiply matrix $\underset{\sim}{F}$ by the assumed (or previously calculated) values of $\underset{\sim}{\omega}_i$, add to the product of matrix $\underset{\sim}{G}$ by the values of $\underset{\sim}{\omega}_b$ calculated in the previous step and add the total to vector $\underset{\sim}{T}$ to find the velocity values $\underset{\sim}{v}_{ki}$ (equation (5.2.10));

e) Multiply the matrices appearing in equation (5.2.17) accordingly by the new values of $\underset{\sim}{\omega}_b$, $(\underset{\sim}{v}_1\omega)_\ell$ and $(\underset{\sim}{v}_2\omega)_\ell$ previously computed and add the result of the products to find the $\underset{\sim}{h}_b$ values;

f) Employ the prescribed velocity boundary conditions and the assumed (or previously calculated) values of $\underset{\sim}{\omega}_i$, together with the values of $\underset{\sim}{\omega}_b$, $\underset{\sim}{v}_{ki}$ and $\underset{\sim}{h}_b$ computed in steps c) to e), to find a new distribution of $\underset{\sim}{\omega}_i$ through equation (5.2.11);

g) Compare the actual values of $\underset{\sim}{\omega}_i$ with their previous values to check if their difference is less than a prescribed tolerance, so the iteration cycle can be terminated;

h) Return to c).

5.3 Transient Problems

As discussed in section 5.1, transient problems of incompressible viscous fluid motion are governed by the set of equations (5.1.1) to (5.1.3). An integral equation equivalent to the kinematic part of the flow as represented by equations (5.1.2) and (5.1.3) has already been derived in section 5.1 (equation (5.1.18)). In what follows, we derive an integral representation for the kinetic aspect of the flow and discuss numerical procedures for the solution of the resulting set of integral equations [38], [92].

Rewriting the vorticity transport equation (5.1.1) as,

$$\nabla^2\underset{\sim}{\omega} - \frac{1}{\nu}\frac{\partial\underset{\sim}{\omega}}{\partial t} = -\frac{1}{\nu}\nabla \times (\underset{\sim}{v} \times \underset{\sim}{\omega}) \qquad (5.3.1)$$

and comparing to equation (2.5.1), we note that (5.3.1) can be interpreted as a (non-linear) non-homogeneous diffusion equation, the non-linearity being included through the convective term in the right-hand side. Thus, an integral equation equivalent to (5.3.1) can be readily obtained as (see equation (2.8.6)),

$$\underset{\sim}{\omega}(p,t_F) + \nu \int_{t_0}^{t_F} \int_{\Gamma} \underset{\sim}{\omega}(S,t) \left[\underset{\sim}{\nabla} u^*(p,S,t_F,t) \cdot \underset{\sim}{n}(S) \right] d\Gamma(S)\, dt$$

$$= \nu \int_{t_0}^{t_F} \int_{\Gamma} u^*(p,S,t_F,t) \left\{ \left[\underset{\sim}{\nabla} \times \underset{\sim}{\omega}(S,t) \right] \times \underset{\sim}{n}(S) \right\} d\Gamma(S)\, dt$$

$$+ \int_{\Omega} \underset{\sim}{\omega}_0(s,t_0)\, u^*(p,s,t_F,t_0)\, d\Omega(s)$$

$$+ \int_{t_0}^{t_F} \int_{\Omega} \left\{ \underset{\sim}{\nabla} \times \left[\underset{\sim}{v}(s,t) \times \underset{\sim}{\omega}(s,t) \right] \right\} u^*(p,s,t_F,t)\, d\Omega(s)\, dt \quad (5.3.2)$$

where $u^*(p,s,t_F,t)$ is the fundamental solution to the diffusion equation, defined in (2.8.3).

The calculation of $\underset{\sim}{\omega}$ throughout the flowfield, at any time t, can be carried out iteratively using the above equation. Following a discussion in page 41, we note that the third integral in (5.3.2) represents the effects of an initial vorticity distribution. Since a stationary fluid cannot co-exist with a non-zero vorticity field, the vorticity distribution changes as a result of a convective process, represented by the last term in (5.3.2). Finally, the boundary integrals in (5.3.2) include the effects of generation (or depletion) of vorticity at the surface Γ, being this process a result of the no-slip condition (see discussion in page 7). The generated vorticity leaves the boundary only through diffusion.

As for the steady-state problem the contribution of the inviscid region of the flow to the computation of $\underset{\sim}{\omega}$ anywhere in the flow is zero. Thus, only the values of $\underset{\sim}{v}$ along Γ and in the viscous region of the flow are needed in the calculation of $\underset{\sim}{\omega}$.

A numerical formulation for the solution of transient problems of incompressible viscous fluid motion as represented by equations (5.1.18) and (5.3.2) will now be derived, following the ideas discussed in [38] and [92] and employing basically the same procedures presented in chapters 3

and 4. For simplicity, only the two-dimensional case is considered, thus the flow motion is described by the scalar equations (5.2.7) and (5.2.8) for the velocity and the following scalar equation for the vorticity,

$$\omega(p,t_F) = \int_\Omega \omega_0(s,t_0)\, u^*(p,s,t_F,t_0)\, d\Omega(s)$$

$$-\int_{t_0}^{t_F}\int_\Omega \left\{ \frac{\partial}{\partial x_1(s)} \left[v_1(s,t)\, \omega(s,t) \right] \right.$$

$$\left. + \frac{\partial}{\partial x_2(s)} \left[v_2(s,t)\, \omega(s,t) \right] \right\} u^*(p,s,t_F,t)\, d\Omega(s)\, dt$$

$$+ \nu \int_{t_0}^{t_F}\int_\Gamma \left[u^*(p,S,t_F,t) \frac{\partial \omega(S,t)}{\partial n(S)} - \omega(S,t) \frac{\partial u^*(p,S,t_F,t)}{\partial n(S)} \right] d\Gamma(S)\, dt \qquad (5.3.3)$$

Integrating by parts the second integral in the above equation gives,

$$\int_{t_0}^{t_F}\int_\Omega \left\{ \frac{\partial}{\partial x_1(s)} \left[v_1(s,t)\, \omega(s,t) \right] \right.$$

$$\left. + \frac{\partial}{\partial x_2(s)} \left[v_2(s,t)\, \omega(s,t) \right] \right\} u^*(p,s,t_F,t)\, d\Omega(s)\, dt$$

$$= \int_{t_0}^{t_F}\int_\Gamma u^*(p,S,t_F,t)\, \omega(S,t) \left[v_1(S,t)\, n_1(S) + v_2(S,t)\, n_2(S) \right] d\Gamma(S)\, dt$$

$$- \int_{t_0}^{t_F}\int_\Omega \omega(s,t) \left[v_1(s,t) \frac{\partial u^*(p,s,t_F,t)}{\partial x_1(s)} \right.$$

$$\left. + v_2(s,t) \frac{\partial u^*(p,s,t_F,t)}{\partial x_2(s)} \right] d\Omega(s)\, dt \qquad (5.3.4)$$

The surface Γ is discretised into S elements and N_b boundary nodes,

the domain Ω sub-divided into L cells, with $N_\ell (=N_i + N_b)$ cells nodes, and the time dimension sub-divided into F time steps. Let us assume, as in the previous section, that the values of the variables within each boundary element and cell are related to their nodal values through suitable interpolation functions. For simplicity, the flow variables are assumed to remain constant on time within each time step, this assumption corresponding to the use of constant time interpolation functions as discussed in section 4.1.1. Clearly, linear or higher order time interpolation functions can easily be introduced, following sections 4.1.2 and 4.1.3. The stepwise variation of the functions permits the analytical evaluation of the time integrals in equation (5.3.3). Applying this equation at the N_i internal nodes in Ω but not in Γ (accounting for (5.3.4)), replacing the resulting space integrals by summations of integrals over individual boundary elements and cells and employing numerical integration schemes to evaluate these integrals (see section 4.1.4), we obtain the following equation in matricial form,

$$\underset{\sim}{\omega}_i = \underset{\sim}{A}_{i\ell}\ (\underset{\sim}{v}_1\omega)_\ell + \underset{\sim}{B}_{i\ell}\ (\underset{\sim}{v}_2\omega)_\ell + \underset{\sim}{D}_{ib}\ \underset{\sim}{h}_b + \underset{\sim}{E}_{ib}\ \underset{\sim}{\omega}_b + \underset{\sim}{T}_i \qquad (5.3.5)$$

where matrices $\underset{\sim}{A}$, $\underset{\sim}{B}$, $\underset{\sim}{D}$ and $\underset{\sim}{E}$ are dependent only on geometrical data, physical properties of the fluid and the time step value, thus they all need to be computed only once during the whole time process (for a fixed time step value). Vector $\underset{\sim}{T}_i$ contains the contribution of the vorticity distribution at the beginning of the step. Note that if (say) linear time interpolation functions are employed, the second and third integrals in equation (5.3.3) also contribute to vector $\underset{\sim}{T}_i$.

Equation (5.3.5) gives a set of N_i algebraic equations relating the values of $\underset{\sim}{\omega}_i$ at the N_i internal nodes to the N_ℓ values of $\underset{\sim}{v}_1\omega$ and $\underset{\sim}{v}_2\omega$ in Ω and the N_b boundary values of $\underset{\sim}{h}_b$ and $\underset{\sim}{\omega}_b$, being $h_b = (\partial\omega/\partial n)_b$.

In principle, an assumed initial distribution of $\underset{\sim}{\omega}_\ell$ at the beginning of the process, together with prescribed velocity boundary

conditions, permits the iterative use of equation (5.3.5) to determine a new distribution of $\underset{\sim}{\omega}_\ell$ at the end of the first time step, and its subsequent progressing with time. Initially, the distribution of $\underset{\sim}{\omega}_\ell$ at the beginning of the time step (together with the velocity boundary conditions) is employed to calculate the velocity values at the N_i internal nodes through (5.2.7) and (5.2.8), whose matricial form is repeated here for convenience,

$$\underset{\sim}{v}_{ki} = \underset{\sim}{F}_{ki\ell}\ \underset{\sim}{\omega}_\ell + \underset{\sim}{H}_{kib}\ \underset{\sim}{v}_{1b} + \underset{\sim}{P}_{kib}\ \underset{\sim}{v}_{2b} \tag{5.3.6}$$

Unlike the steady-state case, we cannot now apply equations (5.2.7) and (5.2.8) to the N_b boundary nodes and directly enforce satisfaction of the velocity boundary conditions. This is due to the fact that in general, the velocity $\underset{\sim}{v}_{kb}$ calculated through (5.2.7) and (5.2.8) using the vorticity distribution obtained from equation (5.3.3) need not necessarily satisfy the no-slip condition at the solid boundaries. In particular, there may be a slip component tangential to the surface. Thus, according to the discussion in page 7, sufficient vorticity must be produced at the boundary Γ to enforce that the velocity field $\underset{\sim}{\bar{v}}$ due to this new vorticity, when combined with that previously determined, reduces the slip velocity to zero. According to the classical definition of the aerodynamics theory [36], a surface across which tangential velocity changes abruptly is a vortex sheet. The velocity induced by the vortex sheet is given by [36],

$$\bar{v}_1(p) = -\frac{1}{2\pi}\int_\Gamma \frac{\omega(S)\ Y_2(p,S)}{r^2(p,S)}\,d\Gamma(S) \tag{5.3.7}$$

$$\bar{v}_2(p) = \frac{1}{2\pi}\int_\Gamma \frac{\omega(S)\ Y_1(p,S)}{r^2(p,S)}\,d\Gamma(S) \tag{5.3.8}$$

where $Y_i(p,S) = X_i(p) - X_i(S)$ $(i=1,2)$.

The requirement that the tangential velocity as calculated from (5.2.7)and (5.2.8) plus (5.3.7) and (5.3.8) satisfies the no-slip

condition then produces the equation,

$$v_t(P) = t_1(P)\left[v_1(P) + \bar{v}_1(P)\right] + t_2(P)\left[v_2(P) + \bar{v}_2(P)\right] \quad (5.3.9)$$

where $t_i(P)$ are the components of the unit vector tangent to the surface Γ at P.

Applying the above equation to the N_b boundary nodes yields the following system of algebraic equations,

$$(\underset{\sim}{P}_{bb} + \underset{\sim}{C})\,\underset{\sim}{\omega}_b = \underset{\sim}{Q}_{b\ell}\,\underset{\sim}{\omega}_\ell + \underset{\sim}{R}_{bb}\,\underset{\sim}{v}_{1b} + \underset{\sim}{Z}_{bb}\,\underset{\sim}{v}_{2b} \quad (5.3.10)$$

where the diagonal matrix $\underset{\sim}{C}$ accounts for the singularity of the kernels in the integrals in (5.3.7) and (5.3.8).

This kinematic treatment of the boundary vorticity distribution, i.e. its calculation through an enforcement of the no-slip condition at solid boundaries, was first stated by Lighthill [31] and later expressed numerically in [34], [35], [37] and [94]. Note that the vorticity generation (or depletion) at the solid boundaries is prescribed rather than actual vorticity values. This avoids employing one-sided difference formulae to calculate vorticity boundary values from values of velocity (or stream function) at points in the vicinity of the boundary, as is usually done in prevailing methods of solution.

A set of N_b equations similar to (5.3.5) can be obtained by applying equation (5.3.3) at the N_b boundary nodes,

$$\underset{\sim}{C}\,\underset{\sim}{\omega}_b = \underset{\sim}{A}_{b\ell}(\underset{\sim}{v}_1\omega)_\ell + \underset{\sim}{B}_{b\ell}(\underset{\sim}{v}_2\omega)_\ell + \underset{\sim}{D}_{bb}\,\underset{\sim}{h}_b + \underset{\sim}{E}_{bb}\,\underset{\sim}{\omega}_b + \underset{\sim}{T}_b \quad (5.3.11)$$

This equation may be rearranged as follows,

$$\underset{\sim}{D}_{bb}\,\underset{\sim}{h}_b = (\underset{\sim}{C} - \underset{\sim}{E}_{bb})\underset{\sim}{\omega}_b - \underset{\sim}{A}_{b\ell}(\underset{\sim}{v}_1\omega)_\ell - \underset{\sim}{B}_{b\ell}(\underset{\sim}{v}_2\omega)_\ell - \underset{\sim}{T}_b \quad (5.3.12)$$

The previous development shows that, with properly specified velocity boundary conditions, transient incompressible viscous flow problems can be efficiently solved by using an iterative process involving equations (5.2.7), (5.2.8) and (5.3.3). Consider that some

time has elapsed since the fluid was set in motion, the actual values of all flow variables are known and the no-slip condition on Γ is satisfied. The following procedure then constitute an iteration loop to advance the solution by one time step:

a) Compute an initial distribution of $\underset{\sim}{\omega}_{\ell}$ using equation (5.3.5), being the $\underset{\sim}{\omega}_{b}$ values evaluated by directly taking the equation to the boundary;

b) Compute new values of $\underset{\sim}{v}_{ki}$ using equation (5.3.6);

c) Compute new vorticity boundary values using equation (5.3.10), where the (known) right-hand side corresponds to the actual slip velocity;

d) Compute new values of $\underset{\sim}{h}_{b}$ using equation (5.3.12);

e) Compute new values of $\underset{\sim}{\omega}_{i}$ using (5.3.5), employing the values of $\underset{\sim}{v}_{ki}$, $\underset{\sim}{\omega}_{b}$ and $\underset{\sim}{h}_{b}$ calculated in steps b) to d);

f) Verify convergence of $\underset{\sim}{\omega}_{\ell}$;

g) Return to b).

6. PROGRAMMING

This chapter describes the computer programs developed throughout this work, employing the theory and numerical procedures derived in chapters 3 and 4. Some results of applications of the programs have already been presented in these chapters.

In developing the programs related to chapter 4, for transient problems, emphasis was placed in simplicity of coding rather than in maximum computer efficiency. The same modular structure was adopted for all programs. In this way, the various moduli that form the programs could be easily modified (for instance, for the testing of different numerical integration schemes, interpolation functions, etc.) and readily implemented. This strategy, however, led to some limitations of the actual programs: when solving practical problems such as the turbine disc analysis of example 4.5.4, the use of disc files was obviously necessary to allow for a large number of cells to be employed in conjunction with time-marching scheme BEM1A and to avoid the need of (unnecessarily) recomputing matrices, thus reducing the required computer CPU time for scheme BEM2. Furthermore, for problems involving a large number of boundary elements like this one, more effective system solver algorithms exploring the sparsity of the system matrix should also be developed. These and other suggestions for improving the efficiency of the programs are further discussed in chapter 7.

The main characteristics of the programs developed are as follows:

Program BEM2DSP: solution of two-dimensional steady potential problems governed by Laplace's or Poisson's equation. Includes constant and linear boundary elements and allows for Dirichlet, Neumann, Cauchy (mixed), Robin or free surface boundary conditions, internal sources, finite, infinite or semi-infinite domains. The theory and examples of applications are discussed in sections 3.1 to 3.7;

Program BEM3DSP: solution of three-dimensional steady potential problems governed by Laplace's equation, employing constant elements (flat triangles). Allows for Dirichlet, Neumann, Cauchy or Robin boundary conditions and finite or infinite domains (section 3.8);

Program BEMASSP: solution of axisymmetric steady potential problems governed by Laplace's or Poisson's equation. Presents the same features as the two-dimensional program (section 3.9);

Program BEM2DTP1: solution of two-dimensional transient potential problems governed by the diffusion equation using time-marching schemes BEM1A or BEM1B with linear boundary elements and triangular cells. Allows for Dirichlet, Neumann, Cauchy or Robin boundary conditions, finite or infinite domains, stepwise constant u and q, stepwise linear u and q or stepwise linear u and quasi-quadratic q (sections 4.1 to 4.5);

Program BEM2DTP2: same, using time-marching scheme BEM2;

Program BEMASTP1: solution of axisymmetric transient potential problems governed by the diffusion equation using time-marching scheme BEM1A with linear boundary elements, triangular cells and stepwise constant u and q. Allows for Dirichlet, Neumann, Cauchy or Robin boundary conditions, finite or infinite domains (section 4.6).

6.1 Description of Program BEM2DSP

The macro flow diagram of the main structure of the program is presented in figure 6.1.1, and the subroutines called by it are shown in figure 6.1.2. The operations performed in each subroutine are described in what follows.

I SUBROUTINE INPUT

In this subroutine, all the input data required by the program are read and printed. The input data consist of the following groups of cards:

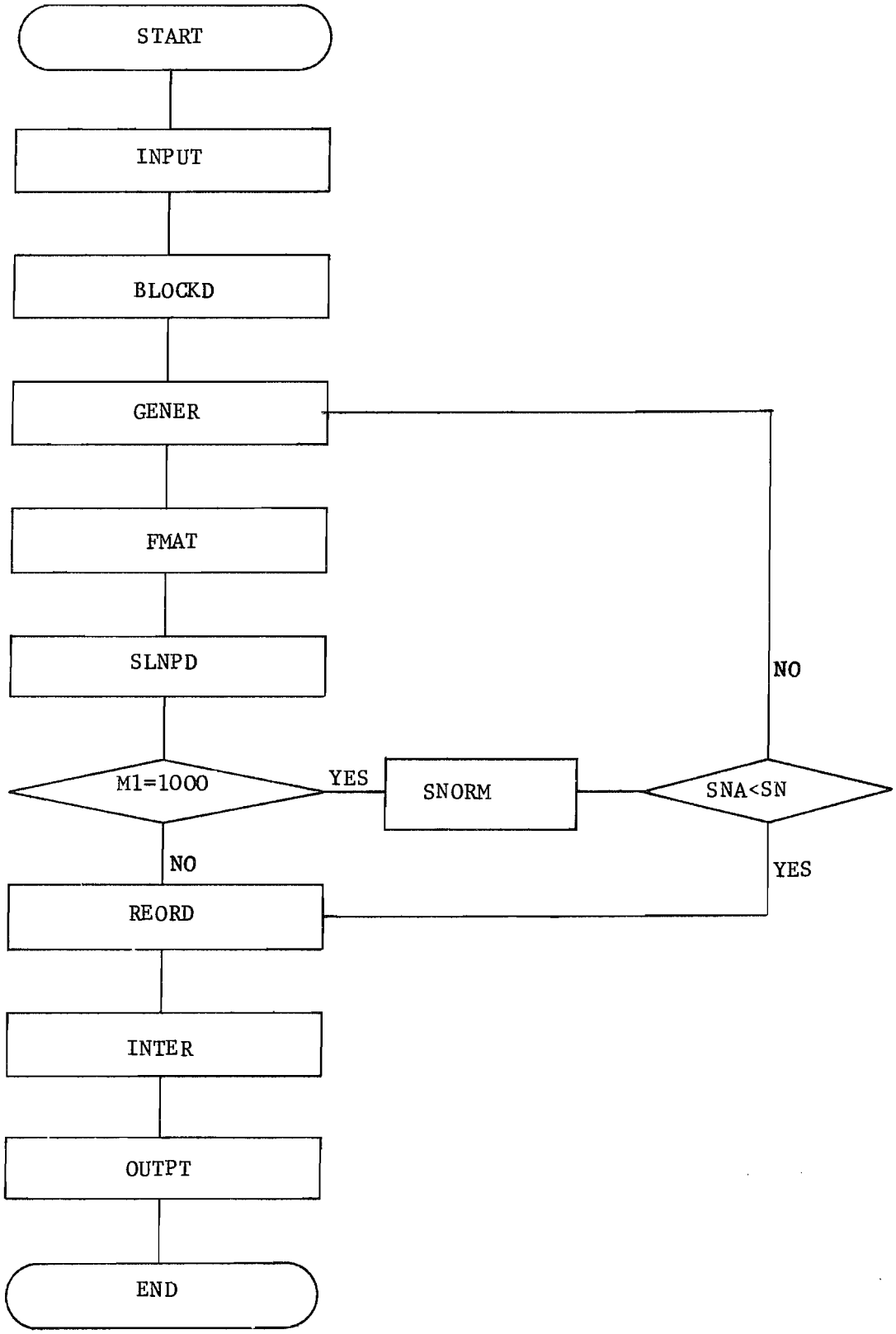

Figure 6.1.1 - Macro flow diagram of program BEM2DSP

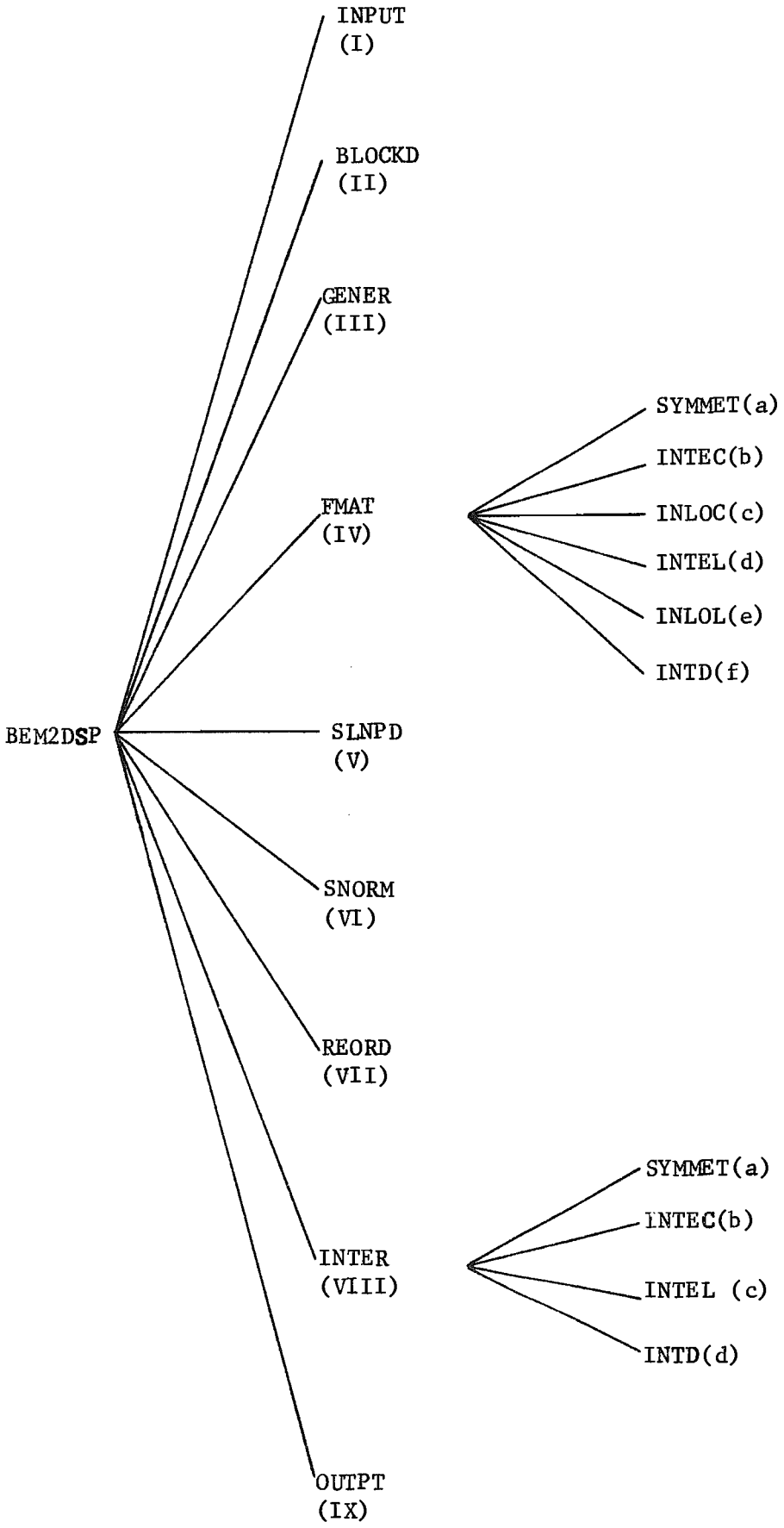

Figure 6.1.2 - Subroutines called by program BEM2DSP

READ: ITP, N, NE, L, NC, NN, M, NS, MC, M1, FA

ITP: code for type of element (0: constant; 1:linear);

N: number of extreme points of boundary elements (including double nodes);

NE: number of boundary elements;

L: number of internal points where the potential and its derivatives in the x_1 and x_2 directions are required;

NC: number of cells;

NN: number of internal points to define the cells;

M: number of surfaces;

NS: code for type of symmetry (0: no symmetry; 1:symmetry with respect to x_1; 2:symmetry w.r.t. x_2; 3:anti-symmetry w.r.t. x_1; 4:anti-symmetry w.r.t. x_2; 5:symmetry w.r.t. x_1 and x_2; 6:anti-symmetry w.r.t. x_1 and x_2; 7:symmetry w.r.t. x_1, anti-symmetry w.r.t. x_2; 8:anti-symmetry w.r.t. x_1, symmetry w.r.t. x_2);

MC: code for type of region (0: bounded; 1:unbounded);

M1: code for type of boundary conditions of the problem (0:Dirichlet, mixed or Robin; number of boundary node with specified potential value: Neumann; 1000:free surface);

FA: specified potential value (Neumann boundary conditions only).

If the boundary conditions are of the free surface type,

READ: NFS, NLS, SN

NFS: number of first node on the free surface;

NLS: number of last node on the free surface;

SN: maximum acceptable error for free surface location.

READ: (IPR(I), NL(I), NFN(I), NLN(I), I=1,M)

IPR(I): code for type of each surface (0: closed; 1: open);

NL(I): number of last node on each surface;

NFN(I): code for the first node on each surface (1: node located over a symmetry axis; 2: node located over an anti-symmetry axis; 0: otherwise);
NLN(I): code for the last node on each surface (as previously).

The above data are necessary for the automatic generation of the connectivity of the boundary elements since multiply-connected regions can be considered. By closed surface, we mean a surface whose first and last nodes form a boundary element (see figure 6.1.3).

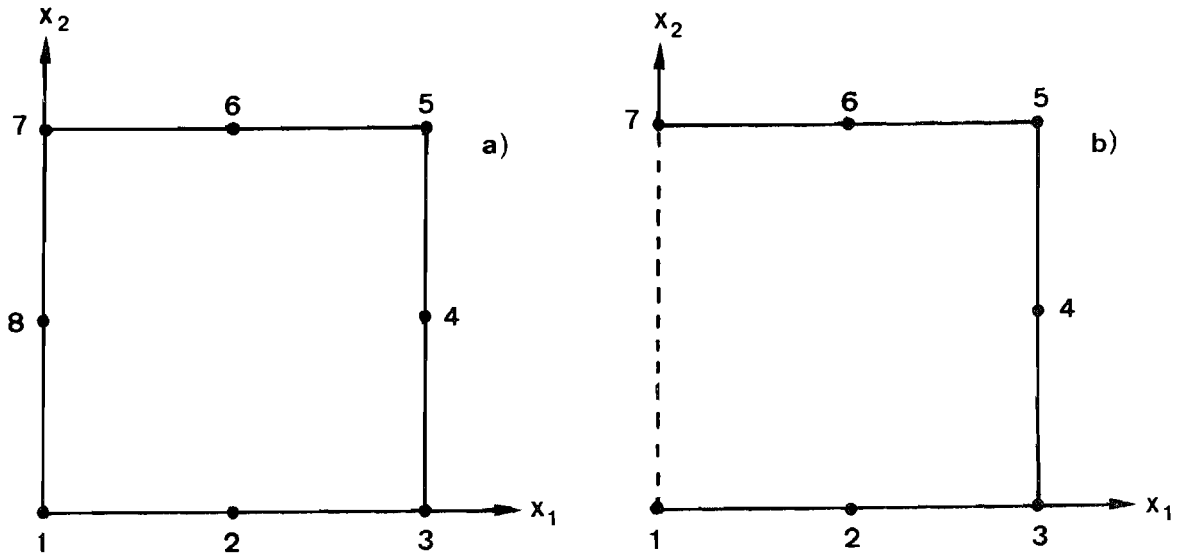

Figure 6.1.3 - Types of surfaces: a) Closed; b) Open

READ: (X1(I), X2(I), I=1, N)
X1(I), X2(I): cartesian coordinates of extreme points of boundary elements (coincident with the boundary nodes for the linear case).

The sequence is given in counter-clockwise direction for external surfaces or in clockwise direction for internal surfaces.

READ: (KODE(I), FI(I), TO(I), I=1, N1)

N1: parameter that equals NE for constant elements or N for linear elements;

KODE(I): code for type of boundary condition at each node (0: prescribed potential; 1: prescribed flux; 2: Robin-type);

FI(I): prescribed value (the value of a/b in equation (3.2.1) or h in equation (3.2.12) if KODE(I)=2);

TO(I): the value of d/a in equation (3.2.1) or u_s in equation (3.2.12) (KODE(I)=2 only).

If there are internal sources,

READ: (X1(I), X2(I), I=N+1, N+NN)

X1(I), X2(I): cartesian coordinates of cell nodes.

READ: (NO1(I), NO2(I), NO3(I), N4(I), (PI(J), J=1,7), I=1,NC)

NO1(I), NO2(I), NO3(I): connectivity of cell I;

N4(I): code for variation of function p (equation (3.3.1)) within each cell (0: constant; 1: given by points);

PI(J): value of function p at each integration point in the cells (if N4(I)=0, only the value of PI(1) is needed).

If the potential and its derivatives with respect to x_1 and x_2 are required at a number of internal points,

READ: (X1(I), X2(I), I=N+NN+1, N+NN+L)

X1(I), X2(I): cartesian coordinates of internal points.

II SUBROUTINE BLOCKD

In this subroutine, the coordinates of integration points and the weighting factors for the Gaussian and Hammer's numerical integration methods are given and kept in COMMON.

III SUBROUTINE GENER

The boundary elements connectivity is generated and their length calculated. If constant elements are employed, the coordinates of the boundary nodes (mid-point of each element) are computed. A parameter for the symmetry loop is set and, if there are internal sources in the problem, the area of the cells is also calculated. All values are printed, so that they can be checked for input errors.

For the case when linear elements are employed, the discontinuities in the boundary conditions at corners or singular points are taken into account through double nodes, i.e. nodes with the same coordinates but different boundary conditions. The zero-length elements formed by them do not affect the computation and therefore are not considered as elements in the program. Note that it is not possible to specify the potential at both nodes forming a double node since this would cause the system matrix to be singular.

IV SUBROUTINE FMAT

This subroutine computes the coefficients of matrices $\underset{\sim}{G}$ and $\underset{\sim}{H}$ in equation (3.1.8) and introduces the prescribed boundary conditions of the problem in such a way that the system matrix $\underset{\sim}{K}$ and the vector $\underset{\sim}{F}$ of independent terms (equation 3.1.11)) are directly assembled.

If the problem under consideration presents symmetry (or anti-symmetry), only one half or one quarter of the actual region needs to be discretised and so, for each position of the source point, we need to reflect the discretised region over the axes of symmetry (or anti-symmetry) in order to form the final system of equations. This means that although only NE (or N) positions of the source point are considered, the integration is performed over the entire region (2NE or 4NE elements). The resulting coefficients, however, are directly condensed such that the final system of equations is of order NE x NE (or N x N). For

computational purposes, it is more convenient to reflect the source points instead of the boundary elements, and this strategy is adopted in the program.

For Neumann problems, a 'normalising' condition (see example 3.1.2) is imposed and the order of the system of equations reduced by one.

IVa SUBROUTINE SYMMET

The coordinates of the source point are reflected over the symmetry axes according to the type of symmetry of the problem.

IVb SUBROUTINE INTEC

The off-diagonal coefficients of matrices $\underset{\sim}{G}$ and $\underset{\sim}{H}$, for constant elements, are computed through numerical integration (see equations (3.1.15)).

IVc SUBROUTINE INLOC

The diagonal coefficients of matrix $\underset{\sim}{G}$, for constant elements, are computed through analytical integration (equation (3.1.16)). The diagonal coefficients of matrix $\underset{\sim}{H}$ are directly taken as π.

IVd SUBROUTINE INTEL

Same as INTEC but for linear elements (see equations (3.1.19)).

IVe SUBROUTINE INLOL

Computes only the diagonal coefficients of matrix $\underset{\sim}{G}$, for linear elements, through analytical integration (equation (3.1.21)). The diagonal coefficients of matrix $\underset{\sim}{H}$ are computed in FMAT through constant potential considerations (equation (3.1.10) or (3.6.9)).

If there are internal sources,

IVf SUBROUTINE INTD

Computes the contribution of the internal sources to the vector $\underset{\sim}{F}$ of independent terms through numerical integration (equation (3.3.3)). The Jacobian in this equation is simply twice the area of the cell.

V SUBROUTINE SLNPD

This is a standard subroutine to solve a system of equations using Gauss elimination, considering a full, non-symmetric, non-positive definite matrix [89].

If there is a free surface,

VI SUBROUTINE SNORM

The calculated potential at every nodal point along the free surface is compared with its elevation; if the difference (SNA) between these two values is greater than the maximum acceptable error (SN), this difference is algebraically added to the elevation of the nodal point and the program returns to subroutine GENER to recalculate the length of the modified elements.

VII SUBROUTINE REORD

In this subroutine, the arrays containing the prescribed and calculated boundary values of u and q are reordered. If a Robin-type condition was specified, the values of q are computed through equations (3.2.1) or (3.2.12).

If there are internal points where the values of u, $\partial u/\partial x_1$ and $\partial u/\partial x_2$ are required,

VIII SUBROUTINE INTER

The values of u, $\partial u/\partial x_1$ and $\partial u/\partial x_2$ are computed by using equations (2.4.5) and (2.4.9). The kernels $\partial u^*(p,S)/\partial x_i(S)$ and $\partial q^*(p,S)/\partial x_i(S)$ $(i = 1,2)$ in (2.4.9) are of the form,

$$\frac{\partial u^*(p,S)}{\partial x_i(S)} = \frac{X_i(p) - X_i(S)}{r^2(p,S)}$$

$$\frac{\partial q^*(p,S)}{\partial x_i(S)} = \frac{2\,Y(p,S)\,[X_i(p) - X_i(S)]}{r^4(p,S)} - \frac{n_i(S)}{r^2(p,S)}$$

where $Y(p,S) = [X_1(p) - X_1(S)]\,n_1(S) + [X_2(p) - X_2(S)]\,n_2(S)$, being $n_i(S)$ the components of the unit normal vector.

This subroutine calls SYMMET, INTEC or INTEL (where the above coefficients are also calculated) and INTD, all of which have been previously described.

IX SUBROUTINE OUTPT

This subroutine outputs the results for boundary and required internal points.

6.2 Description of Program BEM3DSP

The structure of this program is simpler than the previous one, since it does not include options of different types of elements (only flat triangles with piecewise constant u and q variations were implemented), it does not consider free surface problems nor anti-symmetry. Furthermore, the connectivity of the boundary elements is given as input data instead of being automatically generated. But all these features can be easily included in the program since they present no theoretical problems and were not considered only for the sake of simplicity.

The macro flow diagram of the main structure of the program is the same as previously (figure 6.1.1) without the IF statement and the subroutines called by it are the ones labelled I to V and VII to IX in figure 6.1.2, with subroutine FMAT(V) calling only SYMMET(a), INTEC(b) and INLOC(c) and subroutine INTER(VIII) calling SYMMET(a) and INTEC(b). The operations performed in each subroutine are now as follows:

I SUBROUTINE INPUT

READ: N, NE, L, NS, M1, FA

N: number of points to define the boundary elements;

NE: as in 6.1;

L: as in 6.1;

NS: code for type of symmetry (0: no symmetry; 1: symmetry with respect to the plane x_2-x_3; 2: symmetry w.r.t. x_1-x_3; 3: symmetry w.r.t. x_1-x_2; 4: symmetry w.r.t. x_2-x_3 and x_1-x_3; 5: symmetry w.r.t. x_2-x_3 and x_1-x_2; 6: symmetry w.r.t. x_1-x_2 and x_1-x_3; 7: symmetry w.r.t. x_1-x_2, x_1-x_3 and x_2-x_3);

M1: code for type of boundary conditions of the problem (0: Dirichlet, mixed or Robin; number of boundary node with specified potential value: Neumann);

FA: as in 6.1.

READ: (X1(I), X2(I), X3(I), I=1, N)

X1(I), X2(I), X3(I): cartesian coordinates of points defining the boundary elements.

READ: (NO1(I), NO2(I), NO3(I), I=1, NE)

NO1(I), NO2(I), NO3(I): connectivity of the boundary elements. These three values are given in counter-clockwise direction for internal surfaces or in clockwise direction for external surfaces.

READ: (KODE(I), FI(I), TO(I), I=1, NE)

As defined in section 6.1.

If the potential and its derivatives with respect to x_1, x_2 and x_3 are required at a number of internal points,

READ: (X1(I), X2(I), X3(I), I=N+1, N+L)

X1(I), X2(I), X3(I): cartesian coordinates of internal points.

II SUBROUTINE BLOCKD

In this subroutine, the coordinates of integration points and the weighting factors for Hammer's numerical integration scheme are given and kept in COMMON.

III SUBROUTINE GENER

The coordinates of the boundary nodes (centroid of each element) are calculated. A parameter for the symmetry loop is set. The area and unit normal vector for each boundary element are computed, being the latter obtained through the cross-product,

$$\underset{\sim}{n}(I) = \frac{|NO2(I)-NO1(I)| \times |NO3(I)-NO1(I)|}{[|NO2(I)-NO1(I)| \times |NO3(I)-NO1(I)|]}$$

All the above values are printed, so that they can be checked for input errors.

IV SUBROUTINE FMAT

All remarks made for two-dimensional problems are also valid here, being the off-diagonal coefficients of matrices $\underset{\sim}{G}$ and $\underset{\sim}{H}$ now computed through equations (3.8.7), the diagonal coefficients of $\underset{\sim}{G}$ computed by using (3.8.13) and the diagonal coefficients of $\underset{\sim}{H}$ directly taken as 2π.

V SUBROUTINE SLNPD

As in section 6.1.

VI SUBROUTINE REORD

As in section 6.1.

If there are internal points where the values of u, $\partial u/\partial x_1$, $\partial u/\partial x_2$ and $\partial u/\partial x_3$ are required,

VII SUBROUTINE INTER

As in 6.1, being the kernels $\partial u^*(p,S)/\partial x_i(S)$ and $\partial q^*(p,S)/\partial x_i(S)$ $(i=1,2,3)$ in equation (2.4.9) of the form,

$$\frac{\partial u^*(p,S)}{\partial x_i(S)} = \frac{X_i(p)-X_i(S)}{r^3(p,S)}$$

$$\frac{\partial q^*(p,S)}{\partial x_i(S)} = \frac{3Y(p,S)\left[X_i(p)-X_i(S)\right]}{r^5(p,S)} - \frac{n_i(S)}{r^3(p,S)}$$

where $Y(p,S) = \left[X_1(p)-X_1(S)\right] n_1(S) + \left[X_2(p)-X_2(S)\right] n_2(S)$ $+ \left[X_3(p)-X_3(S)\right] n_3(S)$ and $n_i(S)$ are the components of the unit normal vector.

VIII SUBROUTINE OUTPT

As in section 6.1.

6.3 Description of Program BEMASSP

The structure of this program is exactly the same as the one for two-dimensional problems (see figure 6.1.1), as well as the subroutines called by it (figure 6.1.2). Note, however, that the system of coordinates is now cylindrical instead of cartesian, and that some of the subroutines undergo the following modifications:

I SUBROUTINE INPUT

In the first data card, it should be noted that since symmetry with respect to the Z-axis (the axis of revolution) is implied in the formulation, the parameter NS refers only to the R-axis and can take the values 0 (no symmetry), 1 (symmetry) or 2 (anti-symmetry).

II SUBROUTINE BLOCKD

Apart from the data mentioned in section 6.1, the coefficients of the polynomial approximations of the complete elliptic integrals (see appendix A) are also given.

IVb SUBROUTINE INTEC

The off-diagonal coefficients of matrices $\underset{\sim}{G}$ and $\underset{\sim}{H}$, for constant elements, are computed through numerical integration as (see equations

(3.1.6), (3.1.15) and (3.9.7)),

$$H_{ij} = \frac{\ell_j}{2} \sum_{k=1}^{4} \bar{q}^*_{ik} R_k W_k$$

$$G_{ij} = \frac{\ell_j}{2} \sum_{k=1}^{4} \bar{u}^*_{ik} R_k W_k$$

where $\bar{u}^*$ and $\bar{q}^*$ are given in (3.9.4) and (3.9.6), respectively.

IVc SUBROUTINE INLOC

The length of the boundary element under consideration is tested to see if it satisfies equation (3.9.13). If this is not so, the element is divided into a part of length L around the singularity fulfilling condition (3.9.13) and where approximations (3.9.11) and (3.9.12) are valid and the remainder which is to be numerically integrated. This numerical integration is carried out by calling subroutine INTEC while the contribution of the part around the singularity (the whole element if equation (3.9.13) is initially satisfied) is computed through analytical integration (equation (B.4) or (B.5)). The diagonal coefficients of matrix $\underset{\sim}{H}$ are now computed in FMAT through constant potential considerations (equation (3.1.10) or (3.6.9)).

IVd SUBROUTINE INTEL

Same as INTEC but for linear elements, being H_{ij} and G_{ij} now given by (see equations (3.1.6), (3.1.19) and (3.9.7)),

$$h^m_{ip} = \frac{\ell_p}{2} \sum_{k=1}^{4} \bar{q}^*_{ik} \phi^m_k R_k W_k$$

$$g^m_{ip} = \frac{\ell_p}{2} \sum_{k=1}^{4} \bar{u}^*_{ik} \phi^m_k R_k W_k$$

where the interpolation functions $\underset{\sim}{\phi}$ are given in (3.1.17).

IVe SUBROUTINE INLOL

Same as INLOC but for linear elements, thus the contribution of the analytically integrated part of the element to the diagonal

coefficients of matrix $\underset{\sim}{G}$ is given by (B.11), (B.12), (B.14), (B.15) or (B.16).

IVf SUBROUTINE INTD

Same as in section 6.1, being the contribution of the internal sources to the vector $\underset{\sim}{F}$ of independent terms now given by (see equations (3.3.2) and (3.3.3)),

$$\int_{\bar{\Omega}} p(s)\ \bar{u}^*(P,s)\ R(s)\ d\bar{\Omega}(s)$$

VIII SUBROUTINE INTER

Only the value of function u is computed at the required internal points. If its derivatives with respect to the R and Z directions are also required, expressions for the kernels $\partial\bar{u}^*(p,S)/\partial R(S)$, $\partial\bar{u}^*(p,S)/\partial Z(S)$, $\partial\bar{q}^*(p,S)/\partial R(S)$ and $\partial\bar{q}^*(p,S)/\partial Z(S)$, although cumbersome, can be easily derived.

6.4 Description of Program BEM2DTP1

The macro flow diagram of the main structure of the program is shown in figure 6.4.1, and the subroutines called by it are depicted in figure 6.4.2. The operations performed in each subroutine are as follows:

I SUBROUTINE INPUT

The input data required by the program consist of the following groups of cards:

READ: ITP, N, NE, L, NC, NN, M, NS, NBC, NUO

ITP: code for type of analysis (1: stepwise constant u and q, scheme BEM1A; 2: same, scheme BEM1B; 3: stepwise linear u and q, scheme BEM1A; 4: same, scheme BEM1B; 5: stepwise linear u and quasi-quadratic q, scheme BEM1A; 6: same, scheme BEM1B);

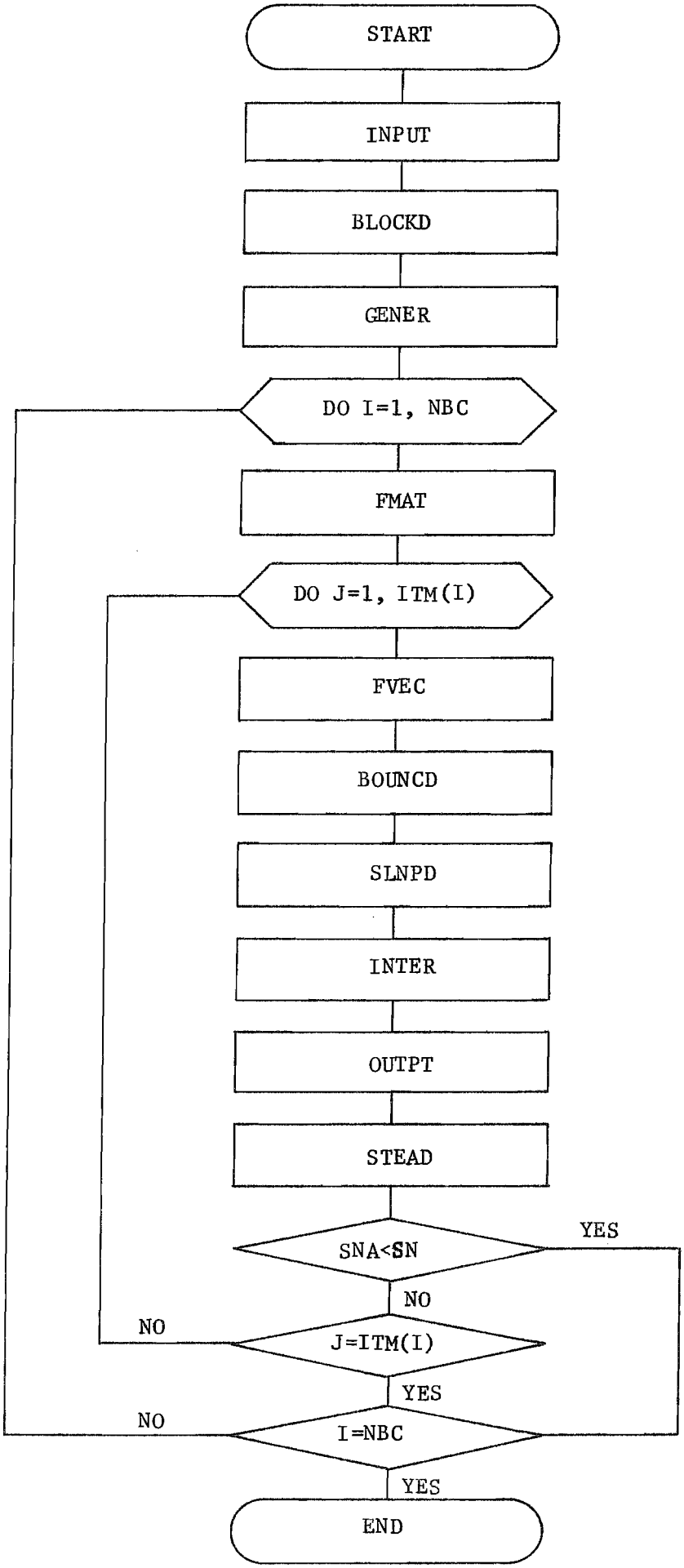

Figure 6.4.1 - Macro flow diagram of Program BEM2DTP1

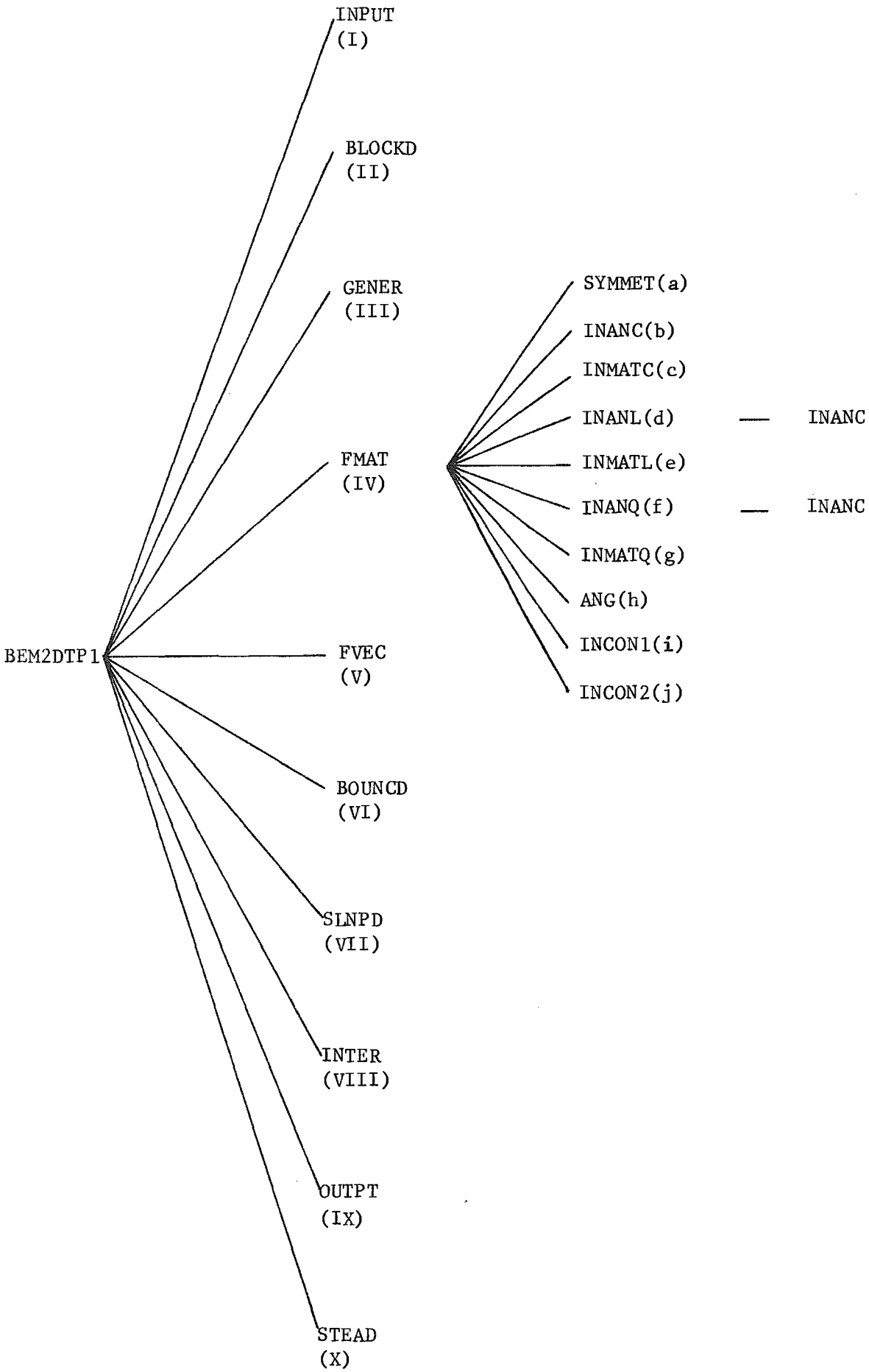

Figure 6.4.2 - Subroutines called by program BEM2DTP1

N: number of extreme points of boundary elements (including doubles nodes);

NE: number of boundary elements;

L: number of internal points where the value of u is required;

NC: number of cells;

NN: number of internal points to define the cells;

M: number of surfaces;

NS: code for type of symmetry (0: no symmetry; 1: symmetry with respect to x_1; 2: symmetry w.r.t. x_2; 3: symmetry w.r.t. x_1 and x_2);

NBC: number of different boundary conditions in time;

NUO: code for variation of initial conditions (0: constant; 1: given by points).

READ: TD, TI, SN

TD: material parameter k;

TI: initial value u_0 (only if NUO = 0);

SN: tolerance for the absolut norm (to consider that a steady-state was reached).

READ: (IPR(I), NL(I), I=1, M)

IPR(I): code for type of each surface (0: closed; 1: open);

NL(I): number of last node on each surface.

READ: (X1(I), X2(I), KODE(I), I=1, N)

X1(I), X2(I): cartesian coordinates of extreme points of boundary elements (coincident with the boundary nodes). The sequence is given in counter-clockwise direction for external surfaces or in clockwise direction for internal surfaces;

KODE(I): code for type of boundary condition at each node (0: prescribed potential; 1: prescribed flux; 2: Robin-type).

If ITP is greater than 2,

READ: (FIO(I), DFIO(I), I=1, N)

FIO(I): initial boundary value of u (the value of a/b in equation (4.5.1) or h in (4.5.4) if KODE(I)=2);

DFIO(I): initial boundary value of q (the value of d/a in equation (4.5.1) or u_s in (4.5.4) if KODE(I)=2).

READ: (ITM(I), TS(I), I=1, NBC)

ITM(I): number of time steps;

TS(I): time step value.

READ: (FI(I1,J), TO(I1,J), J=1,N, I=1, NBC)

$$I1 = \sum_{i=1}^{I} ITM(i)\ TS(i)$$

FI(I1,J): prescribed boundary value at time I1 (the value of a/b in (4.5.1) or h in (4.5.4) if KODE(J)=2);

TO(I1,J): the value of d/a in (4.5.1) or u_s in (4.5.4) at time I1 (KODE(J)=2 only).

READ (X1(I), X2(I), I=N+1, N+NN)

X1(I), X2(I): cartesian coordinates of cell nodes.

READ: (NO1(I), NO2(I), NO3(I), N4(I), (TU(J), J=1,7), I=1,NC)

NO1(I), NO2(I), NO3(I): connectivity of cell I;

N4(I): code for variation of initial conditions within each cell (0: constant; 1: given by points);

TU(J): initial value of u at each integration point in the cells (if N4(I)=0, only the value of TU(1) is needed).

If the value of u is required at a number of internal points,

READ: (X1(I), X2(I), I=N+NN+1, N+NN+L)

X1(I), X2(I): cartesian coordinates of internal points.

II SUBROUTINE BLOCKD

In this subroutine, the following numerical data are given and kept in COMMON:

(a) The coordinates of integration points and the weighting factors for the (six-points) Gaussian numerical integration scheme, employed in the computation of boundary integrals;

(b) The same for the (quintic) Hammer's numerical quadrature, employed in the computation of the domain integral with scheme BEM1A;

(c) The same for the (four-points) Gaussian numerical integration method, employed in the computation of the domain integral with scheme BEM1B;

(d) The coefficients of the polynomial and rational approximations of the exponential-integral and the error functions (see appendix A).

III SUBROUTINE GENER

The boundary elements connectivity is generated and their length calculated. A parameter for the symmetry loop is set. The area of the cells is calculated, as well as the coordinates of the integration points in each cell. All values are printed (apart from the last ones), so that they can be checked for input errors.

IV SUBROUTINE FMAT

This subroutine computes one of the following:

(a) The coefficients of matrices $\underset{\sim}{G}$, $\underset{\sim}{H}$ and $\underset{\sim}{B}$ in equation (4.1.6) and of matrices $\underset{\sim}{G}'$, $\underset{\sim}{H}'$ and $\underset{\sim}{B}'$ in (4.2.1), if ITP=1 or 2;

(b) The coefficients of matrices $\underset{\sim}{G}^1$, $\underset{\sim}{G}^2$, $\underset{\sim}{H}^1$, $\underset{\sim}{H}^2$ and $\underset{\sim}{B}$ in equation (4.1.15) and of matrices $\underset{\sim}{G}'^1$, $\underset{\sim}{G}'^2$, $\underset{\sim}{H}'^1$, $\underset{\sim}{H}'^2$ and $\underset{\sim}{B}'$ in (4.2.2), if ITP=3 or 4;

(c) The coefficients of matrices $\underset{\sim}{G}^1$, $\underset{\sim}{G}^2$, $\underset{\sim}{G}^3$, $\underset{\sim}{H}^1$, $\underset{\sim}{H}^2$ and $\underset{\sim}{B}$ in the BEM1 equivalent of equation (4.5.8) and of the corresponding matrices $\underset{\sim}{G'}^1$, $\underset{\sim}{G'}^2$, $\underset{\sim}{G'}^3$, $\underset{\sim}{H'}^1$, $\underset{\sim}{H'}^2$ and $\underset{\sim}{B'}$ for internal points, if ITP=5 or 6.

All the integrands of the integrals that form the coefficients of the above matrices are strongly dependent on the non-dimensional parameter a defined in (4.1.11) and quickly tend to zero as the value of this parameter becomes large. Thus, a maximum value of a above which the corresponding coefficients in the matrices are taken as zero was then fixed, by trial and error, as 12.

Finally, the matrices are conveniently reordered and stored.

IVa SUBROUTINE SYMMET

The coordinates of the source point are reflected over the symmetry axes according to the type of symmetry of the problem.

IVb SUBROUTINE INANC

The off-diagonal coefficients of matrices $\underset{\sim}{G}$ and $\underset{\sim}{H}$ and all the coefficients of matrices $\underset{\sim}{G'}$ and $\underset{\sim}{H'}$ (which present no singular terms), for the case when ITP=1 or 2, are computed through numerical integration (see equations (4.1.33)).

IVc SUBROUTINE INMATC

The diagonal coefficients of matrix $\underset{\sim}{G}$, for ITP=1 or 2, are computed through analytical integration (see equation (4.1.38)). The diagonal coefficients of matrix $\underset{\sim}{\hat{H}}$ are set to zero (see discussion at the end of section 4.1).

IVd SUBROUTINE INANL

The off-diagonal coefficients of matrices $\underset{\sim}{G}^2$, $\underset{\sim}{H}^1$ and $\underset{\sim}{H}^2$ and all the coefficients of matrices $\underset{\sim}{G}^1$, $\underset{\sim}{G'}^1$, $\underset{\sim}{G'}^2$, $\underset{\sim}{H'}^1$ and $\underset{\sim}{H'}^2$, for ITP=3 or 4,

are computed through numerical integration (equations (4.1.34)).

IVe SUBROUTINE INMATL

The diagonal coefficients of matrix $\underset{\sim}{G}^2$, for ITP=3 or 4, are computed partly by analytical integration and partly by numerical integration (see equation (4.1.42)). The contribution of the analytically integrated part is evaluated in INMATC. The diagonal coefficients of matrices $\underset{\sim}{\hat{H}}^1$ and $\underset{\sim}{\hat{H}}^2$ are set to zero.

IVf SUBROUTINE INANQ

The off-diagonal coefficients of matrices $\underset{\sim}{G}^3$, $\underset{\sim}{H}^1$ and $\underset{\sim}{H}^2$ and all the coefficients of matrices $\underset{\sim}{G}^1$, $\underset{\sim}{G}^2$, $\underset{\sim}{G}'^1$, $\underset{\sim}{G}'^2$, $\underset{\sim}{G}'^3$, $\underset{\sim}{H}'^1$ and $\underset{\sim}{H}'^2$, for ITP=5 or 6, are computed through numerical integration (equations 4.5.10)).

IVg SUBROUTINE INMATQ

Computes the diagonal coefficients of matrix $\underset{\sim}{G}^3$, for ITP=5 or 6, in a similar way as is done in INMATL. The diagonal coefficients of matrices $\underset{\sim}{\hat{H}}^1$ and $\underset{\sim}{\hat{H}}^2$ are set to zero.

IVh SUBROUTINE ANG

Computes the coefficients c_i (equation (4.1.47)).

IVi SUBROUTINE INCON1

This subroutine computes the coefficients of matrices $\underset{\sim}{B}$ and $\underset{\sim}{B}'$, for ITP=1,3 or 5, through numerical integration (equation (4.2.5)).

IVj SUBROUTINE INCON2

The same as INCON1, for ITP=2,4, or 6 (equation (4.2.11)).

V SUBROUTINE FVEC

This subroutine updates the vector of initial conditions using

equation (4.2.1) if ITP=1 or 2, equation (4.2.2) if ITP=3 or 4 or equivalent if ITP=5 or 6.

VI SUBROUTINE BOUNCD

In this subroutine, the vector $\underset{\sim}{F}$ of independent terms is computed through appropriate products of matrices $\underset{\sim}{G}$ or $\underset{\sim}{H}$ by the prescribed boundary conditions for the actual time step plus the product of matrix $\underset{\sim}{B}$ by the initial conditions at the beginning of the step.

VII SUBROUTINE SLNPD

As described in section 6.1.

If there are internal points where the value of u is required,

VIII SUBROUTINE INTER

Computes the value of u at internal points by using equation (2.8.6). If the derivatives of u with respect to x_1 and x_2 are also required, they can be calculated as for the steady-state case.

IX SUBROUTINE OUPT

As described in section 6.1.

X SUBROUTINE STEAD

Computes the absolut norm of the unknowns.

6.5 Description of Program BEM2DTP2

The macro flow diagram of the main structure of this program and the subroutines called by it are presented in figures 6.5.1 and 6.5.2, respectively. The operations performed in each subroutine are now as follows:

I SUBROUTINE INPUT

READ: ITP, N, NE, L, M, NS, NBC, NUO

ITP: code for type of analysis (1: stepwise constant u and q; 2:

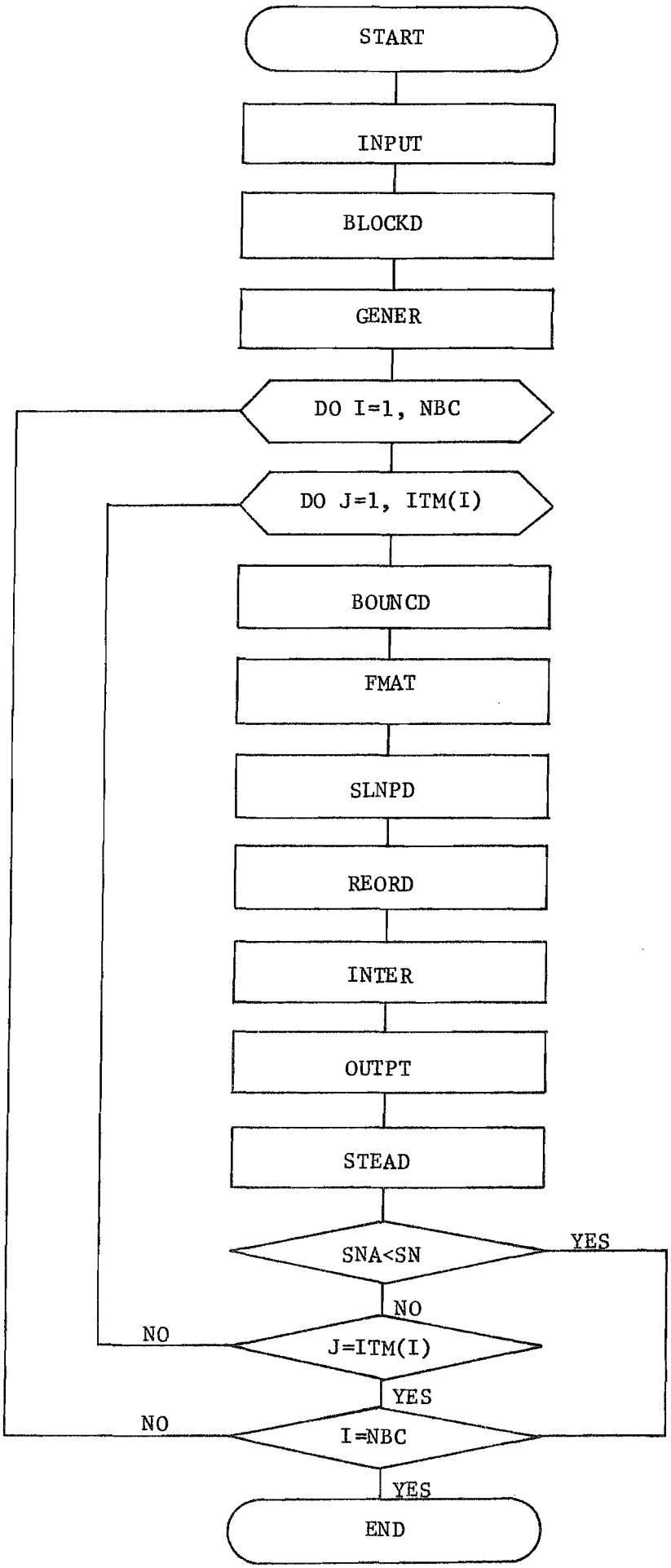

Figure 6.5.1 - Macro flow diagram of Program BEM2DTP2

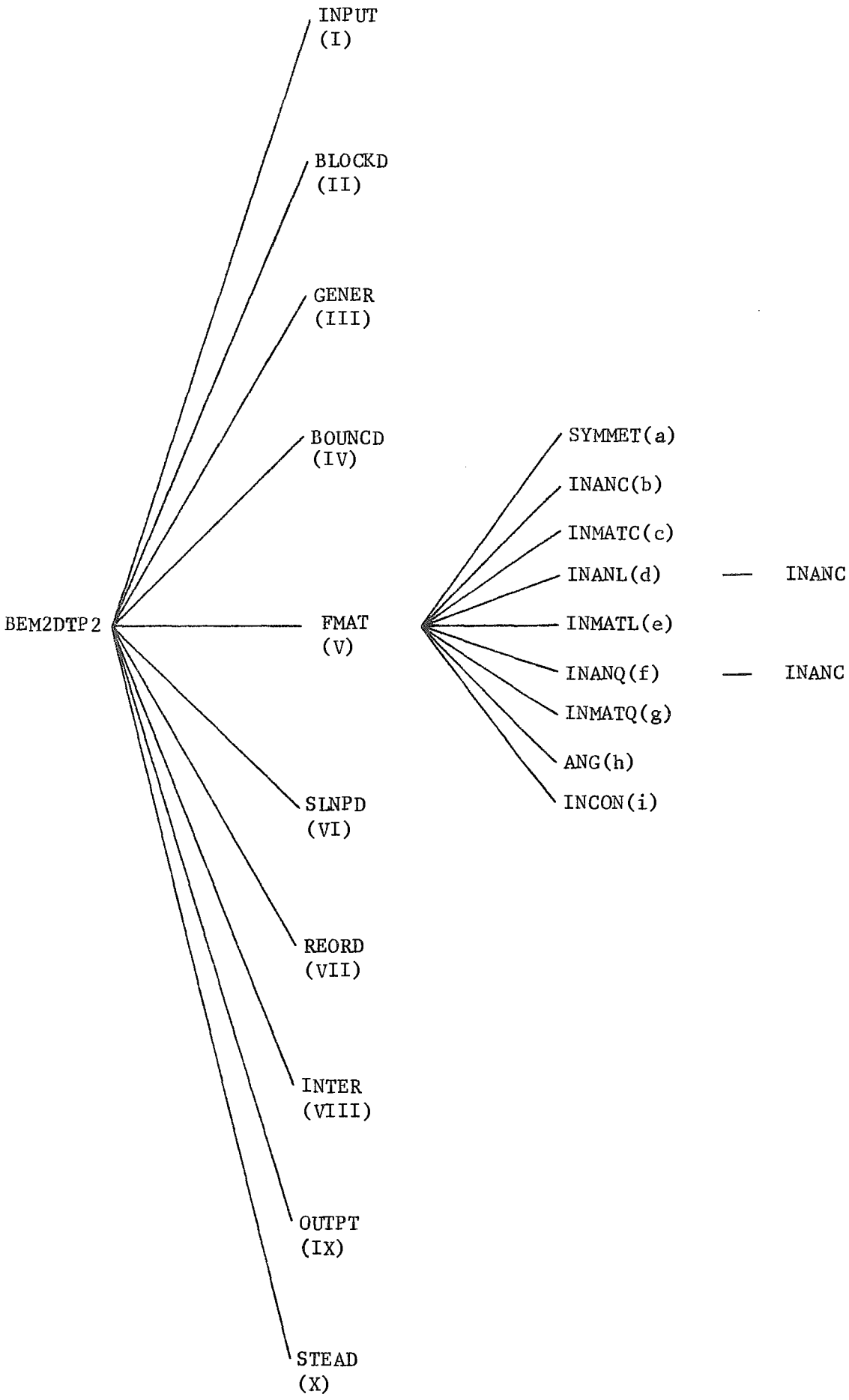

Figure 6.5.2 - Subroutines called by program BEM2DTP2

stepwise linear u and q; 3: stepwise linear u and quasi-quadratic q);

N, NE, L, M, NS, NBC, NUO: as in 6.4.

READ: TD, TI, SN

As in 6.4.

READ: (IPR(I), NL(I), I=1,M)

As in 6.4.

READ: (X1(I), X2(I), KODE(I), I=1,N)

As in 6.4.

If NUO is equal to 1,

READ: (DUO(I), DFUO(I), I=1,N)

DUO(I): initial value u_0 of function u;

DFUO(I): initial value q_0 of function q.

If ITP is greater than 1,

READ: (FIO(I), DFIO(I), I=1,N)

As in 6.4.

READ: (ITM(I), TS(I), I=1,NBC)

As in 6.4.

READ: (FI(I1,J), DFI(I1,J), J=1,N, 1=1,NBC)

As in 6.4.

If the value of u is required at a number of internal points,

READ (X1(I), X2(I), I=N+1, N+L)

As in 6.4.

II SUBROUTINE BLOCKD

In this subroutine,the following numerical data are given and kept in COMMON,

(a) The coordinates of integration points and the weighting factors for the (six-points and two-points) Gaussian numerical integration schemes, employed in the computation of boundary integrals;

(b) The coefficients of the polynomial and rational approximations of the exponential-integral (appendix A).

III SUBROUTINE GENER

The boundary elements connectivity is generated, their length calculated and a parameter for the symmetry loop is set, being all these values printed.

IV SUBROUTINE BOUNCD

This subroutine computes and stores the actual boundary condition values.

V SUBROUTINE FMAT

This subroutine computes one of the following:

(a) The coefficients of matrices $\underset{\sim}{G}_{fF}$ and $\underset{\sim}{H}_{fF}$ (f=1,2,...,F) in equation (4.1.8), if ITP=1;

(b) The coefficients of matrices $\underset{\sim}{G}^{1}_{fF}$, $\underset{\sim}{G}^{2}_{fF}$, $\underset{\sim}{H}^{1}_{fF}$ and $\underset{\sim}{H}^{2}_{fF}$ (f=1,2,...,F) in equation (4.1.17), if ITP=2;

(c) The coefficients of matrices $\underset{\sim}{G}^{1}_{fF}$, $\underset{\sim}{G}^{2}_{fF}$, $\underset{\sim}{G}^{3}_{fF}$, $\underset{\sim}{H}^{1}_{fF}$ and $\underset{\sim}{H}^{2}_{fF}$ (f=1,2,...,F) in equation (4.5.8), if ITP=3.

Matrices $\underset{\sim}{G}_{FF}$ and $\underset{\sim}{H}_{FF}$ (for the case when ITP=1), $\underset{\sim}{G}^{1}_{FF}$, $\underset{\sim}{G}^{2}_{FF}$, $\underset{\sim}{H}^{1}_{FF}$ and $\underset{\sim}{H}^{2}_{FF}$ (for ITP=2) or $\underset{\sim}{G}^{1}_{FF}$, $\underset{\sim}{G}^{2}_{FF}$, $\underset{\sim}{G}^{3}_{FF}$, $\underset{\sim}{H}^{1}_{FF}$ and $\underset{\sim}{H}^{2}_{FF}$ (for ITP=3) are conveniently reordered and stored (they only need to be recomputed when TS(I)$\neq$ TS(I-1)). The boundary conditions for the actual time step are multiplied by some of these matrices to form the vector $\underset{\sim}{F}$ of independent terms. The coefficients of matrices $\underset{\sim}{G}_{fF}$ and $\underset{\sim}{H}_{fF}$

(ITP=1), $\underset{\sim}{G}_{fF}^{1}$, $\underset{\sim}{G}_{fF}^{2}$, $\underset{\sim}{H}_{fF}^{1}$ and $\underset{\sim}{H}_{fF}^{2}$ (ITP=2) or $\underset{\sim}{G}_{fF}^{1}$, $\underset{\sim}{G}_{fF}^{2}$, $\underset{\sim}{G}_{fF}^{3}$, $\underset{\sim}{H}_{fF}^{1}$ and $\underset{\sim}{H}_{fF}^{2}$ (ITP=3), for f=1,2,...,F-1, are accordingly multiplied by the prescribed or calculated boundary values of q and u at previous time steps and the result added to vector $\underset{\sim}{F}$. If the initial conditions of the problem are not zero, the coefficients of matrices $\underset{\sim}{\overline{G}}$ and $\underset{\sim}{\overline{H}}$ in equation (4.3.4) are computed, multiplied by the initial conditions and the result of the product also added to vector $\underset{\sim}{F}$.

Note that the coefficients of the matrices corresponding to the actual time step are calculated using six Gaussian points while the coefficients of the matrices corresponding to the previous time steps are computed using only two integration points, and that the remarks made in section 6.4 regarding the variation of the parameter a are also valid here.

Va SUBROUTINE SYMMET

As described in section 6.4.

Vb SUBROUTINE INANC

The off-diagonal coefficients of matrices $\underset{\sim}{G}_{FF}$ and $\underset{\sim}{H}_{fF}$ (f=1,2,...,F) and all the coefficients of matrices $\underset{\sim}{G}_{fF}$ (f=1,2,...,F-1), for the case when ITP=1, are computed through numerical integration (equations (4.1.33)).

Vc SUBROUTINE INMATC

The diagonal coefficients of matrix $\underset{\sim}{G}_{FF}$, for ITP=1, are computed through analytical integration (equation (4.1.38)). The diagonal coefficients of matrices $\underset{\sim}{H}_{fF}$ (f=1,2,...,F-1) and $\underset{\sim}{\hat{H}}_{FF}$ are set to zero.

Vd SUBROUTINE INANL

The off-diagonal coefficients of matrices $\underset{\sim}{G}_{FF}^{2}$, $\underset{\sim}{H}_{fF}^{1}$ and $\underset{\sim}{H}_{fF}^{2}$ (f=1,2,...,F) and all the coefficients of matrices $\underset{\sim}{G}_{FF}^{1}$, $\underset{\sim}{G}_{fF}^{1}$ and $\underset{\sim}{G}_{fF}^{2}$ (f=1,2,...,F-1), for ITP=2, are computed through numerical

integration (equations 4.1.34)).

Ve SUBROUTINE INMATL

The diagonal coefficients of matrix $\underset{\sim}{G}^{2}_{FF}$, for ITP=2, are computed partly by analytical integration and partly by numerical integration (equation (4.1.42)). The contribution of the analytically integrated part is evaluated in INMATC. The diagonal coefficients of matrices $\underset{\sim}{H}^{1}_{fF}$ and $\underset{\sim}{H}^{2}_{fF}$ (f=1,2,...,F-1), $\underset{\sim}{H}^{1}_{FF}$ and $\hat{\underset{\sim}{H}}^{2}_{FF}$ are set to zero.

Vf SUBROUTINE INANQ

The off-diagonal coefficients of matrices $\underset{\sim}{G}^{3}_{FF}$, $\underset{\sim}{H}^{1}_{fF}$ and $\underset{\sim}{H}^{2}_{fF}$ (f=1,2,...,F) and all the coefficients of matrices $\underset{\sim}{G}^{1}_{FF}$, $\underset{\sim}{G}^{2}_{FF}$, $\underset{\sim}{G}^{1}_{fF}$, $\underset{\sim}{G}^{2}_{fF}$ and $\underset{\sim}{G}^{3}_{fF}$ (f=1,2,...,F-1) are computed through numerical integration (equations (4.5.10)).

Vg SUBROUTINE INMATQ

The diagonal coefficients of matrix $\underset{\sim}{G}^{3}_{FF}$, for ITP=3, are computed in a similar way as is done in INMATL. The diagonal coefficients of matrices $\underset{\sim}{H}^{1}_{fF}$ and $\underset{\sim}{H}^{2}_{fF}$ (f=1,2,...,F-1), $\underset{\sim}{H}^{1}_{FF}$ and $\hat{\underset{\sim}{H}}^{2}_{FF}$ are set to zero.

Vh SUBROUTINE ANG

As described in section 6.4.

If NUO=1,

Vi SUBROUTINE INCON

This subroutine computes the coefficients of matrices $\underset{\sim}{\overline{G}}$ and $\underset{\sim}{\overline{H}}$ through numerical integration (equation 4.3.4)).

VI SUBROUTINE SLNPD

As described in section 6.1.

VII SUBROUTINE REORD

In this subroutine, the values of q are calculated at the nodes with KODE(I)=2 using equation (4.5.4) if ITP=1, (4.5.5) if ITP=2 or (4.5.7) if ITP=3. For the latter, the values of

$$h_f(u_{s,f-1} - u_{f-1}) + h_{f-1}(u_{s,f} - u_f)$$

in equation (4.5.7) are also calculated. All these values are stored.

If there are internal points where the value of u is required,

VIII SUBROUTINE INTER

As described in section 6.4.

IX SUBROUTINE OUTPT

As described in section 6.1.

X SUBROUTINE STEAD

As described in section 6.4.

6.6 Description of Program BEMASTP1

The structure of this program is identical to the one for two-dimensional problems (figure 6.4.1), and the subroutines called by it are therefore the ones shown in figure 6.4.2. However, since only stepwise constant variations for u and q with time-marching scheme BEM1A were considered, only subroutines SYMMET, INANC, INMATC, ANG and INCON1 are now called by FMAT. Again, the system of coordinates adopted is cylindrical instead of cartesian and the subroutines that undergo some modifications are discussed in what follows.

I SUBROUTINE INPUT

In the first data card, it should be noted that the only admissible value for the parameter ITP is 1, therefore this parameter need not be given. Furthermore, since symmetry with respect to the Z-axis is implied, the parameter NS refers only to the R-axis and can assume the values 0 (no symmetry) or 1 (symmetry). In addition to that, initial

boundary values of u and q are not required anymore.

II SUBROUTINE BLOCKD

The data described in (c) (see section 6.4) are not any longer necessary.

IV SUBROUTINE FMAT

This subroutines computes the coefficients of matrices $\underset{\sim}{G}$, $\underset{\sim}{H}$ and $\underset{\sim}{B}$ in the axisymmetric equivalent of equation (4.1.6) and of matrices $\underset{\sim}{G}'$, $\underset{\sim}{H}'$ and $\underset{\sim}{B}'$ in the equivalent of (4.2.1) (see equation (4.6.5)). These matrices are conveniently reordered and stored.

IVb SUBROUTINE INANC

The off-diagonal coefficients of matrices $\underset{\sim}{G}$ and $\underset{\sim}{H}$ and all the coefficients of matrices $\underset{\sim}{G}'$ and $\underset{\sim}{H}'$ are computed through numerical integration. Three different cases are considered: when the coefficient c defined in equation (4.6.6) is less than 0.3 (value determined empirically), equations (4.6.9) and (4.6.12) are employed; when c is greater than 0.3 but the product axc (being the parameter a also defined in (4.6.6)) is less than 1.5, equation (4.6.21) and its equivalent for $\bar{q}^*$ are used; finally, when c is greater than 0.3 and the product axc is greater than 1.5, equations (4.6.18) and (4.6.19) are employed in the calculation.

IVc SUBROUTINE INMATC

The diagonal coefficients of matrices $\underset{\sim}{G}$ and $\underset{\sim}{\hat{H}}$ are computed partly by analytical integration and partly by numerical integration. The contribution of the analytically integrated part is computed through the appropriate set of formulae discussed in appendix C.

IVe SUBROUTINE INCON1

This subroutine computes the coefficients of matrices $\underset{\sim}{B}$ and $\underset{\sim}{B}'$

through a numerical integration over the domain which gives (see equations (4.2.5) and (4.6.3)),

$$B_{ij} = \frac{2\pi}{(4\pi k\Delta t)^{3/2}} \exp\left(-\frac{d_{ij}}{4k\Delta t}\right) I_0\left(\frac{\ell_{ij}}{2k\Delta t}\right) |J|_j R_j W_j$$

If there are internal points where the value of u is required,

VIII SUBROUTINE INTER

Computes the value of u at internal points by using equation (4.6.5).

7. CONCLUSIONS

The present work basically intended to review and extend the range of applications of the Boundary Element Method in connection with steady and transient potential and viscous flow problems.

To this end, chapter 2 started by discussing both the direct and the indirect formulations of the method as applied to steady potential problems governed by Laplace's equation. It was shown that the same integral relationships obtained for the direct formulation through Green's third identity can also be derived employing the weighted residual technique.

Several formulations for the BEM analysis of the diffusion equation were then discussed and boundary integral equations for each case derived by using weighted residual considerations. Since the formulation employing time-dependent fundamental solutions appears to be the most promising for general use, we concentrated our attention on the study of different time-marching schemes that can be adopted in association with it.

Numerical procedures for the solution of the boundary integral equation (3.1) for steady potential problems defined over two-dimensional, three-dimensional or axisymmetric regions were presented in chapter 3. Computer programs incorporating several of the features discussed in this chapter were developed (see chapter 6) and results of applications of such programs presented. For the axisymmetric case, new formulae for the analytical integration of the singular coefficients were derived (see appendix B) and found to be both accurate and efficient. If the solution of geotechnical engineering problems are to be attempted, a more realistic modelling of the soil should consider orthotropy, anisotropy or regions with different material properties. Although not implemented at present, these features can easily be included in the programs as shown in sections 3.4 and 3.5. Fundamental solutions for layered regions can also be derived as shown in section 3.7.

The programs developed (see description in sections 6.1 to 6.3) seem to predict reasonably accurate solutions and to be computationally efficient, thus they can be recommended for general applications. The use of quadratic elements should further improve the overall performance of the BEM since fewer elements (and probably fewer nodes) could be employed with a better description of the geometry and variation of the functions (see section 3.1.3).

The numerical solution of the boundary integral equation (4.1) for two-dimensional transient potential problems was discussed in chapter 4, where comparisons between results obtained with different time-marching schemes were also carried out. The advantages and disadvantages of each time-marching scheme can be summarized as follows:

a) BEM1A: as presently programmed, solutions obtained with this scheme were by far the fastest ones. Its accuracy, in general, was of the same order as that of scheme BEM2 (which produced the most accurate results), with the domain divided into only a few cells. However, as discussed in section 4.4, convergence with decreasing time step values was not always achieved, this problem being associated to truncation errors introduced in the computation of the domain integral. The choice of the domain integration scheme adopted (Hammer's) was largely influenced by its wide application in conjunction with the Finite Element Method. Tests were carried out regarding the number of integration points to be used, but few comparisons were made with other numerical integration schemes (see example 4.4.2). If a large number of cells is employed, implying that some domain integration points are located very near the boundary, a more refined boundary discretisation (or integration) is generally required (see tables 4.4.3 and 4.4.12). The relationship between the distance from the domain integration

points to the boundary and the size of the nearest boundary element needs to be further studied in order that guidelines regarding the boundary and domain discretisations can be set.

Another problem inherent in scheme BEM1A is the total amount of coefficients to be stored in the computer memory. As discussed in section 4.3, this number is dominated by the dimensions of matrix $\underset{\sim}{B'}$ (M x M), being M the product of the number of integration points in each cell (seven at present) by the total number of cells. If the geometry of the problem was such that a large number of boundary elements and cells was required in order to adequately represent it, the dimensions of matrix $\underset{\sim}{B'}$ would be large and, consequently, disc files would be necessary to store all the coefficients. This would probably occur in many practical situations, like the problem analysed in example 4.5.4. But due to the fast variation of the fundamental solution with r a large number of zero coefficients appears in this matrix (as well as in all the other matrices in the formulation), and advantage can be taken of this fact by storing only non-zero coefficients.

b) BEM1B: this scheme required the largest number of input data cards since very refined discretisations were usually needed. This seems to be more dependent on the assumption of linear variation for the function u within each cell than on the domain integration itself, which is accurately performed through a semi-analytical scheme. As pointed out in section 4.4, this approximation is similar to the one for linear finite elements and, as for FEM, great improvement should be obtained if higher order interpolation functions are employed. In fact, the only difference between this scheme and the previous one is the way the domain integral is computed, since the previous scheme does not place any restriction regarding the variation of u within each cell and directly integrates the function $(u^* u_{F-1})$ using a quintic quadrature.

With relation to the examples analysed with this scheme, we note that 4.4.1 and 4.4.3 involve problems with unbounded fluxes at $t = t_0^+$. So, as the time step value decreases, not only the behaviour of the fundamental solution tends to a Dirac delta but also the behaviour of function u itself tends to a step function. The assumption of linear variation of u within each cell then fails to adequately represent this behaviour. This can be clearly seen in tables 4.4.2 and 4.4.11 where the results for scheme BEM1B at early times were very poor; since the calculations at each time step use information from the previous one, these errors propagate, deteriorating the solution. Example 4.4.2 was seen to be particularly sensitive to the domain integration, and even the more accurate scheme BEM1A did not produce good results. It is worth pointing out that further analyses were carried out employing scheme BEM1B, with reasonably accurate solutions.

c) BEM2: this time-marching scheme presented the most accurate solutions and required the smallest number of data cards. It also proved to be convergent with decreasing time step values and refining discretisations. Its main problem, however, was the large computer CPU times reported even for solving some simple problems. This was mainly attributed to the way the corresponding computer program was devised, i.e. to the fact that the matrices accounting for the influence of previous time steps were always recomputed rather than stored. A discussion in section 4.4 showed that drastic reductions in the required CPU times can be achieved by storing these matrices (see table 4.4.14), although the use of disc files would then be necessary for problems involving a large number of boundary elements and time steps since the number of coefficients to be stored is proportional to $N^2 \times F$. Note that, as for scheme BEM1A, advantage can be taken of the sparsity

of the matrices and algorithms developed to store only non-zero coefficients.

Since this scheme appears to be the most promising,mainly if extension to three-dimensional problems are to be attempted, some work still needs to be directed towards improving its computer efficiency. For instance, a more selective time integration scheme could probably be adopted such that, after a certain number of steps, the number of integration points could be dropped to one or even zero. Another idea would be to take average values as representatives of the influence of a certain number of steps: if the actual value of time is large, consider that the influence of steps 1 to 5, for instance, is approximately given by that of step 3 times the number of steps it is representing (5 in this case). Yet another idea is to update the initial conditions after a certain number of steps, i.e. combine schemes BEM1A and BEM2 in order to explore the advantages of both.

Other improvements regarding computer efficiency can be made in all transient programs developed. Since most of the computer time is spent in calculating the coefficients of matrices $\underset{\sim}{G}$ and $\underset{\sim}{H}$ (and $\underset{\sim}{B}$, for schemes BEM1), some other quantities like unit normal vectors, coordinates of integration points, etc., can also be stored. The selective space integration scheme tested, although not presenting significant savings for the simple problems analysed, would probably produce additional savings for large problems. In this case, refined system solver algorithms that take advantage of the sparsity of the system matrix are also of importance.

The use of quadratic boundary elements, as for the steady-state case, should improve the overall performance of the method. On the other hand, the use of stepwise quadratic variations for u and q as discussed in section 4.1.3 implies the computation of a much larger

number of coefficients and the stepwise solution of a system of equations of order 2N x 2N instead of N x N: the advantages of such approximation (if any) remain an open question.

The previous discussion also applies to three-dimensional and axisymmetric problems. Although numerical solutions of equation (4.1) for problems defined over fully three-dimensional regions were not explicitly considered, they follow almost exactly the same procedures derived in chapter 4. In particular, for stepwise constant variations of u and q, the analytical time integration of the fundamental solution and its normal derivative (see equations (4.1.10) and (4.1.13)) produces the incomplete Gamma functions $\Gamma(1/2, a)$ and $\Gamma(3/2, a)$, respectively. The resulting expressions can then be numerically integrated with respect to space following the procedures discussed in section 3.8 and employing polynomial approximations for the incomplete Gamma functions (see equations (4.6.13), (4.6.14) and appendix A). If a step-by-step time marching scheme of the type BEM1 is employed, the domain integration can be performed by using the numerical integration scheme suggested in [67].

The numerical solution of the boundary integral equation (4.1) for problems defined over axisymmetric regions (assuming that all variables are also axisymmetric) was dealt with in section 4.6. The axisymmetric fundamental solution was explicitly obtained by directly integrating the three-dimensional one over a ring (as was done in the steady-state case). Since both the fundamental solution and its normal derivative were expressed in terms of Bessel functions, series expansions of these functions had to be introduced in order to permit the analytical evaluation of the time integrals in the boundary integral equation. The resulting space integrals were calculated numerically, apart from the singular ones. Analytical expressions for the singular integrals were derived in appendix C, where the different situations

that may occur in practice were all accounted for. Results of several analyses were presented, with an accuracy comparable to that of two-dimensional problems. Despite the complexity of the arithmetics involved, the computer CPU times required were not large.

Comparisons between BEM solutions and available FEM solutions showed that, in general, the BEM results are more accurate for equivalent (or even coarser) discretisations. This suggests that computer programs employing the BEM, if efficiently programmed, can be a viable alternative to the FEM for the solution of many practical problems (see example 4.5.4). Note that features like sub-regions, orthotropy and anisotropy, internal sources and semi-infinite regions can be incorporated in the computer programs in a similar way as was done for the steady-state case (see chapter 3).

No error analysis was attempted in the present work. As pointed out in [1], any error analysis which seeks to trace the accumulation of error as it arises from the many different sources (approximation of the geometry of the body, piecewise approximation in space and time of each unknown in equation (4.1), approximate evaluation of integrals using numerical integration schemes, etc.) is likely to be very complicated, if indeed it is possible at all. The analysis performed in [78] only considers errors arising from the piecewise approximation of the functions in space and time and suggests a criterion for determination of the critical time step value (relative to accuracy) somewhat arbitrarily. This criterion was seen to predict rather low critical values and much larger time steps were employed in the problems analysed with no deterioration of the numerical solution.

With regard to stability considerations, we note that the BEM formulation is implicit in character and thus relatively free from stability problems, as can be seen from the results of several of the

examples analysed (for instance 4.4.7, 4.4.8, 4.5.2 and 4.5.3).

Finally, a formulation of the BEM for the solution of problems of incompressible viscous fluid motion governed by the Navier-Stokes equations (together with the continuity equation) was derived, employing the concepts presented by Lighthill [31].

For steady-state problems, the numerical method of solution follows that proposed in [93], where it appears under the name of integral representation method. As showed here, this method is basically an extension of the BEM and as such, the numerical techniques discussed in chapter 3 can be directly applied in its formulation. A numerical result for a square cavity flow problem with Reynolds number equals to 600 was presented in [93], employing linear boundary elements and triangular cells within which the functions ω, $v_1\omega$ and $v_2\omega$ were also assumed to vary linearly. The accuracy of the solution seems to be quite reasonable.

The numerical method of solution of transient problems follows the ones proposed in [38] and [92]. In [92], the method appears as a completely novel technique, totally unrelated to all previous formulations and, according to the authors, requiring the development of entirely new numerical procedures. Again, it was shown here that this formulation is a direct extension of the BEM as applied to the diffusion equation, where the vorticity transport equation is treated as a non-homogeneous diffusion equation, the non-homogeneity accounting for the non-linear convective term.

Some numerical results were presented in [92] for asymptotically obtained steady-state solutions, employing stepwise linear variations for all functions, linear boundary elements and triangular cells with linear interpolation functions. However, no details were given about the numerical integration schemes adopted and numerical problems arising in the formulation.

Clearly, the use of a time-marching scheme of the type BEM2 is impractical in this case due to the presence of the convective term, which would have to be included through a summation of domain integrals. The time-marching scheme adopted in [92] is of the type BEM1B: although the variation of the vorticity within the domain is generally smooth, care has to be taken due to the numerical problems that appear when using very small time step values.

Note that since for transient problems the vorticity boundary values are not computed from a direct enforcement of satisfaction of the no-slip condition at solid boundaries using equations (5.2.7) and (5.2.8) (as was done in the steady-state case), there is no reason to preclude the use of a time-marching scheme of the type BEM1A.

Computer programs for the solution of the above-mentioned problems are currently under way, and it is hoped that the experience gained in the solution of the Laplace and diffusion equations will help in deciding which numerical procedures are best suited for these problems, and that extensions to three-dimensional and axisymmetric analyses can also be developed following the numerical procedures derived in this work.

REFERENCES

1. M.A. JASWON and G.T. SYMM, Integral Equation Methods in Potential Theory and Elastostatics, Academic Press, London, 1977.
2. C.A. BREBBIA, The Boundary Element Method for Engineers, Pentech Press, London, 1978.
3. C.A. BREBBIA and S. WALKER, Boundary Element Techniques in Engineering, Newnes-Butterworths, London, 1980.
4. T.A. CRUSE and F.J. RIZZO (eds.), Boundary Integral Equation Method: Computational Applications in Applied Mechanics, ASME, AMD-11, New York, 1975.
5. T.A. CRUSE, J.C. LACHAT, F.J. RIZZO and R.P. SHAW (eds.), First Int. Symp. on Innovative Numerical Analysis in Applied Engineering Science, CETIM, Versailles, 1977.
6. C.A. BREBBIA (ed.), Recent Advances in Boundary Element Methods, Pentech Press, London 1978.
7. P.K. BANERJEE and R. BUTTERFIELD (eds.), Developments in Boundary Element Methods, Applied Science Publishers, London, 1979.
8. C.A. BREBBIA (ed.), New Developments in Boundary Element Methods, C.M.L. Publications, Southampton, 1980.
9. R.P. SHAW et al. (eds.), Innovative Numerical Analysis for the Engineering Sciences, University Press of Virginia, Charlotesville, 1980.
10. C.A. BREBBIA (ed.), Progress in Boundary Elements, Vol. 1, Pentech Press, London, 1981.
11. I. FREDHOLM, Sur une classe d'equations fonctionelles, Acta Math. 27, 365-390, 1903.
12. V.D. KUPRADZE, Potential Methods in the Theory of Elasticity, Israel Program for Scientific Translations, Jerusalem, 1965.
13. O.D. KELLOGG, Foundations of Potential Theory, Springer, Berlin, 1929.

14. C. SOMIGLIANA, Sopra l'equilibrio di un corpo elastico isotropo,Il Nuovo Cimento, t. 17-19, 1886.

15. P.M. MORSE and H. FESHBACH, Methods of Theoretical Physics, McGraw-Hill, New York, 1953.

16. H.S. CARSLAW and J.C. JAEGER, Conduction of Heat in Solids, 2nd edn, Clarendon Press, Oxford, 1959.

17. G.F. ROACH, Green's Functions: Introductory Theory with Applications, Van Nostrand Reinhold, London, 1970.

18. M.A. JASWON, Integral equation methods in potential theory I, Proc. Royal Society A, 275, 23-32, 1963.

19. G.T. SYMM, Integral equation methods in potential theory II, Proc. Royal Society A, 275, 33-46, 1963.

20. M.A. JASWON and A.R. PONTER, An integral equation solution of the torsion problem, Proc. Royal Society A, 273, 237-246, 1963.

21. J.L. HESS and A.M.O. SMITH, Calculation of potential flow about arbitrary bodies, Progress in Aeronautical Sciences, Vol. 8, D. Küchemann (ed.), Pergamon Press, London, 1967.

22. R.F. HARRINGTON, K. PONTOPPIDAN, P. ABRAHAMSEN and N.C. ALBERTSEN, Computation of Laplacian potentials by an equivalent-source method, Proc. IEE, Vol. 116, No. 10, 1715-1720, 1969.

23. J.R. MAUTZ and R.F. HARRINGTON, Computation of rotationally symmetric Laplacian potentials, Proc. IEE, Vol. 117, No. 4, 850-852, 1970.

24. F.J. RIZZO and D.J. SHIPPY, A method of solution for certain problems of transient heat conduction, AIAA Journal, Vol. 8, No. 11, 2004-2009, 1970.

25. R. BUTTERFIELD and G.R. TOMLIM, Integral techniques for solving zoned anisotropic continuum problems, Proc. Int. Conf. on Variational Methods in Engineering, Vol. 2, C.A. Brebbia and H. Tottenham (eds.), Southampton University Press, Southampton, 1972.

26. G.R. TOMLIM, Numerical Analysis of Continuum Problems in Zoned Anisotropic Media, Ph.D. Thesis, Southampton University, Southampton, 1972.

27. Y.P. CHANG, C.S. KANG and D.J. CHEN, The use of fundamental Green's functions for the solution of problems of heat conduction in anisotropic media, Int. Journal Heat Mass Transfer, Vol. 16, 1905-1918, 1973.

28. R.P. SHAW, An integral equation approach to diffusion, Int. Journal Heat Mass Transfer, Vol. 17, 693-699, 1974.

29. L.C. WROBEL and C.A. BREBBIA, The boundary element method for steady-state and transient heat conduction, Proc. First Int. Conf. on Numerical Methods in Thermal Problems, R.W. Lewis and K. Morgan (eds.), Pineridge Press, Swansea, 1979.

30. L.C. WROBEL and C.A. BREBBIA, A formulation of the boundary element method for axisymmetric transient heat conduction, Int. Journal Heat Mass Transfer, Vol. 24, 843-850, 1981.

31. M.J. LIGHTHILL, Introduction. Boundary layer theory, chapter 2 in Laminar Boundary Layer, L. Rosenhead (ed.), Oxford University Press, 1963.

32. R.B. PAYNE, Calculations of unsteady viscous flow past a circular cylinder, J. Fluid Mechanics, Vol. 4, 81-86, 1958.

33. J.C. WU and J.F. THOMPSON, Numerical solutions of time-dependent incompressible Navier-Stokes equations using an integro-differential formulation, Computer and Fluids, Vol. 1, 197-215, 1973.

34. R.A. SCHMALL and R.B. KINNEY, Numerical study of unsteady viscous flow past a lifting plate, AIAA Journal, Vol. 12, No. 11, 1566-1573, 1974.

35. T. BRATANOW and T. SPEHERT, Computational flow development for unsteady viscous flow, NASA CR-2995, 1978.

36. L.M. MILNE-THOMPSON, Theoretical Aerodynamics, 4th edn, Dover, New York, 1958.

37. J.C. WU, Numerical boundary conditions for viscous flow problems, AIAA Journal, Vol. 14, No. 8, 1042-1049, 1976.

38. C.A. BREBBIA and L.C. WROBEL, The boundary element method, chapter 2 in Computer Methods in Fluids, K. Morgan, C. Taylor and C.A. Brebbia (eds.), Pentech Press, London, 1980.

39. W. POGORZELSKI, Integral Equations and Their Applications, Pergamon Press, Oxford, 1966.

40. T.A. CRUSE, Boundary Integral Equation Methods in Solid Mechanics, Report SM-73-17, Dept. of Mechanical Engng, Carnegie-Mellon University, Pittsburgh, 1973.

41. R. COURANT and D. HILBERT, Methods of Mathematical Physics, Vol. 2, Interscience Publishers, New York, 1962.

42. W.J. STERNBERG and T.L. SMITH, The Theory of Potential and Spherical Harmonics, University of Toronto Press, Toronto, 1944.

43. L.V. KANTOROWICH and V.I. KRYLOV, Approximate Methods of Higher Analysis, Noordhoff, Groningen, 1958.

44. G.F. MILLER, Fredholm equations of the first kind, chapter 13 in Numerical Solution of Integral Equations, L.M. Delves and J. Walsh (eds.), Clarendon Press, Oxford, 1974.

45. V.D. WIDDER, The Laplace Transform, Princeton University Press, Princeton, 1946.

46. M. ABRAMOWITZ and I.A. STEGUN (eds.), Handbook of Mathematical Functions, Dover, New York, 1965.

47. J.C. LACHAT and A. COMBESCURE, Laplace transform and boundary integral equation: application to transient heat conduction problems, in [5].

48. R.A. SCHAPERY, Approximate methods of transform inversion for viscoelastic stress analysis, Proc. Fourth U.S. National Congress on Applied Mechanics, Vol. 2, 1962.

49. J.A. LIGGETT and P.L.F. LIU, Unsteady flow in confined aquifers: a comparison of two boundary integral methods, Water Resources Research, Vol. 15, No. 4, 861-866, 1979.

50. D.A.S. CURRAN, M. CROSS and B.A. LEWIS, Solution of parabolic differential equations by the boundary element method using discretisation in time, Applied Mathematical Modelling, Vol. 4, No. 5, 398-400, 1980.

51. R.F. HARRINGTON, Field Computation by Moment Methods, MacMillan, New York, 1968.

52. A. MARTIN, I. RODRIGUEZ and E. ALARCON, Mixed elements in the boundary theory, in [8].

53. T.A. CRUSE, An improved boundary integral equation method for three-dimensional elastic stress analysis, Computers and Structures, Vol. 4, 741-754, 1974.

54. P. MOON and D.E. SPENCER, Field Theory Handbook, 2nd edn, Springer Verlag, Berlin, 1971.

55. N. PAPAMICHAEL and J.R. WHITEMAN, A numerical conformal transformation method for harmonic mixed boundary-value problems in polygonal domains, J. Appl. Math. Phys. (ZAMP), Vol. 24, 304-316, 1973.

56. R. WAIT and A.R. MITCHELL, Corner singularities in elliptic problems by finite element methods, J. Comp. Phys., Vol. 8, No. 1, 45-52, 1971.

57. C.A. BREBBIA and L.C. WROBEL, Applications of boundary elements in fluid flow, Proc. Second Int. Conf. on Finite Elements in Water Resources, Pentech Press, London, 1978.

58. J.A. LIGGETT, Location of free surface in porous media, ASCE J. Hydraulics Division, Vol. 103, No. 4, 353-365, 1977.

59. C.A. BREBBIA and L.C. WROBEL, Steady and unsteady potential problems using the boundary element method, chapter 1 in Recent Advances in Numerical Methods in Fluids, C. Taylor and K. Morgan (eds.), Pineridge Press, Swansea, 1980.

60. J.J. CONNOR and C.A. BREBBIA, Finite Element Techniques for Fluid Flow, Newnes-Butterworths, London, 1976.

61. V.T. CHOW, Open-Channel Hydraulics, McGraw-Hill, New York, 1959.

62. E.L. WILSON and R.E. NICKELL, Application of the finite element method to heat conduction analysis, Nuclear Engng Design, Vol. 4, 276-286, 1966.

63. B.A. PEAVY, Steady-state heat conduction in an exposed exterior column of rectangular cross-section, J. Res. Natl Bur. Stand., Vol. 69C, 145-151, 1965.

64. P.W. FRANCE, C.J. PAREKH, J.C. PETERS and C. TAYLOR, Numerical analysis of free surface seepage problems, J. Irrigation and Drainage Division, ASCE, Vol. 97, No. IR1, 165-179, 1971.

65. P.C. HAMMER, O.J. MARLOWE and A.H. STROUD, Numerical integration over simplexes and cones, Mathematics of Computation, Vol. 10, 130-137, 1956.

66. G.K. BATCHELOR, An Introduction to Fluid Dynamics, Cambridge University Press, Cambridge, 1967.

67. R.K. NAKAGUMA, Three-Dimensional Elastostatics using the Boundary Element Method, Ph.D. Thesis, Southampton University, Southampton, 1979.

68. O.V. CHANG, Boundary Elements applied to Seepage Problems in Zoned Anisotropic Soils, M.Sc. Thesis, Southampton University, Southampton, 1979.

69. W.L. WOOD, On the finite element solution of an exterior boundary-value problem, Int. Journal Num. Methods Engng, Vol. 10, No. 4, 885-891, 1976.

70. H. GOLDENBERG, External thermal resistance of two buried cables, Proc. IEE, Vol. 116, No. 5, 822-826, 1969.

71. C. SNOW, Hypergeometric and Legendre Functions with Applications to Integral Equations of Potential Theory, Applied Mathematical Series No. 19, National Bureau of Standards, Washington, D.C., 1952.

72. A. ERDELYI et al., Higher Transcendental Functions, Vol. 1, Bateman Manuscript Project, McGraw-Hill, New York, 1953.

73. L.C. WROBEL and C.A. BREBBIA, Axisymmetric potential problems, in [8].

74. O.C. ZIENKIEWICZ and Y.K. CHEUNG, Finite elements in the solution of field problems, The Engineer, Vol. 220, 507-510, 1965.

75. I.S. GRADSHTEYN and I.M. RYZHIK, Table of Integrals, Series and Products, Academic Press, London, 1965.

76. L.C. WROBEL and C.A. BREBBIA, Boundary elements in thermal problems, chapter 5 in Numerical Methods in Heat Transfer, R.Lewis, K. Morgan and O.C.Zienkiewicz (eds.), J.Wiley, Chichester, 1981.

77. C.T. REDDY and D.J. SHIPPY, Alternative integration formulae for triangular finite elements, Int. Journal Num. Methods Engng, Vol. 17, No. 1, 133-139, 1981.

78. K. ONISHI and T. KUROKI, Boundary Element Method in Transient Heat Transfer Problems, Report No. 3, Civil Engineering and Applied Mathematics, The Institute for Advanced Research, Fukuoka University, Japan, 1980.

79. D. CURRAN, M. CROSS and B.A. LEWIS, A preliminary analysis of boundary element methods applied to parabolic partial differential equations, in [8].

80. J.C. BRUCH, JR. and G. ZYVOLOSKI, Transient two-dimensional heat conduction problems solved by the finite element method, Int. Journal Num. Methods Engng, Vol. 8, No. 3, 481-494, 1974.

81. W.L. WOOD and R.W. LEWIS, A comparison of time marching schemes for the transient heat conduction equation, Int. Journal Num. Methods Engng, Vol. 9, No. 3, 679-689, 1975.

82. L.C. WROBEL and C.A. BREBBIA, Time-dependent potential problems, in [10].

83. W. KÖHLER and J. PITTR, Calculation of transient temperature fields with finite elements in space and time dimensions, Int. Journal Num. Methods Engng, Vol. 8, No. 3, 625-631, 1974.

84. O.C. ZIENKIEWICZ and C.J. PAREKH, Transient field problems: two-dimensional and three-dimensional analysis by isoparametric finite elements, Int. Journal Num. Methods Engng, Vol. 2, No. 1, 61-71, 1970.

85. ROLLS ROYCE LTD. (DERBY), Private Communication.

86. G.N. WATSON, A Treatise on the Theory of Bessel Functions, 2nd edn, Cambridge University Press, Cambridge, 1944.

87. A. HAJI-SHEIK and E.M. SPARROW, Transient heat conduction in a prolate spheroidal solid, J. Heat Transfer, Trans. ASME, Vol. 88C, 331-333, 1966.

88. I.H. ABBOTT and A.E. VON DOENHOFF, Theory of Wing Sections, Dover, New York, 1959.

89. C.A. BREBBIA and A.J. FERRANTE, Computational Methods for the Solution of Engineering Problems, Pentech Press, London, 1978.

90. C.A. BREBBIA (ed.), Further Developments in Boundary Element Methods, C.M.L. Publications, Southampton, 1981.

91. K.H. HUEBNER, The Finite Element Method for Engineers, J. Wiley, New York, 1975.

92. J.C. WU and Y.M. RIZK, Integral-representation approach for time-dependent viscous flow, Lecture Notes in Physics, Vol. 90, 558-564, Springer Verlag, New York, 1978.

93. J.C. WU and M.M. WAHBAH, Numerical solution of viscous flow equations using integral representations, Lecture Notes in Physics, Vol. 59, 448-453, Springer Verlag, New York, 1976.

94. Z.M. CIELAK and R.B. KINNEY, Analysis of unsteady viscous flow past an airfoil: Part I - theoretical development, AIAA Journal, Vol. 15, No. 12, 1712-1717, 1977.

APPENDIX A

For convenience of the numerical computation, the special functions that appear throughout the main text can be evaluated by using polynomial and rational approximations as follows [46]:

Complete Elliptic Integrals

$$K(m) = 1.3862944 + 0.1119723\, m_1 + 0.0725296\, m_1^2 + (0.5 + 0.1213478\, m_1 + 0.0288729\, m_1^2)\log(1/m_1) + \varepsilon(m)$$

$$0 \leqslant m < 1, \quad m_1 = 1 - m, \quad |\varepsilon(m)| \leqslant 3 \times 10^{-5}$$

$$E(m) = 1. + 0.4630151\, m_1 + 0.1077812\, m_1^2 + (0.2452727\, m_1 + 0.0412496\, m_1^2)\log(1/m_1) + \varepsilon(m)$$

$$0 \leqslant m < 1, \quad |\varepsilon(m)| < 4 \times 10^{-5}$$

Exponential-Integral

$$E_1(x) = -0.57721566 + 0.99999193\, x - 0.24991055\, x^2 + 0.05519968\, x^3 - 0.00976004\, x^4 + 0.00107857\, x^5 - \log x + \varepsilon(x)$$

$$0 \leqslant x \leqslant 1, \quad |\varepsilon(x)| < 2 \times 10^{-7}$$

$$E_1(x) = (x^4 + 8.5733287401\, x^3 + 18.0590169730\, x^2 + 8.6347608925\, x + 0.2677737343) / [(x^4 + 9.5733223454\, x^3 + 25.6329561486\, x^2 + 21.0996530827\, x + 3.9584969228)\, x\, e^x] + \varepsilon(x)$$

$$1 \leqslant x < \infty, \quad |\varepsilon(x)| < 2 \times 10^{-8}$$

Error Function

$$\operatorname{erf}(x) = 1 - (0.3480242 - 0.0958798\, m + 0.7478556\, m^2)\, m\, e^{-x^2} + \varepsilon(x)$$

$$m = \frac{1}{1+0.47047\, x}, \quad \operatorname{erfc}(x) = 1 - \operatorname{erf}(x)$$

$$0 \leqslant x < \infty, \quad |\varepsilon(x)| \leqslant 2.5 \times 10^{-5}$$

APPENDIX B

In this appendix, the G_{ii} coefficients for axisymmetric steady potential problems are derived by means of analytical integration of the corresponding singular integrals.

Constant Elements

With reference to figure B.1, we can write:

$$R(S) = R(P) - \xi \frac{\ell}{2} \sin \alpha$$
$$Z(S) = Z(P) + \xi \frac{\ell}{2} \cos \alpha \qquad (B.1)$$
$$\gamma = 1 + \frac{\xi^2 \ell^2}{8R(P)R(S)}$$

Thus, the expression to be evaluated is of the form,

$$G_{ii} = \int_{-\ell/2}^{\ell/2} \bar{u}^*(P,S)\, R(S)\, d\bar{\Gamma}(S) = \frac{\ell}{R^{\frac{1}{2}}(P)} \left\{ -\frac{1}{2} \log\left(\frac{\ell^2}{256R(P)}\right) \int_{-1}^{1} R^{\frac{1}{2}}(S)\, d\xi + \frac{1}{2} \int_{-1}^{1} R^{\frac{1}{2}}(S) \log[R(S)]\, d\xi - \int_{-1}^{1} R^{\frac{1}{2}}(S) \log|\xi|\, d\xi \right\} \qquad (B.2)$$

where the first and second integrals are regular and the last one is calculated in the normal sense of improper integrals.

Calling:

$$a = R(P) \quad ; \quad b = -\frac{\ell}{2} \sin \alpha$$
$$c = a + b \quad ; \quad D = a - b \qquad (B.3)$$

the integrals give,

$$G_{ii} = \frac{\ell}{3ba^{\frac{1}{2}}} \left\{ \left[\frac{2}{3} - \log\left(\frac{\ell^2}{256a}\right) \right] (C^{3/2} - D^{3/2}) + C^{3/2} \log C - D^{3/2} \log D + 4a(C^{\frac{1}{2}} - D^{\frac{1}{2}}) - 2a^{3/2} \left(\log \left| \frac{C^{\frac{1}{2}} + a^{\frac{1}{2}}}{C^{\frac{1}{2}} - a^{\frac{1}{2}}} \right| - \log \left| \frac{D^{\frac{1}{2}} + a^{\frac{1}{2}}}{D^{\frac{1}{2}} - a^{\frac{1}{2}}} \right| \right) \right\} \qquad (B.4)$$

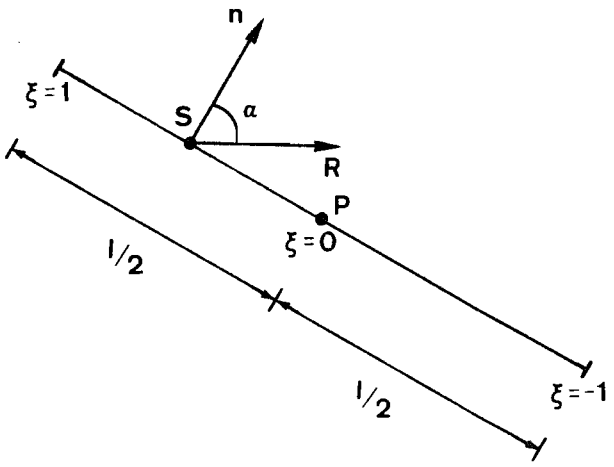

Figure B.1 - Definitions for constant element

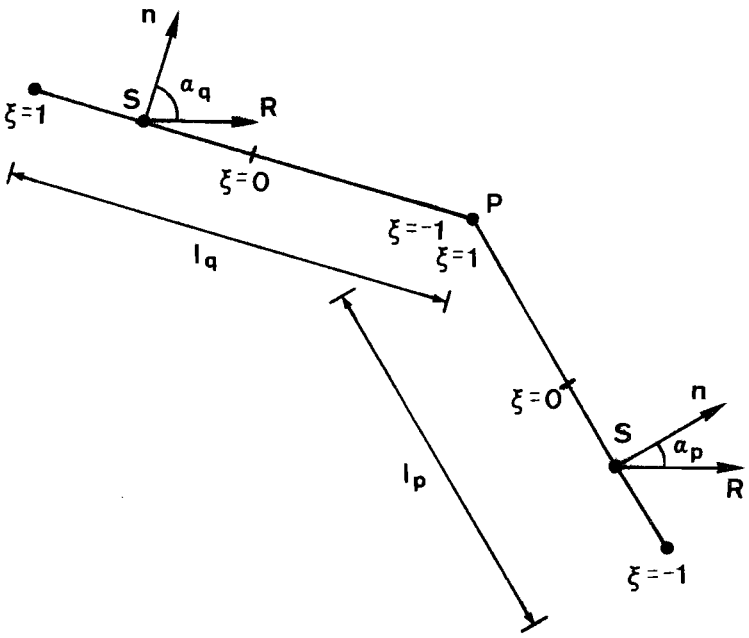

Figure B.2 - Definitions for linear element

For $\sin\alpha = 0$ ($b = 0$), we can take the limit of each term in (B.4) and the expression becomes simply,

$$G_{ii} = 2\ell\left[1 - \log\left(\frac{\ell}{16a}\right)\right] \tag{B.5}$$

Linear Elements

The G_{ii} coefficients now consist of the sum of two terms (see equations (3.1.18) and (3.1.20)),

$$G_{ii} = g_{ip}^{\ 2} + g_{iq}^{\ 1} \tag{B.6}$$

where we have, for element p (with reference to figure B.2),

$$\begin{aligned} R(S) &= R(P) + (1-\xi)\frac{\ell_p}{2}\sin\alpha_p \\ Z(S) &= Z(P) - (1-\xi)\frac{\ell_p}{2}\cos\alpha_p \\ \gamma &= 1 + \frac{(1-\xi)^2\ell_p^{\ 2}}{8R(P)R(S)} \end{aligned} \tag{B.7}$$

and for element q,

$$\begin{aligned} R(S) &= R(P) - (1+\xi)\frac{\ell_q}{2}\sin\alpha_q \\ Z(S) &= Z(P) + (1+\xi)\frac{\ell_q}{2}\cos\alpha_q \\ \gamma &= 1 + \frac{(1+\xi)^2\ell_q^{\ 2}}{8R(P)R(S)} \end{aligned} \tag{B.8}$$

The expressions to be evaluated can now be written as,

$$g_{ip}^{\ 2} = \frac{\ell_p}{2R^{\frac{1}{2}}(P)}\left\{-\frac{1}{2}\log\left(\frac{\ell_p^{\ 2}}{256R(P)}\right)\int_{-1}^{1} R^{\frac{1}{2}}(S)\,(1+\xi)\,d\xi + \frac{1}{2}\int_{-1}^{1} R^{\frac{1}{2}}(S)\log[R(S)]\,(1+\xi)\,d\xi - \int_{-1}^{1} R^{\frac{1}{2}}(S)\log(1-\xi)\,(1+\xi)\,d\xi\right\} \tag{B.9}$$

$$g_{iq}^{\ 1} = \frac{\ell_q}{2R^{\frac{1}{2}}(P)}\left\{-\frac{1}{2}\log\left(\frac{\ell_q^{\ 2}}{256R(P)}\right)\int_{-1}^{1} R^{\frac{1}{2}}(S)\,(1-\xi)\,d\xi + \frac{1}{2}\int_{-1}^{1} R^{\frac{1}{2}}(S)\log[R(S)]\,(1-\xi)\,d\xi - \int_{-1}^{1} R^{\frac{1}{2}}(S)\log(1+\xi)\,(1-\xi)\,d\xi\right\} \tag{B.10}$$

in which R(S) is accordingly given by (B.7) or (B.8) and the last integral in each of the above formulas is calculated in the normal sense of improper integrals.

The final expressions for the G_{ii} coefficients are of the form,

$$g_{ip}^{2} = \frac{\ell_p}{2bR^{\frac{1}{2}}(P)} \left\{ -\frac{v}{3}\left(\frac{2}{3} + A_1\right)\left(C^{3/2} - D^{3/2}\right) - \frac{1}{5b}\left(\frac{2}{5} + A_1\right)\left(C^{5/2} - D^{5/2}\right) \right.$$

$$+ \frac{v}{3}\left(C^{3/2}\log C - D^{3/2}\log D\right) + \frac{1}{5b}\left(C^{5/2}\log C - D^{5/2}\log D\right)$$

$$- \frac{2v}{3}\left[D^{3/2}\left(\frac{2}{3} - \log 2\right) + 2CD^{1/2} - C^{3/2}\left(\frac{8}{3} + A_2\right)\right]$$

$$\left. - \frac{2}{5b}\left[D^{5/2}\left(\frac{2}{5} - \log 2\right) + 2C\left(\frac{1}{3}D^{3/2} + CD^{1/2}\right) - C^{5/2}\left(\frac{46}{15} + A_2\right)\right] \right\} \qquad (B.11)$$

$$g_{iq}^{1} = \frac{\ell_q}{2bR^{\frac{1}{2}}(P)} \left\{ -\frac{v}{3}\left(\frac{2}{3} + A_3\right)\left(C^{3/2} - D^{3/2}\right) + \frac{1}{5b}\left(\frac{2}{5} + A_3\right)\left(C^{5/2} - D^{5/2}\right) \right.$$

$$+ \frac{v}{3}\left(C^{3/2}\log C - D^{3/2}\log D\right) - \frac{1}{5b}\left(C^{5/2}\log C - D^{5/2}\log D\right)$$

$$+ \frac{2v}{3}\left[C^{3/2}\left(\frac{2}{3} - \log 2\right) + 2DC^{1/2} - D^{3/2}\left(\frac{8}{3} + A_4\right)\right]$$

$$\left. - \frac{2}{5b}\left[C^{5/2}\left(\frac{2}{5} - \log 2\right) + 2D\left(\frac{1}{3}C^{3/2} + DC^{1/2}\right) - D^{5/2}\left(\frac{46}{15} + A_4\right)\right] \right\} \qquad (B.12)$$

where:

$$A_1 = \log\left(\frac{\ell_p^{\,2}}{256R(P)}\right) \quad ; \qquad A_3 = \log\left(\frac{\ell_q^{\,2}}{256R(P)}\right)$$

$$A_2 = \log\left|\frac{b(C^{\frac{1}{2}}+D^{\frac{1}{2}})}{4C(C^{\frac{1}{2}}-D^{\frac{1}{2}})}\right| ; \qquad A_4 = \log\left|\frac{b(C^{\frac{1}{2}}+D^{\frac{1}{2}})}{4D(C^{\frac{1}{2}}-D^{\frac{1}{2}})}\right| \qquad (B.13)$$

with $a = R(P) - b$, $v = 1 - a/b$ in equation (B.11) and $a = R(P) + b$, $v = 1 + a/b$ in (B.12), being b, C and D computed as in (B.3).

For $\sin \alpha = 0$ ($b = 0$), these expressions simplify to

$$g_{ip}^{\ 2} = g_{iq}^{\ 1} = \frac{\ell}{2}\left[\frac{89}{30} + 2 \log \left(\frac{8a}{\ell}\right)\right] \qquad \text{(B.14)}$$

in which ℓ equals ℓ_p or ℓ_q, according to the element under consideration.

For the case when $R(P) = 0$, the fundamental solution becomes the three-dimensional one (multiplied by 2π) and the coefficients G_{ii} are equal to $g_{ip}^{\ 2}$ or $g_{iq}^{\ 2}$, being these terms calculated as follows,

$$g_{ip}^{\ 2} = \frac{\pi \ell}{2} \int_{-1}^{1} (1+\xi) \sin \alpha \, d\xi = \pi \ell_p \sin \alpha \qquad \text{(B.15)}$$

$$g_{iq}^{\ 1} = \frac{-\pi \ell_q}{2} \int_{-1}^{1} (1-\xi) \sin \alpha \, d\xi = -\pi \ell_q \sin \alpha \qquad \text{(B.16)}$$

APPENDIX C

In this appendix, the integration of the logarithmic singular terms that appear in the calculation of the G_{ii} and H_{ii} coefficients for axisymmetric transient potential problems is carried out analytically.

Two different cases have to be considered. As discussed in section 4.6, when the coefficient $c \to 0.5$ and the value of x is large throughout the integration interval (a,∞), asymptotic expansions of the Bessel functions can be directly employed. Thus, expanding the exponential-integral in equations (4.6.18) and (4.6.19) in order to isolate the logarithmic term (see equation (4.1.37)), the G_{ii} and $\hat{H}_{ii}$ coefficients can be divided as,

$$G_{ii} = g^{2}_{ip,s} + g^{2}_{ip,ns} + g^{1}_{iq,s} + g^{1}_{iq,ns} \tag{C.1}$$

$$\hat{H}_{ii} = h^{2}_{ip,s} + h^{2}_{ip,ns} + h^{1}_{iq,s} + h^{1}_{iq,ns} \tag{C.2}$$

where the subscript s stands for singular and ns for non-singular. For element p, we can write with reference to figure B.2,

$$\begin{aligned} R(S) &= R(P) + (1-\xi)\ \frac{\ell_p}{2} \sin\alpha_p \\ Z(S) &= Z(P) - (1-\xi)\ \frac{\ell_p}{2} \cos\alpha_p \\ B &= \frac{(1-\xi)^2\ \ell_p^2}{16k\Delta t} \end{aligned} \tag{C.3}$$

and for element q,

$$\begin{aligned} R(S) &= R(P) - (1+\xi)\ \frac{\ell_q}{2} \sin\alpha_q \\ Z(S) &= Z(P) + (1+\xi)\ \frac{\ell_q}{2} \cos\alpha_q \\ B &= \frac{(1+\xi)^2\ \ell_q^2}{16k\Delta t} \end{aligned} \tag{C.4}$$

The expressions to be evaluated are now of the form,

$$g^{2}_{ip,s} = -\frac{\ell_p}{16\pi R^{\frac{1}{2}}(P)}\left\{\log\left(\frac{\ell_p^2}{16k\Delta t}\right)\int_{-1}^{1} R^{\frac{1}{2}}(S)\,(1+\xi)\,d\xi\right.$$

$$\left.+2\int_{-1}^{1} R^{\frac{1}{2}}(S)\,\log(1-\xi)\,(1+\xi)\,d\xi\right\} \qquad (C.5)$$

$$g^{1}_{iq,s} = -\frac{\ell_q}{16\pi R^{\frac{1}{2}}(P)}\left\{\log\left(\frac{\ell_q^2}{16k\Delta t}\right)\int_{-1}^{1} R^{\frac{1}{2}}(S)\,(1-\xi)\,d\xi\right.$$

$$\left.+2\int_{-1}^{1} R^{\frac{1}{2}}(S)\,\log(1+\xi)\,(1-\xi)\,d\xi\right\} \qquad (C.6)$$

$$h^{2}_{ip,s} = \frac{\ell_p\cos\alpha_p}{32\pi R^{\frac{1}{2}}(P)}\left\{\log\left(\frac{\ell_p^2}{16k\Delta t}\right)\int_{-1}^{1} R^{-\frac{1}{2}}(S)\,(1+\xi)\,d\xi\right.$$

$$\left.+2\int_{-1}^{1} R^{-\frac{1}{2}}(S)\,\log(1-\xi)\,(1+\xi)\,d\xi\right\} \qquad (C.7)$$

$$h^{1}_{iq,s} = \frac{\ell_q\cos\alpha_q}{32\pi R^{\frac{1}{2}}(P)}\left\{\log\left(\frac{\ell_q^2}{16k\Delta t}\right)\int_{-1}^{1} R^{-\frac{1}{2}}(S)\,(1-\xi)\,d\xi\right.$$

$$\left.+2\int_{-1}^{1} R^{-\frac{1}{2}}(S)\,\log(1+\xi)\,(1-\xi)\,d\xi\right\} \qquad (C.8)$$

in which R(S) is accordingly given by (C.3) or (C.4) and the last integral in each of the above formulas is calculated in the normal sense of improper integrals.

Carrying out the integrals give,

$$g^{2}_{ip,s} = -\frac{\ell_p}{8\pi b R^{\frac{1}{2}}(P)}\left\{\frac{v}{3}A_1(C^{3/2}-D^{3/2}) + \frac{1}{5b}A_1\,(C^{5/2}-D^{5/2})\right.$$

$$+\frac{2v}{3}\left[D^{3/2}\left(\frac{2}{3}-\log 2\right) + 2CD^{1/2} - C^{3/2}\left(\frac{8}{3}+A_2\right)\right]$$

$$\left.+\frac{2}{5b}\left[D^{5/2}\left(\frac{2}{5}-\log 2\right) + 2C\left(\frac{1}{3}D^{3/2}+CD^{1/2}\right) - C^{5/2}\left(\frac{46}{15}+A_2\right)\right]\right\} \qquad (C.9)$$

$$g^{1}_{iq,s} = -\frac{\ell_q}{8\pi b R^{\frac{1}{2}}(P)} \left\{ \frac{v}{3} A_3 \left(C^{3/2} - D^{3/2}\right) - \frac{1}{5b} A_3 \left(C^{5/2} - D^{5/2}\right) \right.$$

$$- \frac{2v}{3} \left[C^{3/2} \left(\frac{2}{3} - \log 2\right) + 2DC^{1/2} - D^{3/2} \left(\frac{8}{3} + A_4\right) \right]$$

$$\left. + \frac{2}{5b} \left[C^{5/2} \left(\frac{2}{5} - \log 2\right) + 2D \left(\frac{1}{3} C^{3/2} + DC^{1/2}\right) - D^{5/2} \left(\frac{46}{15} + A_4\right) \right] \right\} \qquad (C.10)$$

$$h^{2}_{ip,s} = \frac{\ell_p \cos\alpha}{16\pi b R^{\frac{1}{2}}(P)} \left\{ A_1 \left(C^{1/2} - D^{1/2}\right) + 2v \left[D^{1/2} (2 - \log 2) - C^{1/2} (2 + A_2) \right] \right.$$

$$+ \frac{1}{3b} A_1 \left[C^{1/2} (D-b) + D^{1/2} (C+b) \right] + \frac{2}{3b} \left[D^{3/2} \left(\frac{2}{3} - \log 2\right) \right.$$

$$\left. \left. + 2CD^{1/2} - C^{3/2} \left(\frac{8}{3} + A_2\right) \right] \right\} \qquad (C.11)$$

$$h^{1}_{iq,s} = \frac{\ell_q \cos\alpha}{16\pi b R^{\frac{1}{2}}(P)} \left\{ A_3 \left(C^{1/2} - D^{1/2}\right) - 2v \left[C^{1/2} (2 - \log 2) - D^{1/2} (2 + A_4) \right] \right.$$

$$- \frac{1}{3b} A_3 \left[C^{1/2} (D-b) + D^{1/2} (C+b) \right] + \frac{2}{3b} \left[C^{3/2} \left(\frac{2}{3} - \log 2\right) \right.$$

$$\left. \left. + 2DC^{1/2} - D^{3/2} \left(\frac{8}{3} + A_4\right) \right] \right\} \qquad (C.12)$$

where

$$A_1 = \log \left(\frac{\ell_p^2}{16k\Delta t}\right) \quad ; \quad A_3 = \log \left(\frac{\ell_q^2}{16k\Delta t}\right) \qquad (C.13)$$

with $a = R(P)-b$, $v = 1-a/b$ in equations (C.9) and (C.11), $a = R(P)+b$, $v = 1+a/b$ in equations (C.10) and (C.12), being b, C and D computed as in (B.3) and A_2 and A_4 as in (B.13).

For $\sin\alpha = 0$ ($b=0$), these expressions simplify to

$$g^{2}_{ip,s} = g^{1}_{iq,s} = \frac{\ell}{8\pi} \left[\frac{89}{30} - \log \left(\frac{\ell^2}{4k\Delta t}\right) \right] \qquad (C.14)$$

$$h^{2}_{ip,s} = h^{1}_{iq,s} = \frac{\ell \cos\alpha}{16\pi a} \left[\log \left(\frac{\ell^2}{4k\Delta t}\right) - \frac{17}{6} \right] \qquad (C.15)$$

in which $\cos\alpha = \pm 1$ and ℓ equals ℓ_p or ℓ_q, according to the element under consideration.

The other case to be considered is when the value of the

coefficient c tends to 0.5 but the value of x is small over part of the integration interval (a,∞). In this case, the integrals are divided into two parts (see equation (4.6.21)): evaluation of one results in a quickly convergent series (see equation (4.6.22)) while the asymptotic expansions (4.6.15) and (4.6.16) can now be applied to the other. The value of the coefficient a' was empirically determined to be a' = 1.5/c and this gives

$$B = a'b = 1.5 \left[\frac{[R(P)-R(S)]^2 + [Z(P)-Z(S)]^2}{R(P)\ R(S)} \right] \tag{C.16}$$

Thus, we have for element p,

$$B = \frac{3(1-\xi)^2\ \ell_p^2}{8R(P)\ R(S)} \tag{C.17}$$

being R(S) and Z(S) given by (C.3), and for element q,

$$B = \frac{3(1+\xi)^2\ \ell_q^2}{8R(P)\ R(S)} \tag{C.18}$$

with R(S) and Z(S) computed as in (C.4).

The singular components of G_{ii} and $\hat{H}_{ii}$ can now be written as,

$$g^2_{ip,s} = -\frac{\ell_p}{16\pi R^{\frac{1}{2}}(P)} \left\{ \log\left(\frac{3\ \ell_p^2}{8R(P)}\right) \int_{-1}^{1} R^{\frac{1}{2}}(S)\ (1+\xi)\ d\xi \right.$$

$$\left. - \int_{-1}^{1} R^{\frac{1}{2}}(S)\ \log[R(S)]\ \ (1+\xi)\ d\xi + 2 \int_{-1}^{1} R^{\frac{1}{2}}(S)\ \log(1-\xi)\ (1+\xi)\ d\xi \right\} \tag{C.19}$$

$$g^1_{iq,s} = -\frac{\ell_q^2}{16\pi R^{\frac{1}{2}}(P)} \left\{ \log\left(\frac{3\ \ell_q^2}{8R(P)}\right) \int_{-1}^{1} R^{\frac{1}{2}}(S)\ (1-\xi)\ d\xi \right.$$

$$\left. - \int_{-1}^{1} R^{\frac{1}{2}}(S)\ \log[R(S)]\ (1-\xi)\ d\xi + 2 \int_{-1}^{1} R^{\frac{1}{2}}(S)\ \log(1+\xi)\ (1-\xi)\ d\xi \right\} \tag{C.20}$$

$$h^{2}_{ip,s} = \frac{\ell_p \cos\alpha_p}{32\pi R^{\frac{1}{2}}(P)} \left\{ \log\left(\frac{3\ell_p^2}{8R(P)}\right) \int_{-1}^{1} R^{-\frac{1}{2}}(S)\ (1+\xi)\ d\xi \right.$$

$$\left. -\int_{-1}^{1} R^{-\frac{1}{2}}(S)\ \log[R(S)]\ (1+\xi)\ d\xi + 2\int_{-1}^{1} R^{-\frac{1}{2}}(S)\ \log(1-\xi)\ (1+\xi)\ d\xi \right\} \qquad (C.21)$$

$$h^{1}_{iq,s} = \frac{\ell_q \cos\alpha_q}{32\pi R^{\frac{1}{2}}(P)} \left\{ \log\left(\frac{3\ell_q^2}{8R(P)}\right) \int_{-1}^{1} R^{-\frac{1}{2}}(S)\ (1-\xi)\ d\xi \right.$$

$$\left. -\int_{-1}^{1} R^{-\frac{1}{2}}(S)\ \log[R(S)]\ (1-\xi)\ d\xi + 2\int_{-1}^{1} R^{-\frac{1}{2}}(S)\ \log(1+\xi)\ (1-\xi)\ d\xi \right\} \qquad (C.22)$$

where, again, R(S) is accordingly given by (C.3) or (C.4) and the last integral in each of the above formulas is calculated in the normal sense of improper integrals, being all the others regular.

Comparing expressions (C.19) to (C.22) with (C.5) to (C.8) we notice that one more integral is included in each of the new expressions and apart from that, the only difference between them is in the log term multiplying the first integral. Thus, the analytical evaluation of (C.19) to (C.22) give

$$g^{2}_{ip,s} = g^{2}_{ip,s}\ (C.9) - \frac{\ell_p}{8\pi b R^{\frac{1}{2}}(P)} \left\{ \frac{v}{3}\left[C^{3/2}\left(\frac{2}{3} - \log C\right) - D^{3/2}\left(\frac{2}{3} - \log D\right) \right] \right.$$

$$\left. + \frac{1}{5b}\left[C^{5/2}\left(\frac{2}{5} - \log C\right) - D^{5/2}\left(\frac{2}{5} - \log D\right) \right] \right\} \qquad (C.23)$$

$$g^{1}_{iq,s} = g^{1}_{iq,s}\ (C.10) - \frac{\ell_q}{8\pi b R^{\frac{1}{2}}(P)} \left\{ \frac{v}{3}\left[C^{3/2}\left(\frac{2}{3} - \log C\right) - D^{3/2}\left(\frac{2}{3} - \log D\right) \right] \right.$$

$$\left. - \frac{1}{5b}\left[C^{5/2}\left(\frac{2}{5} - \log C\right) - D^{5/2}\left(\frac{2}{5} - \log D\right) \right] \right\} \qquad (C.24)$$

$$h^{2}_{ip,s} = h^{2}_{ip,s}\ (C.11) + \frac{\ell_p \cos\alpha_p}{16\pi b R^{\frac{1}{2}}(P)} \left\{ v\left[C^{1/2}\left(2 - \log C\right) - D^{1/2}\left(2 - \log D\right) \right] \right.$$

$$\left. + \frac{1}{3b}\left[C^{3/2}\left(\frac{2}{3} - \log C\right) - D^{3/2}\left(\frac{2}{3} - \log D\right) \right] \right\} \qquad (C.25)$$

$$h^{1}_{iq,s} = h^{1}_{iq,s} \quad \text{(C.12)} \quad + \frac{\ell_q \cos\alpha_q}{16\pi b R^{\frac{1}{2}}(P)} \left\{ v\left[C^{1/2}\,(2 - \log C) - D^{1/2}\,(2 - \log D)\right] \right.$$

$$\left. - \frac{1}{3b}\left[C^{3/2}\,(\tfrac{2}{3} - \log C) - D^{3/2}\,(\tfrac{2}{3} - \log D)\right]\right\} \qquad \text{(C.26)}$$

where the coefficients A_1 and A_3 in (C.9) to (C.12) are now computed as,

$$A_1 = \log\left(\frac{3\ell_p^2}{8R(P)}\right) \quad ; \quad A_3 = \log\left(\frac{3\ell_q^2}{8R(P)}\right) \qquad \text{(C.27)}$$

and all the other coefficients are calculated as previously.

For $\sin\alpha=0$ $(b=0)$, these expressions simplify to

$$g^{2}_{ip,s} = g^{1}_{iq,s} = \frac{\ell}{8\pi}\left[\frac{89}{30} - \log\left(\frac{3\ell^2}{2a^2}\right)\right] \qquad \text{(C.28)}$$

$$h^{2}_{ip,s} = h^{1}_{iq,s} = \frac{\ell\cos\alpha}{16\pi a}\left[\log\left(\frac{3\ell^2}{2a^2}\right) - \frac{17}{6}\right] \qquad \text{(C.29)}$$

For the case when $R(P)=0$, the fundamental solution and its normal derivative along the boundary contour become (see equations (4.6.3) and (4.6.4)),

$$\bar{u}^{*}(P,S,t_F,t) = \frac{2\pi}{(4\pi k\tau)^{3/2}} \exp\left(-\frac{d}{4k\tau}\right) \qquad \text{(C.30)}$$

$$\bar{q}^{*}(P,S,t_F,t) = -\frac{1}{8\pi^{\frac{1}{2}}(k\tau)^{5/2}}\left[R(S)\,R_{,n}(S)\right.$$

$$\left. -[Z(P) - Z(S)]\,Z_{,n}(S)\right] \exp\left(-\frac{d}{4k}\right) \qquad \text{(C.31)}$$

The time integrals that appear in the boundary integral equation (4.6.5) can be performed analytically and they give, for stepwise constant variations of u and q,

$$\int_{t_{F-1}}^{t_F} \bar{u}^{*}(i,S,t_F,t)\,dt = \frac{1}{2k(\pi d)^{\frac{1}{2}}}\,\Gamma(\tfrac{1}{2},\, a) \qquad \text{(C.32)}$$

$$\int_{t_{F-1}}^{t_F} \bar{q}^*(i,S,t_F,t)\,dt = -\frac{1}{kd(\pi d)^{\frac{1}{2}}}\left[R(S)\,R_{,n}(S) - [Z(P)-Z(S)]\,Z_{,n}(S)\right]\Gamma(\tfrac{3}{2},a) \tag{C.33}$$

where $d=R^2(S)+[Z(P)-Z(S)]^2$ and $a=d/(4k\Delta t)$.

The coefficients G_{ii} and $\hat{H}_{ii}$ are now obtained by analytically integrating in space the result of the time integrals (C.32) and (C.33). However, since only linear elements are considered in this work, we have that

$$R(S)\,R_{,n}(S) - [Z(P)-Z(S)]\,Z_{,n}(S) = 0 \tag{C.34}$$

and the coefficients $\hat{H}_{ii}$ become identically zero.

In order to compute the coefficients G_{ii}, we expand the incomplete Gamma function in equation (C.32) in series as [75],

$$\Gamma(\tfrac{1}{2},a) = \pi^{\frac{1}{2}} - \sum_{n=0}^{\infty}\frac{(-1)^n a^{n+\frac{1}{2}}}{n!(n+\frac{1}{2})} \tag{C.35}$$

The integrals to be evaluated are now of the form,

$$g_{ip}^{2} = \frac{\ell_p}{8\pi^{\frac{1}{2}}}\int_{-1}^{1} d^{-\frac{1}{2}}\,\Gamma(\tfrac{1}{2},a)\,(1+\xi)\,R(S)\,d\xi \tag{C.36}$$

$$g_{iq}^{1} = \frac{\ell_q}{8\pi^{\frac{1}{2}}}\int_{-1}^{1} d^{-\frac{1}{2}}\,\Gamma(\tfrac{1}{2},a)\,(1-\xi)\,R(S)\,d\xi \tag{C.37}$$

where we have, for element p,

$$R(S) = (1-\xi)\frac{\ell}{2}\sin\alpha \tag{C.38}$$

$$d = (1-\xi)^2\frac{\ell^2}{4}$$

and for element q,

$$R(S) = (1+\xi)\frac{\ell}{2}\sin\alpha \tag{C.39}$$

$$d = (1+\xi)^2\frac{\ell^2}{4}$$

Thus, the final expressions for the coefficients G_{ii} (which

equal g_{ip}^{2} or g_{iq}^{1}) are as follows,

$$g_{ip}^{2} = \frac{\ell_p \sin \alpha_p}{4\pi^{\frac{1}{2}}}\left[\pi^{\frac{1}{2}} - \sum_{n=0}^{\infty} \frac{(-1)^n \ell_p^{2n+1}}{(4k\Delta t)^{n+\frac{1}{2}}\, n!\, (n+\frac{1}{2})(2n+3)\,(n+1)}\right] \quad (C.40)$$

$$g_{iq}^{1} = \frac{\ell_q \sin \alpha_q}{4\pi^{\frac{1}{2}}}\left[-\pi^{\frac{1}{2}} + \sum_{n=0}^{\infty} \frac{(-1)^n \ell_q^{2n+1}}{(4k\Delta t)^{n+\frac{1}{2}}\, n!\,(n+\frac{1}{2})(2n+3)(n+1)}\right] \quad (C.41)$$

and for computer efficiency, each term of the above series can be related to the previous one as,

$$S_n = \frac{(2n+1)(\frac{1}{2}-n)\ \ell^2}{(4k\Delta t)(n+\frac{1}{2})(2n+3)(n+1)}\ S_{n-1} \qquad n=1,2,3,\ldots$$

$$S_0 = \frac{2\ell}{3(4k\Delta t)^{\frac{1}{2}}} \quad (C.42)$$